FUNCTIONAL STUDIES OF CALCIUM ENRICHED TITANIUM SURFACES

Thesis submitted by

Raluca Ioana Mihoc

For the degree of

DOCTOR OF PHILOSOPHY

Divisions of Restorative Dental Sciences
and Biomaterials and Tissue Engineering
UCL Eastman Dental Institute
For Oral Healthcare Sciences
University College London
256 Gray's Inn Road
London WC1X 8LD

-2007-

ProQuest LLC
789 East Eisenhower Parkway
P.O. Box 1346
Ann Arbor, MI 48106-1346

Declaration

"I, Raluca Ioana Mihoc confirm that the work presented in this thesis is my own. Where information has been derived from other sources, I confirm that this has been indicated in the thesis"

ABSTRACT

There exists a clinical requirement for dental implants which will enhance the speed of achievement of osseointegration, its maintenance, and biological and physical properties. Whilst commercially pure titanium remains the material of choice for implant fabrication, a promising approach to enhancing its performance is the surface incorporation of metallic ions, or alkali modification of titanium.

Osteoblast behaviour adjacent to the implant is a key factor in osseointegration and it is known that the response of these cells can be modified by the surface implantation of Ca ions. This process may modify cellular behaviour via a number of physicochemical parameters, three of which were examined in this study using commercially pure titanium, into which Ca ions had been implanted:- topography, calcium ion release, and molecular adsorption.

Surface topography can mediate cellular responses and may be modified by ion implantation. Laser profilometry and white light interferometry were used to measure the roughness of cp Ti surfaces implanted with either biologically active Ca or chemically inert Ar, together with the effects of nitric acid treatment, which is routinely used in implant manufacture.

Ca-ion implantation may also influence cellular responses via accelerated precipitation of calcium phosphate, providing a surface with a chemical composition more similar to that of bone. This may be at least partially due to ion release from the implanted surface. Ion release into water was therefore investigated using ion chromatography and X-ray photoelectron spectroscopy (XPS).

The adsorption of organic molecules (e.g. proteins and peptides) is also important in mediating cellular responses. The effects of Ca-implantation on these processes were investigated using XPS to study the surface adsorption of small model biomolecules (amino acids) from an aqueous solution.

Ion implantation had little effect on surface topography, however, the implanted Ca ions were readily released into an aqueous solution and the surfaces became more receptive to the absorption of certain amino acids. It is concluded that Ca ion implantation is a potentially valuable technique for the surface enhancement of titanium dental implants.

ACKNOWLEDGEMENTS

First and foremost I would like to express my deepest appreciation to Professor J. H. Hobkirk for his continuous support and guidance during this project and throughout my studies in Eastman Dental Institute.

I would like to extend my enormous appreciation to my supervisors Dr. F.H. Jones and Dr. D. Armitage for the hard work and the endless patience that very kindly offered me during this project.

I am indebted many thanks to Dr. R. Chatter for his kind support and guidance with the Zygo and SIMS analysis.

TABLE OF CONTENTS

CHAPTER 3

CHAPTER 4

CHAPTER 5

CHAPTER 6

CHAPTER 7

LIST OF FIGURES

LIST OF TABLES

SCHEMES

To my family

1. INTRODUCTION

Titanium and titanium alloys are widely used in biomedical devices and components, especially as hard tissue replacements for example in cranial reconstruction, as well as in cardiac and cardiovascular applications, because of their desirable properties, such as a relatively low modulus of elasticity, good fatigue strength, formability, machinability, corrosion resistance, and biocompatibility. Commercially pure titanium is also currently the material of choice for making dental implants, an application which has increased considerably over the past three decades.

The expanding use of titanium and its alloys as biomaterials reflects their lower modulus of elasticity, superior biocompatibility and better corrosion resistance when compared to the more conventional stainless steel and cobalt-based alloys.

Titanium was once considered a rare metal, but nowadays it is one of the most important industrial materials. The element was first discovered in England by Gregor in 1790, when it was called mechanite. The name titanium was given in 1795 by Klaproth, who named it after the mythological first sons of the earth, the Titans. In 1887 production of only the impure form of Ti was possible and proper analysis of its properties was not possible until 1901, when Hunter was able to produce enough pure Ti to allow these to be ascertained. In 1938 Kroll developed a process to allow commercial-scale production of Ti. The metal is present in earth as oxide, the chief source of it being dioxide in the mineral ilmenite ($FeTiO_2$) (Brown 1997).

Chemically, titanium is an element in group 4B in the periodic table of elements. It has an atomic number of 22 and an atomic weight of 47.9 (g/mol). Titanium combines the strength of iron and steel with the light weight of aluminium, which accounts for its widespread use in aviation, sports equipment and more relevantly, medical and dental bone replacement devices (Lu et al., 2000). Ti has a low specific gravity (4.5), and a high melting point.

With regards to the chemical composition, commercially pure titanium (cp Ti) contains in very high percentage of titanium (Ti), with the balance being largely oxygen (O), nitrogen (N), hydrogen (H), carbon (C), and iron (Fe) in various

amounts. The American Society for Testing Materials (ASTM) classified Ti in 4 grades, according to the chemical composition, variations in which will influence its properties. Alloying elements are commonly added to titanium to improve the physical and chemical properties. However, a detailed discussion of these is beyond the scope of the current work.

1.1 TITANIUM IN MEDICINE

The applications of titanium and its alloys can be classified according to their biomedical functionalities, including hard tissue replacements, cardiac and cardiovascular applications, dental implants and other applications.

Hard tissue replacements are used because hard tissues (e.g. bone) are often damaged due to accidents, aging, disease and other causes. It is a common practice to surgically substitute the damaged hard tissues with artificial replacements. Depending on the regions in which the implants are inserted and the functions to be provided, the requirements of different endoprosthetic materials vary. Because of the desirable properties mentioned earlier, titanium and titanium alloys are widely used as hard tissue replacements in cranioplasties, joint replacement, and dental implants. As a hard tissue replacement, the low elastic modulus of titanium and its alloys is generally viewed as a biomechanical advantage because this can result in less stress shielding.

Bone, which is very often replaced by titanium and its alloys, is composed from minerals (Ca, Mg, Na, K, some heavy metals, etc) and protein matrix. Hydroxyapatite (calcium phosphate) is the main mineral component of bone. Carbonated-calcium deficient hydroxyapatite is the main mineral of which dental enamel and dentin are comprised. Apatite is a group of phosphate minerals, usually referring to hydroxyapatite, fluorapatite, and chlorapatite, named for high concentrations of OH^-, F^-, Cl^- ions respectively, in the crystal. Bone has relatively high compressive strenght but poor trensile strenght, meaning it resists pushing forces well, but not pulling forces. While bone is essentially brittle, it does have a significant degree of elasticity contributed chiefly by collagen. All bones consist of living cells (osteoblasts, osteocytes, osteoclasts)-

embedded in the mineralised organic matrix (type I collagen) that makes up the osseous tissue.

Apart from hard tissue replacing devices, titanium and titanium alloys are also used commonly in cardiovascular implants because of their unique properties. Early applications included prosthetic heart valves, artificial hearts, protective cases in pacemakers and circulatory devices. Shape memory nickel–titanium alloy (NITINOL) is widely used in intravascular devices, such as stents and occlusion coils. The advantages of titanium in cardiovascular applications are that it is strong, inert, and non-magnetic. It also produces few artefacts under magnetic resonance imaging (MRI), which is a very powerful diagnostic tool. A disadvantage is that it is not sufficiently radio-opaque in finer structures. Artificial hearts made entirely of titanium have in general not been very successful clinically mainly due to problems with blood-clotting occurring on the device surface (Rintoul et al., 1993).

Besides artificial bones, joints, cardiac devices and dental implants, titanium and titanium alloys are often used in bone fracture-fixation (osteosynthesis). Typical implants for osteosynthesis include bone screws, bone plates, maxillofacial implants, etc. Titanium and its alloys with rough surfaces (blasted, plasma sprayed, etched, etc.) or bioactive surfaces which can enhance the deposition of bone-like apatite improve osseointegration because they bond tightly to the bone, thereby reducing relative motions that can otherwise lengthen the bone healing process.

Amongst metals and alloys Ti is the most widely used for dental implants. This is due to its biocompatibility and to the fact that it becomes osseointegrated more rapidly than other metals. According to their position and shape the dental implants can be classified as subperiosteal, transosteal, and endosseous. The most widely used dental implants nowadays are the endosseous ones. They are used widely, as single implants to replace one missing tooth as well as for partially dentate or edentulous patients. The most commonly used endosseous implants are root-form analogues.

The main objective of dental implant treatment is to replace lost teeth in order to restore the function and appearance of the oral cavity.

Insertion of dental implants is based on the "osseointegration" concept that allows dental implants to fuse with bones. This concept was first defined by Brånemark and collaborators in the 1960s as 'a direct structural and functional connection between ordered, living bone and the surface of a load carrying implant' (Albrektsson et al., 1986). The authors suggested criteria of success that indicate the clinical performance of a successful dental implant. They are: absence of implant mobility, absence of radiolucent zones on X-ray, annual bone loss after the first year of < 0.2 mm around the implant, absence of signs and symptoms such as pain, infection, neuropathies, damage to the mandibular canal following placement etc. These criteria are now universally accepted. Since the development of the first implants, there has been considerable debate as to when is the best time to load an implant. In the early days the tissues around implants were allowed to heal and osseointegration occur for up to 6 months before the implant was loaded. The minimum duration allowed for osseointegration has been reduced dramatically since then. Nowadays there are supporters of immediate loading (Esposito, 1998) which is not however universally accepted (Misch 2000).

Whatever the protocol, titanium implants may fail in time (Esposito 1998). The majority of implant failures are related to factors including fractures of prosthetic and fixture components as well as iatrogenic factors. In the minority of the cases implant failures are related to poor osseointegration early on (osseointegration not established) or at a later stage (osseointegration not maintained) Modification of the physical and chemical properties of the Ti surface has been increasingly used as a method of enhancing osseointegration and is a vast topic of increasing scientific interest, which forms the basis of this project.

The ideal material for hard tissue replacement prostheses should possess the following properties: 'biocompatibility' so as to minimise adverse tissue reactions, an excellent resistance to degradation (corrosion) in the human body, acceptable strength, a low modulus to minimize bone resorption, and a high wear resistance to minimize debris generation (Lomg et al., 1998). Besides the above properties, bioactivity, which determines the osseointegratability of the implant, is very important to facilitate cementless anchoring of artificial bones, joints, and dental implants to bones. In order to avoid adverse tissue reactions

arising from hard tissue replacements, a bioinert material, which is stable in the human body and does not react with body fluids and tissues, is preferred. Following implantation into the living body bioinert materials are generally encapsulated by fibrous tissues which isolates them from the surrounding bone. Some bioactive materials, such as hydroxyapatite and bioactive glasses are increasingly used as hard tissue replacements to improve the bonding between implants and bone tissues, because the materials can bond to living bone without the formation of fibrous tissues by creating a bone-like apatite layer on their surface after implantation. Apatite formation is currently believed to be the main requirement for the bone-bonding ability of materials. In this respect, titanium with its native surface oxide, is known to be bioinert, therefore it is difficult to achieve good chemical bonding with bones and form new bone on its surface at the early stage after implantation. Hence, titanium and titanium alloys do not meet all the requirements of the 'ideal' material. In addition, longer human life expectancy and younger patients requiring implants have driven biomedical research from original implant concerns, such as material strength, infection and short-term rejection to consideration of more long-term materials limitations, for instance, wear, fatigue strength, and long-term biocompatibility. The current trend is to use surface modification technologies to address a number of these ever-increasing clinical demands.

Before presenting the Ti modifications, some definitions of the most relevant and frequently used terms mentioned in the area of titanium implants are presented.

A material is defined as 'bio-inert' if it is unable to elicit any response, either favourable or unfavourable, upon contact with the host tissue. The use of this type of material will not harm the host tissue. A material which facilitates tissue growth on its surface and encourages the progression of tissue growth once initiated is defined as 'bio-conductive'. 'Bio-integration' is a term defined as the formation of a biochemical union between the surface of an implant and the host tissue or bone (Steinmann 2000). 'Bio-inductive' materials are materials, which can induce relevant tissue growth.

1.2 MODIFICATIONS OF TITANIUM

Osseointegration of titanium implants is thought to be a result of the presence of a very stable oxide layer at the Ti surface. This layer remains intact on contact with the body tissues and serves as the interface for the chemical interaction between Ti and live tissues. The pure titanium metal does not come into contact with the biological environment (Kasemo 1983). The oxide layer also protects the metal against corrosion. This layer appears in contact with air or water (fluids) and is generally around 0.5-7 nm thick, self-repairing, and strongly resists corrosion (Sunny 1991). Manufacturing procedures as well as the cleaning and sterilization process affect the thickness and the structure of this oxide layer. Osseointegration represents processes that take place between the titanium implant and the bone, at a cellular level. However, processes may occur at a molecular level, between the titanium surface and the organic structures. Improving the titanium surface, by various modifications, the reaction of the inorganic and organic molecules to it may be improved, and clinical results that are more predictable may be obtained when using titanium implants. Therefore, in order to improve the biological, chemical, and mechanical properties, surface modification is often performed. Various surface modification technologies pertaining to titanium and titanium alloys include mechanical treatment, thermal spraying, sol–gel, chemical and electrochemical treatment, and ion implantation from the perspective of biomedical engineering. Recent work has shown that the wear resistance, corrosion resistance, and biological properties of titanium and titanium alloys can be improved selectively using the appropriate surface treatment techniques while the desirable bulk attributes of the materials are retained. The proper surface treatment expands the use of titanium and titanium alloys in the biomedical fields.

Recent clinical research has focused on developing implant materials that produce predictable and rapid healing of the interfacial tissues, both hard and soft. Events leading to the integration of an implant into bone, and consequently to the clinical performance of the restoration under loading, take place largely at the tissue-implant interface. They are dependent on the material that is used to

fabricate the dental implant, the state of the host, the response of the host to the implant, and the behaviour of the material in the host.

The tissue-implant interface

Since the tissue-implant interface plays a major role in osseointegration, a better understanding of events at the interface is needed, and of the effects that biomaterials have on bone and bone cells.

Upon insertion of a titanium implant into the tissues, water adsorption onto the surface results in the formation of an initial hydrated layer known as the 'Helmholtz layer'. The ions and biomolecules present in the surrounding biofluid adhere within this hydrated layer, forming the 'conditioning film' with which cells interact (Lausmaa et al., 1999). The bonding of biomolecules to the surface can occur in several ways, including the long-range and weak van der Waals' interactions and short-range strong chemical bonding, through ionic and covalent bond formation. Inorganic interactions can result in the thickening of the oxide layer through oxidation and hydroxylation, as well as the diffusion of mineral ions or atoms from the bioliquid and tissue into the oxide (e.g. Ca and P-containing mineral ions). Interaction with this conditioning film governs subsequent tissue responses to the implant through the adsorption of larger biomolecules and proteins, which will proceed to form the bone-implant bond. The proteins come first from blood and tissue fluids at the wound site, and later from cellular activity in the interfacial region. Once on the surface, proteins can either desorb, or remain to mediate tissue-implant interactions. If they interact strongly with the surface, they may adopt a structure very different to that in solution (denaturing). The nature of the film deposited on biomaterials, along with the biomechanical conditions surrounding the implantation, can play a major role in the host response (Brunski 2003).

Apart from protein adsorption on the implant's surface, significant changes also occur on the material side of the interface. It is believed that the oxide layer at the implant surfaces undergoes changes in the physiological environment. Commercially pure titanium (cp Ti) implants have an oxide thickness of 2 to 6 nm before implantation, but films on implants removed from human tissues may

be 2 to 3 times thicker (Brunski et al, 2003). Analytical studies of the surface showed that the chemical composition of the oxide film also changed by incorporating calcium, phosphorus, and sulphur. Continued oxide growth after implantation in the body may suggest ongoing events which occur at the tissue-implant interface.

Simultaneously with the events that occur at the titanium surface, ion release from the titanium into the surrounding tissues takes place. Ion release into an experimental medium or any bio-liquid is important because it may be an indication of release into the surrounding tissues *in vitro* and *in vivo*. This may affect the biological and molecular interactions around an implant by inducing hydroxyapatite precipitation and subsequently enhancing bone deposition around the implant. Also, ions released into solution may go through the cell membranes themselves and may have a beneficial effect on the cells but may also have a toxic effect on them. They can also enter the bloodstream and have a systemic effect or potentially be accumulated in body again.

Surface properties play an important role in the dynamics of the interaction between Ti and the surrounding tissues. Various surface modifications have been employed to improve the body reaction to Ti implants.
The bulk properties of biomaterials, such as non-toxicity, corrosion resistance or controlled degradability, modulus of elasticity, and fatigue strength have long been recognized to be highly relevant in terms of the selection of the appropriate biomaterials for a specific biomedical application. The events after implantation include interactions between the biological environment and artificial material surfaces, and the onset of biological reactions, as well as the particular response paths which occur. The material surface plays an extremely important role in the response of the biological environment to artificial medical devices. In implants made of titanium, the normal manufacturing steps usually lead to an oxidized, contaminated surface layer that is often stressed and plastically deformed, non-uniform and rather poorly defined. Such surfaces are clearly not appropriate for biomedical applications and some surface treatment must be performed. Another important reason for conducting surface modification of titanium medical devices is that specific surface properties that

are different from those in the bulk are often required. For example, in order to accomplish biological integration, it is necessary to have good bone formability. In blood-contacting devices, such as dental implants, blood compatibility is crucial. In other applications, good wear and corrosion resistance are also required. The proper surface modification techniques not only retain the excellent bulk attributes of titanium and its alloys, such as relatively low modulus, good fatigue strength, formability and machinability, but also improve the specific surface properties required by different clinical applications. According to these different clinical needs, various surface modification schemes have been proposed.

These methods are classified into mechanical, chemical and physical methods according to the formation mechanism of the modified layer on the surface of titanium and its alloys. The properties of titanium and its alloys can be upgraded to some extent after their surfaces are modified using suitable surface modification technology. With the development of surface engineering, new surface modification technologies will be introduced to improve the properties of titanium and its alloys for meeting the clinical needs.

An overview of the surface modification methods for titanium and its alloys is presented below.

A. MECHANICAL METHODS

1. ***Machining***
2. ***Grinding***
3. ***Polishing***
4. ***Blasting***

B. CHEMICAL METHODS

1. ***Chemical treatment***

- Acid treatment
- Hydrogen peroxide treatment
- Alkali treatment

2. ***Sol–gel coatings***

- TiO_2 coating

- Calcium phosphate coatings
- Titania/hydroxyapatite composite coatings
- Silica coating

3. ***Anodic oxidation***
4. ***Chemical vapour deposition***
5. ***Biochemical modification of titanium and titanium alloys***

C. PHYSICAL METHODS

1. ***Thermal spraying***

- Plasma spraying

  Plasma sprayed hydroxyapatite coating

  Plasma sprayed calcium silicate coating

  Plasma sprayed titanium coating
- Other thermal spraying techniques

2. ***Physical vapour deposition***

- Evaporation
- Ion plating
- Sputtering

3. ***Glow discharge plasma treatment***
4. ***Ion implantation and deposition***

- Oxygen implantation
- Nitrogen implantation
- Carbon implantation and deposition
- Metal ion implantation (Ca, Na, K., etc)

1.2.1 Mechanical modifications

Common mechanical surface modification methods, such as machining (Lausmaa et al., 1990, Lucchini et al., 1996), grinding, polishing (Hignett et al., 1987), and blasting (Marinucci et al., 2006, Buser et al., 1999, Baleani et al., 2000, Desagne et al., 1999, and Wennerberg et al., 1996) involve physical treatment, shaping, or removal of the surface of the material. The typical objective of mechanical modification is to obtain specific surface topographies

and roughness, remove surface contamination, and / or improve adhesion in subsequent bonding steps.

Increased surface roughness has been shown to enhance the mechanical interlocking between the macromolecules of the implant surface and the bone (Cochran 1999). This has resulted in a greater resistance to compression, tension, shear, and stress. All these properties increase the degree of cellular attachment of osteoblast-like cells. They also increase the removal torque, (the torque applied on the implant in order for it to be removed), which demonstrates that implants with roughened surfaces have enhanced contact with bone. Implants with increased surface roughness show higher success rates compared with those with smooth surfaces (Lazzara et al., 1999, Binon et al., 2000, Buser et al., 1991).

1.2.2 Chemical modifications

Chemical methods include chemical treatment (acid, alkali, H_2O_2, heat, and passivation treatments), electrochemical treatment (anodic oxidation), sol–gel, chemical vapour deposition (CVD), and biochemical modification. During the chemical and electrochemical treatments, and biochemical modification, chemical, electrochemical or biochemical reactions occur, respectively, at the interface between titanium and a solution.

Kasemo et al. (1986) stated that biologic tissues interact mainly with the outermost atomic layer of an implant, the "primary interaction zone". Modifications are made at this "primary interaction zone". It has been shown that the physico-chemical nature of the implant surface can influence macromolecular binding.

Among the physico-chemical properties that have been modified in order to improve the bone-implant interface are: surface energy, surface charge, and surface composition (Baier et al., 1988). Procedures that have been undertaken to increase the surface energy have included heat treatments in the range of 500°-600°C, acid cleaning and passivation (Kilpadi et al., 2000), glow discharge and the use of charged surfaces (Taborelli et al., 1997, Rupp et al., 2006).

Chemical modifications employed include the preparation of sol-gel titania layers, treatment with hydrogen peroxide (Ohtsuki et al., 1997), treatment with alkali solution (with and without heat treatment) and etching with sulphuric and hydrochloric acids (Kim et al., 1996).

Rough surfaces are generally created by the use of coatings, blasting (sand blasting), acid etching, or a combination of the last two (sand blasting and acid etching (SLA)). Other methods of increasing surface roughness include anodic oxidation, machining and grinding.
Two popular techniques for producing coating are plasma spraying and ion beam sputtering. The most common coatings are hydroxyapatite (HA) and plasma sprayed titanium (TPS).

A. Chemical treatment

1. Acid treatment

Acid treatment is often used to remove oxides and contamination so as to obtain clean and uniform surface finishes.
Takeuchi et al. (2003) investigated the decontamination efficiency of three acids, $Na_2S_2O_8$, H_2SO_4, and HCl on the Ti surface. The authors found that HCl was an excellent decontamination agent because it could easily dissolve titanium salts and did not weaken the Ti surfaces.
Vanzilotta et al., (2006) investigated the influence of surface treatments of commercially pure titanium samples on *in vitro* bioactivity. Commercially pure (cp) titanium (Ti) sheets were submitted to three different surface treatments, including, for all samples, etching with an HCl/H_2SO_4 solution. Part of each etched sample was further submitted either to anodic oxidation by using an H_3PO_4 solution or to thermal oxidation. The samples were analysed by using scanning electron microscopy (SEM), profilometry and photoelectron X-ray spectroscopy (XPS). The *in vitro* assessment was carried out through the immersion of samples in simulated body fluid (SBF). *In vitro* testing was carried out by SEM and by the determination of calcium (Ca) content in solution by atomic absorption spectrometry (AAS). The non-treated titanium samples were

used as the control group. Their study showed that, after up to 7-day exposure, a calcium phosphate layer precipitated only on samples submitted to at least one of the three treatments used. This result, based on SEM images, is in good agreement with Ca content and XPS analysis, in which remarkable effects of surface modifications on Ti samples are highlighted. The results suggested that suitable surface treatments, such as employed here, may improve *in vitro* titanium bioactivity in a SBF solution at 37° C. This behaviour may suggest a possibility of a further favourable *in vivo* response.

Acid etching generally may lead to a thin surface oxide layer (< 10 nm). These oxide layers have been shown to grow slowly in air, from ~ 3 to ~ 6 nm during a 400-day period (Sittig et al., 1999). The oxide is predominantly TiO_2, but residues from the etching solution are frequently observed, particularly chemicals containing fluorine. Also some treatments can lead to hydrogen incorporation in the surface region below the oxide (Taborelli et al., 1997). These residues can remain even after post-thermal treatment of the etched surfaces. In addition, the acid treatment was often used in combination with other treatment methods to improve the properties of titanium and its alloys. Wen et al. (1997, 1998) reported that the bioactivity of Ti alloy could be improved by two-step chemical treatments employing ($HCl + H_2SO_4$) and an alkaline solution.

Nitric acid passivation of cp Ti has been recommended as it is thought to modify the oxide layer, minimise corrosion and remove debris embedded in the surface during machining (Kilpaldi et al., 1998). Nitric acid passivation of metallic implants prior to surgical implantation aims to modify the oxide layer in order to prevent ion release from the bulk metal into the immediate biological vicinity of the implant, which may have an adverse effect on the integration process (Lacefield 1999). Lee et al., (2006) studied the effects of passivation treatment (34% nitric acid passivation, 400°C heated in air, and aged in 100°C de-ionised water) and surface modification (2 h and 8 h vacuum-brazed treatments) on the ion dissolution and nano-surface characteristics of Ti-6Al-4V exposed in Hanks solution with 8.0 mM ethylene diamine tetra-acetic acid (EDTA) at 37°C. The results indicated that the original nano-surface characteristics and microstructure would influence the ion dissolution but not change the capability

of the Ca and P adsorption upon immersion. After soaking in Hanks / EDTA solution, the adsorbed non-elemental Ca and P for all groups of specimens were observed by XPS analysis, and the AES depth-profile analysis indicate that the oxide films of all groups of specimens thicken with the longer immersion periods. The increasing oxide thickness may be the factor in the improved dissolution resistance at the longer immersion periods. The relationship between lower dissolution rate and thicker oxide films was observed for all groups of specimens. The results suggest that the dissolution kinetics were governed by the metal ion transport through the oxide film in this study.

2. Hydrogen peroxide treatment

Titania gel coating can improve the bioactivity of titanium implants because titania gels can induce the formation of apatite when soaked in a simulated body fluid (SBF) (Kangasniemi et al., 1994, Peltola et al., 1998, 1999, and Ohtsuki et al., 1994).

Titanium surfaces have been shown to react with H_2O_2 producing Ti-peroxy gels (Tengvall et al., 1992, 1998). From a surface engineering point of view, the H_2O_2-titanium interaction offers a method for chemical dissolution and oxidation of titanium surfaces (Walivaara et al., 1993, 1994) as well as pre-treatment for apatite precipitation (de Oliveira et al., 2007, Pan et al., 1996, 1998, Ohtsuki et al., 1997). An amorphous titania gel layer can be formed by treating Ti in an H_2O_2 / 0.1 M HCl solution. The reaction between titanium and the H_2O_2 solution results in the formation of a layer of amorphous titania gel on the Ti surface. The thickness of the titania gel layer depends on the duration of the chemical treatment (Wang et al., 2002). Pan et al. (1996, 1998) suggested that the oxide had a two-layer structure consisting of a thin (< 5 nm) and dense inner oxide and an outer porous layer. Subsequent heat treatment above 300 °C gradually transformed the gel from the amorphous to crystalline state. The as-treated amorphous gel layer transformed mainly to anatase if the treatment temperature was below 600 °C while the rutile phase was dominant above 700 °C. Thermal treatments at temperatures lower than 600 °C hardly changed the morphology of the pores of the gel layer. Large spherical particles of titania have been reported to appear after heat treatment at 700 °C, apparently due to the coalescence of small particles. Further increasing the temperature to 800 °C

results in a fully densified titania layer. The titania gel processed between 400 and 500 °C possesses the anatase structure and exhibits excellent bioactivity. A higher temperature raises the rutile content in the gel and degrades its bioactivity.

Recently Tavares et al., (in press) evaluated whether controlled chemical oxidation of titanium (Ti) with sulphuric acid (H_2SO_4)/hydrogen peroxide (H_2O_2) can influence *in vivo* bone formation. The authors concluded that a controlled chemical oxidation of Ti implants significantly enhances contact osteogenesis and suggested that this treatment may be beneficial for early loading of implants.

3. Alkali treatment

Alkali and heat treatments were first introduced by Kim et al., (1996) to improve the bioactivity of some implant materials. The method enables the formation of a biologically active bone-like apatite layer on the surface of bioactive ceramics, (Wei et al., in press, Hench et al., 1993), and hydroxyapatite (Legeros et al., 1993). A simple chemical method was established for inducing bioactivity in Ti and its alloys. When pure Ti, Ti-6Al-4V, Ti-6Al-2Nb-Ta, and Ti-15Mo-5Zr-3Al substrates were treated with 10 M NaOH aqueous solution and subsequently heat-treated at 600°C, a thin sodium titanate layer was formed on their surfaces (Kim et al., 1996). Subsequently, treated substrates formed a dense and uniform bonelike apatite layer on their surfaces in simulated body fluid (SBF) with ion concentrations nearly equal to those of human blood plasma. This indicated that the alkali- and heat-treated metals bonded to living bone through the bonelike apatite layer formed on their surfaces in the body. The apatite formation on the surfaces of Ti and its alloys was assumed to be induced by a hydrated titania layer which was formed by an ion exchange of the alkali ion in the alkali titanate layer and the hydronium ion in SBF. The resultant surface structure changed gradually from the outermost apatite layer to the inner Ti and its alloys through hydrated titania and titanium oxide layers. This provided not only the strong bonding of the apatite layer to the substrates but also a uniform gradient of stress transfer from bone to the implant. The described chemical surface modification was therefore expected to allow the use of bioactive Ti and its alloys as artificial bones even under load-bearing conditions. However, the

authors concluded that, as they established a single treatment condition in their study (10 M NaOH at 60^{0}C for 24 h and subsequent heat treatment at 600 ^{0}C for 1 h), it was not clear how concentration, temperature, and duration of alkali treatment, as well as the subsequent heat treatment would affect the resultant ability to induce apatite formation for each Ti alloy. They stated that these factors should be optimised to develop functionally gradient bioactive Ti and its alloys for use as a bone substitute.

Osteoblastic differentiation in bone marrow cells on the alkali- and heat-treated titanium, and apatite-formed titanium were examined by Nishio et al., (2000). They found that apatite formation played an important role in osteoblastic differentiation. Bone-like apatite-formed on titanium after alkali- and heat-treatment was observed to provide the most favourable conditions for bone marrow cell differentiation.

Alkali- and heat-treated titanium bonds to bone tissue directly, but titanium that is only alkali-treated does not. Both alkali and heat treatments are essential in order to acquire the bone bonding ability (Nishiguchi et al., 1999). The authors analysed the detaching failure loads of untreated, alkali-treated, and alkali- and heat-treated titanium 8–16 weeks after implantation. After 8 weeks, the failure loads of the alkali- and heat-treated titanium group were significantly higher than those of the alkali-treated titanium and control titanium groups. After 16 weeks, the alkali- and heat-treated titanium group showed a failure load significantly higher than that of the same group at 8 weeks and those of alkali-treated and control titanium groups at 16 weeks. The failure loads of alkali-treated and control titanium groups did not increase over the 8-week loads.

Since the introduction of alkali and heat treatment to improve the bioactivity of titanium and its alloys by Kim et al. (1996), many researchers have further investigated the mechanism and optimized the treatment process for better bioactivity (Sandrini et al., in press, Jonášová et al. 2002, 2004, Wang et al., 2002, 2003, Liang et al., 2003, Lu et al., 2004). Lee et al. (2002) investigated the bioactivity and surface changes on surface treated Ti–In–Nb–Ta and commercial Ti–6Al–4V alloys using *in vitro* tests which employed simulated body fluids. Porous networked layers of sodium titanate ($Na_2Ti_5O_{11}$ or $Na_2Ti_6O_{13}$) were formed on the surface of titanium alloys after surface modification by alkali and heat treatments. The pore size of the inner porous

reticular structures in the Ti–In–Nb–Ta alloy was finer than that of the Ti–6Al–4V alloy, whereas the thickness of the sodium titanate layer on the Ti–In–Nb–Ta alloy was half that of the Ti–6Al–4V alloy. It thus appears that the corrosion resistance to alkalis is enhanced on the Ti–In–Nb–Ta alloy.

Titanium treated in NaOH and then immersed in SBF formed inhomogeneous and non-uniform apatite (Jonášová et al., 2004). Etching of titanium by HCl under an inert atmosphere was found to produce a uniform micro-roughened surface that provided improved conditions for in situ apatite formation. After alkali treatment in NaOH, apatite nucleation was found to be homogenous and the thickness of the precipitated apatite layer increased continuously with time. The treatment of titanium by a two step HCl and subsequent NaOH process appears to be a suitable method to enhance the bone-bonding ability of the surface.

A plasma-sprayed titanium surface is thought to be suitable for bone ingrowth. The materials can endure shear forces that can break the bones. Alkali and heat treatment of such porous titanium implants leads to significantly higher bonding shear strength in the canine femora push-out model 4 weeks after implantation. This alkali- and heat-treated porous titanium may be useful in clinical situations, such as cementless total hip arthroplastry and total knee arthroplastry (Nishiguchi et al., 2001).

Lee et al. (2004) showed that a nanosized porous layer of sodium titanate ($Na_2Ti_5O_{11}$ or $Na_2Ti_6O_{13}$) was formed on the surface of the plasma sprayed titanium implants after alkali and heat treatments. The average pore size on the surface of the alkali- and heat-treated implant was about 150 nm. This implant had good bone bonding strength after 4 weeks of healing because of the mechanical interlocking in the micrometer-sized rough surface and the large bonding area between the bone and implant caused by the nanosized porous surface structure.

B. Sol–gel coatings

The sol–gel process is widely used to deposit thin (< 10 μm) ceramic coatings. Compared to conventional thin film processes, it allows for better control of the chemical composition and microstructure of the coating, preparation of

homogeneous films, reduction of the densification temperature, and finally simpler equipment and lower cost.

Many coatings, such as titanium oxide (TiO_2), calcium phosphate, and TiO_2–calcium phosphate composite have been prepared on titanium and its alloys for biomedical applications. Some silica-based coatings have also been produced using the sol–gel technique.

Huang et al., (in press) prepared a titania containing calcium and phosphate with rough and porous structure. The *in vitro* bioactivity was examined by immersing the samples into the simulated body fluid (SBF). The results show that only 3 days of immersion in SBF, apatite was formed on the surface, and after 6 days, nearly all the surface covered by apatite. This indicates that the layer can induce the formation of apatite in simulated body fluid.

Meretoja et al., (2007) compared titania (TiO_2-coated), titania-silica (TiSi)-coated, and uncoated (cp Ti) titanium fibre meshes as scaffolds for bone engineering. The authors noted that the sol-gel coatings resulted in enhanced initial bone contact and distribution of bone tissue, whereas uncoated implants showed bone formation mainly in the centre of the scaffolds. They concluded that TiO_2-based sol-gel coatings may be used in tissue engineering to gain more uniform distribution of bone throughout titanium fibre mesh scaffolds.

Collagen coatings of Ti alloys improve the early cells adhesion of cell (Bierban et al., 2006). TiO_2 coating (titania coatings) synthesized by the sol–gel process are widely used in the optical, electrical, and catalytic fields (Samuneva et al., 1993, Trapalis et al., 1993).

The bonding strength of titania coatings synthesized on titanium substrates using the sol–gel technique was investigated by Pätsi et al., (1998). In their work, three different pretreatments were used, namely sodium hydroxide treatment, plasma cleaning, and titanium nitride coating. The effects of the temperature, heating in vacuum, and titanium surface roughness were studied. The maximum attachment strengths were achieved by a 1 h treatment in 10 M sodium hydroxide solution. All the samples showed the ability to form a calcium phosphate layer in simulated body fluids (Pätsi et al., 1998). It is believed that the sol–gel titania rich in Ti–OH groups can induce calcium phosphate formation and may therefore be able to contribute to enhanced bonding to bones.

The possibility of modifying the surface area, porosity, composition, adsorption capacity, and dissolution rate using the sol–gel technique is very attractive in the fields of medicine and dentistry. Calcium phosphate coatings, especially hydroxyapatite coatings, are commonly used in orthopaedic applications. The sol–gel method is a relatively simple way to prepare hydroxyapatite coatings on titanium alloys because of the easy formation of the oxide coatings at a relatively low temperature.

Hydroxyapatite (HA) coatings have been employed in an attempt to make Ti implants osteoconductive and maximize bone growth. HA is of interest as it closely resembles the mineral component of natural bone. Osteoconductivity of a bioactive material is thought to be related to its ability to form a thin layer of calcium phosphate on its surface as a consequence of reactions with body fluids (Strnad et al., 2000).

The hydroxyapatite coatings synthesized by the sol–gel method are typically bioactive but have poor adhesion strength to the substrate. On the other hand, titanium dioxide (TiO_2) coatings strongly adhere to titanium but their bioactivity is limited. Hence, a composite titania/hydroxyapatite coating can take advantage of the high adhesion strength of TiO_2 and bioactivity of calcium phosphate.

Kim et al. (2004) deposited hydroxyapatite on titanium by means of a titania (TiO_2) buffer layer using the sol–gel method. The HA layer showed a typical apatite phase at 400°C. The phase intensity increased above 450°C. The HA and TiO_2 films of thicknesses of approximately 800 and 200 nm, respectively, adhered tightly to each other and to the Ti substrate. The bonding strength of the HA / TiO_2 double layer was markedly improved when compared to that of a single HA coating on Ti. The improvement in the bonding strength with the insertion of a TiO_2 buffer layer was attributed to the enhanced chemical affinity of TiO_2 towards the HA layer as well as Ti substrate. Human osteoblast (HOS)-like cells cultured on the HA/TiO_2 coating surface proliferated in a similar manner to those on the single TiO_2 coating and Ti. However, the alkaline phosphatase (ALP) activity of the cells on the HA / TiO_2 double layer was greater than on the single TiO_2 and Ti. The corrosion resistance of Ti was also improved by the presence of the TiO_2 coating.

The role of silica gel in the formation of bone-like apatite on the substrate has been investigated by many researchers. Karlsson et al., (1989) proposed that silicate chelating was an essential step in the formation and mineralization of hard tissues. Yoshida et al. (1999) investigated the silica coatings produced on titanium by the sol–gel technique. The formation of both thin SiO_2 and SiO_2/F-hybrid films by the sol–gel dipping process gave rise to excellent surface properties including high bonding strength to the metal substrate, small amounts of leached titanium ions and high hydrophobicity. With these important findings, the bond strength of dental resin cements to titanium can be improved, the release of titanium ions from the substrate can be mitigated, and accumulation of dental plaque on intraoral dental devices can be reduced.

C. Anodic oxidation

Anodic oxidation is a simple and effective method to modify the surface of titanium and its alloys for better biocompatibility and bioactivity. The anodic oxide film exhibits a variety of different properties that depend on the composition and microstructure of the materials and processing parameters, such as anode potential, electrolyte composition, temperature, and current. Anodic oxidation encompasses electrode reactions in combination with electric field driven metal and oxygen ion diffusion leading to the formation of an oxide film on the anode surface.

Yang et al. (2004) indicated that anodic oxidation in an H_2SO_4 solution combined with subsequent heat treatment was an effective method to prepare bioactive titanium. After anodic oxidation, the surface was observed to be covered with porous titania of the anatase and/or rutile phase. In simulated body fluids, the titanium anodically oxidized during spark discharge induced apatite formation on its surface. The induction period of apatite formation decreased with increasing amount of either the anatase or rutile phase.

D. Chemical vapour deposition

Chemical vapour deposition is a process involving chemical reactions between chemicals in the gas phase and the sample surface resulting in the deposition of a non-volatile compound on the substrate. It is different from physical vapour deposition (PVD), which typically employs techniques, such as evaporation and

sputtering involving no chemical reactions. CVD is widely adopted in the industry to produce organic and inorganic films on metals, semiconductors, and other materials. The application of diamond coatings on cemented tungsten carbide (WC-Co) tools has been the subject of much attention in recent years in order to improve cutting performance and tool life in orthodontic applications (Jackson et al., 2007). Chemical vapour deposition and sol-gel methods are used in the surface engineering of artificial heart valve discs (Jackson et al., 2006).

E. Biochemical modification

Biochemical modification of biomaterials utilises biological and biochemical knowledge of cellular function, adhesion, differentiation and remodelling. The objective of modification is to induce specific cell and tissue response by means of surface-immobilized peptides, proteins, or growth factors. However, it is also important that biochemical modification improves the biocompatibility of the surface, the bulk properties cannot be adversely affected, and so the concept of a bio-mimetic surface to guide cell behaviour on an ultra thin layer consisting of bioactive molecules has been introduced (Xiao et al., 2001). A variety of techniques, such as silanized titania (Xiao et al., 1997, 1998), photochemistry (Weber et al 1998), self-assembled monolayers (Iwasaki et al., 2003, Abe et al., 2005, Majewski et al., 2006, Schuler et al., 2006, Abe et al., 2005) protein resistance, and protein immobilization (Tosatti et al., 2003) have been used on titanium and titanium alloys. These technologies exploit either physical adsorption via van der Waals', hydrophobic, or electrostatic forces, or chemical bonding. On account of the existence of a surface TiO_2 film, the modified layer does not make direct contact with the substrate. Since TiO_2 is a relatively inert surface, only a few organic reagents, such as organosilanes, organophosphates, and photosensitive chemicals, are able to form strong chemical bonds.

Covalent attachment of organosilanes has proven to be a simple and versatile method to enhance surface properties, such as wettability, adhesion, and surface activity. Silane chemistry is used on the titanium surface to enhance metal–metal and metal–polymer adhesion, convert semiconducting TiO_2 films into electrodes (Finklea et al., 1979), immobilize enzymes, and conduct

chromatography. It is also useful to graft biomolecules onto the titanium implant surface for improvement in biocompatibility. Photochemistry can also be used to graft biomolecules onto titanium surface (Xiao et al., 2001).

Self-assembled monolayers (SAMs) have become an important research technique to produce surfaces with a very well defined chemical composition. SAMs have often been used as model surfaces for various biological assays including the study of cell-surface interaction and the influence of the surface chemistry on the spontaneous mineralization caused by contact with simulated body fluid (Scotchford et al., 1998, Tanahashi et al., 1997). Self-assembled monolayers of alkaline phosphates or phosphonates have been used on titanium surfaces to tailor selected physico-chemical properties of the surface, such as wettability and electrical charge (Tosatti et al., 2002, Hofer et al., 2001). The effects of the surface chemistry on protein adsorption and cell adhesion have also been studied (Sigal et al., 1998, Tegoulia et al., 2001, Holmlin et al., 2001). Protein-resistant and protein immobilization technologies are often used to modify the surface of titanium and titanium alloys. In many cases, integration of the implant with the newly formed tissue is desired. Thus, the adsorption of cell-adhesive proteins or bioactive proteins is an important aspect of the healing process. Bone morphogenetic protein can be immobilized on the surface of Ti–6Al–4V to enhance the bioactivity (Puleo et al., 2002). Plasma polymerization of allyl amine has also been used to provide functional groups for immobilization of biomolecules on Ti–6Al–4V surfaces. The amount of protein weakly and strongly bound to metallic biomaterials can be controlled by the choice of the surface treatment and immobilization chemistry. BMP-4 bound to Ti–6Al–4V having a high density of amino groups using a two-step carbodiimide immobilization scheme appears to induce significant osteoblastic activity in pluripotent C3H10T1/2 cells. In other applications, protein adsorption may lead to a deleterious physiological response depending on the type and nature of the adsorbed proteins (Xiao et al., 2001). For example, non-specific protein adsorption may impair the performance of blood or serum in contact with stents or diagnostic sensors.

The native oxide on titanium is beneficial to the adhesion of many proteins. However, in some applications, it is necessary to reduce surface protein adsorption, for example in blood-contacting devices, such as stents and

sensors. The simplest approach to controlling protein adsorption is to passivate the surface with a layer of an inert protein, such as albumin (Xiao et al., 2001). Immobilization of poly (ethylene glycol) (PEG) on the titanium surface has long been known to decrease protein adsorption (Jeon et al., 1991, Morra et al., 2001). Some researchers have reported the chemisorption of a polycationic comb-like graft copolymer and poly(L-lysine)-graft-poly(ethylene glycol) (PLL-g-PEG) onto negatively charged metal oxide surfaces by a simple dipping process in an aqueous solution of the polymer (Kenausis et al., 2000, Huang et al., 2001). When the appropriate polymer is chosen, such coated surfaces can be stable and protein resistant for days even in the presence of fibrinogen or full human serum. At physiological pH, the poly(L-lysine) chains display positively charged amino groups ($-NH_3^+$) that interact with negatively charged metal oxides, such as TiO_2, Ta_2O_5, Nb_2O_5, and SiO_2 thus leading to a densely packed layer of PEG chains at the metal-oxide substrate surface.

1.2.3 Physical modifications

During some surface modification processes, such as thermal spraying and physical vapour deposition, chemical reactions do not occur. In this case, the formation of a surface modified layer, films or coatings on titanium and its alloys are mainly attributed to the thermal, kinetic, and electrical energy. In the thermal spraying process, the coating materials are thermally melted into liquid droplets and coated to the substrate at a high speed (kinetic energy). Physical vapour deposition leads to film growth by reaction between a substrate surface and an adjacent vapour which supplies the coating material in the form of atoms, molecules or ions, generated from a target and transported to the substrate surface on which condensation and reaction with atoms of the surface lattice take place. The generation of atoms, molecules or ions from targets can be accomplished by resistance heating, electron beam, laser or electrical discharge in vacuum. Glow discharge plasma treatment and ion implantation are also categorized as physical methods, although they influence the surface chemistry.

A. Thermal Spraying

Thermal spraying is a process in which materials are thermally melted into liquid droplets and introduced energetically to the surface on which the individual particles stick and condense. The coating is formed by a continuous build-up of successive layers of liquid droplets, softened material domains and hard particles. Thermal spraying requires a device that creates a high temperature flame or a plasma jet. Therefore, thermal spraying is often divided into flame spraying and plasma spraying. The principal difference between flame and plasma spraying is the maximum temperature achievable.

Plasma sprayed hydroxyapatite coating, because of its similarity to the mineral phase of natural hard tissues, is considered to be a bioactive material. Bone can be regarded as an organic matrix with the inclusion of an inorganic filler with a crystal size in the submicron range. About 70% of the mineral fraction of bone has an HA-like structure and the use of HA as an orthopaedic biomaterial has been suggested and clinically demonstrated. However, the mechanical properties of HA are quite poor, making it unsuitable as bulk a material in applications where high loads or strains occur. The concept of using plasma spraying to produce HA coatings on endoprosthesis was first proposed in Japan in 1975. It has been shown that implants with an HA surface develop a strong connection with the bone tissue in a short time (Driskell et al., 1994, Lacefield et al., 1993). The relatively poor bonding between a plasma sprayed HA coating and titanium is one of the main disadvantages of the technique. The bonding strength of the HA coating on titanium decreases with longer immersion time in simulated body fluids (SBF) (Kwek et al., 2002). Another disadvantage is the resorption and degradability of HA coatings in a biological environment. This may lead to disintegration of the coating resulting in the loss of both the coating–substrate bonding strength and implant fixation. There also exists the threat of coating delamination and formation of particulate debris (Bauer et al., 1991, Collier et al., 1993). The thickness of the HA coating affects both its resorption and mechanical properties. A thicker coating usually exhibits poorer mechanical properties. The suggested optimum thickness is about 50 μm in order to avoid fatigue failure while still providing reasonable coating

bioresorption and consistent bone growth (Wang et al., 1993, Yang et al., 1997).

A plasma sprayed titanium coating increases the surface area of the bone to implant interface, and increases roughness for initial stability, while the surface has a stronger bond to implant interface than uncoated implant surfaces (Lee et al., 2004). Plasma-sprayed titanium coatings with porous structure have been used in tooth root, hip, knee and shoulder implants. The porous surface improves fixation via the growth of bone into the coating forming a mechanical interlock. Vercaigne et al., (1998) evaluated the biological and mechanical properties of the implant with a titanium coating and investigated the effects of the surface roughness on the bone response. No correlation was observed between the percentage of bone contact and surface roughness. The percentage of bone contact after 3 months of installation was very low. The loosening of particles during or after implant placement endangers the safe application of very rough coatings, but with the advent of improved plasma spraying techniques and post processing, rough coatings that show no particle release have been produced. Lee et al. (2004) investigated the mechanical stability and *in vivo* behaviour of implants of three surface designs: smooth surface (SS), rough titanium surface with a plasma-sprayed coating (PSC), and an alkali- and heat-treated titanium surface (AHT) after plasma spraying. Four weeks after the implants had been implanted in dog bone, the pull-out forces of the SS, PSC, and AHT implants were determined. The AHT implant showed good bone-bonding strength after 4 weeks of healing because of the mechanical interlocking in the micrometer-sized rough surface and the large bonding area between the bone and implant, as a result of the nanosized porous surface structure. During this healing period, new bone on the surface of AHT implant underwent higher growth than that on the PSC implant, results which have been confirmed by Liu et al., (2004).

B. Physical vapour deposition

Physical vapour deposition (PVD) is a technique used to deposit thin films of various materials onto various surfaces by physical means, as compared to chemical vapour deposition. The physical vapour deposition process can be described succinctly as follows. In vacuum, the target materials are evaporated

or sputtered to form atoms, molecules or ions that are subsequently transported to the substrate surface, on which condensation and sometimes some reactions with the materials surface take place leading to film growth. Physical vapour deposition processes include evaporation, sputtering, and ion plating.

C. Glow discharge plasma treatment

Glow discharge plasma is a low-temperature, low-pressure gas in which ionization is controlled by energetic electrons. Glow discharge plasma treatment has been well established for cleaning and surface processing in the microelectronics industry (Mittal et al., 1979) and has attracted much interest in biomaterials research in which it is used for the surface modification of bulk polymers and production of thin polymer coatings (plasma polymerization).

D. Ion implantation

Ion implantation is a technique developed for the semiconductor industry to introduce dopant ions into the surface layer of a material (Sze 1985). Detailed description of the method is given in Chapter 2. It has been proposed as a method of enhancing biological response to the surface. This method is very advantageous because in general is controllable, fast, homogeneous, reproducible and useful for creating model surfaces of known composition. Ion implantation allows the alteration of the chemical, physical and optical properties of a solid and is commonly used to alter the composition, structure and morphology of the near surface layers. Various surface properties may be modified by ion implantation, like mechanical, chemical, electrical and optical properties (Townsend et al., 1994). Mechanical properties include microhardness, friction, adhesion, and wear. Chemical properties altered by ion implantation include corrosion, passivation, diffusion, and reactivity. Electrical properties include resistivity, photoconductivity, electron mobility, and semiconductivity, meanwhile optical properties include colour, reflectivity, transmission and opteoelectronics.

Annealing is the process of heat treatment, and subsequent slow cooling of the substrate. This can be performed after ion implantation has taken place. Its

aims are ion activation, moving the dopant ion within the surface layer, and restructuring the surface after it has been damaged.

Ion beam technology has contributed significantly to the modification of biomaterials (Hanawa et al., 1997). The surface modification techniques can be divided into two categories: formation of a surface-modified layer or that of a thin film that can be totally different from the substrate. For instance, ion implantation and ion beam mixing can produce a surface-modified layer. The wear resistance and bone conductivity can be improved by nitrogen and calcium ion implantation, respectively. The advantage of the surface-modified layer is the graded composition and an obscure interface between the surface layer and substrate making surface delamination less of a problem. Addition of thin films can also be used to improve bone conductivity, corrosion resistance, and wear resistance. Examples are apatite, TiO_2, and TiN, respectively. During film formation, control is easier and the film materials can be selected irrespective of the substrate. However, weak adhesion of the thin film to the substrate can be a problem especially in the case of high film stress or thermal mismatch.

Different ions have been implanted into titanium with a view to improving its properties, including oxygen, calcium, nitrogen, argon, and fluoride.

N implantation results in the formation of titanium nitride. Its good electrical conductivity and excellent performance as an adhesive layer make TiN an interesting material in microelectronic applications, for example as a diffusion barrier between silicon substrates and aluminium metallisations (Price et al., 1993, Hedge et al., 1993). TiN also has high hardness and remarkable resistance to wear and corrosion, and is therefore commonly used in products such as cutting tools. Because of its intrinsic biocompatibility, TiN is also a suitable material for orthopaedic implants and has been used as a coating on the heads of hip prostheses to improve their wear and fatigue resistance (Mandl et al., 2002). TiN is the material of choice as the hard coating on dental implants and dental surgical tools. N implantation of the titanium improves the wear and corrosion resistance of the material (Yeung at el., in press, Buchanan et al., 1987). The structure and properties of nitrogen ion implanted titanium and titanium alloys have been investigated by many researchers (Liu et al., in press,

Krupa et al., 1996, 1999, Berberich et al., 2001, Wen et al., 2002). Krupa et al., (1996, 1999) implanted nitrogen into OT-4-0 (Ti–0.7Mn–0.7Al) titanium alloy using conventional ion implantation and investigated the changes in the surface structure and the effect of nitrogen ion implantation upon the corrosion resistance. The structure obtained by implanting ions at the rate of 1×10^{18} cm^{-2} was similar to those implanted with lower doses and was composed of nanocrystalline TiN (10–150 nm in diameter). Examination of the corrosion resistance showed that nitrogen ion implantation increased the corrosion resistance of the OT-4-0 alloy in a 0.9% NaCl solution. The best corrosion resistance was achieved with a nitrogen ion dose of 1×10^{17} cm^{-2}.

Oxygen implantation improves the wear resistance, corrosion resistance, and biocompatibility of titanium and its alloys (Fraker et al., 1983).

Carbon does not worsen the biocompatibility of titanium alloys and is widely used as a coating on metal implants (De Maetzu et al., 2007). Carbon has been implanted to or deposited on titanium using ion implantation and deposition technologies, and found to improve the mechanical properties, corrosion resistance and biocompatibility. The implanted ions are bound either to titanium to form titanium carbides or to carbon atoms to form C-C bonds near the surface. Implantation at moderate doses (5×10^{15}–1×10^{17} cm^{-2}) creates a layer of nanocrystalline titanium carbide TiC with a cubic lattice (Fm3m) and a-Ti matrix.

Fluorine has been implanted into titanium to improve the antibacterial effect (Nurhaerani et al., 2006, Yoshinari et al., 2001). F-implanted specimens were observed to significantly inhibit the growth of both *P. gingivalis* and *A. actinomycetemcomitans* (Yoshinari et al., 2001). It has also been reported that several fluoride salts with polyvalent cations, such as Cu^{2+}, Sn^{2+}, and Al^{3+} exhibit a direct antibacterial effect, and titanium tetrafluoride seeded with bacteria exhibits similar growth inhibition zones to those of these salts (Skartveit et al., 1990).

Krupa et al., (2005, 2004, 1999) investigated the effects of phosphorus ion implantation on the corrosion resistance and biocompatibility of titanium. The sample was implanted with 1×10^{17} P^+ cm^{-2} and the ion energy was 25 keV. The process led to the surface layer becoming amorphous and the formation of TiP. It also increased the corrosion resistance after short-term as well as long-

term exposures to SBF. The phosphate layers formed on the titanium surface during exposure did not affect the corrosion resistance and the biocompatibility of the titanium was confirmed under specific conditions. With regard to the viability of osteoblasts, their function as measured by ALP activity, and ability to spread on the investigated surfaces, no difference was found between the modified and control titanium specimens.

Sodium has also been implanted into titanium and its alloys to improve the bone conductivity by inducing the formation of apatite on their surface in body fluids (Pham et al., 2000, Maitz et al., 2005, 2002a, 2002b). Sodium ion implantation into Ti was shown to incorporate sodium titanate within the surface layer and produce morphologically rugged surfaces. The titanate formation occurred by Na reacting with Ti in the presence of oxygen. Sodium-implanted Ti surfaces were found to be sensitive to inducing apatite precipitation from simulated body fluids. The surface reactivity was associated with a titania hydrogel film formed by the hydrolysis of sodium titanate. The surface hydroxyl groups were thought to be not the chemically specific sites for apatite nucleation. The apatite formation seems to be related to an unspecific effect based on the electrical double layer at a negatively charged titania hydrogel surface which tends to increase the supersaturation for apatite precipitation near the surface. Three factors are thought to affect the supersaturation level: surface bound titanate and hydroxyl anions, the pH dependent deprotonation equilibrium, and the microtopography facilitating a surface potential superposition.

Calcium ion implantation is a promising method to enhance the surface bioactivity of titanium and to improve the biocompatibility of Ti and its alloy (Park et al., in press, Nayab et al., 2007, Hanawa et al., 1996). Calcium-ion implantation of titanium surfaces has been obtained by implanting Ca ions with acceleration energy of 18 keV, ion beam density of 50 μAcm and krypton as the assist gas (Hanawa et al., 1993). The nature of the modified layer depended on the quantity of ions implanted. Hanawa et al. carried out numerous studies on Ca ion implantation (Hanawa et al., 1993, 1994, 1995, 1997, 1999) and revealed that the bone conductivity of titanium was improved by calcium ion implantation (Hanawa et al., 1993). This was thought to be because calcium ion implantation expedited calcium phosphate precipitation on titanium. After the calcium ion implanted titanium was soaked in Hank's solution for 30 days, a

calcium phosphate layer formed on the surface. Osteogenic cells were activated to form osteoid tissues and a large amount of new bone was observed to form early on calcium ion implanted titanium compared to unimplanted titanium, even only two days after implantation into rat tibia. The improvement in the bone conductivity of calcium-implanted titanium is due to the modified surface. The surface of calcium implanted titanium was postulated to consist of calcium titanate at ion implant doses of 10^{16}–10^{17} ions cm^{-2}, and both calcium oxide and calcium titanate were found to be formed when the implant dose is 10^{18} cm^{-2}, although actually the papers show little direct evidence for this (Hanawa et al., 1998).The outermost surface in both cases is possibly calcium hydroxide .The modified surface layers are very thin and about 6, 8, and 13 nm on the specimens implanted with 10^{16}, 10^{17}, and 10^{18} cm^{-2}, respectively. This modified layer operates as a substrate with improved hard-tissue compatibility. The calcium implanted titanium surface was found to be more positively charged due to dissociation of hydroxyl radicals (Hanawa et al., 1998). A larger number of phosphate ions from the body fluid adsorbed on the calcium implanted titanium surface. Calcium ions were also gradually released from the surface of calcium implanted titanium into certain solutions (Hanawa et al., 1996a, and 1996b). It was postulated that this may cause supersaturation of calcium ions in the body fluid next to the surface resulting in acceleration of calcium phosphate precipitation.

Krupa et al. (2001) investigated the effects of calcium implantation and formation of calcium phosphate precipitates on the corrosion resistance of titanium. The titanium surface was implanted with calcium ions at a dose of 1×10^{17} cm^{-2} and the ion energy was 25 keV. The conditions under which implantation was carried out were selected so that the calcium concentration was maximum on the surface. The corrosion resistance was examined by electrochemical methods in a simulated body fluid (SBF) at a temperature of 37°C. Calcium ion implantation with a dose of 1×10^{17} cm^{-2} resulted in amorphisation of the surface layer and increased the corrosion resistance under stationary conditions in SBF. Calcium phosphate formed on the titanium surface during exposure did not affect the corrosion resistance.

Calcium and phosphorus have also been co-implanted into titanium and titanium alloys to enhance their mechanical properties and biocompatibility

(Wieser et al., 1999, Krupa et al., 2001, Tsyganov et al., 2002, Bauman et al., 2002). A hydroxyapatite surface layer with a continuous transition to the titanium substrate can be produced by implanting successively calcium and phosphorus into titanium under different conditions. Krupa et al. (2001) found that implantation of titanium with Ca and P ions, both separately and in combination increased its corrosion resistance in SBF.

Calcium ions were also implanted into titanium to immobilize bisphosphonates on the surface of titanium (Yoshinari et al., 2001). Here, the modified layer that was about 7–12 nm thick consisted of $CaTiO_3$ and TiO_2. This modified layer was comparatively stable, and so immobilized bisphosphonate could remain on the modified surface. Bisphosphonates are a new class of drugs that have been developed to treat diseases related to bones and calcium metabolism. These compounds are potent inhibitors of bone resorption and inhibit soft tissue calcification *in vivo*. In the dental field, the compounds prevent periodontal destruction and decrease the formation of dental calculus. *In vitro*, many of the bisphosphonates inhibit the crystal formation of calcium phosphate blocking the transformation of amorphous calcium phosphate into hydroxyapatite and the dissolution of these crystals. Bisphosphonates are also reported to alter the morphology of osteoclasts both *in vitro* and when administered *in vivo*. On dental implants, the use of bisphosphonates is expected to promote osteogenesis at the bone tissue/implant interface by inhibiting the activity of osteoclasts and immobilization of bisphosphonates on titanium implants is therefore considered by some worker to be important.

It has been shown that the architecture of the tissues adjacent to a titanium implant is greatly affected by the implant surface configuration. This includes both chemical and structural properties. The surface chemistry and energy are reported to determine the type and the orientation of adsorbed molecules, and consequently cellular attachment. It is known that osteoblasts and chondrocytes are sensitive to subtle differences in surface roughness and surface chemistry (Boyan et. al., 1995). As established by Larsson (1996), early phases of cortical bone formation in rabbits are determined by the surface roughness and the oxide film thickness on 99.7% commercially pure titanium (cp Ti). It has been shown that by increasing the surface roughness the mechanical interlocking between the macromolecules of the implant surface and the bone (Cochran

1999) is enhanced. This results in a greater resistance to tension, shear, stress and compression. As a result, the degree of cellular attachment of osteoblast - like cells will increase, as well as the torque removal (the torque applied on the implant in order to break the bond between the implant and the surrounding tissues). This demonstrates that implants with roughened surfaces have enhanced contact with bone. Implants with increased surface roughness show higher success rates compared with those with smooth surfaces (Binon et al., 2000 and Buser et al., 1991). It has recently been shown in studies at the UCL Eastman Dental Institute that cells respond differently at gene level to different surface topography (Brett et al., 2004).

Also, studies conducted by the Biomaterials and Tissue Engineering group of the UCL Eastman Dental Institute, have shown that bone-derived cells (both primary alveolar bone cells and MG-63 osteosarcoma cell line) respond differently to Ti surfaces when implanted with Ca ions. For example, cell adhesion experiments have indicated that fewer cells attach to Ca-implanted Ti ($^{40}Ca^{+}$, 40 keV, 1×10^{17} ions cm^{-2}), but implantation with other ions of similar mass ($^{39}K^{+}$, $^{40}Ar^{+}$) did not lead to such a drop in cell attachment (Nayab et al., 2003). However, despite this reduced cell adhesion, scanning electron micrographs showed highly spread cells with an increase cell to substrate ratio on Ca-Ti surfaces compared with those on control non-implanted Ti discs. Subsequently, a remarkable increase in cell proliferation was also observed on this particular surface compared with a non-implanted cp-Ti control (Nayab et al., 2003). Also Ca-Ti, in contrast to K-Ti, Ar-Ti and Ti samples significantly enhanced cell spreading and subsequent cell growth (Nayab e al., 2004). The effect of ion dose of Ca-Ti samples on cells was also examined (Nayab et al., 2005). High dose (10^{17} ions cm^{-2}) Ca-Ti resulted in significantly enhanced cell spreading, cell size, the formation of 'focal adhesion plaques' and the expression of $\alpha5\beta1$ integrin (a mediator of cell adhesion). In contrast, no marked differences were observed in cell behaviour on lower dose (10^{16} or 10^{15} ions cm^{-2}) Ca-Ti compared with control Ti. Pre-immersion of the discs in culture medium was found to significantly enhance subsequent cell adhesion on Ca (high)-Ti, and was found to be correlated with the presence of Ca- and P-rich particles on this surface at certain time points. Cell proliferation was also found

to be significantly increased on the high dose Ca-Ti surface (Nayab e al., in press). Furthermore, when the cells were synchronised at the G1/S boundary and then released from 'arrest', cultures grown on Ca-Ti more rapidly re-entered and progressed through the S and G2/M phases of the cell cycle than those on Ti. Ca-Ti also showed a significantly higher proportion of mitotic cells, again indicating that this surface enhanced cell cycle progression. The effects of Ca implantation on cell function were also assessed, by measuring the production of essential bone-associated constituents. Bone morphogenetic protein receptor-IB, bone sialoprotein and particularly osteopontin were significantly up-regulated in the MG-63 cells cultured on Ca-Ti compared with control Ti, while alkaline phosphatase and osteonectin levels were not altered (Nayab et al., in press). The presence of notably elevated levels of osteopontin mRNA in the cells indicated that the effects of the Ca-Ti surface were mediated, at least partly, via gene activation.

The reasons for this behaviour are not yet understood, therefore it is important to fully characterise the surface in terms of both topography and chemistry to attempt to rationalise the effects.

It is likely that a number of physicochemical processes influence cellular responses to the newly-challenged implant surface. Among them are physical damage to the surface during the surface modification processes, as it is known that cells can be sensitive to sub-micron changes in surface morphology, surface energy, crystal structure etc. Also ion release is important for any material in the biological environment. For ion implanted materials, ions are physically embedded in the lattice. However, there is some evidence that they may be released into solution where they will influence adsorption processes and may enter the cells themselves. Surface oxide layer thickness plays a role. The natural oxide layer may dissolve and become thinner, or may oxidise and thicken. All may influence cellular responses to inserted titanium. Interaction with species in solution is another factor which may influence cells. These may be inorganic (e.g. the formation of calcium phosphate layers, thought to be important in osseointegration of implant materials) or organic (e.g. the

adsorption of biomolecules required for cellular adhesion or specific cell functions).

Some attempt has been made in the past to characterise Ti surfaces (Shinawi 2003), but many of these studies were inconclusive, and the characteristics of Ca implanted Ti (Ca-Ti) are still not fully understood. Those studies however, provided a starting point for this work, which has extended the understanding of the Ca-Ti surface and sub-surface composition and resulting reactivity quite considerably.

This thesis describes studies on some of the aspects of titanium and modified titanium surfaces which may influence interactions with cells and tissues during osseointegration. These are:

1. The changes (if any) that occur in the surface topography with surface modification by titanium plasma spraying, sand blasting and acid etching, ion implantation and nitric acid treatment.
Different surfaces with known measured topographic characteristics were examined. These had shown different cell responses when used in gene expression experiments (Brett et al., 2004). A study was also carried out to ascertain whether ion implantation and nitric acid treatment affected surface topography. Ion implantation of cp Ti samples was known to modify the chemical composition of titanium, which is likely to play a role in determining the cell response to titanium (Nayab et al., 2003, 2006, in press). It is important to ascertain whether the implantation process modifies the topography of the titanium and to what extent this might influence cellular reactions to the implanted surfaces.

2. To study ion release into water from ion implanted titanium discs.
As discussed above, the effects of ion microdissolution from titanium surfaces are important. By calcium-ion implantation, calcium phosphate precipitation on titanium is accelerated. It is believed that microdissolution of calcium ions into the bioliquid induces the precipitation of calcium phosphate on the material by supersaturation of the bio-liquid near the material (Hanawa et al., 1996).

Previous studies have concentrated on analysis of the titanium surface. This study looks at ion release from modified titanium by analysis of the solution. Also the effect of ion release on the surface and sub-surface layers of titanium are studied using surface analytical techniques

3. To study the adsorption of amino acids at the titanium surface.
As discussed above, protein adsorption on titanium surfaces is very important. As proteins are highly complex molecules, amino acids were used in this study because they are the building blocks of proteins and their structures are much simpler. Simple chemical surface modifications have been shown to influence adsorption on titanium surfaces (Kilpadi et al., 2000). Alkali treatments, mainly NaOH, have been employed to improve protein or amino acid adsorption at the titanium surface. These methods have also been shown to enhance the precipitation of calcium phosphate and to increase the thickness of the oxide layer. Ion implantation is a good method for modifying the surface properties of model implant materials in order to study parameters that may influence osseointegration at a fundamental level.

4. To attempt to deposit Ca on the Ti surface by alternative methods to Ca ion implantation. These methods are potentially cheaper and readily available in any chemical laboratory. The methods employed were alkali treatments, which have been shown to accelerate apatite formation.

1.3 LIST OF REFERENCES

Abe, Y., Hiasauzuki, K., Akagawa, Y. (2005)
New surface modification of titanium implant with phospho-amino acid.
Dental Materials Journal 24(4): 536-540

Andrade, M.C., Filgueiras, M.R.T., Ogasawara, T. (1999)
Nucleation and growth of hydroxyapatite on titanium pretreated in NaOH Solution: Experiments and thermodynamic explanation
Journal of Biomedical Materials Research 46(4): 441-446

Baier, R.E, Meyer, A.E. (1988)
Implant surface preparation.
International Journal of Oral and Maxillofacial Implants 3: 9-20

Baleani, M. Viceconti, M., Toni, A. (2000)
The effect of sandblasting treatment on endurance properties of titanium alloy hip prostheses.
Artificial Organs 24(4): 296-299

Baumann, H., Bethge, K., Bilger, G., Jones, D., Symietz, I. (2002)
Thin hydroxyapatite surface layers on titanium produced by ion implantation
Nuclear Instruments & Methods in Physics Research Section B- Beam Interactions with Materials and Atoms, 196(3-4) 286-292.

Berberich, F., Matz, W., Kreissig, U., Richeter, E., Schell, N., Möller, W. (2001)
Structural characterisation of hardening of Ti–Al–V alloys after nitridation by plasma immersion ion implantation.
Applied Surface Science 179(1-4): 13-19

Binon, P. (2000)
Implant and components: Entering the new millennium.
International Journal of Oral and Maxillofacial Implants 15: 76-94

Boyan, B.D., Hummert, T.W., Kieswetter, K., Schraub, D., Dean, D., Schwartz, Z. (1995)
Effect of titanium surface characteristics on chondrocytes and osteoblasts *in vitro*.
Cells and Materials 5(4): 323-334

Brånemark, P. I., Zarb, G. A., Albrektsson, T (1985)
Tissue-integrated prostheses. Osseo-integration in clinical dentistry.
Carol Stream, IL: Quintessence Publishers: 11-76, 129-143

Braceras, I., Alava, J.I., Oñate, J.I., Brizuela, M., Garcia-Luis, A., Garagorri, N., Viviente, J.L., de Maetzu, M.A. (2002)
Improved osseointegration in ion implantation-treated dental implants.
Surface and Coatings Technology 158-159: 28-32

Brett, P.M., Harle, J., Salih, V., Mihoc, R., Olsen, I., Jones, F.H., Tonetti, M. (2004)
Roughness response genes in osteoblasts.
Bone 35(1): 124-133

Brunski, J.B. (2003)
In vivo response to biomechanical loading at the bone/dental-implant interface.
Advanced Dental Research 13: 99-119

Buchanan, R.A., Rigney Jr. E.D., Williams, J.M. (1987)
Ion implantation of surgical Ti-6Al-4V for improved resistance to wear-accelerated corrosion.
Journal of Biomedical Materials Research 21(3): 355-366

Buser, D., Schenk, R., Steinemann, S., Fiorellini, J.P., Fox, C.H., Stich, H. (1991)
Influence of surface characteristics on bone integration of titanium implants. A histomorphometric study in miniature pigs

Buser, D. Nydegger, T. Oxland, T. Cochran, D.L. Schenk, R.K., Hirt, H.P. Snetivy, D., Nolte, L.P. (1999)
Interface shear strength of titanium implants with a sandblasted and acid-etched surface: A biomechanical study in the maxilla of miniature pigs.
Journal of Biomedical Materials Research 45 (2): 75-83

Cohran, D.L (1999)
A comparison of endosseous dental implant surfaces
Journal of Periodontology 70: 1523-1539

Collier, J. P., Surprenant, V. A., Mayor, M. B., Wrona, M., Jensen, R. E., Surprenant, H.P. (1993)
Loss of hydroxyapatite coating on retrieved, total hip components.
Jourrnal of Arthroplasty 8: 389-395

De Oliveira, P. T., Zalzal, S. F., Beloti, M. M., Rosa, A. L., Nanci, A. (2007)
Enhancement of *in vitro* osteogenesis on titanium by chemically produced nanotopography.
Journal of Biomedical Materials Research A 80(3): 554-564

De Maetzu, M. A., Braceras, I., Alava, J. I., Sanchez-Garces, M. A., Gay-Escoda, C. (2007)
Histomorphometric study of ion implantation and diamond-like carbon as dental implant surface treatments in beagle dogs.
International Journal of Oral and Maxillofacial Implants 22(2): 273-279

Degasne, I. Basle, M.F. Demais, V. Hure, G. Lesourd, M. Grolleau, B. Mercier, L., Chappard, D. (1999)
Effects of roughness, fibronectin and vitronectin on attachment, spreading, and proliferation of human osteoblast-like cells (Saos-2) on titanium surfaces.
Calcified Tissue Interface 64(6): 499-507

Driskell, T. D. (1994)
Early history of calcium phosphate.
Materials and Coatings, ASTM publication, Philadelphia 3-17

Esposito, M., Hirsch, J.M., Lekholm, U., Thomsen, P. (1998)
Biological factors contributing to failures of osseointegrated oral implants
European Journal of Oral Science 106: 527-551

Finklea, H.O., Murry, R.W. (1979)
Effects of silanization on titanium dioxide electrodes.
Journal of Physical Chemistry B 83: 353-359

Fraker, A.C. Ruff, A.W. Sung, P. Van Orden A.C., Speck K.M. (1983)
Titanium alloys in surgical implants.
In: H.A. Luckey and F. Kubli, Editors, ASTM Special Technical Publication 796, Philadephia : 206–219.

Fujibayashi, S., Nakamura, T., Nishiguchi, S., Tamura, J., Uchida, M., Kim, H. M., Kokubo, T. (2001)
Bioactive titanium: Effect of sodium removal on the bone-bonding ability of bioactive titanium prepared by alkali and heat treatment.
Journal of Biomedical Materials Research 56 (4): 562-570

Hanawa, T., Ukai, H., Murakami K. (1993)
X-ray photoelectron spectroscopy of calcium-ion-implanted titanium.
Journal of Electron Spectroscopy and Related Phenomena 63: 347- 354

Hanawa, T., H. Ukai, K. Murakami, and K. Asaoka, (1995)
Structure of surface-modified layers of calcium-ion-implanted Ti6Al4V and Ti56Ni.
Materials Transactions Jim, 36(3)438-444.

Hanawa, T., Asami, K., Asaoka, K. (1996a)
AES Studies on the dissolution of surface oxide from calcium-ion-implanted titanium in nitric acid and buffer solutions.
Corrosion Science 38(11): 2061-2067

Hanawa, T., Asami, K., Asaoka K. (1996b)
Microdissolution of calcium ions from calcium-ion-implanted titanium
Corrosion Science 38: 1579-1594

Hanawa, T., Hiromoto, S., Asami, K. (2001)
Characterization of the surface oxide film of a Co–Cr–Mo alloy after being located in quasi-biological environments using XPS.
Applied Surface Science 183(1-2): 68-75

Hanawa, T. (1997)
Early bone formation around calcium-ion- implanted titanium inserted into rat tibia.

Journal of Biomedical Materials Research 36(1): 131-136

Hanawa, T., Kon, M., Doi, H., Ukai, H., Murakami K., Hamanaka, H., Asaoka, K (1998)
Amount of hydroxyl radial on calcium-ion- implanted titanium and point of zero charge of constituent oxide of the surface-modified layer.
Journal of Material Science: Materials in Medicine 9: 89-92

Hanawa, T. (2004)
Metal ion release from metal implants.
Materials Science and Engineering: C: 24, (6-8): 745-752

Hench, L.L., Andersson, Ö. (1993)
Bioactive glass.
In: L.L. Hench and J. Wilson, Editors, An Introduction to Bioceramics,
World Scientific, Singapore: 41–62

Hignett, B., Andrew, T. C., Downing, W., Duwell, E.J., Belanger, J., Tulinski, E.H. (1987)
Surface cleaning, finishing and coating.
In: W.G. Wood, Editors, Metals Handbook vol. 5, American Society for Metals, Metals Park, OH: 107–127

Huang, N. P. Michel, R. Voros, J. Textor, M. Hofer, R. Rossi, A. Elbert, D.L. Hubbell J.A. and Spencer, N.D.(2001)
Poly(L-lysine)-g-poly(ethylene glycol) layers on metal oxide surfaces: surface-analytical characterization and resistance to serum and fibrinogen adsorption.
Langmuir 17: 489-497

Huang, P., Xu, K., Han. Y. (in press)
Formation mechanism of biomedical apatite coatings on porous titania layer.
Journal of Material Science Materials in Medicine

Iwasaki, Y., Saito, N. (2003)
Immobilization of phosphorylcholine polymers to Tisupported vinyldimethylsilyl monolayers and reduction of albumin adsorption.
Colloids Surfaces B Biointerfaces 32: 77-83

Jackson, M. J., Robinson, G. M., Ali, N., Kousar, Y., Mei, S., Gracio, J., Taylor, H., Ahmed, W. (2006)
Surface engineering of artificial heart valve disks using nanostructured thin films deposited by chemical vapour deposition and sol-gel methods.
Journal of Medical Engineering and Technology 30(5): 323-329

Jackson, M. J., Sein, H., Ahmed, W., Woodwards, R. (2007)
Novel diamond-coated tools for dental drilling applications.
Journal of Medical Engineering and Technology 31(2): 81-93

Jeon, S. I., Lee, J. H., Andrade, J .D., Degennes, P.G. (1991)
Protein - surface interactions in the presence of polyethylene oxide.

Journal and Colloid Interface Science 142: 149-157

Jonášová, L., Müller, F.A., Helebrant, A., Strnad, J., Greil, P. (2002)
Hydroxyapatite formation on alkali-treated titanium with different content of Na+ in the surface layer.
Biomaterials 23(15): 3095-3101

Jonášová, L., Müller, F.A., Helebrant, A., Strnad, J., Greil, P. (2004)
Biomimetic apatite formation on chemically treated titanium.
Biomaterials 25(7-8): 1187-1194

Karlsson, K.H. Fröberg K., Ringbom, T. (1989)
A structural approach to bone adhering of bioactive glasses.
Journal Non-Crystalline Solids 112: 69-77

Kasemo B (1983)
Biocompatibility of Titanium Implants: Surface Science aspects
Journal of Prosthetic Dentistry 49(6): 832-837

Kasemo, B., Lausmaa, J. (1986)
Surface science aspects on inorganic biomaterials.
CRC Critical Review of Biocompatibility 2: 335-380

Kenausis, G. L., Voros, J., Elbert, D. L., Huang, N. P., Hofer, R., Ruiz-Taylor, L., Textor, M., Hubbell, J. A., Spencer, N.D. (2000)
Poly (L-lysine)-g-poly(ethylene glycol) layers on metal oxide surfaces: attachment mechanism and effects of polymer architecture on resistance to protein adsorption.
Journal of Physical Chemistry B 104: 3298-3307

Kilpadi, D.V., Lemons, J.E., Liu, J., Ganesh, N., Raikar, N. (2000)
Cleaning and heat – treatments effects of unalloyed titanium implant surfaces.
International Journal of Oral and Maxillofacial Implants 15: 219-230

Kim, H.W., Koh, Y.H., Li, L.H., Lee, S., Kim, H.E (2004)
Hydroxyapatite coating on titanium substrate with titania buffer layer processed by sol-gel method.
Biomaterials 25: 2533-2546

Kim, H.M. Miyaji, F., Kokubo, T., Nakamura, T. (1996)
Preparation of bioactive Ti and its alloy via simple chemical surface treatment
Journal of Biomedical Materials Research 32: 409-417

Kim, H.M. Miyaji, F., Kokubo, T., Nakamura, T. (1996)
In situ measurements of ion-exchange processes in single polymer particles: laser trapping microspectroscopy and confocal fluorescence microspectrosopy.
Journal of Biomedical Materials Research 33: 524-531

Krupa, D., Jezierska, E., Baszkiewicz, J., Kamiński, M., Wierzchoń, T., Barcz, A. (1996)

Effect of nitrogen ion implantation on the structure and corrosion resistance of OT-4-0 titanium alloy.
Surface and Coatings Technology 79 (1-3): 240-245

Krupa, D., Baszkiewicz, J., Jezierska, E., Wierzchoń, T., Barcz, A., Fillit, R. (1999)
Effect of nitrogen-ion implantation on the corrosion resistance of OT-4-0 titanium alloy in 0.9% NaCl environment.
Surface and Coatings Technology 111: 86-91

Krupa,D.,Baszkiewicz,J.,Kozubowski,J.,Barcz,A.,Sobczak,J.,Bilinski,A., Lewanswoska-Szumiel, M., Rajchel, B. (2001)
Effect of calcium-ion implantation on the corrosion resistance and biocompatibility of titanium.
Biomaterials 22(15): 2139-2151.

Krupa, D., Baszkiewicz, J., Kozubowski, J., Barcz, A., Sobczak, J., Bilinski, A., Rajchel, B. (2001)
The influence of calcium and/or phosphorus ion implantation on the structure and corrosion resistance of titanium.
Vacuum 63: 715-719

Krupa,D.,Baszkiewicz,J.,Kozubowski,J.,Barcz,A.,Sobczak,J.,Bilinski,A., Lewanswoska-Szumiel, M., Rajchel, B. (2002)
Effect of phosphorus-ion implantation on the corrosion resistance and biocompatibility of titanium.
Biomaterials 23(16): 3329-3340.

Krupa, D., Baszkiewicz, J., Kozubowski, J., Lewandoswska-Szumiel, M., Barcz, A., Sobczak, J., Bilinski, A., Rajchel, B. (2005)
Effect of calcium and phosphorus ion implantation on the corrosion resistance and biocompatibility of titanium.
Biomedical Materials Engineering 14(4): 525-536

Krupa, D., Baszkiewicz, J., Kozubowski, J., Mizera, J., Barcz, A., Sobczak, J., Bilinski, A., Rajchel, B. (2005)
Corrosion resistance and bioactivity of titanium after surface treatment by three different methods: ion implantation, alkaline treatment and anodic oxidation.
Analytical and Bioanalytical Chemistry 381(3): 617-625

Kweh, S. W. K., Khor, K. A., Cheang, P. (2002)
An in vitro investigation of plasma sprayed hydroxyapatite (HA) coatings produced with flame-spheroidized feedstock.
Biomaterials 23: 775-785

Lacefield, W. R. (1993)
An introduction to bioceramics.
World Scientific, Singapore, In: L.L. Hench and J. Wilson, Editors 223-233

Larsson, C., Thomsen, P., Aronsson, B.O., Rodhal, M., Lausmaa, J., Kasemo, B., Ericsson, L.E. (1996)
Bone response to surface modified titanium implants: studies on the early tissue response to machined and electropolished implants with different oxide thicknesses.
Biomaterials 17(6): 605-616

Lausmaa, J., Kasemo, B., Mattsson, H. (1990)
Surface spectroscopic characterization of titanium implant materials.
Applied Surface Science 44: 133-147

Lausmaa, J., Lofgren, P., Kasemo, B. (1999)
Adsorption and coadsorption of water and glycine on TiO_2.
Journal of Biomedical Materials Research 44 (3): 227-242

Lazzara, R.J., Testori, T., Trisi, P., Porter, S.S., Weinstein, R.L. (1999)
A human histological analysis of osseotite and machined surfaces using implants with two opposing surfaces.
International Journal of Periodontics and Restorative Dentistry 19: 117-129

Lee, B.H., Kim, J.K., Kim, Y.D., Choi, K., Lee, K.H. (2004)
In vivo behaviour and mechanical stability of surface-modified titanium implants by plasma spray coating and chemical treatments.
Journal of Biomedical Materials Research 69 A : 279-284

Lee, B.H., Kim, J.K., Kim, Y.D., Shin, J., Lee, K.H. (2002)
Surface modification by alkali and heat treatments in titanium alloys.
Journal of Biomedical Materials Research 61: 466-471

Legeros, R.Z., LeGeros, J.P. (1993)
Dense hydroxyapatite.
In: L.L. Hench and J. Wilson, Editors, An Introduction to Bioceramics, World Scientific, Singapore: 139–180

Li, P., Ohtsuki, C., Kokubo, T., Nakanishi, K., Soga, N., de Groot, K. (1994)
The role of hydrated silica,titania and alumina in inducing apatite on implants.
Journal of Biomedical Materials Research 28: 7-12.

Li, P., Kangasniemi, I., de Groot ,K., Kokubo, T. (1998)
Bonelike hydroxyapatite induction by a gel-derived titania on a titanium substrate.
Journal of the American Ceramic Society 77(5): 1307-1312

Liu, X. M., Wu, S. L., Chan, Y. L., Chu, P. K., Chung, C. Y., Chu, C. L., Yeung, K. W., Lu, W. W., Luk, K. D. (in press)
Surface characteristics, biocompatibility, and mechanical properties of nickel-titanium plasma-implanted with nitrogen at different implantation voltages.
Journal of Biomedical Materials Research

Liu, X., Chu, P., Ding, C. (2004)
Surface modification of titanium, titanium alloys, and related materials for biomedical applications.
Material Science and Engineering 47(3-4):49-61

Lu, G., Bernasek, S. I., Schwartz, J. (2000)
Oxidation of a polycrystalline titanium surface by oxygen and water.
Surface Science 458: 80-90

Lu, X., Leng, Y. (2004)
TEM study of calcium phosphate precipitation on bioactive titanium Surfaces.
Biomaterials 25: 1779-1785

Lucchini, J. P. , Aurelle, J. L., Therin, M., Donath, K., Becker, W. (1996)
A pilot study comparing screwshaped implants. Surface analysis and histologic evaluation of bone healing.
Clinical Oral Implants Research 7 (4): 397-404

Maitz, M.F. Pham, M. T. Matz, W. Reuther, H. Steiner G.(2002)
Promoted calcium-phosphate precipitation from solution on titanium for improved biocompatibility by ion implantation,
Surface & Coatings Technology 158: 151-156.

Maitz, M.F. Pham, M. T. Matz, W. Reuther, H. Steiner G, Richter, E. (2002)
Ion beam treatment of titanium surfaces for enhancing deposition of hydroxyapatite from solution.
Biomolecular Engineering, 19(2-6): 269-272.

Maitz, M. F., Poon, R. W., Liu, X. Y., Pham, M. T., Chu, P. K. (2005)
Bioactivity of titanium following sodium plasma immersion ion implantation and deposition.
Biomaterials 26(27): 5465-5473

Majewski, P. J., Allidi G. (2006)
Synthesis of hydroxyapatite on titanium coated with organic self-assembled monolayers.
Materials Science and Engineering: A 420(1-2): 13-20

Marinucci, L., Balloni, S., Becchetti, E., Belcastro, S., Guerra, M., Calvitti, M., Lilli, C., Calvi, E. M., Locci, P. (2006)
Effect of titanium surface roughness on human osteoblast proliferation and gene expression *in vitro*.
International Journal of Oral and maxillofacial Implants 21(5): 719-725

Meretoja, V. V., Tirri, T., Aaritalo, V., Jansen, J. A., Narhi, T. O. (2007)
Titania and Titania-Silica Coatings for Titanium: Comparison of Ectopic Bone Formation within Cell-Seeded Scaffolds.
Tissue Engineering 13(4): 855-863

Misch, C.E. (1999)

Contemporary implant dentistry
2nd Ed. Mosby, St. Louis

Mittal, K.L. (1979)
Surface Contamination: Genesis, Detection and Control vol. 1.
In: K.L. Mittal, Editors Plenum Press, New York: 3–46.

Morra , M. (2001)
Water in Biomaterials Surface Science.
Wiley, Chichester, UK

Nayab, S., Shinawi, L., Hobkirk, J., Tate, T. J., Olsen, I., Jones, F. H. (2003)
Adhesion of bone cells to ion-implanted titanium.
Journal of Materials Science: Materials in Medicine 14(11): 991-997

Nayab, S., Jones, F. H., Olsen, I. (2004)
Human alveolar bone cell adhesion and growth on ion-implanted titanium.
Journal of Biomedical Materials Research A 69(4): 651-656

Nayab, S., Jones, F. H., Olsen, I. (2005)
Effects of calcium ion implantation on human bone cell interaction with titanium.
Biomaterials 26: 4717.

Nayab, S., Jones, F. H., Olsen, I. (2007)
The human bone cell cycle is modulated by calcium ion-implantation of titanium.
Biomaterials 28(1): 38-44

Nayab, S., Jones, F. H., Olsen, I. (in press)
Effects of calcium ion-implantation of titanium on bone cell function *in vitro*.
Journal of Biomedical Materials Research A

Nishiguchi, S. Nakamura, T. Kobayashi M., Kim, H.M. Miyaji F.. Kokubo, T (1999)
The effect of heat treatment on bone-bonding ability of alkali-treated titanium.
Biomaterials 20: 491-497

Nishiguchi, S., Kato, H., Neo, M., Oka, M., Kim, H.M., Kokubo, T.,Nakamura, T. (2001)
Alkali- and heat-treated porous titanium for orthopaedic implants.
Journal of Biomedical Materials Research 54: 198-203

Nishio, K., Neo, M., Akiyama, H., Nisguchi, S., Kim, H.M, Kokubo, T., Nakamura, T. (2002)
Journal of Biomedical Materials Research 52: 652-657
Nurhaerani, V., Arita, K., Shinonaga, Y., Nishino, M. (2006)
Plasma-based fluorine ion implantation into dental materials for inhibition of bacterial adhesion.
Dental Materials Journal 25(4): 684-692

Ohtsuki, C., Iida, H., Hayakawa, S., Osaka, A. (1997)

Bioactivity of titanium treated with hydrogen peroxide solutions containing metal chlorides.
Journal of Biomedical Materials Research 35: 39-47

Pan, J., Thierry, D., Leygraf, C. (1996)
Hydrogen peroxide toward enhanced oxide growth on titanium in PBS solution: blue coloration and clinical reference.
Journal of Biomedical Materials Research 30(3): 393-402

Pan, J., Liao, H., Leygraf, C., Thierry, D., Li, J (1998)
Variation of oxide films on titanium induced by osteoblast-like cell culture and the influence of an H_2O_2 pretreatment.
Journal of Biomedical Materials Research 40 (2): 244-256

Park, J. W., Park, K. B., Suh, J. Y. (in press)
Effects of calcium ion incorporation on bone healing of Ti6Al4V alloy implants in rabbit tibiae.
Biomaterials

Patsi, M., Hautaniemi, J. A., Rahiala, H., Peltola, T., Kangasiemi, I. (1998)
Influence of sol and surface properties on in vitro bioactivity of sol-gel-derived TiO2 and TiO2-SiO2 films deposited by dip-coating method.
Journal Sol–Gel Science and Technology 11: 55-61

Peltola, T., Patsi, M., Rahiala, H., Kangasiemi, I., Yli-Urpo, A. (1998)
Calcium phosphate induction by sol-gel-derived titania coatings on titanium substrates *in vitro*.
Journal of Biomedical Materials Research 41(3): 504-510

Peltola, T., Jokinen, M. Rahiala, H. Levanen, E., Rosenholm, B. Kangasiemi, I., Yli-Urpo, A. (1999)
Calcium phosphate formation on porous sol-gel-derived SiO_2 and $CaO-P_2O_5-SiO_2$ substrates *in vitro*.
Journal of Biomedical Materials Research 44: 12-19

Pham, M.T., Matz, W., Reuther, H., Richter, E., Steiner, G., Oswald, S. (2000)
Surface sensitivity of ion implanted titanium to hydroxyapatite formation.
Journal of Materials Science Letters 19(5): 443-445

Pham, M.T. Maitz, M. Matz, F.W. Reuther, H. Richter, E. Steiner, G.(2000)
Promoted hydroxyapatite nucleation on titanium ion-implanted with sodium,
Thin Solid Films 379(1-2): 50-56

Price, B., Borland, J.O., Selbrede, S. (1993)
Properties of chemical-vapour-deposited titanium nitride.
Thin Solid Films 236 (1-2): 311-318

Puleoa, D .A., Kissling, R. A., Sheu, M. S. (2002)
A technique to immobilize bioactive proteins, including bone morphogenetic protein-4 (BMP-4) on titanium alloy.

Biomaterials 23(9): 2079-2087
Rintoul, T.C., Bulter, K.C., Thomas, D.C., Carriker, J. W., Maher, T. R., Kiraly, R. J., Massiello, A., Himely, S. C., Chen, J. F., Fukamachi, K. (1993)
ASAIO J. 39 (3): 168-176

Rupp, F. Scheideler, L. Olshanska, N. de Wild, M. Wieland, M. Geis-Gerstorfer J. (2005)
Enhancing surface free energy and hydrophilicity through chemical modification of microstructured titanium implant surfaces.
Journal of Biomedical Materials Research 76(2): 323-334

Samuneva, B., Kozhukharov, V., Trapalis, C., Kranold, R. (1993)
Sol-gel processing of titanium-containing thin coatings Part I Preparation and Structure.
Journal of Material Science. 28: 2353-2361

Scotchford, C. A., Cooper, E., Legget,t G. J., Downes, S.1998)
Growth of human osteoblast-like cells on alkanethiol on gold self-assembled monolayers: The effect of surface chemistry.
Journal of Biomedical Materials Research 41: 431-439

Schuler, M., Owen, G. R., Hamilton, D. W., de Wild, M., Textor, M., Brunette, D. M., Tosatti, S.G.P. (2006)
Biomimetic modification of titanium dental implant model surfaces using the RGDSP-peptide sequence: A cell morphology study.
Biomaterials 27(21): 4003-4015

Shinawi, L. A. (2003)
Ion implantation as a route to enhancing osseointegration on modified titanium surfaces.
PhD thesis, UCL

Sigal, G. B., Mrksics, M., Whitesides, G.M. (1998)
Effect of surface wettability on the adsorption of proteins and detergents.
Journal of American Chemical Society. 120: 3464-3472

Sittig, C., Textor, M., Spencer, N.D., Wieland M., Vallotton, P.H. (1999)
Surface characterization.
Journal of Material Science: Materials in Medicine 10(1): 35-46

Steinmann S.G (2000)
Titanium-the material of choice?
Periodontology 17: 7-21

Sood, D. K., Drawl, W. R., Messier, R. (1992)
The effect of carbon ion implantation on the nucleation of diamond on Ti-6Al-4V alloy.
Surface and Coatings Technology 51: 307-312

Strnad, Z., Strnad, J., Urban, K. (2000)

Effect of plasma- sprayed hydroxyapatite coating on the osteoconductivity of commercially pure titanium implants.
International Journal of Oral and Maxillofacial Implants 15: 483-490

Sunny, M.C., Sharma, C.P. (1991)
Titanium-protein interaction: changes with oxide layer thickness.
Journal of Biomaterial Application 6: 22-29

Sze, S.M. (1985)
Diffusion and ion implantation.
In: Sze, S.M. Semiconductor devices, Physics and Technology P 381-427
Wiley & Sons, New York

Taborelli, M., Jobin, M.,Francois, P.,Vaudaux, P.,Tonetti, M.,Szmucler-Moncler, S., Simpson, J.P. (1997)
Influence of surface treatments developed for oral implants on the physical and biological properties of titanium.
Clinical Oral Implant Research 8(3): 208-216

Takeuchi, M. Abe, Y. Yoshida, Y. Nakayama, Y. Okazaki, M., Kagawa,Y. (2003)
Acid pre-treatment of titanium implants.
Biomaterials 24: 1821-1827

Tanahashi ,M., Matsuda, T. (1997)
Surface functional group dependence on apatite formation on self-assembled monolayers in a simulated body fluid.
Journal of Biomedical Materials Research 34 (3): 305-312

Tavares, M.G., Tambasco, O. P., Nanci, A., Hwthorne, A. C., Rosa, A. L., Xavier, S. P. (2007)
Treatment of a commercial, machined surface titanium implant with H_2SO_4/H_2O_2 enhances contact osteogenesis.
Clinical Oral Implants Research (in press)

Tegoulia, V. A., Rao, W., Kalambur, A. T., Rabolt, F., Cooper, S.L. (2001)
Surface properties, fibrinogen adsorption, and cellular interactions of a novel phosphorylcholine-containing self-assembled monolayer on gold.
Langmuir 17: 4396-4403

Tengvall, P, Lundström, I. Sjoqvist, L., Elwing, H.,. Bjursten, L.M. (1989)
Titanium-hydrogen peroxide interaction: model studies of the influence of the inflammatory response on titanium implants.
Biomaterials 10 (3): 166-173

Tengvall, P. Elwing, H. Sjoqvist, L. Lundström, I Bjursten, L.M. (1989)
Interactions between hydrogen peroxide and titanium.
Biomaterials 10 (2): 118-125

Tosatti, S., De Paul, S. M., Askendal, A., Van de Vondele, S., Hubbell, J. A., Tengvall, P., Textor, M. (2003)

Peptide functionalized poly(lysine)-*g*-poly(ethylene glycol) on titanium: resistance to protein adsorption in full heparinized human blood plasma.
Biomaterials 24 (27): 4949-4958

Townsend, P. D., Chandler, P. J.,Zhang, L. P. (1994)
Optical effects of ion implantation.
Cambridge University Press

Trapalis, C. Kozhukharov, V. Samuneva B. Stefanov, and P. (1993)
Sol-gel processing of titanium-containing thin coatings Part II : XPS Studies.
Journal of Material Sciences 28: 1276-1281

Vanzilotta, P. S., Sader, M. S., Bastos, I. N., Soares, G. A. (2006)
Improvement of *in vitro* titanium bioactivity by three different surface treatments.
Dental Materials 22(3): 275-282

Vanzilotta, P. S., Sader, M. S., Bastos, I. N., Soares, G. A. (2006)
Improvement of in vitro titanium bioactivity by three different surface treatments.
Dental Materials 22(3): 275-282

Walivaara, B Lundström I., Tengvall, P (1993)
Clinical Materials 12 (3): 141-148

Wang, B. C., Lee, T. M., Chang, E., Yang, C. Y. (1993)
The shear strength and the failure mode of plasma-sprayed hydroxyapatite coating to bone: the effect of coating thickness.
Journal of Biomedical Materials Research 27(10): 1315-1327

Wang, X. X., Hayakawa, S., Tsuru, K., Osaka, A. (2002)
Bioactive titania-gel layers formed by chemical treatment of Ti substrate with a H_2O_2/HClsolution.
Biomaterials. 23(5): 1353-1357

Wei, D., Zhou, Y., Jia, D., Wang, Y. (in press)
Characteristic and *in vitro* bioactivity of a microarc-oxidized TiO(2)-based coating after chemical treatment.
Acta Biomaterials

Wen, F., Dai, H. N., Huang, H., Sun, Leng, Y. X., Chu, P. K. (2002)
Controlling synthesis of Ti–O/Ti–N gradient films by PIII
Surface and Coatings Technology 156: 208-213

Wen, H.B,. Wolke, J.G., Wijn, J.R., Liu, Q., Cui, F.Z., de Groot, K. (1997),
Fast precipitation of calcium phosphate layers on titanium induced by simple chemical treatments.
Biomaterials 18: 1471-1478

Wen, H.B., Liu, Q., Wijn, J.R., de Groot, K. (1998)
Preparation of bioactive microporus titanium surface by a new two-step chemical treatment.

Journal of Material Science: Materials in Medicine 9(3): 121-128

Wennerberg, A., Albrektsson, T., Lausmaa, J. (1996)
Torque and histomorphometric evaluation of cp titanium screws blasted with 25 and 75 μm sized particles of Al_2O_3.
Journal of Biomedical Materials Research 30(2): 251-260

Wennerberg, A., Albrektsson, T., Johansson, C., Andersson, B. (1996)
Experimental study of turned and grit-blasted screw-shaped implants with special emphasis on effects of blasting material and surface topography.
Biomaterials 17(1): 15-22.

Wieser, E., Tsyganov, I., Matz, W., Reuther, H., Oswald, S., Pham, Richter,E. (1999)
Modification of titanium by ion implantation of calcium and/or phosphorus.
Surface & Coatings Technology 111(1): 103-109.

Xiao S.J., G. Kenausis, Textor M. (2001)
Titanium in Medicine.
In: D.M. Brunette, P. Tengvall, M. Textor and P. Thomsen, Editors, Springer, Berlin: 417–455.

Xiao, S.J., Textor, M., Spencer, N.D., Sigrist, H. (1998)
Covalent attachment of cell-adhesive, (Arg-Gly-Asp)-containing peptides to titanium surfaces.
Langmuir 14: 5507-5512

Xiao, S.J., Textor, M., Spencer, N.D., Wieland, M., Keller, B., Sigrist, H. (1997)
Immobilization of the cell-adhesive peptide Arg–Gly–Asp–Cys (RGDC) on titanium surfaces by covalent chemical attachment.
Journal of Material Science: Materials in Medicine 8: 867-875

Yang, B., Uchida, M., Kim, H. M., Zhang, X., Kokubo, T. (2004)
Preparation of bioactive titanium metal via anodic oxidation treatment.
Biomaterials 25: 1003-1012

Yang, C. Y., Wang, B. C., Lee, T. M. (1997)
Intramedullary implant of plasma-sprayed hydroxyapatite coating: An interface study.
Journal of Biomedical Materials Research 36 (1): 39-48

Yang, B.C,. Weng, J., Li, X.D., Zhang, X.D. (1999)
The order of calcium and phosphate ion deposition on chemically treated titanium surfaces soaked in aqueous solution.
Journal of Biomedical Materials Research 47: 213-221

Yeung, K. W., Poon, R. W., Chu, P. K., Chung, C. Y., Liu, X. Y., Lu, W. W., Chan, D., Chan, S. C., Cheun, K. M. (in press)

Surface mechanical properties, corrosion resistance, and cytocompatibility of nitrogen plasma-implanted nickel-titanium alloys: A comparative study with commonly used medical grade materials.
Journal of Biomedical Materials Research A

Yoshida, K., Kamada, K., Sato, K., Hatada, R., Baba, K., Atsuta, M. (1999)
Thin sol-gel-derived silica coatings on dental pure titanium casting.
Journal of Biomedical Materials Research B Applied Biomaterials 48: 778-785

Yoshinari, M., Oda, Y., Kato, T., Okuda, K., Hirayama, A. (2000)
Influence of surface modifications to titanium on oral bacterial adhesion *in vitro.*
Journal of Biomedical Materials Research 52(2): 388-394

Yoshinari, M., Oda, Y., Kato, T., Okuda, K., Hirayama, A. (2001)
Influence of surface modifications to titanium on antibacterial activity in vitro,
Biomaterials, 22(14): 2043-2048.

2. EXPERIMENTAL

2.1 INTRODUCTION

This chapter details the materials and methods common for all the experiments and the techniques used throughout the experiments to characterise Ti and modified Ti surfaces, and also used to analyse solutions in which samples were immersed.

The surface analytical techniques used were chosen to provide information about both surface topography and surface chemistry, and also to gain additional insight into sub-surface chemistry.

The physical properties of interest in the current research were the surface topography and roughness in order to follow alterations that may appear on the surface following various surface modifications. The techniques used for the measurement of these were scanning electron microscopy (SEM), laser profilometry (LP), and white light interferometry (WLI).

Chemical surface modifications to commercially pure titanium employed in this work included ion implantation, nitric acid treatment, alkali treatments, and modifications caused by immersion of Ti in solution or adsorption of amino acids onto Ti and modified Ti surfaces. Techniques used include X-ray photoelectron spectroscopy (XPS), which provided detailed analysis of the immediate surface region in terms of composition and chemical states. The second technique was depth-profiling XPS, which was used to examine the deeper layers of titanium samples.

Another technique used which provided information indirectly about the stability of Ti surfaces was ion chromatography (IC). This technique provided information through analysis of the solutions in which the Ti samples were immersed.

This chapter will give detailed explanations of the basic theories of these techniques. For a more complete description, please refer to appropriate reference textbooks. Also specific details of each analytical technique applied

will be presented. These include experimental parameters and settings of various instruments and details of sample cleaning and preparation.

Throughout the study, the substrate for the experiments was commercially pure titanium (cp Ti) discs polished in house. A mirror finish was essential to obtain on the Ti samples, as smooth surfaces are prerequisite for the surface analysis techniques applied in the current work. The presence of prominent surface features such as peaks will create shadows thus hindering the detection from other surface areas (valleys). In addition to surface characterisation problems, a rough surface will also interfere with the ion implantation process itself resulting in preferential ion implantation and inhomogeneous doping of the Ti substrate.

A detailed description of the polishing methods employed is presented below.

2.2 POLISHING OF TITANIUM DISCS IN-HOUSE

Titanium discs (8 mm diameter and 1 mm thick) made of grade 1 commercially pure titanium (cp Ti), (99.6 %, Goodfellow Cambridge Limited, Cambridge, U.K.) were used for all experiments. The exception was when the cp Ti samples were provided polished by the Straumann Institute (Switzerland) and were grade 4. However, there are only minute differences between the two grades with regards to composition, and they have similar mechanical properties (Boyer et al., 1994).

The in-house samples were polished using two polishing methods throughout this research. The first technique used was a well-established technique previously developed in the Unit, and the second was a newer one, developed in the Unit as well because a continuing improvement of the quality of the polishing has been attempted.

Table 2.1 presents a list with the materials and instruments used in the polishing process.

Material	Remarks	Manufacturer
Ti disc	CP Ti 99.6% Grade 1	Goodfellow Cambridge Ltd England
SiC paper	1200	Struers A/S Denmark
SiC paper	2400	Struers A/S Denmark
OP Chem cloth		Struers A/S Denmark
OPS	Colloidal silica suspension	Struers A/S Denmark
Polishing machine	Struers Rotopol II	Struers A/S Denmark
Hydrogen Peroxide	5%	BDH laboratory supplies Poole England
Wax	Modelling wax	Associated Dental Products Ltd England
Toluene	99.8% HPLC grade	BDH laboratory supplies Poole England
Acetone	HPLC grade	BDH laboratory supplies Poole England
Mounting jig	Made for fixing Ti discs during polishing	Biomaterials EDI 256 Gray's Inn Road London WC 1X0L8
Ultrasonic bath	Sonorex Transistor	Bandelin Electronics, Berlin, Germany
Tissue culture wells	24 well plates	Beckton Dickinson Labware, France

Table 2. 1 Table of materials and instruments used for the polishing of the cp Ti samples.

2.2.1 Polishing method 1

Before polishing, the Ti discs were mounted on a custom built jig (30 mm diameter) for fixing Ti discs during polishing (Biomaterials, EDI) made of poly (methylmethacrylate) resin (PMMA). The samples were fixed onto the resin jigs using molten wax (Associated Dental Prod. Ltd. England) that was left to set for a minimum of 2 h prior to polishing.

The mounted jigs were placed on a rotating Struers Rotopol-II machine (Struers Ltd., Glasgow), to allow for their positioning on the polishing stage. The polishing protocol is detailed in table 2.2.

The discs were mechanically ground in two stages using silicon carbide grit-polishing discs (SiC)(grades 2400 and 1200)(Struers, A/S Denmark), at 300 rpm, while applying a constant downward force of 25 N for 45 seconds, and a constant supply of water to keep the discs wet, using a Struers Rotoforce-I (Struers Ltd., Glasgow). Following the grinding, the discs were then polished to a mirror finish using a chemical cloth (Struers, A/S Denmark) at 150 rpm, with a downward force of 20 N, for 4 minutes, with no additional water, but under a

mixture of 0.1 μm colloidal silica suspension (OPS) and 5% H_2O_2 (BDH laboratory supplies, Poole, England), (4 : 1 silica : H_2O_2). After the polishing was finished, the samples were manually removed from the jigs and placed in a glass beaker for cleaning. The remaining traces of wax were dissolved ultrasonically in an ultrasonic bath (Sonorex Transistors, Bandelin Electronics, Berlin, Germany) in toluene (99.8% HPLC grade, Sigma-Aldrich, Germany) for 5 minutes, using successive baths of solvent until no traces of wax were detected. The process of ultrasonic cleaning was then repeated using acetone (HPLC grade, BDH laboratory supplies, Poole, England), and finally distilled water. Each cleaning period was for 5 minutes, and was performed three times in both the acetone and the distilled water, a fresh solution being used for each stage. Finally, the discs were placed with the polished side facing up on paper towels to draw the liquid off the surface. The discs were then dried using compressed air and stored in 24 well plates (Beckton Dickinson Labware, France). Gloves were worn during sample preparation to avoid contamination of the discs, which were handled using plastic tweezers on the edges only.

Stage	Force (N)	Time	Speed (RPM)	Polishing disc	Lubricant
1	25	45 s	300	1200 grit SiC	water
2	25	45 s	300	2400 grit SiC	water
3	20	4 min	150	OP chem cloth	OPS + 5 % H_2O_2 ratio 4:1

Table 2. 2 Protocol 1 for polishing titanium discs.

2.2.2 Polishing method 2

The differences from the previous method were in the mounting procedure for the samples, in the polishing and cleaning methods, and also in the storage of the samples following polishing.

Mounting of the Ti discs was performed on a mounting jig (block) used in protocol 1 using double sided adhesive tape (Struers A/S Denmark). The adhesive tape was placed with one side on the mounting jig. On the other (adhesive) side, the Ti discs were fixed for polishing. Seven cp Ti discs were fitted on to a mounting block. The advantage using this mounting procedure is

that it was much quicker than in the previous protocol, which was quite time consuming when using wax. Another advantage with regards to the mounting is that the samples could be polished immediately after mounting, which was not the case in the previous protocol.

The cp Ti discs were polished to a mirror finish using 1200 and 2400 grade silicon carbide-grit (SiC) paper for 5 minutes at 5 N force and 300 rpm. In between the stages the samples were placed upside down in a beaker of distilled water in an ultrasonic bath for 30 seconds. After the grinding, the process was followed by 0.1 μm colloidal silica suspension (OPS) plus 30% H_2O_2 (10% v/v) with the polisher set at 10 minutes, 5 N and 150 rpm. Cleaning was then performed by ultra-sonication in acetone, propan-2-ol (IPA) and ultra-pure water (UPW) for 5 minutes respectively. Less cleaning was required as a result of the elimination of contamination from the mounting wax.

Following cleaning, the samples were dried with compressed air and stored in Al foil in a desiccator until use. This was used instead of tissue culture well plates to minimise possible damage which may occur to the surface during sample transportation for experiments. Potential contamination of the samples was again minimised by using plastic tweezers, and handling the discs on their edges only.

Stage	Force (N)	Time	Speed (RPM)	Polishing disc	Lubricant
1	5	5 min	300	1200 grit SiC	water
2	5	5 min	300	2400 grit SiC	water
3	20	10 min	150	OP hem. cloth	OPS + 5 % H_2O_2 ratio 4:1

Table 2.3 Protocol 2 for polishing titanium discs.

2.3 ION IMPLANTATION

2.3.1 Introduction

Ion implantation allows the alteration of the chemical, physical and optical properties of a solid and is commonly used to alter the composition, structure

and morphology of the near-surface layers. Various surface properties may be modified, such as mechanical, chemical, electrical and optical (Townsend et al., 1994). Mechanical properties include microhardness, friction, adhesion, and wear. Chemical properties altered by ion implantation include corrosion resistance, passivation, diffusion, and reactivity. Electrical properties include resistivity, photoconductivity, electron mobility, and semiconductivity, while optical properties include colour, reflectivity, transmission and opteoelectronic behaviour.

Ion implantation is a process in which ionised atoms or molecules are accelerated through an electrostatic field into the substrate to be implanted. Neil Bohr proposed the theory of ion implantation in 1913. The technique, however, was developed much later and Shockley obtained the first patent for ion implantation in 1957, describing the lattice damage brought about by the implantation process (Ziegler et al., 1988).

Ion implantation offers a number of advantages over other surface modification techniques including the ability to control implantation energy, species, and species purity, while allowing accurate dose and depth control, which is applicable to most ions and achievable at low or even ambient temperature (Townsend et al., 1994). In addition to speed, it is possible to control dopant mass as well as homogeneity and reproducibility of the surface modified layer, which is not prone to the fracture or delamination that is often associated with surface coatings. Ion implantation does not impair the mechanical bulk properties of the substrate, and also allows for multiple implantations of variant species into the substrate. On the other hand, disadvantages of the technique include possible damage to the substrate crystal lattice caused by the collision of the dopant ions with the substrate as a result of the implantation process. In addition the technique is limited to the surface region and is unsuitable for bulk doping.

Bombardment of the surface by the primary ion beam results in a cascade of collisions within the surface atoms causing some particles to be dislodged from their molecular sites. These are known as sputtered particles (Brown 1989). Surface sputtering limits the achievable dose of implantation in what is referred as to as sputter limited implantation (Townsend et al., 1994). The depth of the implantation varies from a few nanometers to several micrometers depending

on the energy of implantation and the mass of the incident ion as well that of the substrate atoms (Ziegler 1988).

The implanter employs an ion source; the most commonly used being the Freeman ion source. The entire ion source is enclosed within a shielded high voltage enclosure and is floated at up to 50 keV with respect to local ground. The generated ions in the primary ion beam are extracted at the preset energy and accelerated towards a mass analyser magnet which deflects the primary beam allowing only the passage of ions with the chosen mass / charge ratio (a.m.u. / z). Acceleration / deceleration lenses may be then used to select the required implantation beam energy before the beam is directed into the main chamber in the earthed end-station. The substrate to be implanted is mounted onto a movable stage vertically positioned in the chamber and is scanned through the stationary ion beam. The stage can be moved out of the beam to allow for beam current measurement. The main chamber and the controls are all enclosed in a class 100 clean room.

2.3.2 Ion implantation in the current study

The implantation of the cp Ti discs used in this study was carried out by Dr. T. Tate at Imperial College, London, using a Wickham 200 ion implanter. This implanter is equipped with a Freeman ion source, a graphite arch chamber and a tungsten filament, and is maintained at a background pressure of 2×10^{-7} mbar. The beam was set at energy of 40 keV and the ion beam passes through a mass analysing magnet to achieve 1 a.m.u. resolution.

In this study calcium (Ca) and argon (Ar) ions were implanted into cp Ti discs. The ion doses used for implantation were for Ca-Ti samples, $^{40}Ca^{+}$ at a dose of 1×10^{17} ions cm^{-2} using an implantation energy of 40 keV. For Ar-Ti discs the same dose and implantation parameters ($^{40}Ar^{+}$, 1×10^{17} ions cm^{-2}, 40 keV) were used. Argon, being chemically inert, was selected as a control to assess the effects of the implantation process itself, if any. It has the same atomic mass with Ca (40), so it should implant in a similar manner, resulting in comparable if not identical lattice deformation, yet producing a diverse surface chemistry.

This ion dose was chosen because higher ion doses of 1.4×10^{17} were found to produce experimental difficulties, with the Ca ions reacting with the oxygen and potentially other species residually present in the implanter instead of the target Ti (Shinawi 2003). In her work, simulations which utilised a low implantation energy similar to that quoted in the literature were found to result in implanted ions at a near surface depth resulting in the sputtering of this modified layer which reduced the possibility of acquiring a high dose implantation. Thus an energy of 40 keV was chosen, based on the simulations which proposed a deeper ion distribution into the Ti substrate, making the implantation more efficient and the designated dose achievable. An implantation dose of 1×10^{17} ions cm^{-2} was seen to give a maximum concentration at the immediate surface for Ca-Ti. This dose was shown to extend to a maximum depth of ~ 600 Å (0.06 μm). For the Ca ion the depth sputtered was 598.6 Å, slightly more than for the Ar ion (542.9 Å) (Shinawi 2003).

For implantation, the cp Ti samples were mounted onto stainless steel plates. The amount of sputtering of stainless steel during implantation was negligible. The plates were cleaned in acetone and water in the same procedure used for sample cleaning. Two mounting methods were used. In the first method, nail varnish was used as an adhesive to attach the samples to the plate and allowed to dry overnight. Care was taken to avoid nail varnish pooling around the samples. The plates were then placed vertically on the implanter. Following implantation, the samples were removed from the implantation plates using acetone and cleaned by ultrasonication in HPLC grade acetone for 15 minutes and then deionised water for 5 minutes.

The second mounting method was developed to avoid cleaning in acetone and water the ion implanted samples, because immersion will result in surface modification of the ion implanted samples. In the second method, specially made stainless steel plates were used. There were two plates made, one plate had small depressions to accommodate each a Ti disc. The second plate had holes in it at the size of a Ti disc and was used to cover the first plate were the cp Ti discs were mounted, leaving free for implantation the whole surface of a Ti disc. The plates were fixed one to the other using small screws.

After implantation, the samples were removed from the plates using plastic tweezers, wrapped in Al foil and placed in the dessicator until used.

2.4. SCANNING ELECTRON MICROSCOPE (SEM)

2.4.1 Introduction

A scanning electron microscope (SEM) is a microscope which uses electrons rather than light to obtain images. It enables imaging to a resolution in the micrometer and sub-micrometer range. The information is obtained instantaneously, which makes it a very widely used analysis method for examining the microstructure of materials. Advantages of the technique include a large depth of field allowing large areas of the surface to be focused on simultaneously while maintaining high resolution.

A voltage is applied across the tungsten filament in the electron gun to generate an electron beam at energies between 2 keV and 40 keV. The beam is accelerated down the beam column to the surface. As the beam passes through the beam column, it is condensed by a condenser lens to `de-magnify' the electron beam and limit the current in the beam, which is then passed though a scan generator causing it to move and scan across the specimen after being focused by the objective lens. As the electron beam hits the sample surface it results in various interactions with the material in what is known as the interaction volume. Although radiation is generated in this volume, it is not easily absorbed as it escapes undetected from the sample. Meanwhile the ejected secondary electrons from the near surface region can either be back-scattered electrons with a broad energy span or outer shell atomic electrons of low energy. These are collected by a backscatter detector or a secondary electron detector respectively and are then converted to voltage and amplified. The backscatter mode is used to investigate compositional variation in the sample as it depends on the atomic number, while the unscattered electrons are used to provide high-resolution imaging. The amplified voltage of unscattered electrons alters the intensity of the spot of light on the cathode-ray tube (CRT) producing an image that consists of thousand of spots of varying intensity on the face of the CRT which correspond to the sample surface (Goodhew et al., 2000). The electron column in the SEM must be at a vacuum in order to generate and maintain a stable beam. Gas present in the column can

react with the electron source causing it to burn out, as well as hindering the transmission of the beam through the column.

2.4.2 SEM used in the current study

The SEM used in current work was a Stereoscan 90B which contains two pumps, a rotary and a turbo, which keep the system pressure of 10^{-4} mmHg. The secondary electron detector was set at a voltage of 15 kV.
For the analysis with SEM, the samples must be able to withstand the vacuum environment and to be electrically conductive, conditions which are met by the samples used in current work. If the samples are not conductive, they need to be plated with a suitable medium such as gold or carbon.
The samples were fixed on the SEM screw using conductive carbon tags. The images obtained were digitally scanned in TIFF format and imported into the Paint programme in Microsoft Office for presentation.

2.5 LASER PROFILOMETRY

2.5.1 Introduction

Topography refers to the external characteristics of a surface. It is made up of features defined as roughness, waviness and form. Nevertheless, only the roughness component is analysed, as the last two parameters are usually filtered, or separated out from the recorded measurement data. This is done using different filter types. A filter is an electronic, mechanical, optical, or mathematical transformation of a profile to attenuate (remove) wavelength components of the surface outside the range of interest for a measurement. Roughness is what is left when errors of form and waviness are removed. Different parameters are used to quantify surface roughness. They characterize three basic aspects of the surface topography: height, spacing and spatial or textural characteristics. Height parameters measure the vertical variations (depths of grooves and pits), and they can be divided into two categories:

a. Height description of a statistical nature which gives average values (R_a, R_q, R_z) b. Extreme value height description, like R_{max}, which depend on isolated occurrences.

Roughness average (R_a) represents the average deviation of a surface profile from the mean reference line within the sampling length. The mean line is defined so that equal areas of the profile lie above and below it and is the most commonly used parameter. It is known to be quite stable and insensitive to occasional high peaks or deep valleys (Wennerberg, et al., 2000). R_q represents the root mean square parameter corresponding to R_a. It is often used as an alternative to R_a. It gives larger numerical values than the equivalent R_a values. R_q it is more sensitive to extreme numerical values than R_a. R_{max} is the maximum peak-to-valley height within the sampling length. Total surface area represents the actual or projected total area measured.

In the literature, very different R_a and R_q values are reported for similar surfaces. They depend on the different instruments used for analysis (Wennerberg, et al., 2000). The different values are a result of using different measuring equipment, different lengths of measurement (for example R_q will increase with the root of the measuring length), and the use of either 2-D or 3-D evaluations. In addition, different filter sizes may have been used to separate roughness, waviness, and form. All of the above factors clearly reflect the difficulties in interpreting data from different studies without suitable standards for oral implants.

The parameters measured in these experiments were R_a, and total surface area. R_q, was analysed but found to vary in a very similar manner to R_a, and hence was not reported extensively in this work.

Objects are scanned as they are moved in the x and y directions of the fixed laser beam. The system uses the laser triangulation principle to measure extremely fine vertical displacements on the contour of surfaces. The laser spot is focused on the object to be measured, and the light from the laser is then reflected or scattered back into a fixed photo-detector, which receives a maximum signal when the surface is at its focal point. When the object is moved, the height variations encountered along the surface are expressed as

displacement of the spot on the photo-detector since the start of the scan. The position of the spot on the detector is converted into an electric signal that is proportional to the height of each point on the scanned profile. By combining the three co-ordinates obtained from the height measured by the laser with the position of the sample in the x and y axes, a digitised colour coded 3-D image of the surface profile is produced. Dimensional measurements can then be easily made from these images using the software provided with the system.

2.5.2 LP used in the current study

The surface roughness of the samples was measured with a Proscan 1000 scanning laser profilometer (Scantron Industrial Products Ltd., Taunton, England, UK). This is a PC controlled non-contact 3-D surface profiling and measuring system which employs a highly accurate laser displacement sensor to scan the surfaces on a motorised x / y table.

The sensor used (KL131A) has a working distance of 10 mm and a measuring range of 400 ± 200 μm. The laser beam used is a semiconductor laser with a wavelength of 780 nm, a beam diameter of 12-35 μm and a lateral resolution of 0.02 μm.

The parameters analysed with laser profilometry in this work were: the roughness average (R_a), the root-mean-square roughness (RMS or R_q) and the total surface area. The step size was 5 μm in both the x- and y-directions. Each point recorded was averaged from eight readings at that point.

To estimate roughness averages R_a and root mean squared roughness R_q, 5 points were selected on each sample and the R_a and R_q values measured across 5 mm in both the x- and the y-directions. The averages of the 10 recorded values and their standard deviations were calculated.

A surface filter was used to calculate the surface roughness. It removes the general shape of the object but leaves the roughness. The filter can be set at values between 01 - 99, where 01 is the smallest and 99 the largest filter. It operates by performing a warpage filter and subtracting this from the original scan. The result is that the roughness is left. A warpage filter removes the surface texture or roughness of an object to leave the general shape of the

object. It takes a point in the scan and assigns that point as the 'centre scan point' of the rectangular filter. The filter size selected represents how many points are taken either side of this 'centre scan point'.
For scans which were not horizontal 'Auto levelling' was used. The scan finds the best-fit arithmetic plane for the scan by taking a minimum of 3 points from the surface of the object. When this is done, the Proscan 1000 is adjusted to make the scan effectively horizontal.

2. 6 WHITE LIGHT INTERFEROMETRY (WLI)

2.6.1 Introduction

This is a three-dimensional, imaging surface structure analyser. It is a non-contact technique that provides both imaged surface details of test parts and accurate measurements to characterize these details. The system uses scanning white light interferometry to image and measure the microstructure and topography of surfaces in three dimensions.
The system consists of an interferometric microscope linked with a computer. Light from a white light source in the microscope passes through a narrow band filter and the objective. It is split inside the interferometer into two light waves: one goes to the surface intended for analysis and the other to an internal, high quality reference surface. Both light waves are then recombined inside the interferometer undergoing constructive and destructive interferences. Their interaction results in a fringe pattern consisting of light and dark bands, which are one and a half wavelengths apart. This phase difference is automatically quantified by the precision movement of the reference surface via piezoelectric transducers. The resulting image is analysed by the solid–state video camera and the accompanying `Metro-Pro' control software. Vertical measurements, normal to the surface, are performed interferometrically. Lateral measurements in the plane of the surface are calculated using the pixel size from the field of view of the used objective.
The technique offers a high resolution with depths up to 100 μm with 0.1 nm resolution and 0.4 nm RMS repeatability, independent of objective lens

magnification. Results are displayed as colour images as well as plot and numeric representation (Rochow et. al., 1994). In this research the R_a was measured, which is a value of the arithmetic mean of the roughness height, (Ungerbook et al 1994).

2.6.2 WLI used in the current study

In the current analysis, a Zygo 3D optical interferometric microscope (Zygo – New View 200) was utilised to measure the R_a and R_q values of Ti samples with various surface topographies. The system was also used to investigate the surface topography of cp Ti samples prior to and following ion implantation and nitric acid treatment. A 10x Mirau objective, which offers a magnification of 200x was used resulting in a field of view area of 0.23 x 0.37 mm and lateral resolution of 1.12 microns.

2.7 X-RAY PHOTOELECTRON SPECTROSCOPY (XPS)

2.7.1 Theoretical background to XPS.

Figure 2.1 presents a photo of the XPS instrument used in the current work.

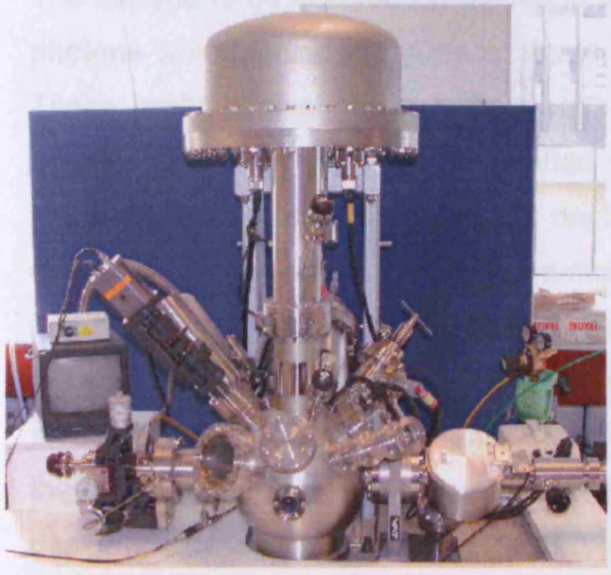

Figure 2. 1 Photo of the XPS used in the current study.

XPS, also known as electron spectroscopy for chemical analysis (ESCA), was developed by Kai Siegbahn in the 1960s. The technique is based on the photoelectric effect, which was explained by Einstein in the early 1900s.

The photoelectric effect occurs when a photon of light, of sufficient energy, directly transfers its energy to electrons within an atom, resulting in the emission of the electrons (photoelectrons), without energy loss.

When a photon impinges upon an atom, one of three events may occur (Ratner et al., 1997):

1. The photon can pass through with no interaction.
2. The photon can be scattered by an atomic orbital electron leading to partial energy loss.
3. The photon may interact with an atomic orbital electron with total transfer of the photon energy to the electron, leading to electron emission from the atom.

In the first case, no interaction occurs. The second option is referred to as 'Compton scattering' and can be important in high-energy processes. The third process accurately describes the photoemission that is the basis of XPS.

XPS utilizes photons with energy in the X-ray region of the electromagnetic spectrum to excite core electrons from the surface analysed through ionization of the atoms. The ejected electron is called a photoelectron (Ratner et al., 1997).

The surface to be analysed is placed in ultrahigh vacuum and is irradiated with photons which ionise the surface atoms, resulting in photoemission electrons. These emitted electrons are then separated according to their energy and counted. As the energy of the emitted electrons is unique to the atomic or molecular environment from which it originates, XPS offers fingerprinting of the chemical composition as well the chemical status of the analysed surface. The number of emitting electrons relates to the concentration of the emitting atom in the sample (Vickerman 1997). The system requires a photon source to produce X-ray photons. The most suitable materials for the production of photons are thermally conductive metals such as these most commonly used in the anode design, Al Kα and Mg Kα ($h\nu$ = 1486.6 eV, and $h\nu$ = 1253.6 eV). Twin anode sources are available where one can switch between Al and Mg, which coat either side of the X-ray anode. This however produces X-rays with different

transitions giving rise to Al and Mg $K_{\alpha 1,2}$ as well as the weaker $K_{\alpha 3,4}$ and $K_{\alpha 5,6}$ radiations which in turn result in the satellite features seen to lower binding energy of the main photoelectron peaks. Alternatively, in monochromatic X-ray source the X-ray beam is diffracted allowing a single energy of light to be obtained. This minimises satellite features in the collected spectra. It is also thought that monochromated sources result in less sample heating than the twin anode, since they are not as close to the sample surface as the twin anodes are.

In addition to the photon source, XPS requires an electron detection system to record a spectrum and establish the distribution of the electrons' binding energies. A concentric hemisphere analyser (CHA) is commonly used. As a voltage is applied between the two hemisphere, the electron passing through the gap are deflected by the electrostatic field with only electrons of an energy equal to the preset pass energy being allowed to pass through the analyser. To measure the spectrum of photoelectron kinetic energies, the photoelectrons approaching the analyser are slowed down to the pass energy using a retarding potential prior to entering the gap between the two hemispheres. As these exit the analyser they pass into an electron multiplier system, known as channeltron. The XPS chamber must be maintained under ultra high vacuum (UHV) of 10^{-9} – 10^{-10} mbar in order for the emerging electrons to travel to the analyser without suffering inelastic collisions and consequent energy loss and to retain a contaminant free surface through the analysis period; otherwise molecules in the air will land on a surface and change its properties. Even at a pressure of 10^{-6} mbar a layer of gas atoms will form on the surface in about 3 seconds (assuming every atom to strike the surface sticks to the surface). To maintain such pressure the main metal chamber is evacuated using a combination of pumps including turbo pumps, ion pumps, and titanium sublimation pumps. Once UHV is achieved, it is best maintained by inserting samples into a 'fast entry lock' and then transferring them into the main chamber without breaking vacuum. The fast entry lock is usually maintained at a pressure of 10^{-6} mbar or less (Vickerman 1997).

The obtained XPS spectrum shows the intensity of the photoelectron signal as a function of binding energy (E_B). XPS is best described as a semi-quantitative analysis. A widescan (survey) spectrum gives instant analysis of the surface

chemistry, while narrow scans of specific energy regions offer information regarding peak energies, intensities and shapes. The binding energies are affected by both intra and extra atomic relaxations which rearrange electrons in a final state effect. The E_B of core electrons depends on the chemical environment of the atom which can create chemical shifts.

The following information can be gained from XPS (Ratner et al., 1997):

1. Identification of all elements present (except hydrogen and helium) at concentrations > 0.1 atomic %.
2. Information about the molecular environment (oxidation state, bonding atoms, etc).
3. Semi quantitative determination of the approximate elemental surface composition (error < ± 10 %).
4. Non-destructive elemental depth profiles 10 nm into the sample and surface heterogeneity assessment using angular dependent XPS studies and photoelectron with differing escape depths.

Main drawbacks of XPS are its relative lack of sensitivity (~1% detection limit and spatial resolution (Paynter, 1999).

2.7.2 XPS spectra

The understanding and analysis of XPS spectra require an appreciation of the spectral features that are observed. XPS analysis are typically performed by first taking a wide scan or survey scan spectrum, often covering a range of 1000 eV, and then looking in more detail over smaller ranges (20 eV) at specific features found in the survey scan spectrum. The spectra have two axes: x and y. The x- axis is generally labeled 'binding energy'. Since binding energy has meaning for the chemistry and structure of the surface, it is most common to plot XPS spectra in terms of binding energy. The y- axis represents 'intensity' or 'number of counts'. The survey scan provides information on:

1. Instant analysis of surface elemental composition and identity of any impurities present.

2. Background. This appears as a climbing intensity and is due to secondary electrons emitted from the sample with lower kinetic energy and, therefore, apparent higher binding energy than the peaks.
3. Auger electron peaks. Core holes can be created by photoemission. Electrons can drop back from higher levels to fill the core hole. This causes emission of a second electron called Auger electron.

The high-resolution spectra can be used to assess three parameters:

Peak energies

The binding energy of an electron is the difference between the initial state (the atom), and the final state (the ion). The binding energy of an electron is dependent on the atomic number of the element and the atomic orbital that is was emitted from:

1. The lower the atomic number the lower the binding energy, because there is less effective nuclear charge to bind the electrons.
2. Electrons have a negative charge and the nucleus has a positive charge. Therefore the closer the electron is to the nucleus the greater its binding energy. For titanium, the core occupied atomic orbitals are 1s, 2s, 2p, 3s, 3p from nucleus out. Therefore we would expect 1s to have the highest binding energy and 3p the lowest. In fact, the 1s atomic orbital is too strongly bound to be excited by Al Kα photons. The binding energies of electrons in the other core-level atomic orbitals are in order 2s > 2p > 3s > 3p.
3. The greater the positive charge on an atom the greater its binding energy. For example, Ti^0 has a lower binding energy than Ti^{4+}.
4. The electronegativity of the atom to which atoms are bonded will affect the binding energy. For example, binding energy for carbon (C) in hydrocarbons (i.e. bonded to C and H only) appears at 285 eV, whereas C bound to oxygen (O), (C-OH or C-O-C) appears ~ 1.5 eV higher, while C-F appears 2.91 eV higher (Beamson et al., 1992).

Peak shapes

Peak shape can be changed by the initial and final state effects. Some of the most important include:

1. Relaxation. This represents re-arrangement of the remaining electrons after photoemission.
2. Spin-orbital splitting. Some peaks occur as a doublet peak. This is caused by spin-orbit splitting and occurs with p, d, or f orbitals. Electrons closer to the nucleus show greater spin-orbital coupling. For titanium, the Ti2p shows spin-orbit splitting. The two peaks are labeled $Ti2p_{3/2}$ and $Ti2p_{1/2}$.
3. Shake up satellites. These represent photoelectrons that have lost energy through promotion of valence electrons from an occupied energy level to an unoccupied energy level. They appear at higher apparent binding energies.
4. Chemical shifts. If an element in a solid state exists in a number of chemical states with similar binding energies, there will be some overlapping of their peaks. This can give very complex peak shapes. For detailed analysis peak fitting should be performed.

Peak areas

The intensity of a photoelectron peak of a particular element is dependent on the X-ray flux, the photoionisation cross section for the atomic orbital, inelastic free mean path of the photoelectron, the area from which the photoelectron is detected, the angular efficiency, detection efficiency and spectrometer transmission. If the same experimental conditions are used for the peaks for each element, then the experimental parameters (constant) may be taken together as a single factor, T. The parameters that are dependent on atomic core level and photoelectron energy, may be combined as the 'atomic sensitivity factor', σ,

$I=nT\sigma$ where I is the peak intensity, n is the number of atoms of the element per unit volume, T is the experimental constants, σ is the sensitivity factor, which includes the photoionisation cross-section (a measure of the probability of the electronic transition for the particular initial and final states involved), the inelastic mean free path (a measure of how far the photoelectron can travel without losing energy), and the spectrometer transmission function (a measure of the sensitivity of the spectrometer for a photoelectron of a particular kinetic energy).

For a material of two components, the experimental constants cancel each other so the measured ratio of the peak area intensities is given by:

$I_a / I_b = n_a\sigma_a / n_b\sigma_b$

In order to estimate the actual ratio of elements present on the material, the intensity (peak area) ratio is measured and corrected using published atomic sensitivity factors.

2.7.3 XPS used during current study

XPS spectra were recorded using an ESCALAB 220i X-ray photoelectron spectrometer (Vacuum Generator, East Grinsted, UK) with typical base pressure of < 3 x 10^{-9} mbar. The analysis chamber was equipped with both a monochromated and twin anode Al Kα X-ray source ($h\nu$=1486.6 eV) of 1 mm spot size and a 300 mm diameter 180° hemispherical electron energy analyser. A magnetic objective lens was used for enhanced sensitivity. The analysing chamber was maintained under UHV with a baseline pressure of 1 x 10^{-9} torr.
Spectra were recorded at normal emission, in constant analyser energy (CAE) mode using pass energies of 100 eV and a step size of 1 eV for the survey spectra and pass energy of 20 eV and a 0.1 eV step size for the narrow scan spectra. The monochromated Al Kα source was set at a 1 mm spot size and 10 mA, while the twin anode was run at a current of 20 mA at a voltage of 15 kV. Both were run utilising the large area XL lens. All the spectra were recorded at normal emission angle.

Charge compensation

As most of the samples in the current work are metallic and are conductive, charge compensation was not necessary, so there was no need to use an electron gun to flood the samples which is a standard procedure to compensate for charging effects.
For the powder amino acid samples analysed in this study, charge compensation was achieved by placing a tantalum-conducting mask over the sample to ensure good electrical contact and flooding the sample with low energy (4 eV) electrons. This corrects for the fact that the insulating samples would otherwise acquire a positive charge as photoelectrons are emitted from

the surface, which would result in shifts in the binding energy positions of the photoelectron peaks.

Qualitative Assessment

A qualitative analysis of the XPS spectra was made using CasaXPS and Sigmaplot software. The data obtained from the XPS analysis was saved in the CasaXPS software, and then imported in the Sigmaplot software in order to be able to interpret the results. Using Sigmaplot, the background was removed and then the data was normalised to the Ti 2p peak maximum (for Ti samples), or to C 1s peak maximum (for the amino acid powder samples).The regions of interest for the study were Ti 2p, C 1s, N 1s, O 1s, Ca 2p, S 2p, Na 1s, and survey. These regions were displayed as graphs. The spectra for each region were displayed on the same x- and y- scale, although the scales for different regions were not similar. The following assessments of the spectra graphs were made: number of peaks, peak shape and intensity, and binding energies of the peaks.

Quantification

In addition, quantitative analysis was performed using CasaXPS software and quantification tables, which give elemental ratios of the elements present on the surface, are presented. The ratios give an indication of whether the concentration of a particular element has increased or decreased relative to titanium for the discs and relative to carbon, for the powders. However, the sensitivity factor of each element should be taken into account when quantifying XPS data. Sensitivity factors are instrument dependent and related to the photoionisation cross-section and the mean free path. There are several published lists of atomic sensitivity factors, which are derived from measuring a whole series of compounds using a specific spectrometer (Wagner et al. 1981) of atomic ratios is corrected using Wagner's published atomic sensitivity factors. All XPS spectra will contain climbing background intensity due to inelastically scattered electrons. It is essential to isolate the intensity due to the primary peak by defining a baseline or subtracting a background prior to the peak area

measurement. The simplest background is a linear line drawn between two points on either side of the primary peak. Other models are available to subtract the backgrounds which include the Shirley background, which was used in the current study. This approximates the intensity of the secondary electrons by assuming that the background intensity at any point is proportional to the total photoelectron intensity above the background to the lower E_B. Another method to subtract the backgrounds is the Tougaard approach which is a mathematical technique.

Data display

All XPS files were transferred into CasaXPS software allowing them to be converted from the native .dts files to Vamas file format and then to text files, which can be imported into the Sigmaplot software to produce graphs. The raw data consists of two columns: the x axis represents the binding energy and the y axis represents the intensity or counts per scan. A flat linear background was stripped off mathematically by excluding the average of the last ten data points in the intensity column

$$I_2 = I_1 - (\text{average of last ten data points in } I_1),$$

where I is the column representing signal intensity. Having stripped off the background a new column is generated that contains the intensity of the signal recorded with the low end of the scale at zero intensity.

The maximum of the Ti intensity column was then found allowing all spectra to be normalised to the Ti $2p_{3/2}$ peak maximum relevant to each sample for referencing. This allows direct comparison between spectra.

To normalise, all intensities were then divided by the Ti maximum intensity

$$I_3(x) = I_2(x)/Max\ I_2(Ti)$$

Where x represents the element under consideration e.g.

$$I_3(Ti) = I_2(Ti)/ Max\ I_2(Ti)$$

$$I_3(C) = I_2(O)/ Max\ I_2(Ti)$$

Finally, a Sigmaplot graph was obtained for presenting the XPS spectra.

2.8 DEPTH PROFILE XPS

2.8.1 Introduction

XPS depth profiling is used to study metals, oxide, ceramics, semiconductors, and metal coatings. Depth profiling can be used to identify the elements present as a function of depth into a solid; applications include thin films, the composition at buried interfaces, and the depth distribution of ion implants in materials.

Depth profiles deep into the sample surface (to a micron or more) can be generated by ion etching the surface, and then analysing the bottom of the etching crater at regular time intervals using XPS. However, for organic material, structural information will be lost due to damaging effects of the ion beam. In addition, the ion beam will induce scrambling and knock-in of atoms at the bottom of the crater reducing the accuracy of the analysis-the longer the etching time (the deeper the crater), the more degraded will be the accuracy of the depth profiles (Ratner et al., 1997).

The depth profile XPS functions in the same as XPS but using an argon (Ar^+) ion beam to incrementally etch the surface away. The advantages include the ability to analyse subsurface structures. The principal disadvantage is that the beam produces artefacts. Changes in chemical state can occur with preferential etching resulting in incorrect compositions being recorded if not assessed carefully.

2.8.2 Depth profile XPS used in the current study

Depth profiles were performed on the samples using XPS by etching the surface of the sample with an Ar^+ ion beam at 6 keV. The etch current was maintained at 0.4 mA throughout the experiments. XPS survey and region data were recorded for up to 26 levels after times of 0, 5, 10, 20, 30, 50, 70, 110, 190, 350, 670, 1030, 1390, 1750, 2110, 2470, 3070, 4270, 4870, 5470, 6670, 7870, 9070, 10270, 11470 s respectively. Acquisition was halted once the

oxygen to titanium ratio became less than 0.1. The pressure in the chamber was maintained at 1 $x10^{-7}$ torr throughout by controlling the inflow of Ar gas.
The data for the XPS depth profiling was quantified using Shirley background subtraction and Wagner sensitivity factors. As no Ar was observed on any of the surfaces prior to etching, it was excluded from the quantifications.
The standard errors in the elemental ratios recorded for the surface analysis are in the region of ± 0.01. The possible errors in the elemental ratios shown in the depth-profiling results are likely to be higher in depth profiling because is likely that they will suffer from preferential etching.

2.9 ION CHROMATOGRAPHY

2.9.1 Introduction

Ion chromatography is a process that allows the separation of ions and polar molecules based on the charge properties of the molecules. It can be used for almost any kind of charged molecule including large proteins, small nucleotides and amino acids, with the experimental solution to be separated collectively known as the analyte. It is often used as a first step in protein purification.
Ion-exchange chromatography (IEC or IC) methods have been in use since 1850, when H. Thompson and J. T. Way, researchers in England, treated various clays with ammonium sulphate or carbonate in solution to extract the ammonia and release calcium. In 1927, the first zeolite mineral column was used to remove interfering calcium and magnesium ions from solution to determine the sulphate content of water. The modern version of IEC was developed during the wartime Manhattan Project, and in the early 1970s ion chromatography was developed by Hamish Small and co-workers at Dow Chemical Company as a novel method of IEC usable in automated analysis. IC uses weaker ionic resins for its stationary phase and an additional neutralizing stripper, or suppressor, column to remove background eluent ions. It is a powerful technique for determining low concentrations of ions and is especially useful in environmental and water quality studies, among other applications. Ion chromatography is used for analysis of aqueous samples in parts-per-million

(ppm) quantities of common anions (fluoride, chloride, nitrite, nitrate, and sulphate) and common cations (lithium, sodium, ammonium, and potassium) using conductivity detectors. The chromatography also has the capability to analyse aqueous samples for parts-per-billion (ppb) quantities of hydrazine, monomethylhydrazine (MMH), and unsymmetrical dimethylhydrazine (UDMH). Ion chromatography is a form of liquid chromatography that uses ion-exchange resins to separate atomic or molecular ions based on their interaction with the resin. Its greatest utility is for analysis of anions for which there are no other rapid analytical methods. It is also commonly used for cations and biochemical species such as amino acids and proteins. Most ion-exchange separations are done with pumps and metal columns. Ion chromatography is one of the few techniques existent that can provide quantitative analysis of anions at the ppb level. This technique is used to determine ions in liquids and ionic contamination on the surfaces of wafers, chips, and packages. Aqueous solutions, which may require filtration, dilution, and/or cleaning to remove interferences, are required for analysis. Solid samples are extracted with water to remove ions from the sample surface. Organic liquids may also be extracted with water to obtain an aqueous solution of ions for analysis. The minimum sample required is approximately 10 ml for liquids and 2-3 cm^2 for solids and there are no upper limits.

A sample is introduced, either manually or with an autosampler, into a sample loop of known volume. A buffered aqueous solution known as the mobile phase carries the sample from the loop onto a column that contains some form of stationary phase material. This is typically a resin or gel matrix consisting of agarose or cellulose beads with covalently bonded charged functional groups. The target analytes (anions or cations) are retained on the stationary phase but can be eluted by increasing the concentration of a similarly charged species that will displace the analyte ions from the stationary phase. For example, in cation exchange chromatography, the positively charged analyte could be displaced by the addition of positively charged sodium ions. The analytes of interest must then be detected by some means, typically by conductivity or UV/Visible light absorbance.

2.9.2 IC used in the current study

The cations (Ca^{2+}) were measured on a Dionex ICS 1000 system (Dionex, UK) equipped with an AS50 autosampler, using a 20 mM MSA (Methanesulfonic acid, BDH, UK) solution in deionised water mobile phase, at a flow rate of 1 ml / min with a CS12A column and a CAES suppressor. This MSA solution was used as the eluent. The ICS-1000 is an integrated and preconfigured system that performs isocratic IC separations using suppressed conductivity detection. In this method, cations were eluted using a 4 x 250 mm IonPac® CS12A separator column. The cations were detected via conductivity.
All results were calibrated against a 5-point calibration curve using a predefined calibration routine. Coupled with AutoSuppression®, the ICS-1000 provides high performance with ease of use. Chromeleon® software package was used for data analysis.

Cation Reagent and Standard Solution Preparation:

Calibration was carried out with standard solutions containing 0.1, 0.2, 0.5 and 1 ppm of calcium. An injection loop of 20 µl was used.
The initial standard solution was prepared using either:
a. Sodium chloride (Sigma) and calcium chloride ($CaCl_2.2H_2O$, BDH, UK) as reagents. The initial stock solution made was 100 ppm from 36.68 mg $CaCl_2 \cdot 2 H_2O$ + 25.42 mg sodium chloride (NaCl) in 100 ml volumetric flask.
b. A solution which contained six standard cations (from Six Cation-II Standard, Dionex Corporation, California, lot # 040602, Product No. 046070). The solution contained 500 ppm calcium chloride. The pH of the initial standard solution was 3.0 ± 0.3.The initial stock solution made was 5 ppm (from 500 ppm) in 100 ml volumetric flask. From this solution, serially diluted 0.01, 0.1, 0.2, and 1 ppm standard solutions were prepared (1 ml 5 ppm in 499 ml, 5 ml 5 ppm in 245 ml, 10 ml 5 ppm in 240 ml, 5 ml 5 ppm in 20 ml).
The data were imported into Microsoft Excel and presented as graphs. Details of each experiment are given separately in Chapter 4.

2.10 LIST OF REFERENCES

Beamson, G., Briggs, D. (1992)
High resolution XPS of organic polymers: the Scienta ESC 300 database.
Wiley & Sons, Chichester

Boyer, R., Welsch, G., Collings, E. W.1994
Materials Properties Handbook: Titanium Alloys.
Eds. ASM International, Materials Park, OH.

Brown, W. L. (1989)
Ion beam induced chemical changes in molecular solids.
Nuclear Instruments and Methods B 37-38: 270-274

Goodhew, P. J., Humphrey, F. J., Beansland, R. (2000)
Electron microscopy and analysis.
Taylor and Francis, Boca Raton, USA

Paynter, R. (1999)
Basic principles of X-ray photoelectron spectroscopy.
http//goliath.inrs-ener.Quebec.ca/commerce/xps-techn.html

Ratner, B.D., Castner, D.G. (1997)
Electron spectroscopy for chemical analysis.
In: Vickerman, J.C. Surface analysis: principal techniques P 43-98
Wiley & Sons, Chichester

Townsend, P. D., Chandler, P. J., Zhang, L. P. (1994)
Optical effects of ion implantation.
Cambridge University Press

Ungerbock, A., Rahn, B. (1994)
Methods to characterise the surface roughness of metallic implants.
Journal of Material Science: Material in Medicine 5: 434-440

Vickerman, J., C. (1997)
Surface analysis; the principal techniques.
Wiley & Sons, Chichester

Ziegler, J. F. (1988)
Ion implantation.
Science and Technology, 2nd edition, Boston; London Academic Press

Wagner, C. D.1981
Empirical atomic sensitivity factors for quantitative analysis by electron spectroscopy for chemical analysis.
Surface and interface analysis 3 (5): 211-225

3. SURFACE CHARACTERISATION OF COMERCIALLY PURE TITANIUM AND MODIFIED TITANIUM SURFACES

3.1. INTRODUCTION

The attachment of cells to titanium surfaces is an important phenomenon in the area of clinical implant dentistry. It is well known that the biocompatibility of commercially pure titanium and its alloys is strongly related to their surface properties, with both the composition of the protecting oxide film naturally present on the surface and the surface topography playing important roles (Masaki et al., 2005, Links et al., 1998). The biological response to an implanted material is governed by the surface chemistry, surface topography and surface energy (Ratner et al., 1987). The titanium surface can either be chemically or physically modified, or both, in order to improve biomaterial–tissue integration. Different treatments are used to the modify titanium surfaces, such as: hydroxyapatite coatings, oxide blasting treatments, chemical etching and anodic or thermal oxidation. Full details of these techniques are given in Chapter 1.

As the behaviour of the cells, such as adhesion, proliferation and morphologic changes are greatly affected by the surface properties, a major consideration in designing implants has been to create surfaces that will promote desirable responses by the cells and tissues contacting the implants. To achieve this, the titanium implant surface can be modified in various ways, for example roughening the surface, with the consequence that it can improve bony apposition, tissue adhesion, and cell migration. Surface roughness has a significant influence on cell response, as extensive research had shown some time ago. Previous *in vivo* studies have shown that both heat treatment and acid etching of a titanium implant surface significantly enhance osseointegration (Smith et al., 1991). Also recent studies showed that a controlled chemical oxidation of Ti implants significantly enhanced contact osteogenesis and suggested that this treatment may be beneficial for early loading of implants (Tavares et al., in press). Vanzilotta et al., (2006) showed that etching with an HCl/H_2SO_4 solution might improve *in vitro* titanium bioactivity in a SBF solution

at 37°C. This behaviour may suggest a possibility of a further favourable *in vivo* response.

The surface area of the bone–implant interface is positively correlated with an increasing roughness of the titanium implant surface (Natan 1983). In addition, bone deposition was induced on roughened titanium surfaces whereas smooth surfaces were almost entirely covered by fibrous tissue. This was confirmed by Carlsson et al. (1988), who showed that irregular (grit-blasted and plasma sprayed) or porous dental implant surfaces favoured bone growth and apposition, whereas smooth surfaces resulted in a fibrous tissue response. Brunette (1988) reviewed in detail the effects of implant surface topography on the behaviour of cells and showed that considerable differences occurred with different cells on dental implant surfaces of different topography.

Thomas et al. (1987) found that roughened surfaces had an increased implant surface area which resulted in a greater surface coverage by bone, as compared with the smooth polished surfaces. In their study, the most extensive bone-implant interface was observed on acid-treated surfaces (hydrochloric acid/sulphuric acid [HCl / H_2SO_4]) and hydroxyapatite-coated implants.

Michaels et al. (1989) determined that a higher percentage of osteoblast-like cells attached to roughened commercially pure titanium surfaces produced by sandblasting than to smoother surfaces, which had been polished with 1 µm diamond paste. This was later confirmed Keller et al. (1994). Buser et al. (1991) reported that increasing the roughness of the surface was correlated with increased bone-implant contact (BIC). They demonstrated significant differences in the percentage of bone-implant contact for implants with various treatment surfaces. The least BIC (20-25%) was seen for electro polished and acid pickled (medium grit 0.12-0.25 µm; HF / HNO_3). Sand blasted surfaces (with large grit, 0.25-0.50 µm) and titanium plasma sprayed had higher percentages of BIC (30-40%) with the largest values being for SLA and acid treated surfaces (large grit 0.25-0.50 µm; HCl / H_2SO_4) with 50-60% and hydroxyapatite coated implants with 60-70%. The same tendency was observed when the three different sandblasted surfaces were compared, with the roughest of the three showing the highest BIC. The direct comparison between SL (sandblasted with large grit 0.25-0.50 µm) and SLA (sandblasted with large grit 0.25-0.50 µm and acid treated with HCl / H_2SO_4 surfaces, both sandblasted

with the same grit size, revealed a significant difference, with an increase of almost 60% for the SLA sample. The authors assumed that this difference may be attributed to the acid treatment with HCl and H_2SO_4. The results from this study are in concordance with the results in biomechanical studies carried out earlier by Steinmann et al. (1986) which showed consistently higher removal torque for TPS implants when compared with smooth implants.

It is well known that osteoblasts initially respond in a differential manner to titanium surface roughness. Martin et al. (1995) studied the effect of surface roughness on osteoblast proliferation and differentiation. Five different titanium surfaces with different roughness were analysed. Higher levels of cellular attachment were found *in vitro* on rough surfaces of titanium with irregular morphologies when compared with smoother surfaces.

The effects of chemical modification (acid etching alone) on the osseointegration without adding particulate matter (TPS or hydroxyapatite) or embedding surface contaminants (grit particles) had been examined. There have been several studies on the effect of acid treatment, such as a mixture of HCl / H_2SO_4 or hydrofluoric acid/nitric acid (HF / HNO_3) (Klokkevold et al., 1997). The purpose of this study was to look at the effect of acid etching alone without sand blasting of the implant surface. The removal torque of screw-shaped titanium implants with an acid etched (HCl / H_2SO_4) surface (Osseotite) was compared to that of implants with a machined surface. It was found that the chemically etched implant surface quadrupled the removal torque as compared to a machined surface. This test has been widely used as a measure of implant anchorage and osseointegration, although it is destructive and its direct clinical validity has never been established. The authors concluded that chemical etching of the titanium implant surface significantly increased the strength of osseointegration when compared to a machined surface.

It must be specified that alteration in the surface topography will result in an altered surface chemistry. In an evaluation of 34 different examined Ti dental implants with topographical features related to machining, sandblasting, acid etching and plasma spraying, Morra et al. (2003) concluded that the surface topography was not the only variable controlling the biological response, and that the surface chemistry varied accordingly to the topographical properties.

As surface chemistry is also known to play a significant role in the tissue behaviour toward the implant upon immersion into the body, some modification of the chemistry will be presented below. For a more detailed description of the modification of surface chemistry please refer to Chapter 1.

Various strategies for modifying the surface chemistry have been employed, some of which aimed to promote hydroxyapatite (HA) precipitation (as Ti itself is not able to promote HA precipitation). These largely involved pre-treatment (in solution or through thermal oxidation) or the provision of ceramic or glass coatings rich in calcium and phosphate ions to enhance the biological response by achieving true bone bonding at the interface. Other strategies have focussed on controlling the cellular response rather than HA formation.

A short review of the modifications mentioned above is listed below. Pre-treatment can be carried out by: nitric acid passivation, H_2O_2 treatment, calcium and phosphate containing solutions, and alkali solutions. Coatings can be ceramic, glass and protein. Less common methods of modifying the surface include peptide immobilisation and reaction with antibiotics.

Passivation was repeatedly found to result in the thinning of the oxide layer, unless coupled with thermal aging of the surface in boiling water or through heating, which resulted in more favourable cellular responses after long exposure times (Ku et al., 2002). A detailed discussion about passivation is given in Chapter 4.

Pre-treatment in alkali solution resulted in Ca and phosphate deposition on the cp Ti surface (Yang et al., 1999). Treatment of cp Ti with NaOH to form sodium hydrogels at the surface layer was reported to induce apatite deposition in a simulated body fluid (SBF) environment (Kim et al., 1999). Jones (2001) listed several methods of Ti surface modification among which was the inclusion of Ca ions into Ti plates through immersion in aqueous Ca solutions. This was reported to result in the formation of calcium hydroxide and/or calcium titanate, which, upon immersion in HBSS was found to induce apatite formation not found on un-treated cp Ti.

H_2O_2 treatment resulted in oxidation and hydroxylation of the surface, as well as the production of Ti-peroxy gels, which were thought to enhance calcium phosphate nucleation (Brunette et al., 2001). Exposure to H_2O_2 solutions containing various metal chlorides was found to create bioactive Ti surfaces

(Jones 2001). Tavares et al., (in press) found that treatment of a commercial, machined surface titanium implant with H_2SO_4 / H_2O_2 enhances contact osteogenesis.

Hydroxyapatite coatings are used to enhance osseointegration and short-term exposure revealed that such surfaces provide more osteophilic substrates than cp Ti resulting in more extensive bone-implant integration. The force required to detach hydroxyapatite coated Ti from bone was found to be higher than that for Ti at periods of around 12 weeks (Tengvall et al., 1992)

Implants coated with HA have been shown to display a biological profile superior to uncoated implants as judged by: lack of local or systemic toxicity, absence of fibrous tissue between implant and bone, and capacity to bond directly to the bone. HA coatings also promoted faster bony adaptation, resulting in a reduced healing time (Misch, 1999).

However, the disadvantages of the coatings are fragility, risk of fracture, and increased cost. Esposito (1998), after an extensive literature review of the causes of implant failure, stated that hydroxyapatite-coated implants showed increased susceptibility to infection, and double the failure rate compared with TPS implants, with failure after 36 months of function due to peri-implantitis.

There is a general agreement that the early stages of healing are the most critical in determining the biological response, whereas long-term studies have shown no significant differences in the host tissue surrounding integrated Ti implants prepared by different methods. It would therefore seem logical to attempt to modify Ti surfaces to accelerate short-term bone formation on Ti through direct incorporation of Ca and/or phosphate ions. This can be achieved by numerous methods, one of which is ion implantation. Various ions have been implanted into titanium. Initially the majority of experiments which involved ion implantation were carried out to modify the physical properties of the cp Ti with the aim of increasing the wear and corrosion resistance through the implantation of C, O, and N into Ti (Krupa et al., 1996, 1999, 2005). A more detailed description of ion implantation was given in Chapter 1.

The most significant reports were those claiming to enhance osseointegration by improving the chemical properties of cp Ti via Ca ion implantation. In order to

improve the biocompatibility of titanium and its alloys, Hanawa et al. (1993, 1995) used calcium ions for the implantation and found that this accelerated the precipitation of calcium phosphates; this effect was more pronounced in pure titanium than in titanium alloys. They examined the chemical composition and structure of the surface layers thus formed and found that, during the calcium-ion implantation, the thickness of the oxide layer increased and the implanted ions occurred in this layer in the form of calcium oxide (CaO) and the complex calcium and titanium oxide ($CaTiO_3$). The enhancement of phosphate deposition, found by the authors *in vitro* and *in vivo* was related to the amount of Ca ions implanted. In *in vivo* examinations (Hanawa et al., 1997), calcium-ion implantation also appeared to be advantageous for the growth of the bone tissue.

In order to understand the mechanisms by which physical and chemical surface properties of cp Ti and Ca implanted Ti (Ca-Ti) will influence cell behaviour it is essential to present the characteristics of these surfaces first. This chapter gives a compete overview of the surface characteristics of the material and the surface topography and it examines the roughness, surface and sub-surface composition of cp Ti and as implanted Ca-Ti.

The cp Ti used in current work was grade 1 according to the ASTM grading list (ASTM 67), except the Ti samples provided by the Straumann Institute which were grade 4. There are 4 grades in this list and the grading is based on the percentage by weight content of oxygen and iron. ASTM gives the following composition (in maximum %) for a grade 1 cp Ti sample: 0.03% N, 0.1% C, 0.0125% H, 0.18% Fe, 0.20% O, Ti balance. Grade 1 has a maximum O content of 0.18% by weight and a maximum Fe content of 0.2% by weight and is the softest of all 4 grades. Grade 4 Ti has similar composition with grade 1 and contains slightly more Fe and O (0.05% N, 0.1% C, 0.015% H, 0.5% Fe, 0.4% O, Ti balance). All grades of Ti contain maximum concentrations of C, H, and N of 0.1%, 0.015% and 0.3% respectively (Brown 1997).

Analysis of the surface topography was carried out using scanning electron microscopy (SEM), laser profilometry (LP) and white light interferometry (WLI) to visualize the surface features and measure the surface roughness. Surface chemistry was analysed using X-ray photoelectron spectroscopy and XPS depth

profiling, to map the distribution of elements (with the exception of hydrogen) through the implanted surface.

3.2 SURFACE TOPOGRAPHY OF TITANIUM DISCS

It has been shown above that surface topography of titanium influences the biological response. As a result, by modifying the topography the response of the cells to it may be changed in a way that could potentially improve osseointegration.

Ion implantation of cp Ti is known to modify its chemical composition, which may to play a role in determining the cell response to this metal (Nayab et al., 2003, 2005, 2007, in press). It is important to determine if the implantation process modifies the topography of the titanium, as this characteristic may influence the cell reaction to the implanted surfaces.

The objective of this study was to characterize the titanium surface using several methods of measuring the surface topography and also to assess whether various surface modifications affect the surface roughness. The methods employed were laser profilometry and white light interferometry (WLI). The parameters analysed in these experiments were R_a, R_q and total surface area. As R_q values were found to vary in the same way with R_a, are not presented here.

Initially, smooth Ti (SMO), sand blasted and acid etched Ti (SLA) and titanium plasma sprayed Ti (TPS) were analysed. The discs were provided polished by the Straumann Institute (Switzerland). All the discs were nitric acid treated (passivated) using high concentration (70%) HNO_3 for 10 min.

Subsequently discs polished in-house were analysed after polishing carried out using two polishing procedures, and after Ca implantation. The aim was to assess the quality of the in-house polishing using both methods, and also to assess whether Ca implantation will modify the surface roughness.

In a final experiment discs supplied by Straumann were assessed before and after calcium and argon implantation and also after nitric acid treatment. The aim of this experiment was to explore whether ion implantation and nitric acid

treatment will influence the surface roughness, and also to compare the roughness of supplied samples with that of the in-house specimens, to assess the relative quality of the polishing.
For all of the experiments described below, the following techniques were used:

a) SEM

Scanning electron microscopy (SEM) allows a visual assessment of surface topography and is widely used in industry and in biological studies. However, this method provides only a qualitative roughness measurement. Details of the parameters (voltage, vacuum, etc) used for the SEM in the current work were given in Chapter 2.

b) Laser profilometry

Areas of 16 mm^2 (4 mm x 4 mm) were measured on all the samples. The step size was 5 μm in both the x- and y- directions and R_a was measured. Similar length scales were used for all the samples. In addition, the actual surface area was measured and recorded for each sample.
Smaller areas of 25 x 10^4 μm^2 (500 μm x 500 μm) were also analysed on the smooth (SMO), sand blasted and acid etched (SLA), and titanium plasma sprayed samples (TPS) analysed in the first experiment. The step size was 1 μm. R_a and the total surface area were measured for these samples. These analyses were carried out to compare how the area measured and the step size might influence the roughness values, and to observe how these values may be compared with roughness values recorded with WLI, as a similar step size was employed.

c) White light interferometry

Surface roughness was measured by white light interferometry, using a Zygo 3D optical interferometric microscope. A 10× Mirau objective, offering a magnification of 200× was used. An area of 0.36 mm × 0.27 mm was measured, with a lateral resolution of 1.12 μm. For each sample, an average and standard deviation roughness value was calculated from the analysis of three different

regions of the sample. Their mean R_a values were compared statistically using the t- test. The R_a and surface area were recorded.

3.2.1. Roughness measurements of topographically different surfaces

Surfaces with different topographic characteristics were examined. The motivation was to assess the chosen methods for measuring roughness across the range of textures which can be exhibited by titanium surfaces. Two discs of each smooth (SMO), titanium plasma sprayed (TPS), and sand blasted and acid etched (SLA) samples provided by the Straumann Institute (Waldenburg, Switzerland) were analysed using laser profilometry (LP) and white light interferometry (WLI).

The aim of this experiment was to verify the suitability of the techniques and to establish differences between techniques (if any). These surfaces have shown different cell responses when used in gene expression experiments (Brett et al., 2004).

Appearance

Figure 3.1 shows the general appearance of a commercially pure titanium sample provided by the Straumann Institute (Switzerland).

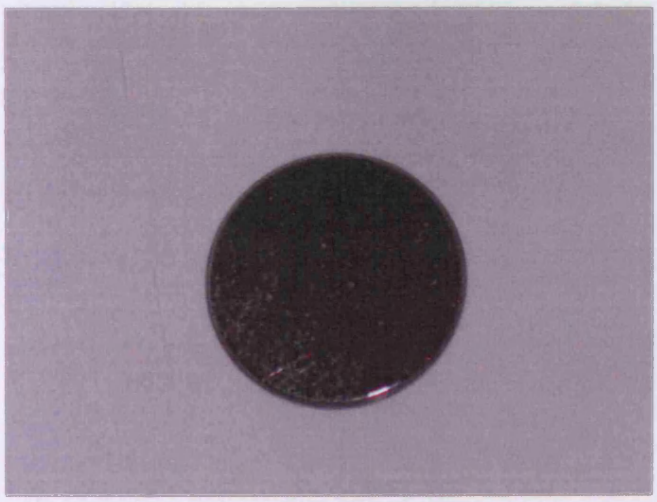

Figure 3. 1 Picture of a commercially pure titanium sample (SMO) supplied by the Straumann Institute.

The polished commercially pure titanium discs (SMO samples) had no distinct colour, were shiny silver and had a mirror finish. No scratches or pits were visible on the samples with the naked eye. This clean appearance indicates that the surface had been successfully polished. The appearance of the cp Ti, mainly the surface colour, is related to the thickness of the oxide film present on the surface and the preparation methods, as observed by Ungersböck et al. (1994). They used standard reflected light microscopy and interference contrast microscopy to study the surface colour, and found that samples which were anodized to a fine finish displayed a gold colour, whereas samples which were anodised then roughened by blasting were dark gold. The gold/yellow tint observed on smooth Ti was reported to arise from the oxide layer, as opposed to the grey areas of metallic Ti. Ti plates which were hand ground, blasted with Al_2O_3 or electro polished did not display any interference colours. The fact that the SMO did not change colour suggested that the oxide layer present on the surface was too thin as to give rise to any interference colours. This finding was also noted by Lausmaa et al. (1985) when describing their samples. As the oxide layer is reported as being less than 10 nm thick little interference effect would be expected.

Figure 3.2 shows the general appearance of a sandblasted and acid etched sample supplied by the Straumann Institute (Switzerland).

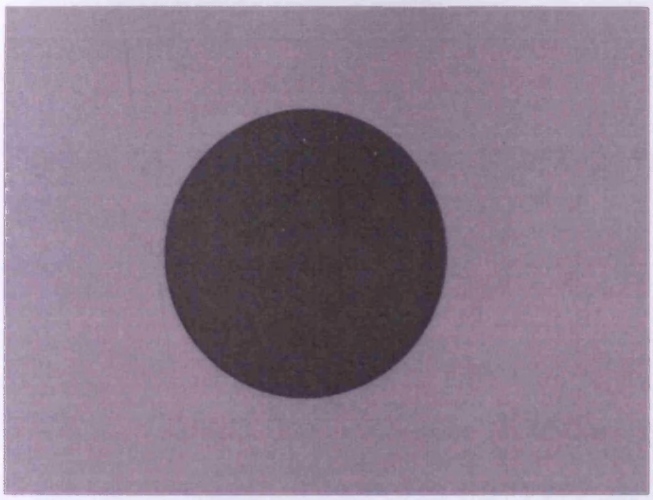

Figure 3. 2 Picture of a sandblasted and acid etched sample supplied by the Straumann Institute (Switzerland).

The sand blasted and acid etched (SLA) samples appeared visibly rougher than the smooth samples, had an irregular surface and were matt dark grey in colour.

Figure 3.3 shows the general appearance of a titanium plasma sprayed sample.

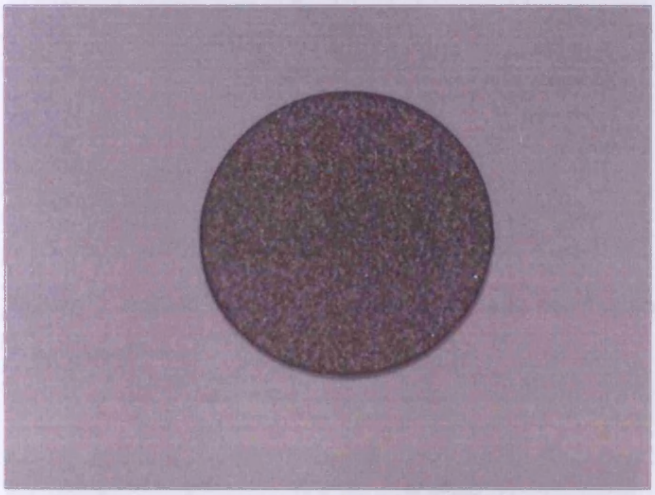

Figure 3. 3 Picture of a titanium plasma sprayed sample (TPS) supplied by the Straumann Institute (Switzerland).

The titanium plasma sprayed samples (TPS) appeared rough, with an irregular surface and was matt pale grey. It appeared rougher than the SMO and than the SLA, and showed different texture and colour from the two.

Topography

Figures 3.4, 3.5, and 3.6 present SEM images of SMO, SLA, and TPS samples at various magnifications.

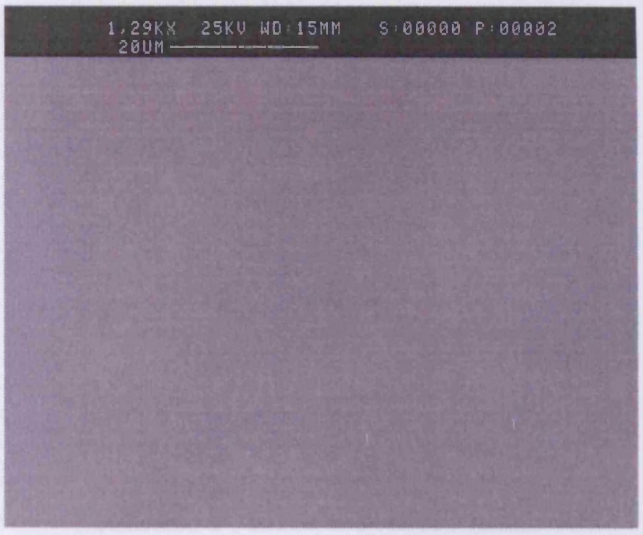

Figure 3. 4 SEM images of a commercially pure titanium (SMO) sample recorded at 1290 x magnification.

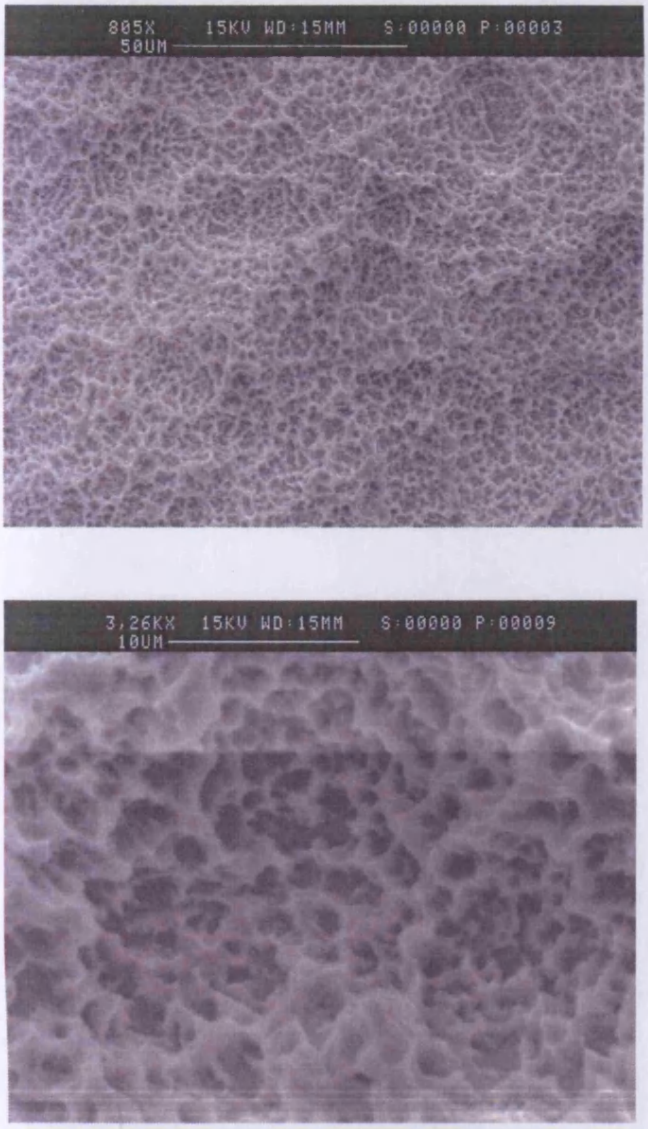

Figure 3. 5 SEM images of a sandblasted and acid etched (SLA) titanium sample recorded at 102 x (row 1), 802 x (row 2) and 3260 x magnifications (row 3).

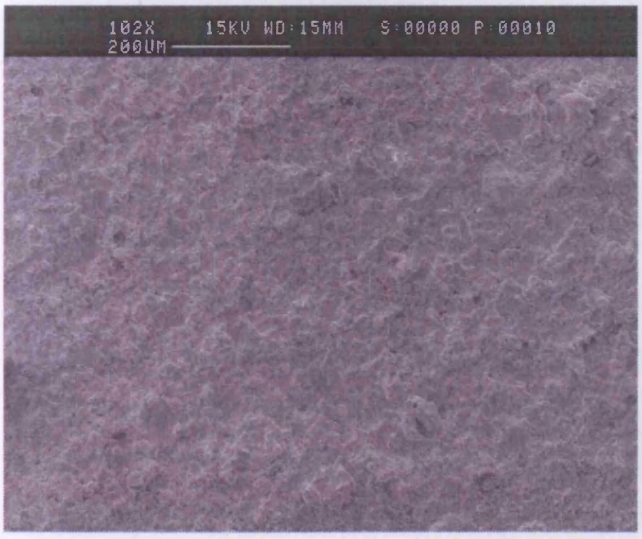

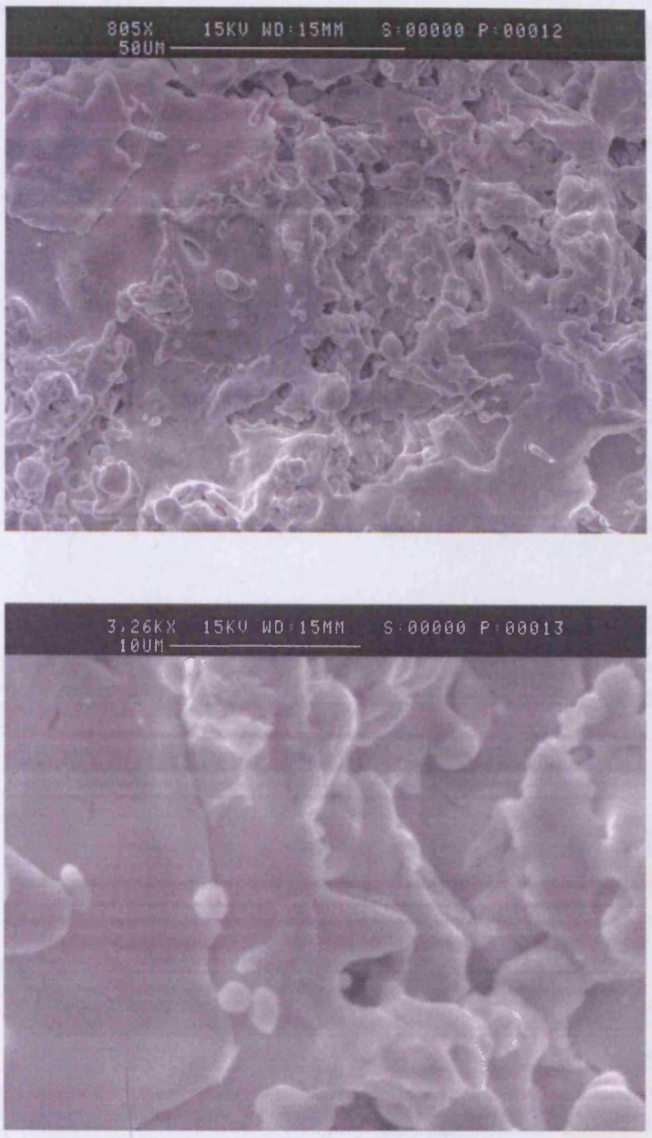

Figure 3. 6 SEM images of a titanium plasma sprayed (TPS) titanium sample recorded at 102 x (row 1), 802 x (row 2) and 3260 x magnifications (row 3).

The SMO sample was the smoothest of the three. The overall appearance was smooth and the surface did not show scratches, pits or grooves from the polishing.

The SLA and TPS samples appeared rougher at a 102 x magnification than the SMO sample, and also the TPS sample appeared much rougher than the SLA sample. For the SLA discs, the silica grains appeared to have eroded the metal to various depths; sharp ridges and pits of various diameters were easily recognized. On larger magnifications (802 x, 3260 x), the SLA samples presented craters and micropits as a result of the etching and the sandblasting, as described by Buser at al. (1991). The TPS samples had a highly

heterogeneous and undulating topography. They presented an irregular surface with cavities and small globular protuberances from the titanium plasma spraying. This appearance was made more evident when looking at images recorded at a magnification of 802 x or 3260 x. SEM images for SLA and TPS obtained in this study were similar with the images presented for these samples by Buser et al. (1991).

Figures 3.7, 3.8, and 3.9 present images recorded with laser profilometry (LP) for cp Ti (SMO), sand blasted and acid etched (SLA) and titanium plasma sprayed (TPS) samples over an area of 4 mm x 4 mm.

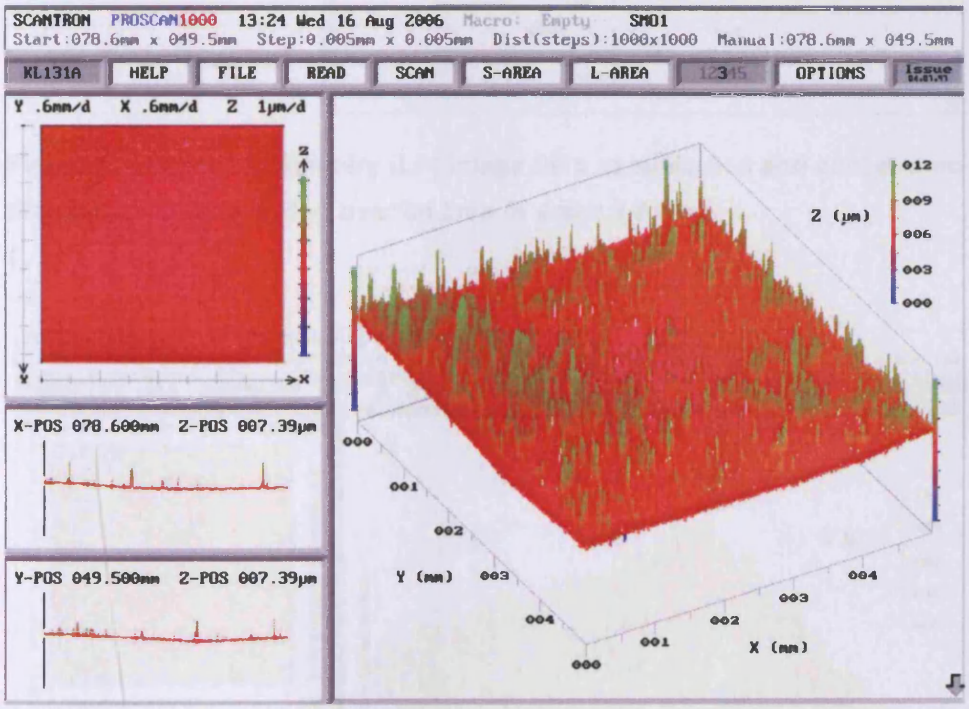

Figure 3. 7 Laser profilometry (LP) image for a cp Ti (SMO) sample recorded over an area of 4 mm x 4 mm.

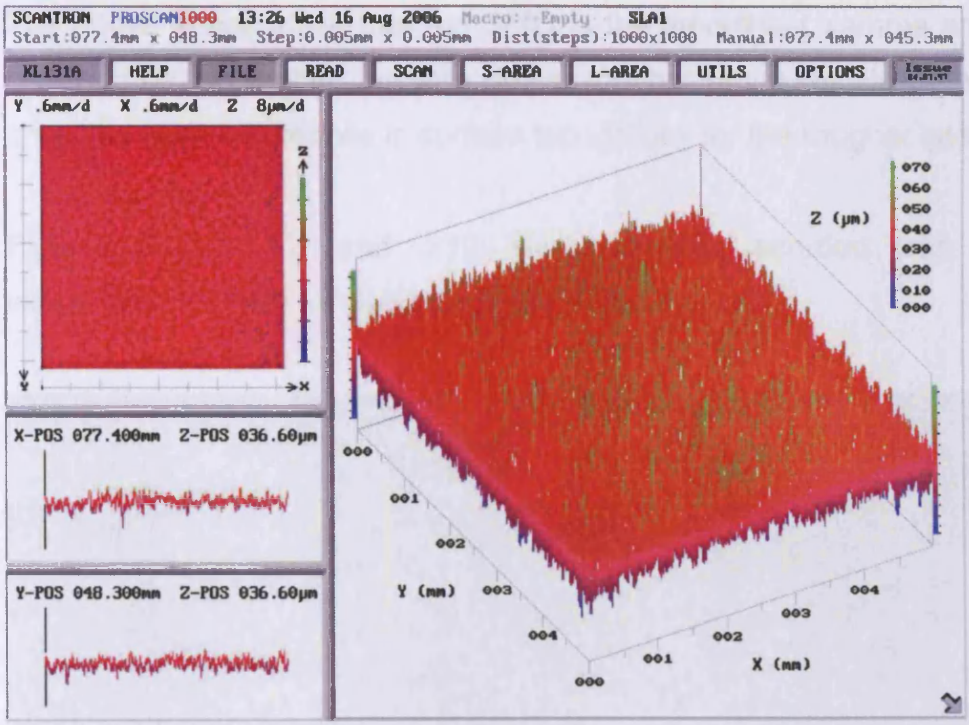

Figure 3. 8 Laser profilometry (LP) image for a sandblasted and acid etched (SLA) titanium sample recorded over an area of 4 mm x 4 mm.

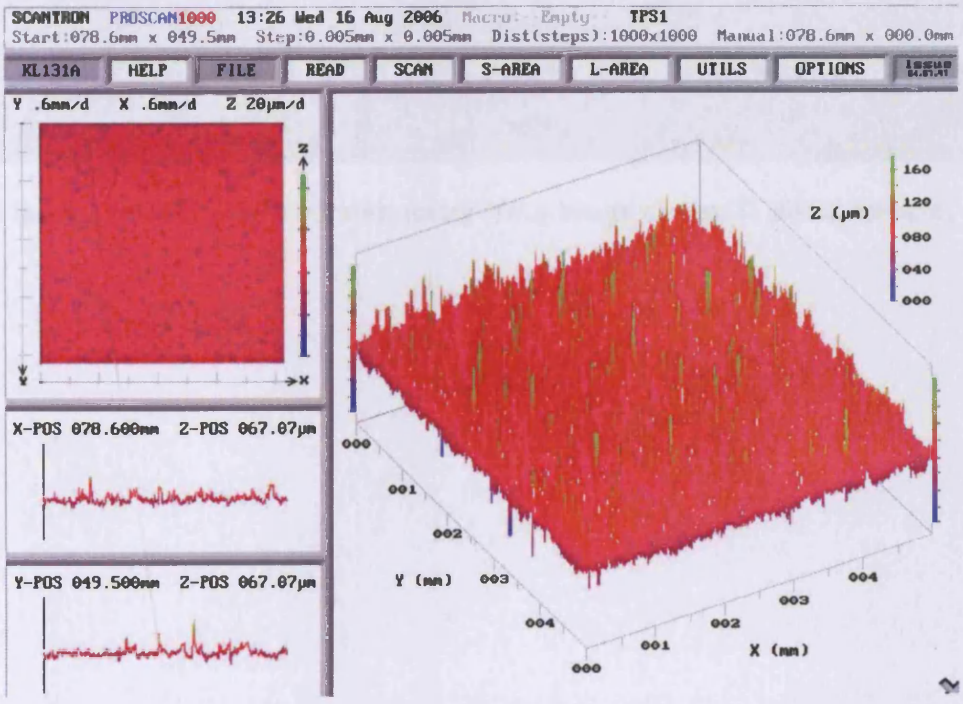

Figure 3. 9 Laser profilometry (LP) image for a titanium plasma sprayed (TPS) titanium sample recorded over an area of 4 mm x 4 mm.

The above image show that the SMO is the smoothest sample and both SLA and TPS being rougher, but with similar roughness values. However it does not show the main differences in surface topography for the rougher samples.

Figures 3.10, 3.11, and 3.12 show images recorded with white light interferometry (WLI) for SMO, SLA and TPS samples.

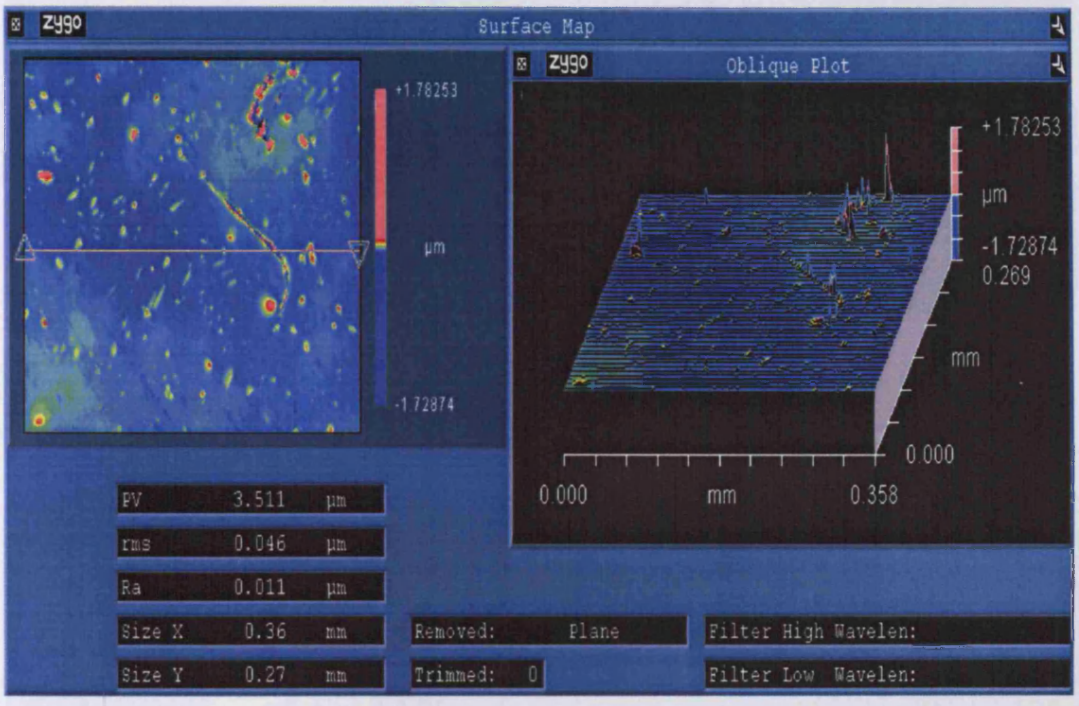

Figure 3. 10 White light interferometry (WLI) image of a cp Ti (SMO) sample.

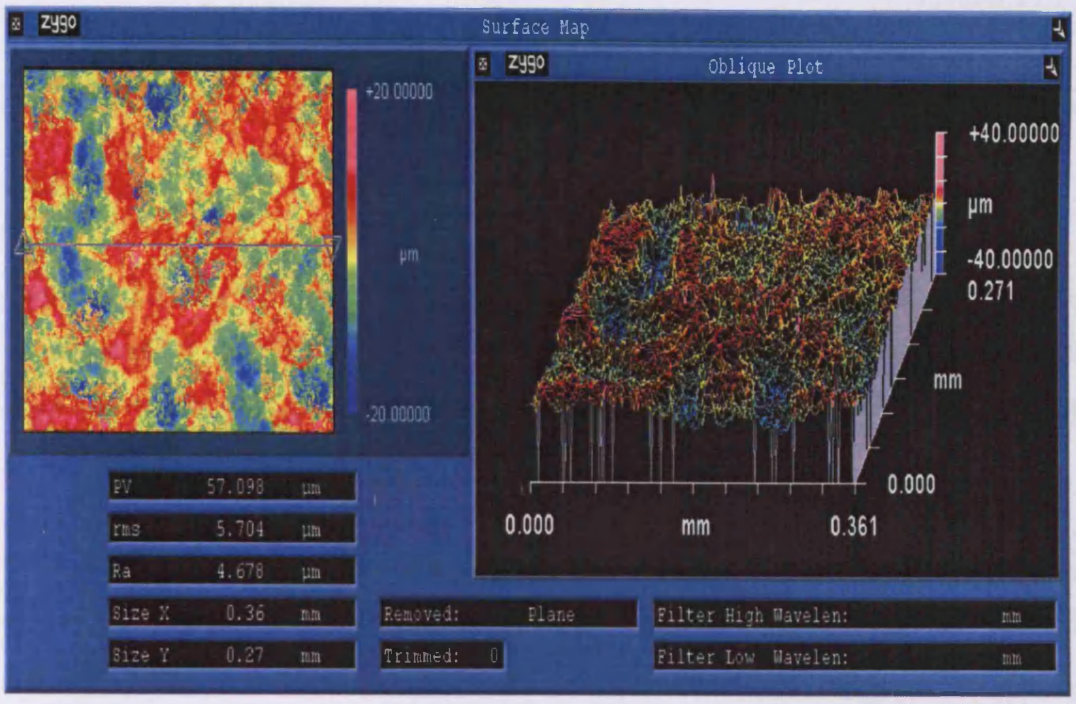

Figure 3. 11 White light interferometry (WLI) image of a sandblasted and acid etched (SLA) titanium sample.

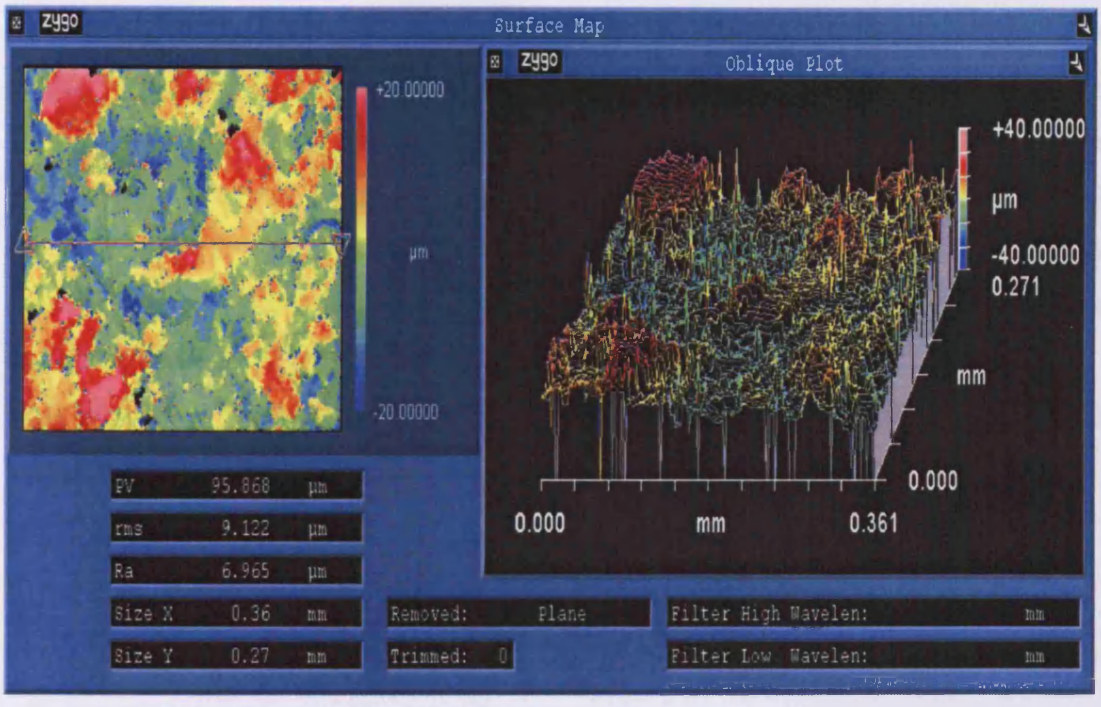

Figure 3. 12 White light interferometry (WLI) image for a titanium plasma sprayed (TPS) titanium sample.

Compared to the LP images, these pictures clearly show the difference in the surface topography between the samples. The SMO surface looks the

smoothest from the three and has few spikes. The SLA and TPS surfaces have an irregular, roughened form from the profile when looking at an oblique plot.

Roughness

Figures 3.13, 3.14, and 3.15 show the mean roughness (R_a) values (averages and standard deviations) for the smooth (SMO), sand blasted and acid etched (SLA), and titanium plasma sprayed (TPS) surfaces, measured with LP over a large area (4 mm x 4 mm) and WLI.

From the laser profilometry image recorded for the SMO sample over an area of 4 mm x 4 mm (figure 3.7) it can be noticed that the SMO sample was not strictly flat and showed a slight curvature from the profile. When measuring the R_a for this sample, an average value of 0.23 ± 0.04 μm (figure 3.13) was recorded over an area of 4 mm x 4 mm. It was decided to use a surface filter in the software to remove the general shape of the object but leave the roughness of the sample (details about the filter were given in Chapter 2). Various filters were applied and it was found out that if the curvature was removed, increasing the size of the filter did not modify the roughness values. In this experiment it was found that a filter with a nominal value of 2 as defined by the manufacturer removed the curvature and influenced significantly the R_a. Increasing the filter size did not change the roughness further. After applying the filter, the R_a decreased significantly ($p<0.05$) to an average of 0.15 ± 0.02 μm.
The SLA and TPS samples were effectively flat so the application of the filter was not necessary.

Figure 3. 13 Comparison between Ra values for SMO sample using unfiltered and filtered LP on a large area (4 mm x 4 mm).

Figure 3.13 presents a comparison between R_a values for SMO samples using LP (un-filtered and filtered) on a large area (4 mm x 4 mm). Figure 3.14 shows a comparison between R_a values for SMO, SLA and TPS samples using LP (un-filtered) on a large area (4 mm x 4 mm) and WLI.

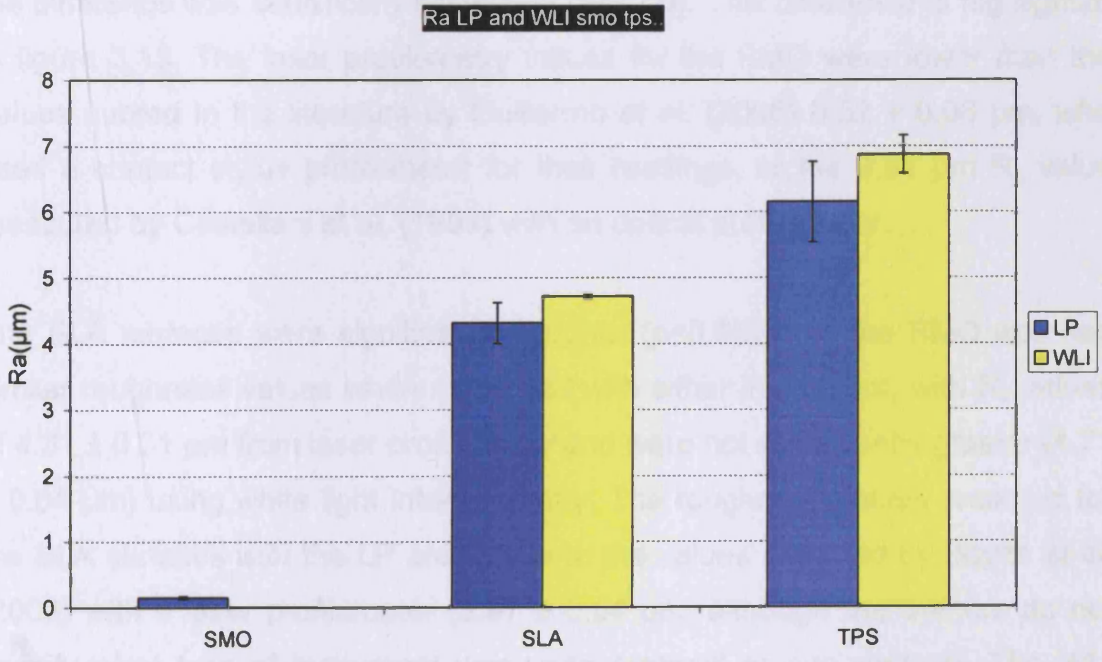

Figure 3.14 Comparison between Ra values for SMO, SLA and TPS samples measured using filtered LP on a large area (4 mm x 4 mm) and WLI.

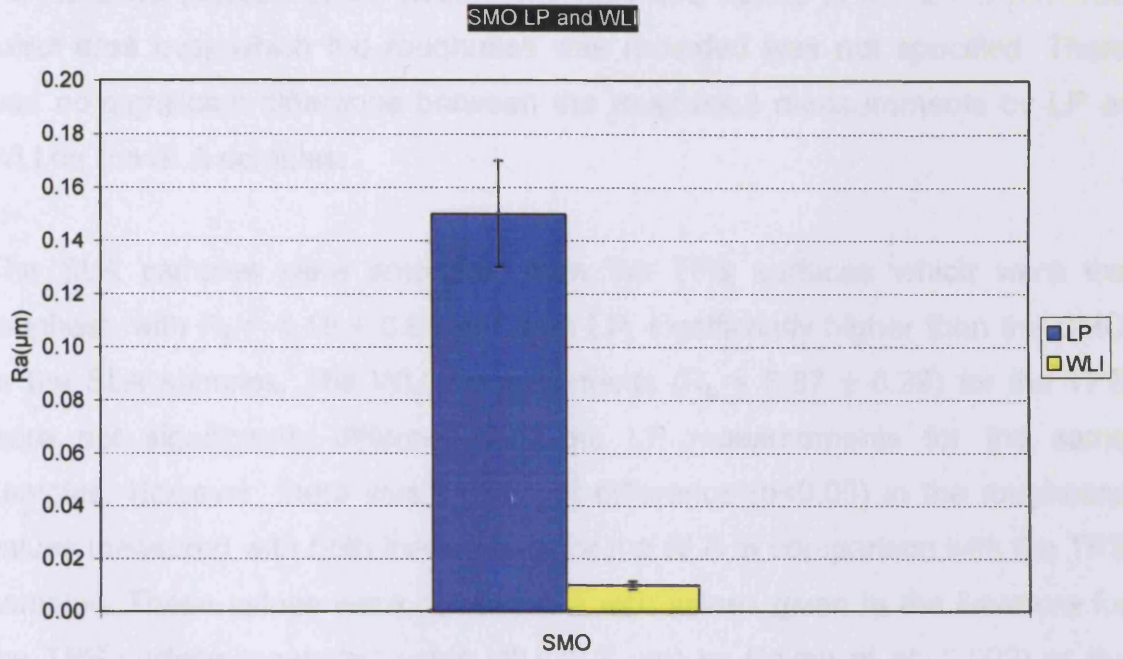

Figure 3.15 Comparison between Ra values for SMO sample measured using filtered LP on a large area (4 mm x 4 mm) and WLI.

The SMO surfaces were clearly the smoothest of the three types, with R_a values of 0.15 ± 0.02 µm from laser profilometry and 0.015 ± 0.002 µm from white light interferometry. As observed, LP gave over ten times the R_a value of WLI and the difference was statistically significant ($p<0.05$). This difference is highlighted in figure 3.15. The laser profilometry values for the SMO were lower than the values quoted in the literature by Guillermo et al. (2005) 0.32 ± 0.06 µm, who used a contact stylus profilometer for their readings, or the 0.31 µm R_a value measured by Castellani et al. (1999) with an optical profilometer.

The SLA surfaces were significantly rougher ($p<0.05$) than the SMO and had similar roughness values when measured with either instrument, with R_a values of 4.31 ± 0.31 µm from laser profilometry and were not significantly greater (4.71 ± 0.04 µm) using white light interferometry. The roughness values recorded for the SLA surfaces with the LP are similar to the values recorded by Boyan et al. (2002) with a laser profilometer (3.97 ± 0.04 µm, although the authors do not specify what type of instrument was used (contact or non-contact). The WLI roughness values measured for the SLA discs were similar to those quoted in

the literature (Borsari et al., 2005), who recorded values of 4.1 ± 0.3 μm. The exact area over which the roughness was recorded was not specified. There was no significant difference between the roughness measurements by LP or WLI for the SLA samples.

The SLA samples were smoother than the TPS surfaces which were the roughest, with R_a = 6.15 ± 0.61 μm from LP, significantly higher than the SMO or the SLA samples. The WLI measurements (R_a = 6.87 ± 0.29) for the TPS were not significantly different from the LP measurements for the same samples. However, there was significant difference ($p<0.05$) in the roughness values measured with both instruments for the SLA in comparison with the TPS samples. These values were comparable with values given in the literature for the TPS surface measured using WLI (5.2 μm) by Boyan et al. (2002) or the roughness values (R_a) of 5.21 μm measured by Lossdörfer et al. (2004) with a laser profilometer.
In general, the values measured using WLI were reasonably similar and not significantly different to those using LP for the SLA, slightly smaller, but again not statistically significant for the TPS surfaces, but were over an order of magnitude smaller for the SMO surfaces. This was probably due to the SMO discs being very smooth and the smallest curvature being detected as roughness; in addition the WLI is more precise, especially for small height differences. Another possible explanation is that the LP has reached its limitation and cannot give much smaller readings for smooth areas than those presented by the SMO sample with the filter applied.

In this study all the samples analysed had roughness values similar to those in the literature for both instruments. However, is still difficult to make an exact comparison of the roughness recorded as details of the samples' preparation (in our case we do not know the exact details of polishing or SLA and TPS sample preparation) or instruments used are rarely quoted, similarly exact descriptions of the techniques used for roughness measurements are often lacking.

Table 3.1 below shows the actual surface area for SMO, SLA and TPS samples measured with the laser profilometry in mm^2. In measuring the surface area the

filter was not applied for the SMO sample as this does not influence the surface area measurement.

Sample	Area (mm^2)
SMO	16
SLA	23.3
TPS	23.9

Table 3. 1 The actual surface area for SMO, SLA and TPS samples measured with unfiltered laser profilometry over an area of 4 mm x 4 mm.

From the above table it can be observed that the smoothest samples (SMO) had an actual surface area of 16 mm^2, a value which coincides with the area measured (4 mm x 4 mm). The SLA samples had a total surface area of 23.3 mm^2 which was greater than the actual area measured and the area measured of the smoothest sample (16 mm^2). This confirmed again that the SLA samples were much rougher than the smooth samples. Furthermore, the large area increase will provide a greater area for bone contact and a greater active area for each sample, potentially increasing the activity and ion-release rates. The roughest samples were the TPS samples, with an actual surface area of 23.9 mm^2, which again was greater then the actual area measured or the area measured for the SMO samples, but was very similar to the SLA surface area. Their appearance confirmed that they were rougher than the SMO samples but of similar topography to the SLA samples.

To see if differences in the surface area and the step size influenced the roughness measurements, an area of 0.25 mm^2 (0.5 mm x 0.5 mm), almost 10 times smaller than the previous area measured was chosen. The step size was 1 μm and was very similar to the step size used for the WLI measurements (1.12 μm). This was chosen to see whether the same step size would give similar R_a measurements for both techniques. The R_a and the total surface area for all the samples were measured.

Figures 3.16, 3.17 and 3.18, present images recorded with the laser profilometer for a cp Ti (SMO) sample, a sandblasted and acid etched (SLA), and a titanium plasma sprayed (TPS) titanium sample taken over a small area

(0.5 mm x 0.5 mm). Table 3.2 shows a comparison in the R_a values measured with LP for the small and large areas. In recording the R_a the filter was applied for the SMO sample for both large and small areas but was not applied for the SLA and TPS samples.

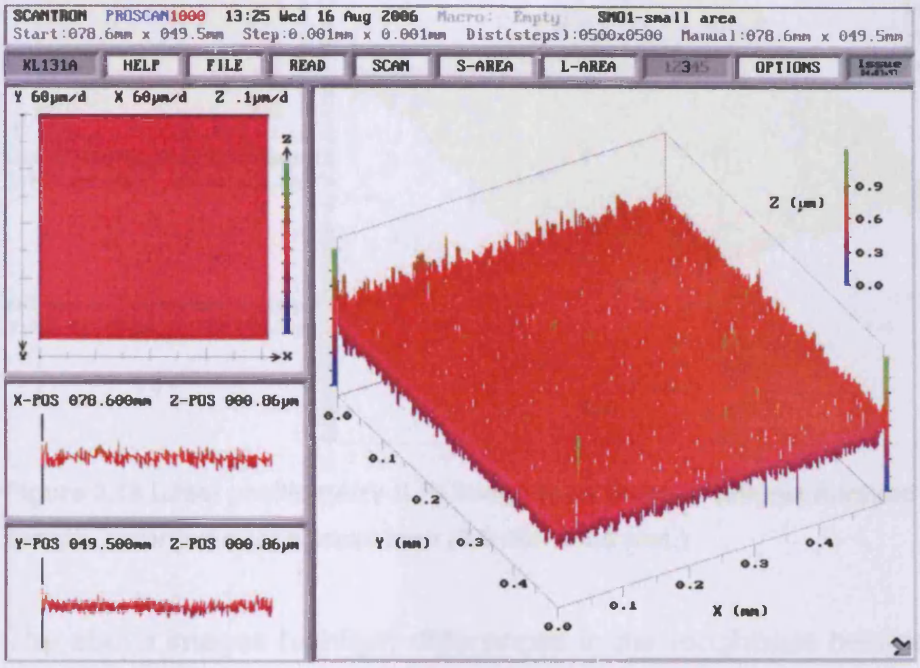

Figure 3.16 Laser profilometry (LP) image for a cp Ti (SMO) sample recorded over a small area (0.5 mm x 0.5 mm.)

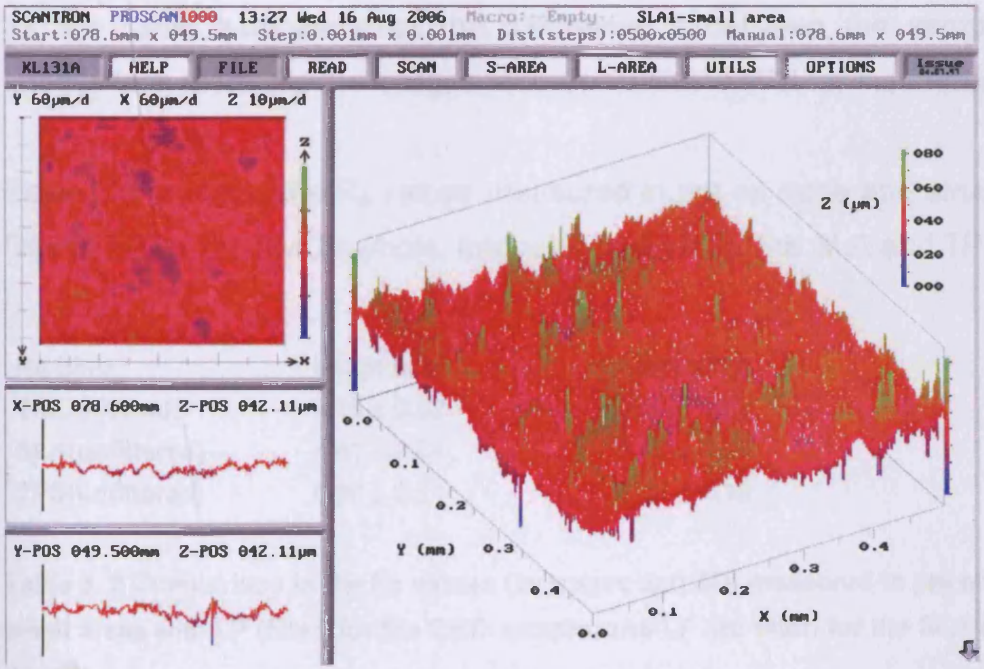

Figure 3.17 Laser profilometry (LP) image for a sandblasted and acid etched (SLA) titanium recorded over a small area (0.5 mm x 0.5 mm.)

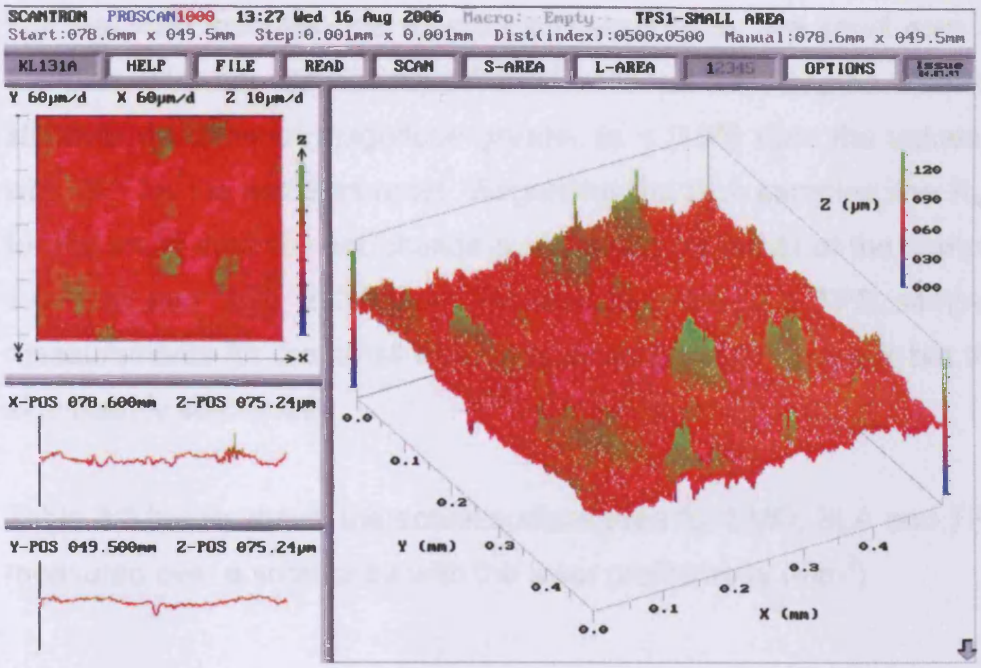

Figure 3.18 Laser profilometry (LP) image for a titanium plasma sprayed (TPS) titanium sample recorded over a small area (0.5 mm x 0.5 mm.)

The above images highlight differences in the roughness between the samples. The SMO sample is flat and smooth and both the SLA and TPS do not present a flat surface but more irregular and are rougher than the SMO sample. It is much clearer in these images compared to the images recorded over large area for the same samples what the difference is between the samples. These images look more like the images recorded with the WLI for the same samples.

Table 3.2 presents the R_a values measured in µm on large and small area with filtered LP for the SMO sample, and unfiltered LP for the SLA and TPS sample.

Ra (µm)	Large area	Small area
SMO(filtered)	0.15 ± 0.02	0.12 ± 0.03
SLA(unfiltered)	4.41 ± 0.64	3.86 ± 0.66
TPS(unfiltered)	6.66 ± 0.54	5.48 ± 1.16

Table 3. 2 Comparison in the Ra values (averages and SD) measured in µm on large and small areas with LP (filter) for the SMO sample, and LP (no filter) for the SLA and TPS samples.

For the SMO samples, the R_a values measured for the small area for the two samples were not significantly different between the samples. The values were still over an order of magnitude greater ($p < 0.05$) than the values measured with WLI for the same samples. Regarding the SLA samples, the R_a measured for the small area did not change significantly for either of the samples (4.41 ± 0.64 µm and 3.86 ± 0.66 µm respectively). For the TPS samples, the R_a measurements for the small area decreased for both samples, but this was not significantly statistically.

Table 3.3 below shows the actual surface area for SMO, SLA and TPS samples measured over a small area with the laser profilometry (mm^2).

Sample	**Area (mm^2)**
SMO	0.25
SLA	0.95
TPS	0.71

Table 3. 3 actual surface area (mm^2) for SMO, SLA and TPS samples measured over a small area (0.5 mm x 0.5 mm) by laser profilometry.

The SMO samples had an actual surface area of 0.25 mm^2, which coincided to the actual surface area measured (0.5 mm x 05 mm).
The SLA samples showed an almost 4 times increase in the actual surface, and the TPS samples had a total surface area of 0.75 mm^2, which increased three times when compared with the actual area measured for the same sample, or the total surface area measured for the SMO samples. There is a major difference in the increase of the surface area for the small area for the SLA and the TPS samples compared with the large area, where the surface area increased by 1/3 only. This may be due to the fact that a small step size was used in recording the scan and, as both the SLA and the TPS have a rough and irregular surface, a small step size allowed a more detailed measurement of the surface.

The area of the surface analysed and the step size did not appear to markedly influence the LP roughness measurements but did influence the total surface

area measured in relation to the topography of the samples. Also the roughness values measured with LP on a small area with the filter applied were again over 10 times greater for the SMO samples when compared with the WLI samples. However, there was no significant difference in the roughness measurements between large and small areas for the SLA and the TPS samples. As the step size for the small area LP and the WLI measurements were the same, it appeared that the difference in the roughness values between both the techniques could not be attributed to this factor.

3.2.2 Roughness measurements of commercially pure titanium discs polished in-house.

In order to assess the surface roughness of samples polished at the Eastman, six samples were polished using the first polishing method (details in Chapter 2). Their surfaces was assessed using both laser profilometry and white light interferometry. R_a values and total surface area were calculated. As the picture for the cp Ti discs from the LP looked different from the previous SMO samples in terms of the sample's curvature, a filter in the software was again necessary to be used to correct this. A surface filter no 2 was chosen, as in previous experiments, to remove curvature effects on the sample.

Appearance

Figure 3.19 presents a picture of both unpolished and in-house polished commercially pure titanium.

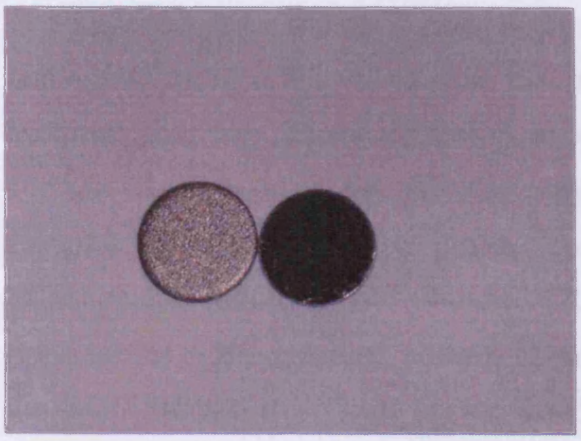

Figure 3.19 Picture of unpolished (left) and polished (right) cp Ti discs.

The surface of un-polished Ti appeared matt silver-grey.

The surface of polished cp Ti was similar to the surface of the SMO sample described earlier, appearing shiny silver with a mirror finish. Minor scratches were visible with the naked eye on a few of the samples. This was due to the softness of Ti and its poor abrasion resistance. However it proved very difficult to capture photographically the details of the surface of the polished sample as this was highly reflective.

Topography

The figures presented below show images taken with SEM, LP and WLI for cp Ti sample polished in-house.

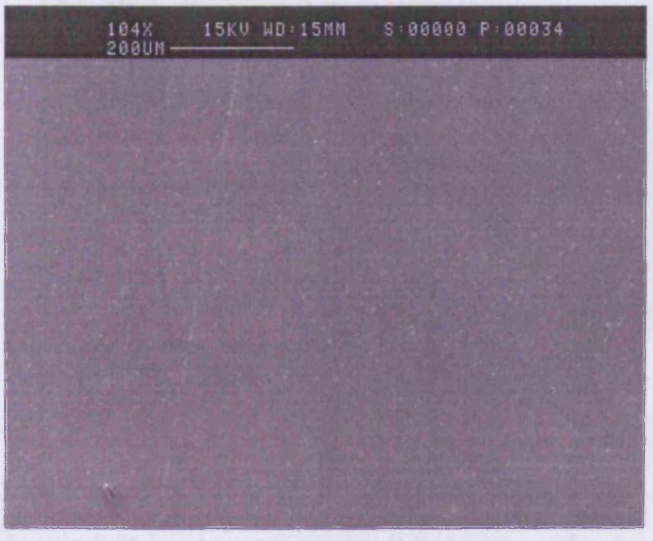

Figure 3.20 SEM image for commercially pure titanium sample (cp Ti) recorded at 104 x magnification.

The SEM image for the cp Ti sample (figure 3.20) shows a smooth surface, with some dots representing silica from the polishing, grooves and scratches, again from the polishing. These surface features are randomly distributed across the surface. Scratches on the surface may also appear due to handling of the samples. The SEM image of the in-house polished sample was similar to the SEM image recorded by Shinawi (2003) for her polished samples. The appearance of the polished sample above was different from the appearance of the SMO sample described earlier, as the SEM image recorded for the above sample shows more scratches and impurities on the sample. The features observed for the samples in the SEM are not in agreement with the SEM sample description by Ameen et al. (1993). These authors demonstrated the presence of pitting and pores on the surface of cp Ti, prepared to either a rough finish to simulate the surface of an implant or to smooth finish, to resemble an abutment. However, they believed that these are related to the hydrocarbon overlayer.

Images recorded with LP (without and with the filter) for a cp Ti sample polished in-house are presented below (figures 3.21 and 3.22).

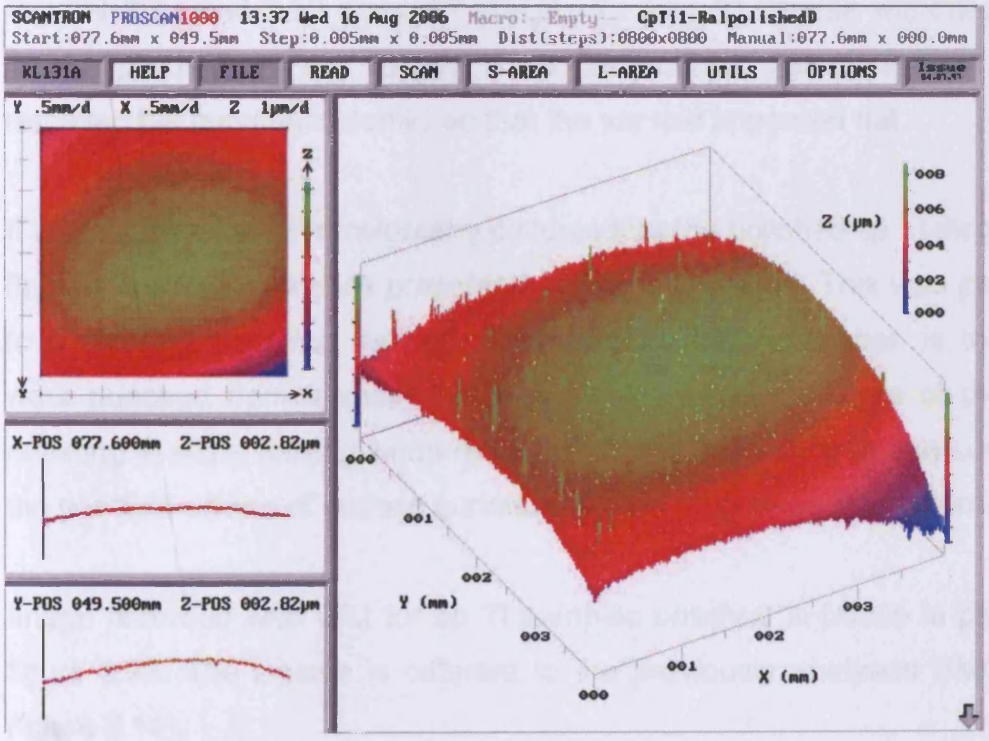

Figure 3.21 Laser profilometry (LP) image without a filter for a cp Ti sample polished in-house recorded over an area of 4 mm x 4 mm.

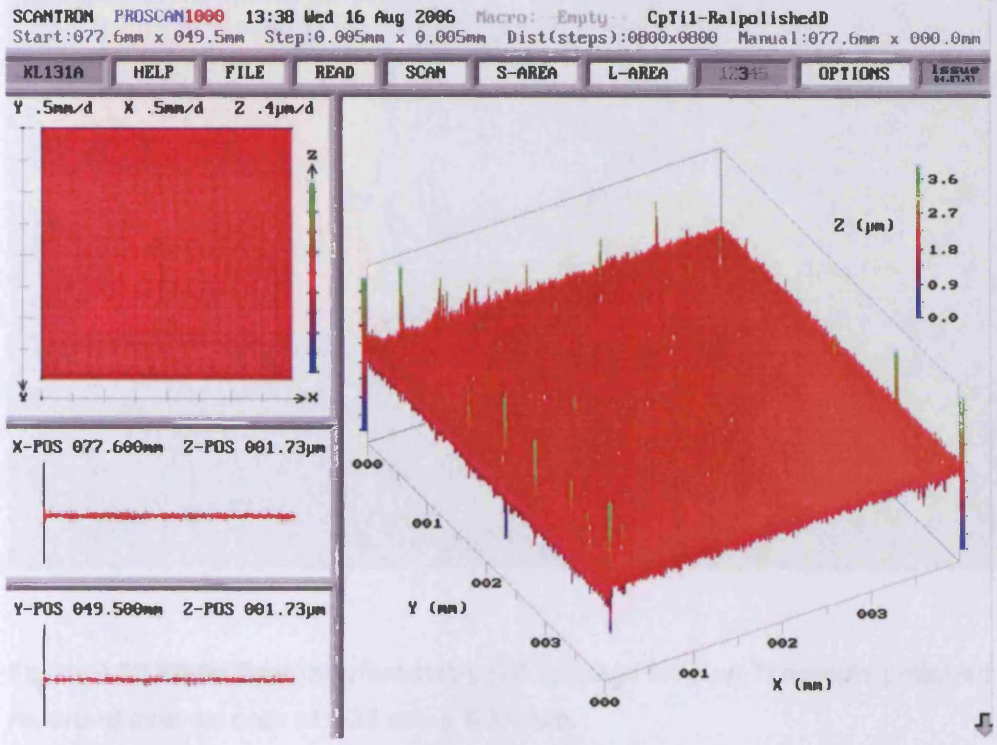

Figure 3.22 Laser profilometry (LP) image of a cp Ti sample polished in-house recorded over an area of 4 mm x 4 mm using a no 2 filter.

Figures 3.21 and 3.22 show LP images for a cp Ti sample without and with a filter applied. From the images it can be noticed that application of a filter removed the curvature (dome) so that the sample appeared flat.

It is clear from the LP profilometry pictures that the polished cp Ti discs were not flat like the SMO samples presented above, but domed. This was possibly due to a different polishing method. Another possible explanation is that as they were punched from a sheet this may have caused curvature of the samples resulting in slight rocking when mounted. It was interesting to see subsequently the possible effects of surface curvature on the roughness measurements.

Image recorded with WLI for cp Ti samples polished in-house is presented in figure 3.23. The z-scale is different to the previously analysed SMO samples (figure 3.10).

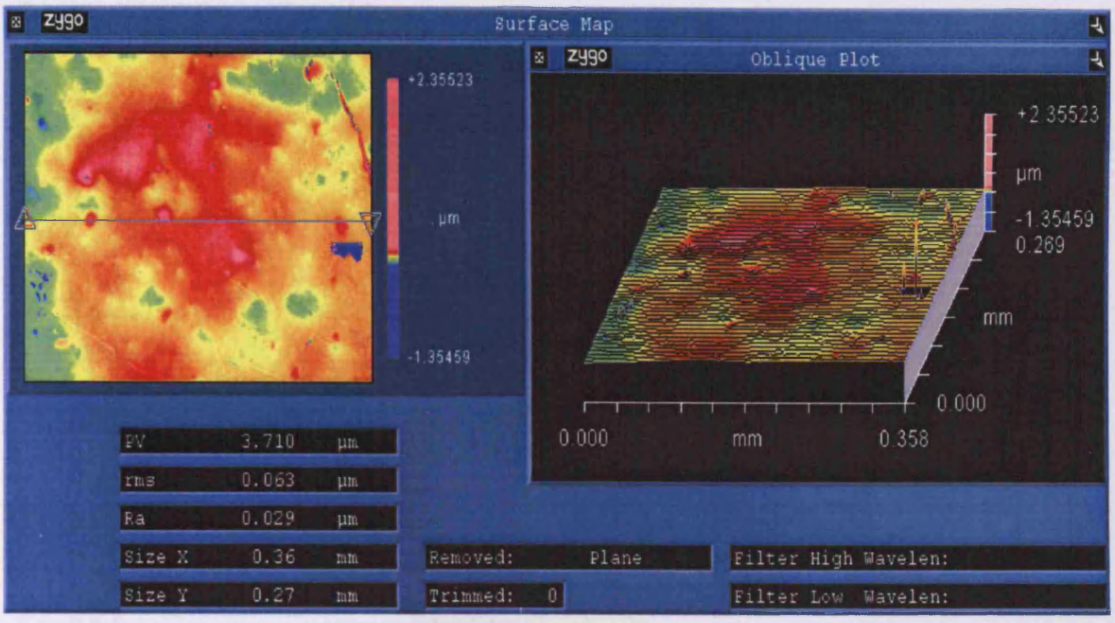

Figure 3.23 White light interferometry (WLI) image for a cp Ti sample polished in-house recorded over an area of 0.36 mm x 0.27 mm.

The WLI images for the cp Ti sample show a reasonably smooth sample with some irregularities on the surface, pits and very few spikes.

Roughness

Figure 3.24 presents the R_a values (averages and SD) measured for cp Ti samples (in µm) with LP (unfiltered) and WLI.

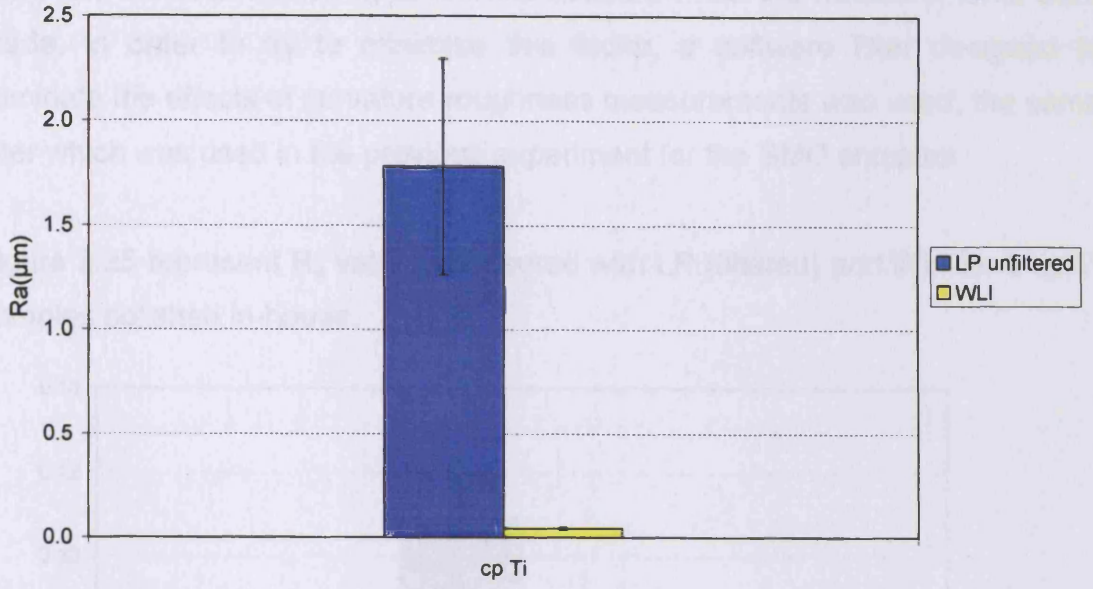

Figure 3. 24 Comparison between Ra values (average and standard deviation) for a cp Ti samples polished in-house and measured with unfiltered LP and WLI.

The R_a average value for the cp Ti samples was very high, with an average of 1.78 ± 0.5 µm. The R_a average values measured with the WLI had very small values, significantly lower than the LP roughness measurements ($p<0.05$) and significantly different ($p<0.05$) to the values recorded with the WLI for the SMO samples described earlier (experiment 3.3.1), and were in the region of 0.04 ± 0.01 µm. The average value recorded for the WLI was smaller than the R_a values recorded by Yoshinary et al. (2000) of 0.07 ± 0.01 µm on cp Ti surfaces. These had been polished mechanically to 1200 grit then polished using 0.3 µm alumina and finally ultrasonically cleaned with acetone, and had similar surface roughness as assessed with WLI measurements to those described by Shinawi (2003) using the same instrument. Chauvy et al. (1998) described R_q values of 0.08 µm on cp Ti surfaces. Since R_q values are usually higher than R_a values it may be proposed that again the measurements in this study were broadly in agreement with the literature.

It is clear from the figure that a discrepancy exists between the roughness values measured with the laser profilometer and the white light interferometer, with the LP values very high when compared with the WLI values. These very

high R_a values for the laser profilometry are probably due to the curvature of the samples, which was not fully taken into account when the measurements were made. In order to try to minimise this factor, a software filter designed to eliminate the effects of curvature roughness measurements was used, the same filter which was used in the previous experiment for the SMO samples.

Figure 3.25 represent R_a values measured with LP (filtered) and WLI for 6 cp Ti samples polished in-house.

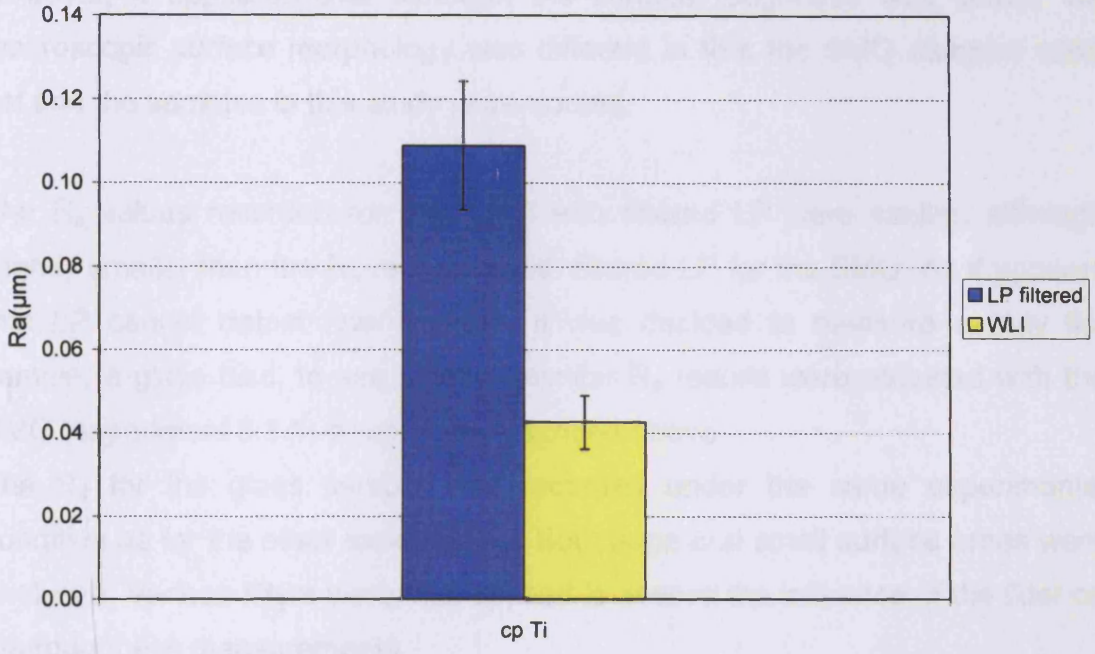

Figure 3.25 Comparison between Ra (average and standard deviation) for cp Ti samples polished in-house measured with filtered LP and WLI (n = 6.)

It can be observed that following application of the filter the R_a values measured with the LP were over 10 times smaller, more uniform, and approaching the WLI values compared with the unfiltered roughness measurements presented before. The average R_a value for the six samples measured with laser profilometry after the filter was applied was significantly lower ($p<0.05$), 0.11 ± 0.02 µm, than the unfiltered value (1.78 ± 0.4 µm). However, the LP roughness value (average) recorded for the six cp Ti samples with the LP after the filter was used was still significantly greater ($p<0.05$)) than the R_a average value measured with WLI for the same six cp Ti samples (0.04 ± 0.006 µm), as found

in the previous experiment for the SMO samples (section 3.3.1). Application of the filter appears to be very important in recording the roughness for the samples where the surfaces are curved, as it removes the curvature effects and allows only the roughness to be measured.

The R_a measurements were again different when using both methods of surface analysis: LP and WLI. The values measured using WLI were similar to those measured from SMO (Straumann polished) surfaces (0.015 ± 0.002 μm). However, it appeared that although the surface roughness was similar the macroscopic surface morphology was different in that the SMO samples were flat and the samples in this study were domed.

The R_a values recorded for the cp Ti with filtered LP were similar, although slightly smaller than the R_a recorded with filtered LP for the SMO. As it appears that LP cannot detect finer surface, it was decided to measure a truly flat sample, a glass disc, to see whether similar R_a results were obtained with the SMO (experiment 3.3.1) or cp Ti as described above.

The R_a for the glass sample was recorded under the same experimental condition as for the other experiments. Both large and small surface areas were analysed. Various filters were also applied to assess the influence of the filter on the roughness measurements.

It was found that the R_a (average) for the glass sample over a large area (4 mm x 4 mm) was 0.09 ± 0.01 μm, not significantly different from the R_a recorded for the cp Ti samples. There was also no difference in the R_a recorded over large and small areas.

It is clear now that the difference in the R_a values recorded with LP and WLI for the smooth samples may be partly due to the resolution limit of LP at the bottom of its measurement range.

3.2.3 Roughness measurements of commercially pure titanium discs polished in-house before and after Ca ion implantation.

Six samples polished in-house were assessed before and after Ca implantation using white light interferometry to observe whether Ca ion implantation would modify the surface roughness. R_a roughness measurements are presented below.

Appearance

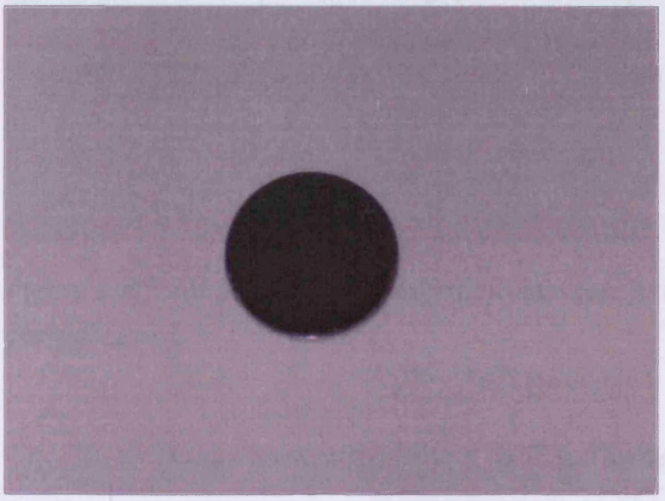

Figure 3.26 Picture of a calcium implanted titanium sample (Ca-Ti).

Looking at the Ca-Ti samples it could be noticed that their colour or texture did not change visibly following ion implantation. The Ca-Ti surfaces (implanted with $^{40}Ca^{+}$ at a dose of 1 x 10^{17} ions cm^{-2}, using an implantation energy of 40 keV) were similar to the cp Ti and were shiny silver. This was in contrast to Hanawa's samples (1997), which were described as 'gold' after Ca ion implantation, or with the Ca implanted Ti analysed by Krupa (2001) whose samples were subsequently light yellow. This difference in colour was attributed to the oxidation process which occurs at the surface, but may also be due to different implantation procedures, which may result in different surface and sub-surface characteristics of the samples. Indeed, the implantation was carried out at an in energy of 18 keV by Hanawa. In Krupa's experiment, the implantation was

carried out using 1×10^{17} Ca^{+} / cm^{2} and the ion energy was 25 keV, different from the conditions in the current study, which employed 40 keV.

Topography

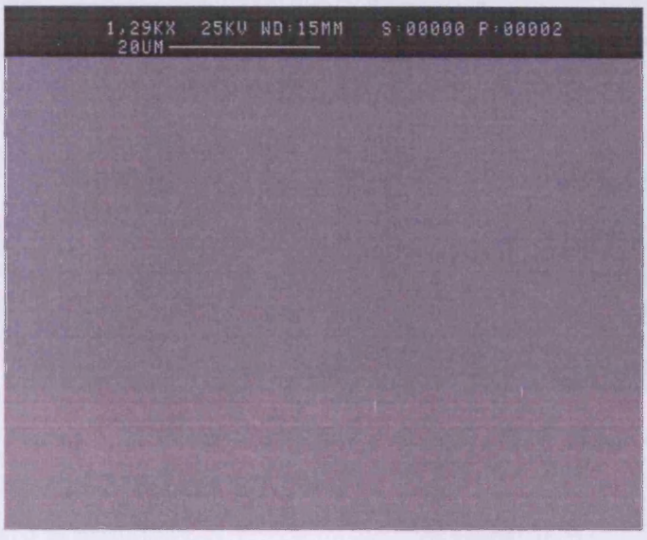

Figure 3.27 SEM image for Ca implanted titanium sample (Ca-Ti) recorded at 1290 x magnification.

The SEM image shows that the Ca-Ti samples had a similar appearance to the cp Ti samples and were generally smooth with no scratches and grooves. If the implantation process had changed the surface in any way, it was evident that it was beyond the capabilities of the SEM to detect them.

Images for a Ca-Ti sample recorded by WLI are presented in figures 3.28.

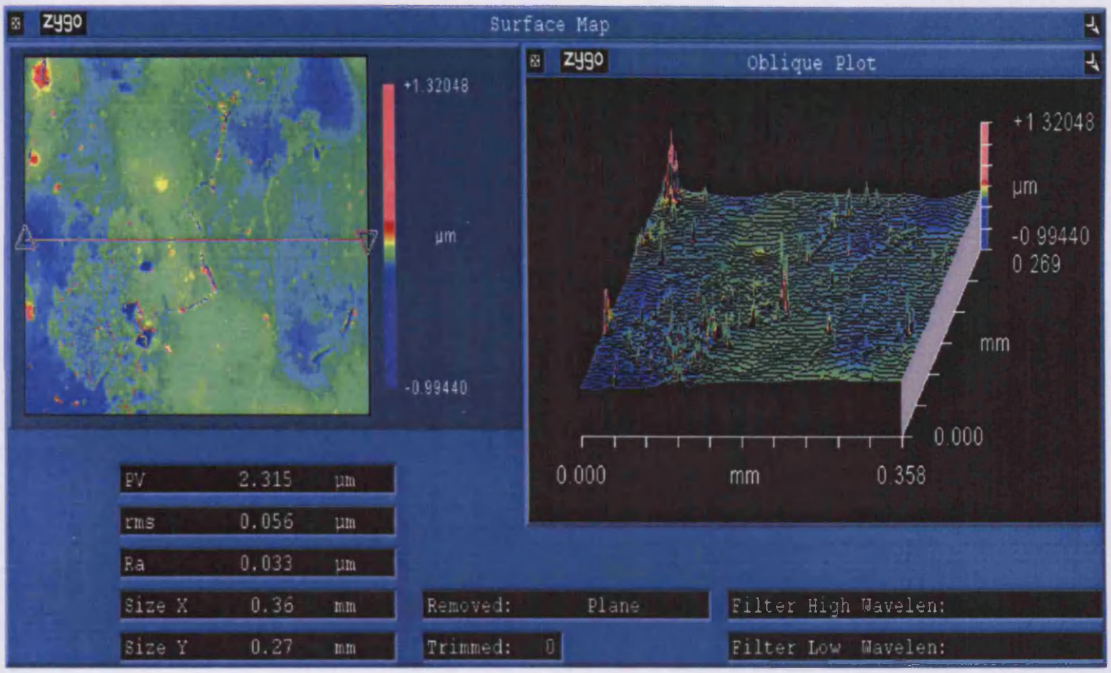

Figure 3. 28 White light interferometry (WLI) image of a Ca-Ti sample recorded over an area of 0.36 mm x 0.27 mm.

From the above figure it can be noticed that the Ca-Ti sample had a fairly smooth surface, with some irregularities and few spikes. When compared with the WLI image for the cp Ti samples (figure 3.23), the Ca-Ti sample was not very different and presented slightly more surface spikes and pits.

Roughness

The R_a values (average and SD for 6 cp Ti samples) measured with the white light interferometer are presented in figures 3.29 and 3.30.

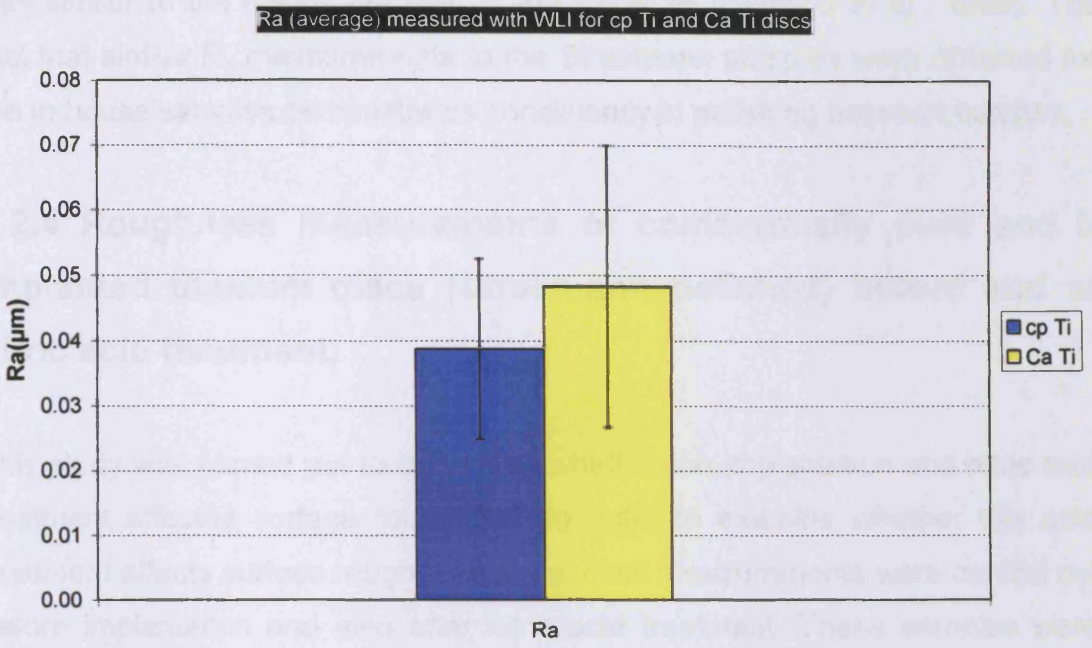

Figure 3. 29 Comparison between Ra values (average and SD) measured with WLI for titanium samples polished in-house before (cp Ti) and after (Ca-Ti) Ca ion implantation.

The R_a average values measured with WLI for the cp Ti samples increased slightly, but not significantly, from 0.04 ± 0.01 µm before ion implantation to 0.05 ± 0.02 µm after. The average value for cp Ti measured with WLI was comparable with the WLI values measured for previous samples polished in-house (0.04 ± 0.01 µm), but was significantly bigger ($p < 0.05$) than the average R_a value measured with the WLI for the SMO samples provided by Straumann (0.015 ± 0.00 µm). The average value for Ca-Ti measured with WLI was smaller than the R_a measured for Ca-Ti samples by Yoshinari et al. (2000). The authors reported a R_a average value for Ca-Ti of 0.1 ± 0.01 µm. This difference may be due to the fact that this Ca-Ti was implanted with 5×10^{17} ions/cm^{2,} at a voltage of 41 keV. They found that the Ca-Ti promoted more bacterial adhesion (P. Gingivalis and A. Actynomicetenscomitans) than cp Ti, thus potentially promoting the adhesion of plaque on surfaces exposed to the oral cavity, even though the Ca implantation is beneficial for bonding to hard tissue.

Implantation of cp Ti with Ca did not produce a significant increase in the surface roughness, as measured with the white light interferometer (WLI). This

was similar to the results reported in the literature (Hanawa et al., 1996). The fact that similar R_a measurements to the Straumann samples were obtained for the in-house samples demonstrates consistency in polishing between batches.

3.2.4 Roughness measurements of commercially pure and ion-implanted titanium discs (Straumann polished) before and after nitric acid treatment.

This study was carried out to determine whether ion implantation and nitric acid treatment affected surface roughness. In order to examine whether this acid treatment affects surface roughness, roughness measurements were carried out before implantation and also after nitric acid treatment. These samples were used in *in vitro* cell experiments at the UCL Eastman Dental Institute.

Commercially pure titanium discs (cp Ti) supplied by the Straumann Institute (Waldenburg, Switzerland) were used throughout the experiments. From these samples, a large number were implanted with calcium and argon (details of the implantation were given in chapter 2). Following implantation, all the discs (implanted and non-implanted) were treated with nitric acid (10% HNO_3 for 10 minutes) to examine whether this treatment had an influence on the surface roughness. 6 cp Ti, 6 Ar-Ti and 6 Ca-Ti samples were analysed prior to nitric acid treatment with white light interferometry. All samples were randomly selected from their corresponding batch of samples. Their average R_a values were compared statistically using the t- test.

Following nitric acid treatment, randomly selected cp Ti, Ar-Ti and Ca-Ti samples (6 of each) were again analysed using white light interferometry, and their mean R_a values compared in the same way. Again, their average R_a values were compared statistically using the t- test.

The discs were kept wrapped in aluminium foil in the desiccator at all times to minimise contamination, only being removed when required for analysis. R_a was measured. For the R_a, for each type of disc, an average was calculated from 6 samples.

Appearance

The cp Ti (SMO) and Ca-Ti samples looked similar to the previously described SMO samples and were shiny silver. The Ar-Ti surfaces looked similar to the cp Ti and Ca-Ti samples.

After nitric acid treatment the implanted samples changed colour to dark silver. This behaviour for the Ca-Ti samples is in agreement with Ca-Ti samples polished in-house and passivated following the same protocol, where the samples also went dark silver (details in Chapter 4).

Topography

The pictures and SEM images recorded for the SMO, Ca-Ti and Ar-Ti samples looked similar to previous pictures and images presented before and are not shown for this experiment.

Presented below are images from the WLI for SMO, Ca-Ti and Ar-Ti before and after nitric acid treatment. Figure 3.30 presents images taken with WLI for the SMO sample before and after nitric acid treatment.

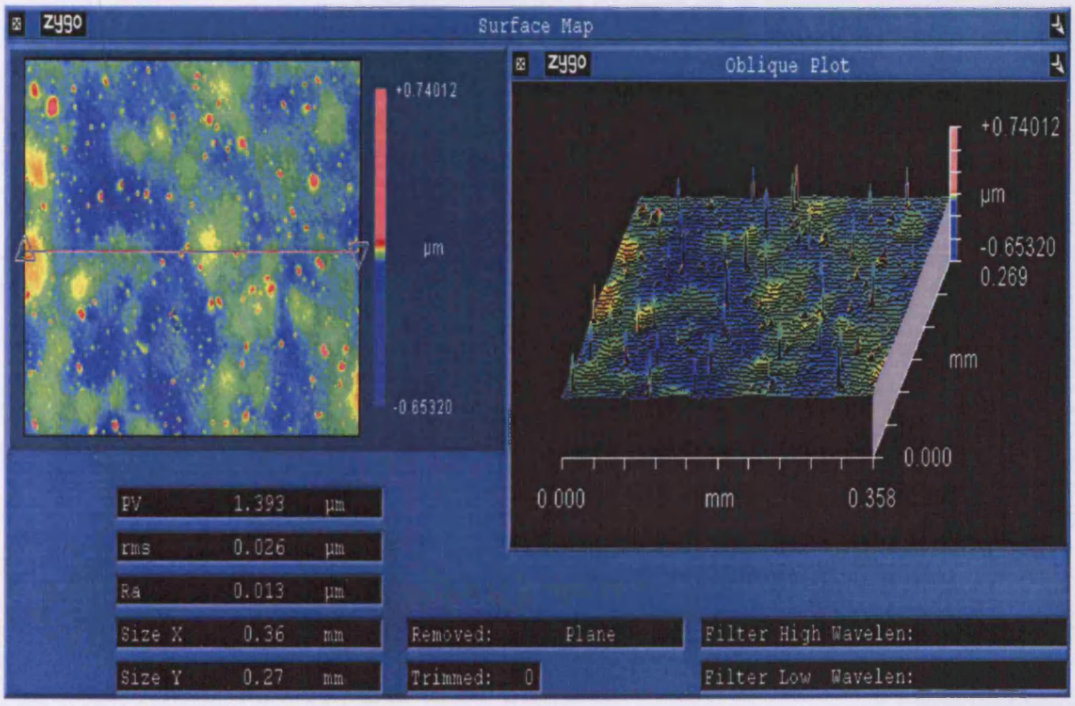

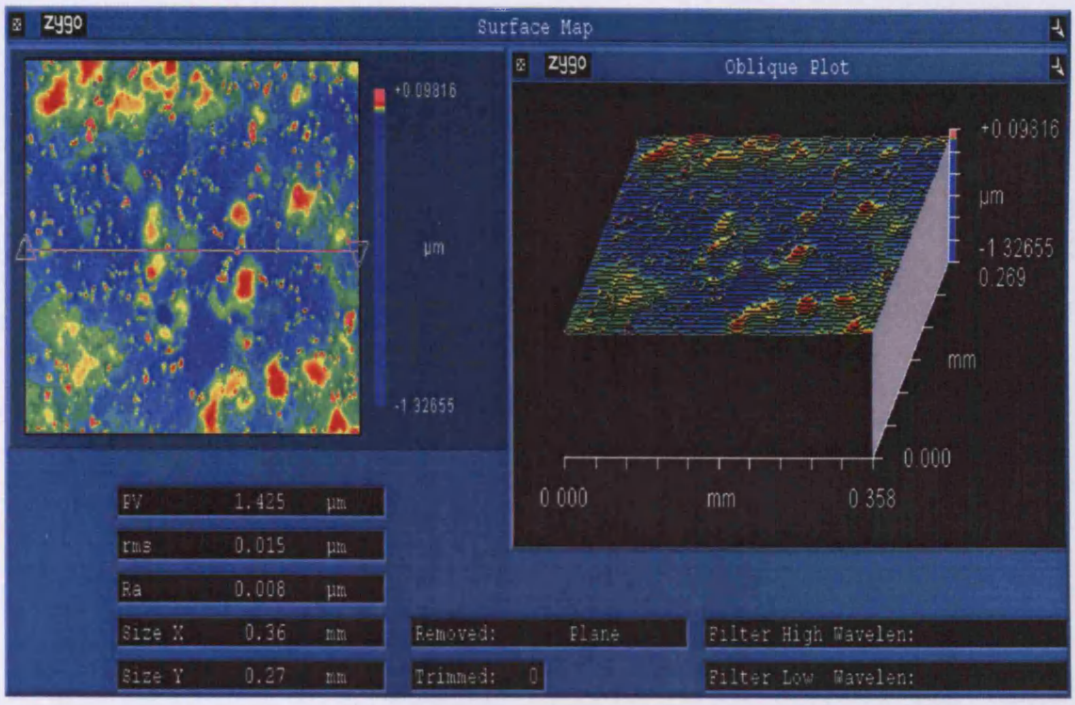

Figure 3. 30 White light interferometry (WLI) image of a cp Ti sample recorded over an area of 0.36 mm x 0.27 mm before (first row) and after (second row) nitric acid treatment.

Before treatment with HNO_3, the samples looked rough with irregular surface, spikes and dots. After treatment, the surfaces appeared smoother, without spikes and were less irregular.

Figure 3.31 presents images taken with WLI for the Ca-Ti sample before and after nitric acid treatment.

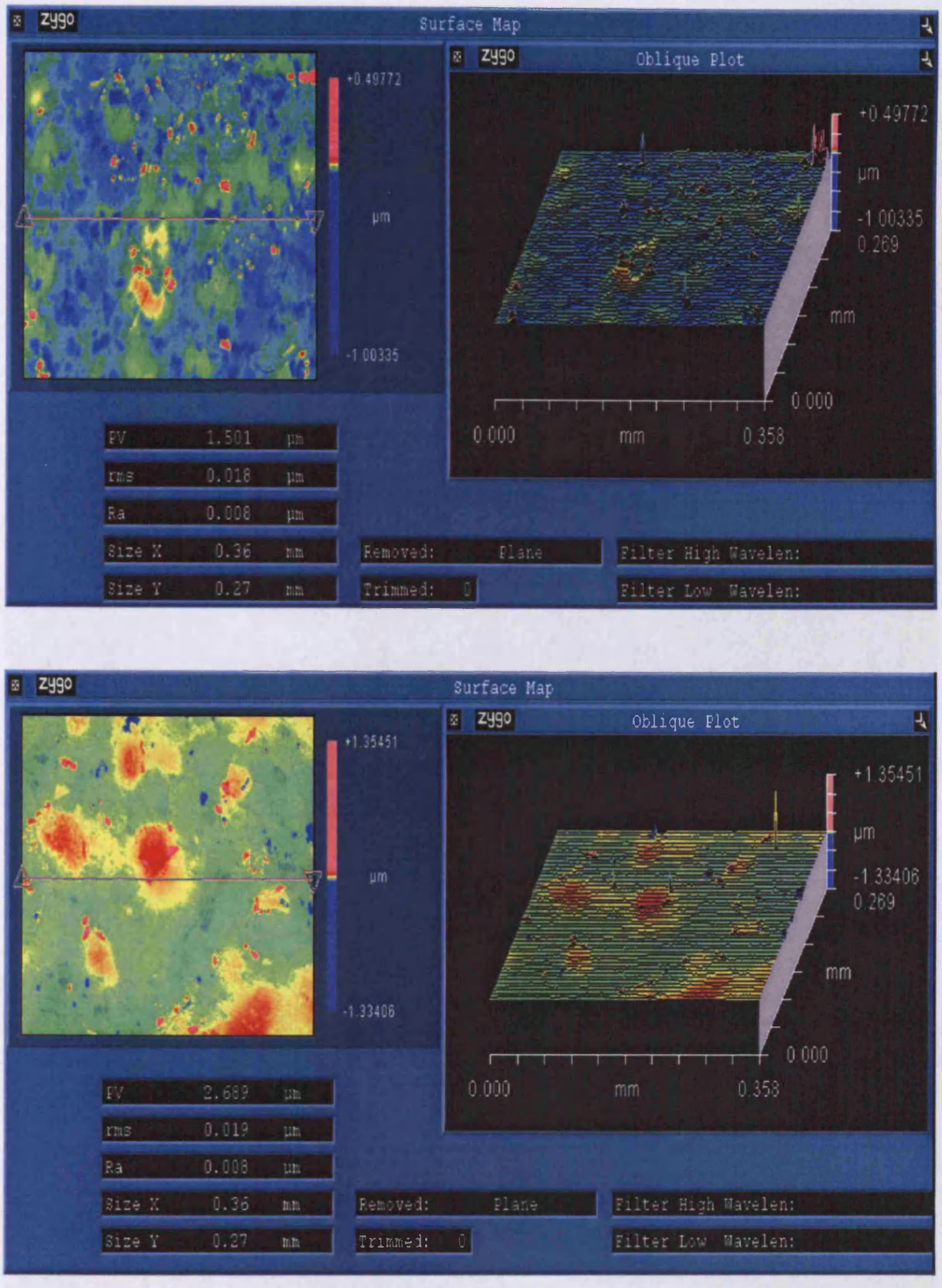

Figure 3. 31 White light interferometry (WLI) image of a Ca-Ti sample recorded over an area of 0.36 mm x 0.27 mm before (first row) and after (second row) nitric acid treatment.

Before HNO_3 treatment, the Ca-Ti sample looked slightly smoother than the SMO sample presented previously, with only a few spikes present on the surface, fewer than for the SMO sample. However, as the z-scale is highly

exaggerated they could be round particles (dust). After HNO_3 treatment, the surface looked smoother and the spikes were almost entirely removed.

Figure 3.32 presents images recorded with WLI for the Ar-Ti sample before and after nitric acid treatment.

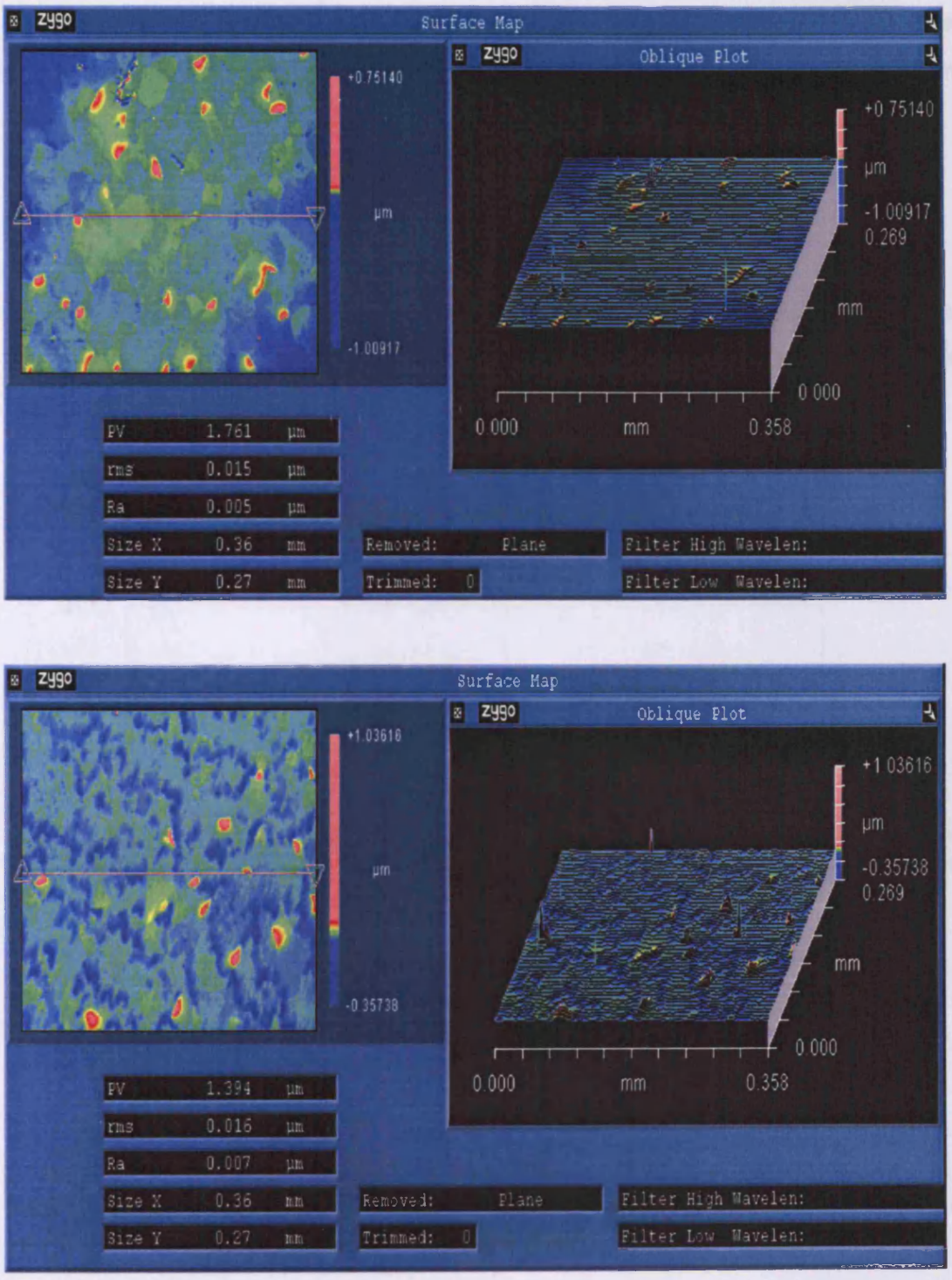

Figure 3. 32 White light interferometry (WLI) image of an Ar-Ti sample recorded over an area of 0.36 mm x 0.27 mm before (first row) and after (second row) nitric acid treatment.

Before HNO_3 treatment the sample looked smooth with almost no spikes present on the surface. Treatment with HNO_3 did not change significantly the appearance of the surface, with some spikes and dots still present.

From the above figures it can be noticed that the samples are flat and present some irregularities on the surface, which are less pronounced after treatment with HNO_3.

Roughness

Figure 3.33 presents results for R_a roughness values (averages) measured with white light interferometry (WLI) for the cp Ti, Ca-Ti and Ar-Ti surfaces, before and after nitric acid treatment (HNO_3).

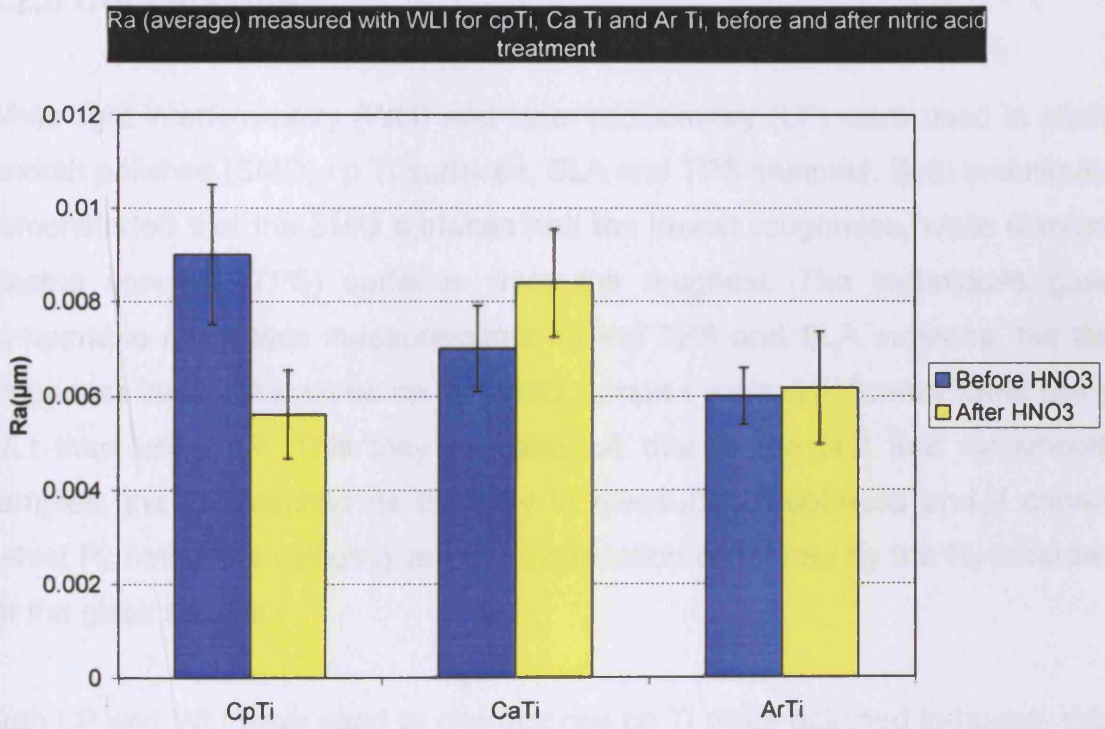

Figure 3. 33 Comparison between Ra values (average) measured with WLI for cp Ti, Ca-Ti, and Ar-Ti before and after nitric acid treatment (HNO_3).

From the left column of the figure 3.33 it can be observed that before nitric acid treatment, the roughness values (averages) for all the samples looked similar, and no significant difference were detected between the samples.
The R_a (average) values (right column), decreased after nitric acid treatment for the cp Ti samples to 0.006 μm. However, this decrease was not statistically significant. The R_a average value for the Ca-Ti samples increased, but not significant, to 0.008 μm. The R_a average value for the Ar-Ti samples remained unchanged following nitric acid treatment. The non-implanted samples were the smoothest. Nitric could be cleaning the surface of polishing debris, but does not modify the roughness as measured with WLI for cp Ti, Ca-Ti and Ar-Ti.

As a conclusion, there was no significant difference between the variation in the R_a values (averages and SD) measured with WLI between the cp Ti and ion implanted samples, before and after nitric acid treatment.

3.2.5 Conclusions

White light interferometry (WLI) and laser profilometry (LP) were used to study smooth polished (SMO) cp Ti surfaces, SLA and TPS samples. Both techniques demonstrated that the SMO surfaces had the lowest roughness, while titanium plasma sprayed (TPS) surfaces were the roughest. The techniques gave comparable roughness measurements for the TPS and SLA surfaces, but the roughness values measured on the SMO samples were significantly lower using WLI than using LP. This may probably be due to the fact that for smooth samples, the LP reached its capacity in measuring roughness and it cannot detect R_a below the values given, an explanation confirmed by the R_a recorded for the glass sample.

Both LP and WLI were used to characterise cp Ti discs polished in-house. WLI only was used to characterise cp Ti polished in-house before and after Ca ion implantation. The R_a values measured with LP for the cp Ti samples were found initially to be much greater than the values given in the literature and also much greater than the R_a values measured with WLI for the same six cp Ti samples.

This was most likely due to surface curvature and the use of a filter to remove this effect was explored. The filter indeed removed the curvature and gave much smaller roughness results, which were comparable with the R_a values for the SMO Straumann polished samples and also with the values quoted in the literature. However, the values were still significantly higher than the values recorded for the same samples with the WLI, for the reasons given above.
Analysing in-house polished cp Ti following refinement to the technique, the same results were obtained, which confirmed that a good polishing method which gave roughness values similar to the literature for both experiments had been developed.

WLI was also used to compare the roughness of smooth polished cp Ti (samples supplied by Straumann), and samples implanted with Ca and Ar ions before and after nitric acid treatment. Neither ion implantation nor nitric acid treatment was found to influence the surface roughness of the samples, which remained unchanged. The roughness values measured for the Ca-Ti samples gave similar values with the R_a values measured the for Ca-Ti (in-house polished Ti) samples. These consistent results confirmed once again that quality polished Ti samples (both cp Ti and Ca-Ti), comparable with manufacturer's samples, were obtained at the Eastman.

Undeniably, LP and WLI can measure roughness, but they gave consistently different results when very smooth samples were analysed. This is consistent with the literature (Wenneberg, 2000), who found that different techniques gave different roughness measurements.
It appears that Ca ion implantation has no impact on the surface topography as measured with WLI. This may suggest that any changes in cells response cannot be due to topography as measured at this level. It is still possible, however, to have topography changes at lower level (atomic scale changes) not resolved by WLI, which might still affect cells response. Another possibility is that cells response could be purely due to chemical changes at the surface, with no influence from surface topography changes.

3.3 SURFACE CHEMISTRY

3.3.1 XPS surface studies

As indicated earlier, it is now accepted that surface properties will influence the initial response of the body to the implanted material. These interactions occur at the atomic level and are highly dependant on the surface chemistry of the biomaterial, which will influence the type and orientation of adsorbed molecules. As described in Chapter 1, physical and chemical properties of titanium play an important role in the response of the body following placement of an implant. Titanium has a native oxide layer present on the surface. This layer develops in contact with air or water (fluids), is generally around 0.5-7 nm thick, self-repairing, and strongly resists corrosion (Sunny, 1991). It is passive and is strongly attached to the surface and does not disintegrate in the physiological environment. It is this oxide layer which makes this material biocompatible and encourages osseointegration when dental implants are placed in the body.

Modifications have been made to Ti surfaces in order to improve the long-term clinical results of dental implants as clinical failures of osseointegration are still reported (Esposito, 1998). It has been shown that even subtle differences in the surface composition can modify cell response even when surface roughness is kept constant (Links et al., 1998)

It is therefore very important to characterize the surface of cp Ti and Ca-Ti in order to understand changes in their characteristics. The surface chemistry of the cp Ti and Ca-Ti was investigated by a number of analytical techniques to compensate for the limitations of each technique. XPS was employed for the analysis of the surface, but this instrument has a detection limit of 100-150 Å into the surface. Complemented with XPS depth profiling it was possible to get a profile of the distribution of the Ca ions into the depth of the sample.

Experimental

A very large number of titanium samples (over 600 cp Ti and 100 Ca-Ti) were analysed throughout this study with XPS to characterise the cp titanium surface. Two operating modes of XPS, a monochromated Al Kα X-ray source and an Al Kα twin anode source were used to analyse the surface during this time, so differences in Ti 2p spectra will be highlighted where they are due to the excitation source. Representative spectra and quantification will be presented for both cp Ti and Ca-Ti samples. Also, as two different polishing methods were used throughout the study, a comparison between the polishing method early on and toward the end will be given by presenting a table with the average composition over lots of samples for both polishing methods.

Qualitative analysis was carried out on the sample and included survey, Ti 2p, O 1s, C 1s, N 1s and Ca 2p spectra. This was based on the elements present in the oxide layer and also organic and inorganic contaminants. The Ca-Ti spectra are presented together with those for the cp Ti for comparison. Quantitative analysis was also performed using CasaXPS software. A quantification table showing elemental ratios for the elements present on the surface and a table showing atomic percentages are presented (details of the analysis were given in Chapter 2).

Results and discussion

Table 3.4 shows the average composition as elemental ratios from numerous samples for both polishing methods.

Date	C/Ti	N/Ti	O/Ti
2003	1.30 ± 0.52	0.11 ± 0.10	2.83 ± 0.47
2004	0.84 ± 0.27	0.07 ± 0.02	2.44 ± 0.08
2005	0.77 ± 0.17	0.03 ± 0.02	2.44 ± 0.25
2006	0.72 ± 0.13	0.02 ± 0.01	2.45 ± 0.09

Table 3. 4 Elemental ratios (average and standard deviation) for cp Ti samples polished in–house during the duration of the project using different polishing methods

Two different polishing methods were employed. The main differences were in the mounting of the samples, and their cleaning after polishing. The samples were mounted on a plastic jig using wax (method 1), or double-sided adhesive tape similar to that used by the Straumann Institute in their polishing protocol. Cleaning of the samples (details in Chapter 2) also differed between the two methods. Initially, 3 cycles of 5 min duration in each of acetone, propan-2-ol and UPW was used. This was subsequently reduced to 1 min per solvent and finally the acetone step was removed. These changes were made as the samples were no longer mounted on wax, which was a major source of contamination compared with the tape, and hence requiring more thorough cleaning.

From the quantification table it can be seen that the C/Ti and N/Ti ratios decreased as the polishing and cleaning processes were refined. The C/Ti ratio decreased significantly ($p < 0.05$) from 1.30, for the first polished samples (average from 12 discs) to smaller values later on (0.77 and 0.84 respectively). The N/Ti ratio also decreased, again significantly ($p < 0.05$), from 0.11 to 0.03. This decrease confirms that a continuous improvement in the polishing was achieved. This may be due to both the mounting of the samples, and improved handling of the discs during and following polishing.

The tables below (3.5-3.6) present atomic percentage and ratios of elements detected on cp Ti and Ca-Ti samples. The averages were calculated from 30 cp Ti samples and 22 Ca-Ti samples. From this point onwards for clarity only ratios are presented.

Sample	C 1s %	Ca 2p %	N 1s %	O 1s %	Ti 2p %
Cp Ti	19.5 ± 3.5	0.1 ± 0.1	0.6 ± 0.3	56.2 ± 2.9	22.8 ± 1.9
Ca-Ti	17.0 ± 0.8	4.8 ± 0.1	0.3 ± 0.3	55.4 ± 0.9	22.6 ± 0.6

Table 3. 5 Quantification of atomic percent ratios (including the average ratios and standard deviation for cp Ti samples analysed with a monochromated X-ray source.

Sample	C/Ti	Ca/Ti	N/Ti	O/Ti
cp Ti ratios	0.86 ± 0.19	0.00 ± 0.01	0.03 ± 0.01	2.48 ± 0.27
Ca-Ti ratios	0.75 ± 0.05	0.21 ± 0.01	0.02 ± 0.01	2.45 ± 0.09

Table 3. 6 Elemental ratios calculated for cp Ti and Ca-Ti samples (average + SD) analysed with a monochromated X-ray source.

Figure 3.34 presents the widescan spectrum of a representative polished cp Ti and Ca-Ti surface analysed using the monochromated X-ray source.

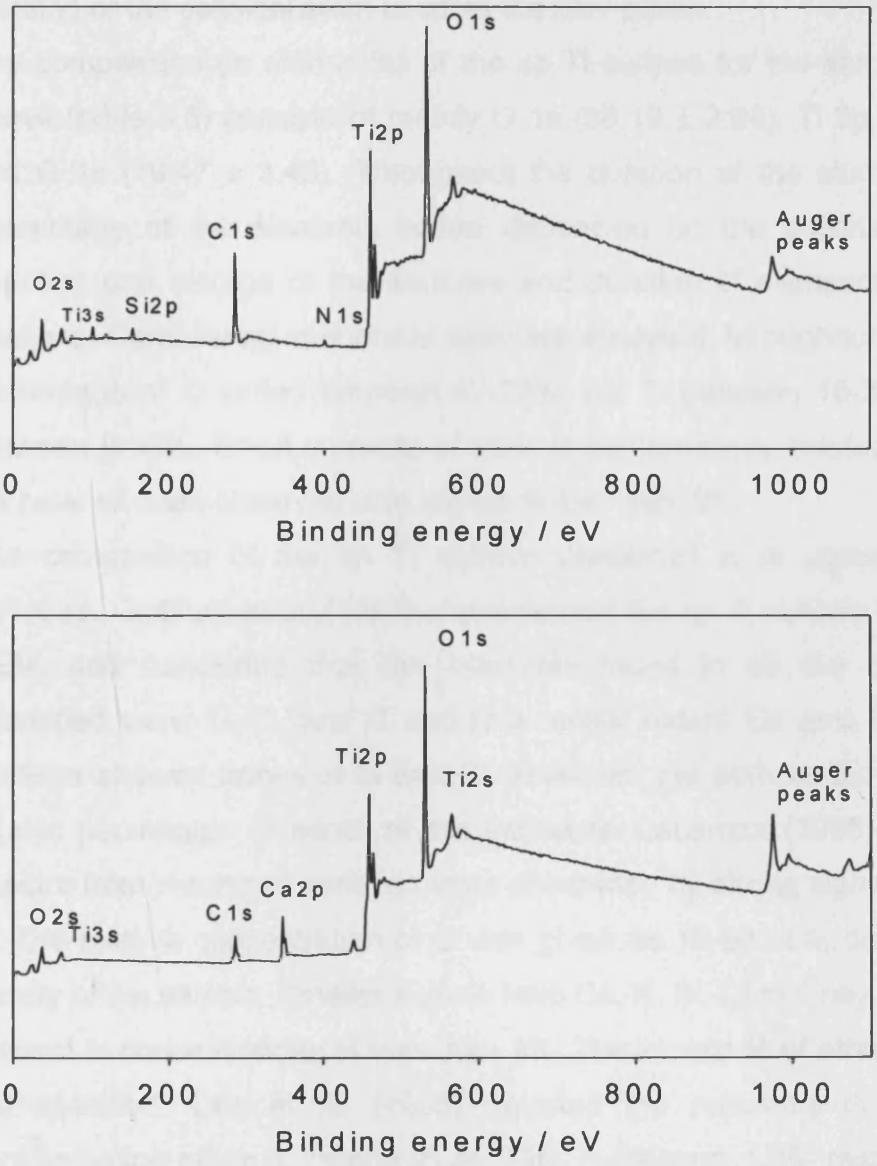

Figure 3. 34 The XPS widescan spectrum of a representative cp Ti sample (row 1) and Ca-Ti sample (row 2) analysed using a monochromated X-ray source.

The survey spectrum for cp Ti (figure 3.34, first row) is characterised by a variety of peaks at different intensities and binding energies. There are two strong peaks at E_B=530.4 and 458.9 eV which are due to the O 1s and Ti 2p photoelectrons from the oxide layer present on the surface of the sample. There is another prominent peak of lesser intensity at 285 eV from C 1s photoelectrons which are present on the surface as a result of contamination. There is a small intensity peak at 400 eV which is the N 1s binding energy. There is a small peak at ~ 152 eV and one minimal at ~ 345 eV and represent minute amount of Si and Ca and all are due to contamination. It is probable that the Si found on some of the samples may come from the SiC paper used for grinding or the colloidal silica used as the final polish.

The composition (in atomic %) of the cp Ti surface for the samples presented above (table 3.5) consists of mainly O 1s (56.19 ± 2.94), Ti 2p (22.81 ± 1.87), and C 1s (19.47 ± 3.48). Throughout the duration of the study however, the percentage of the elements varied depending on the polishing procedures, handling and storage of the samples and duration of exposure to air prior to analysis. Considering numerous samples analysed throughout this study the percentage of O varied between 47-72%, the Ti between 15-32%, and the C between 9-38%. Small amounts of various contaminants existed: N, Si, Al and Ca have all been observed with atomic % less than 2%.

The composition of the cp Ti surface presented is in agreement with the literature. Olefjford et al. (1993) characterized the cp Ti surface using XPS and SEM, and concluded that the elements found in all the dental implants examined were Ti, O, and C and to a lesser extent Ca and N. Some of the systems showed traces of Si and Cl. However, the authors did not specify the atomic percentage of either of the elements. Lausmaa (1996) found that the spectra from machined surfaces were dominated by strong signals of Ti, O, and C. The relative concentration of C was given as 10-80 at%, depending on the history of the sample. Smaller signals from Ca, N, Si, Cl etc may be occasionally present in concentrations of less than 1%. The atomic % of other elements was not specified. Ong et al. (1995) reported the presence of Al, Si and N contamination on cp Ti (grade 2) at 1-3%, 1-2% and < 2% respectively, which again is in agreement with the above data. Esposito et al. (1999), after examination of the surfaces of implant dental fixtures, stated that Si was only

detectable on samples stored in glass vials and not those stored in plastic vials, concluding that Si ion leaching from the glassware used was the source of Si detected on the samples. Occasionally, Cl and P may be detected on the samples, probably from water or glassware used during preparation of the samples. Al may be also found on the surface, as found very rarely on the samples presented in this study, and it was concluded that it came from the aluminium foil with which the samples were wrapped. Esposito et al. (1999) mentioned the presence of minute amounts of various contaminants on the surface, which may be either from the fabrication process or handling and storage of the samples. Ameen et al. (1993) reported the N percentage present on the surface of implants to be 6.02%, much higher than the percentage found for our samples. Additional peaks at $E_B \sim 24$ eV, ~ 37 eV, and ~ 61 eV can also be distinguished and are due to Ti 3p, O 2s, and Ti 3s photoelectrons respectively.

In conclusion, a standard cp Ti contains primarily Ti, O and C on the surface, which is in agreement with the literature (Lausmaa et al. 1996). Small quantities of other elements like N, Ca, Si, Cl, P etc. are present, which are surface contaminants and are very difficult to entirely eliminate from the surface.
The survey spectrum of a representative Ca-Ti sample analysed using a monochromated X-ray source (figure 3.34, second row) is similar to the cp Ti spectrum, showing on the surface mainly Ti, O and less amount of C. The atomic percentages and elemental ratios (tables 3.5, 3.6) of Ti (21-28%), O (49-59%), O/Ti (1.9-2.8) and C (12-31%), C/Ti (0.5-1.2) varied throughout the experiments. Again the high variability in the O and C concentration may be due to the samples' history, storage and duration in air prior to analysis. Also, it was found that the variability was related to the time which passed between implantation and analysis. Later on in the following chapters it will be shown that the samples which were analysed nearer to the implantation time behaved more uniformly than samples analysed following many months of storage. This was also observed by Shinawi (2003), who used Ca-Ti samples implanted under the same conditions as the samples in this work and noticed that as the time from the implantation increases, the variability in O and C concentration increases.

In addition to the elements discussed above, calcium is present on the Ca-Ti surface appearing at ~ 340 eV in a percent ranging from 2-4.5 %. However, the percentage and the Ca/Ti ratio started to vary among the samples as the time from the implantation increased, from an initial fairly constant Ca/Ti ratio (average) of 0.22 to a Ca/Ti ratios (average) varying from 0.21 to 0.11. This may explain the increasing in the variability of the samples behaviour as the time from implantation increases.
Very small amounts of other elements may be present on the surface, like in this case F at 685 eV and N at 400 eV, and they are usually contaminants. Their concentration is less than 1%.

In conclusion the Ca-Ti sample contains on the surface mainly Ti and O and small amounts of C and Ca. Other elements may be present on the surface from contamination (N, F, Al, etc.). The composition is similar with the composition of the Ca-Ti reported in the literature (Hanawa, 1993, 1996, Krupa, 2001).

Figure 3.35 presents a Ti 2p spectrum of a representative polished cp Ti and a Ca-Ti analysed using a monochromated X-ray source.

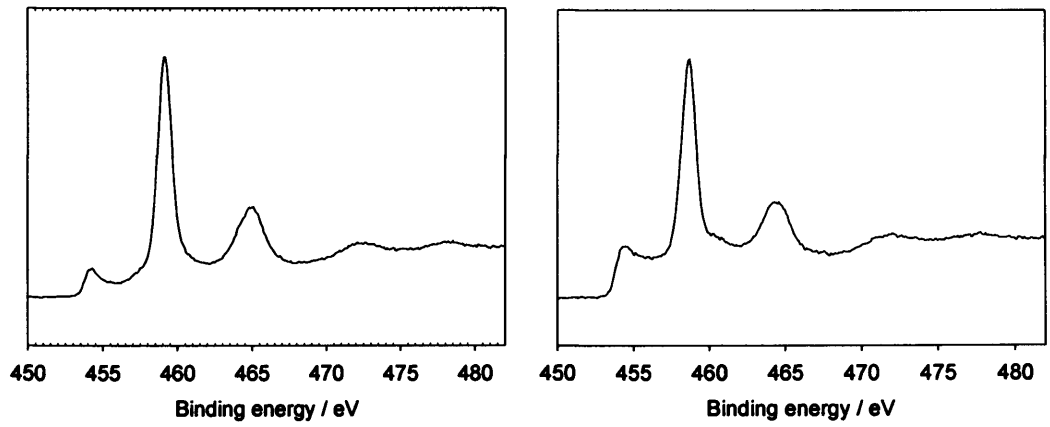

Figure 3. 35 XPS spectra of Ti 2p region of a cp Ti (left) and Ca-Ti (right) sample analysed using a monochromated X-ray source.

The Ti 2p spectrum for cp Ti consists of two peaks as a result of spin-orbit splitting and shows peaks for Ti^0, and Ti^{4+}, species and contributions from Ti^{3+} and probably also Ti^{2+}. The prominent peaks at 459.2 eV and 465 eV (spin orbit splitting) are the $2p_{3/2}$ and $2p_{1/2}$ peaks due to Ti^{4+} (Lausmaa et al. 1990) which represent the majority of the oxide layer. The Ti metal (Ti^0) underneath the oxide

layer was seen at the lower end of the binding energy scale at 454.3 eV. The fact that the metal can be detected means that the thickness of the oxide layer is within the detection limit of the XPS (~100 Å). The oxide layer consists mainly of titanium dioxide (TiO_2), but other oxides may be present including Ti_2O_3 and TiO. However, Ameen et at (1993) have shown the Ti^0 peak at ~455 eV is detectable with XPS only on the surface of a smooth polished Ti, and is not detectable on an unpolished, rough Ti sample. The authors explained this as to be caused either to the reduced effective sampling depth on the rough Ti or an increased oxide layer thickness.

The right-hand graph in figure 3.35 presents the Ti 2p spectrum of a representative Ca-Ti sample analysed using a monochromated X-ray source.
In comparison, the Ti 2p spectrum is different to that of control cp Ti in terms of peak shape and peak position. The Ti^{4+} peak position is similar to the cp Ti and appears at ~ 458.7 eV, but the peak at lower binding energy is broader and slightly shifted by ~1 eV to higher E_B (454.7 eV), due to thickening of the oxidised surface layer and the presence of greater amount of sub-oxide species. As a result of the shifting, this peak will no longer be referred to as Ti^0, but Ti^{n+}, where $n < 4$, as the range of binding energies over which intensity is observed corresponds to those of reduced oxide species. The fact that Ti^0 is not detected is confirmed by research of Krupa et al. (2001), who analysed cp Ti implanted with Ca to a dose of 1 x 10^{17}ions/cm^2 at energy 25 keV. The authors did not detect the Ti^0 on the surface of the Ca-Ti, only Ti^{4+} and Ti^{3+}, which indicated, together with the increase in the O composition, an increase in the oxide layer following implantation. In another publication by the same group of researchers the Ti^0 peak was not detectable following P ion implantation into cp Ti. These modifications are due to the change in the surface chemistry, to an increase in the thickness of the oxide layer and probably to the formation of Ti^{3+} and Ti^{2+} arising from re-oxidation after implantation. Also the formation of TiC during implantation would contribute to the modifications which appeared at the lower binding energy.
Below are presented representative Ti 2p spectra for two cp Ti samples polished using the same method but analysed using a monochromated X-ray source (on the left) and on the right twin anode source (right).

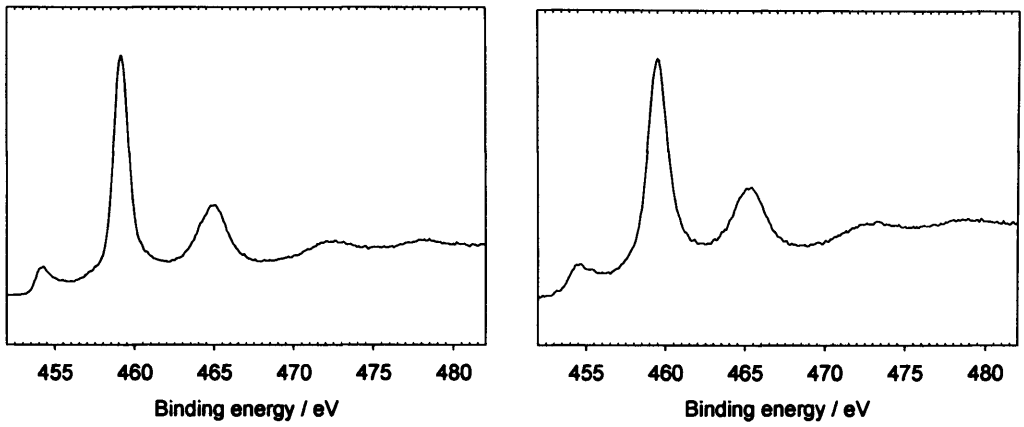

Figure 3. 36 XPS spectra of Ti 2p region of a polished cp Ti disc analysed using a monochromated X-ray source (left) and twin anode source (right).

It can be noticed that the same features are seen in the spectra but that the Ti^0 peak is more defined for the sample analysed using a monochromated X-ray source than for a twin anode source and that the feature is less defined for the latter. This may be due to the additional broadness of the X-ray lines and to the satellite intensities superimposed on the Ti^0 peak in the spectra obtained with the twin anode source. The Ti^{4+} peak is noticeably broader for the twin anode source.

Figure 3.37 presents the O 1s spectrum of a representative in-house polished cp Ti disc (left) and Ca-Ti disc (right) analysed using a monochromated X-ray source.

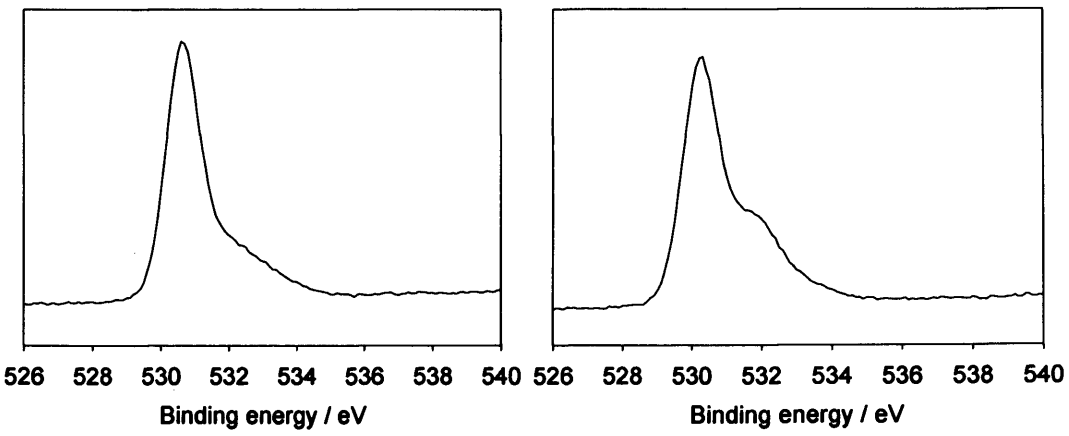

Figure 3. 37 XPS spectra of O 1s region of a representative cp Ti (left) and Ca-Ti (right) sample analysed using a monochromated X-ray source.

The O 1s spectrum for cp Ti (fig.3.37, left) shows a single peak at ~ 530 eV due to O as O^{2-} (Hanawa et al., 1995, Pham et al., 2000). The slight shoulder at higher binding energy represents O in the OH group and H_2O at ~532 eV (Pham et al., 2000) and also other O-containing organic compounds likely to be present on the surface. It is possible that the O is present in organic species like C=O, C-OH, and COOH as carbon is present on the surface, as stated and in the literature (Lausmaa 1996, Kilpadi 1998a).

The O/Ti ratio (table 3.6) on cp Ti varied between 2.44 and 3.88. Theses values are significantly ($p < 0.05$) lower than the 4.54 value reported by Yang et al. (2001). In the literature it was reported that differences in the surface roughness will modify the O atomic percent, with smooth surfaces having more O on the surface than rough surfaces (Ameen et al., 1993). However, in this case differences in the surface roughness cannot be the cause of different O/Ti ratios, as all the samples were polished to a mirror finish following similar protocols and had similar roughness, as presented earlier in this chapter. This difference may be attributed to time in air prior to analysis, as stated by Lausmaa et al. (1996), which will cause an increase in the contamination, represented by an increase in the hydroxide levels, and this will cause an increase in the O/Ti ratio.

Figure 3.37 (right) shows the O 1s spectrum of a representative Ca-Ti sample analysed using a monochromated X-ray source. The O 1s region, is similar in shape with the O 1s for the cp Ti, presents a first peak at 530.5 eV, and the shoulder representing O in OH group [TiOH or Ca $(OH)_2$], (Feng et al., 2002) at ~ 531 eV and H_2O at ~ 533 eV is more pronounced. This may be due to the fact that the oxide layer present on the surface has thickened. The shoulder at higher binding energy due to hydroxyl is more pronounced that the one for cp Ti, a fact confirmed in research carried out by Hanawa et al. (1996b) who stated that the proportion of hydroxyl radicals in total oxygen atoms is much larger for Ca-Ti than cp Ti. This was attributed to the fact that calcium hydroxide forms easily on the surface of Ca-Ti (as Ca easily reacts with moisture in ambient air), inducing more hydroxyl radical on Ca implanted Ti than cp Ti.

The O/Ti ratio varies throughout the study from 1.98-3.01, due to the modification of the oxide layer or the contamination present on the surface and length of time exposed to air.

Figure 3.38 presents a C 1s spectrum of a representative polished cp Ti (left) and Ca-Ti sample (right) analysed using a monochromated X-ray source.

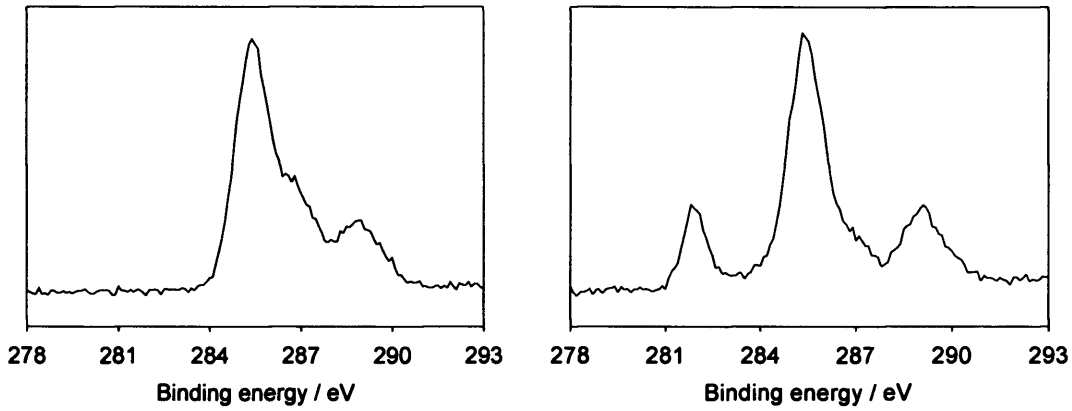

Figure 3. 38 XPS spectra of C 1s region of a cp Ti (left) and Ca-Ti (right) sample analysed using a monochromated X-ray source.

The C 1s spectrum for the cp Ti sample (figure 3.38, left) shows three peaks of similar width but decreasing intensity, as the binding energy increases (285.6 eV, 286.9 eV, and 289 eV). The lowest binding energy peak, which is the most intense, represents hydrocarbon bonds. The middle binding energy peak represents carbon linked to a single oxygen atom -C- O (Kilpadi et al., 1998a), C-OH (Lausmaa et al., 1990), or C-O-C bonds. The third peak corresponds to carbon atoms from the carboxylate -COO^- (Kilpadi et al., 1998a), COOH acid group, O-*C*=*O* (Mantel et al., 1994). All the carbon present on the surface is due to contamination. The C/Ti ratio varies between 0.77 and 2.79. This is in agreement with Lausmaa et al. (1990), but significantly lower ($p<0.05$) than the values presented by Yang et al. (2001) which may explain the high O/Ti ratio recorded. This variation in the ratio may also be attributed to the time of exposure to air prior to analysis. The level of C on cp Ti is reported to increase with increased air exposure (Mouhy et al., 1998). It was also noticed that the C/Ti ratio was smaller for samples which were ultrasonically cleaned in acetone and ultra-pure water before being used in the experiments.

The C 1s spectrum for the Ca-Ti sample (figure 3.38, right) presents the 3 peaks similar to the cp Ti sample and a fourth, at a lower binding energy. The lowest binding energy peak is seen at 281.9 eV and is assigned to titanium carbide formed during the ion implantation process. This was not detectable on the cp Ti surface. The binding energy peak at 285 eV is due to CH bonds. The second peak (~287 eV) is attributed to C bound to a single O atom, while the peak at the highest binding energy (~289 eV) is attributed to C bound to two O atoms. The measured C/Ti ratio varied throughout the project between 0.5 and 1.2. The high variability in the C/Ti ratio may be attributed to an increased time from implantation, as reported also by Shinawi (2003). It was also noticed that the ratio was smaller for samples which were ultrasonically cleaned in acetone and ultra-pure water before being used in the experiments.

Figure 3.39 shows the Ca 2p spectrum of a representative cp Ti (left) and Ca-Ti (right) sample analysed using a monochromated X-ray source.

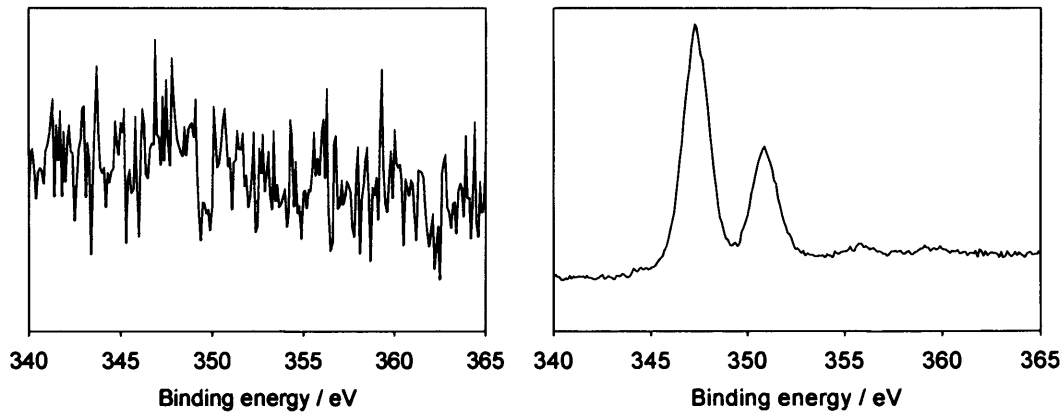

Figure 3. 39 XPS spectra of the Ca 2p region of cp Ti (left) and Ca-Ti (right) samples analysed using a monochromated X-ray source.

Ca is not normally present on a cp Ti surface, as seen from figure 3.39 (left). Occasionally, if cleaning is not thorough or impure water is used, calcium can be present in very small quantities as a contaminant. The presence of Ca on the cp Ti surface is reported in the literature as being due to CaO and $CaCO_3$ (Krupa, 2001). Only minute amounts of Ca may be compositional, as reported in the literature (Hanawa et al., 1996), although the authors did not specify a percentage for the Ca. The maximum percentage of Ca allowed in grade 1 cp Ti

is not specified in ASTM 67, which gives the following composition (in max %) for a cp Ti sample: 0.03% N, 0.1% C, 0.0125% H, 0.18% Fe, 0.20% O, Ti balance, which suggests that only tiny traces are permissible.

The Ca 2p spectrum for the Ca-Ti sample (figure 3.40, right) presented with a simple spin orbit doublet, with Ca $2p_{3/2}$ and Ca $2p_{1/2}$ binding energies of 347.3 eV and 351 eV due to Ca^{2+}. These were attributed by Krupa et al., (2001) and Hanawa et al., (1998) to CaO and $Ca(OH)_2$. They stated that calcium hydroxide forms very easily on the surface of Ca-Ti (as calcium easily reacts with moisture in ambient air), inducing more hydroxyl radical on Ca implanted Ti than cp Ti. As a result calcium oxide and calcium titanate are covered by calcium hydroxide in air at the outermost surface of the Ca-Ti sample (Hanawa, 1998). However, in the Ca 2p spectrum for the Ca-Ti sample analysed, calcium titanate ($CaTiO_3$), with the $2p_{3/2}$ peak at E_B = 346.9 eV, was not detected on the surface.

From the analysis of the Ca 2p spectrum it can be concluded that as calcium was not present on the cp Ti sample, the Ca present on the surface was clearly the result of the Ca ion implantation.

Nitrogen can be a contaminant on titanium surfaces. As Chapter 5 presents details of amino acid adsorption and XPS data is used extensively, it is important to consider the N 1s spectra for cp Ti and Ca-Ti here.

Figure 3.40 presents the N 1s spectrum of a representative polished cp Ti disc (left) and Ca-Ti disc (right) analysed using a monochromated X-ray source.

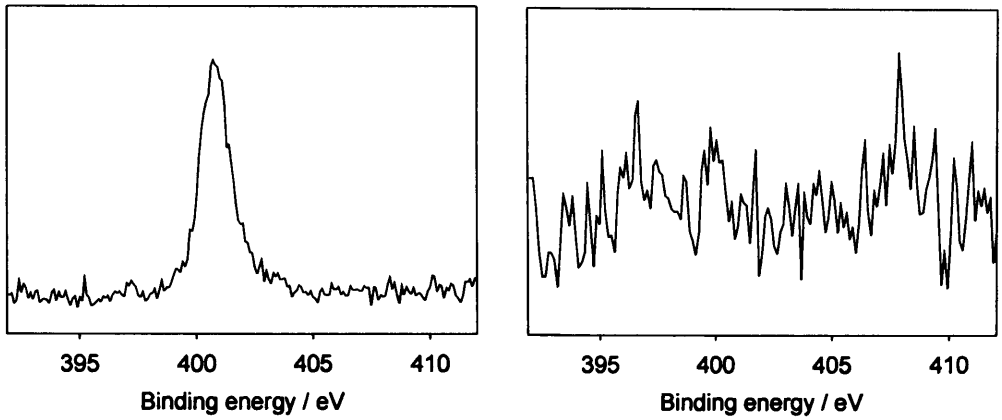

Figure 3. 40 XPS spectra of N 1s region of cp Ti (left) and Ca-Ti (right) samples analysed using a monochromated X-ray source.

The N 1s spectrum for cp Ti (figure 3.40, left) indicated that nitrogen was present on the cp Ti surface as N-(C, H) species, presenting a single N 1s photoelectron peak at ~400.5 eV. This is probably due to surface contamination; likely sources are adsorption from air or cleaning solvents, and also proteins (Feng et al., 2002). Sometimes a second peak was present at ~ 401.1 eV, caused by organic contamination (proteins), as mentioned by Feng et al. (2002). The N/Ti ratio was small, varying from 0.3 ± 0.1 to 0.03 ± 0.02 (table 3.6). It is clear that the range of variation was very wide, and was caused by polishing, cleaning and handling procedures, storage of the samples, and time in air prior to analysis.

The Ca-Ti samples generally showed no quantifiable signal due to N (figure 3.40, right). However, in rare cases a very small peak was observed, at around 400 eV due to N in NH_2 caused by minimal contamination and a minimal peak at ~397.5 eV which was attributed to the presence of nitride species at the surface, probably TiN caused by the implantation process. The N atomic percentage varies very little between 0.1-0.3%, and the N/Ti ratio between 0.1-0.2. It appears that the N contamination does not change as the time from the implantation increases, since the samples did not vary with regards to the amount of N present on the surface.

3.3.2 XPS depth profiles

Presented below in figures 3.41-3.46 and tables 3.7-3.10 are the depth profiles of a cp Ti sample, the Ti 2p, O 1s and C 1s spectra recorded throughout the etching and the O/Ti, Ca/Ti and C/Ti profiles of a Ca-Ti sample.

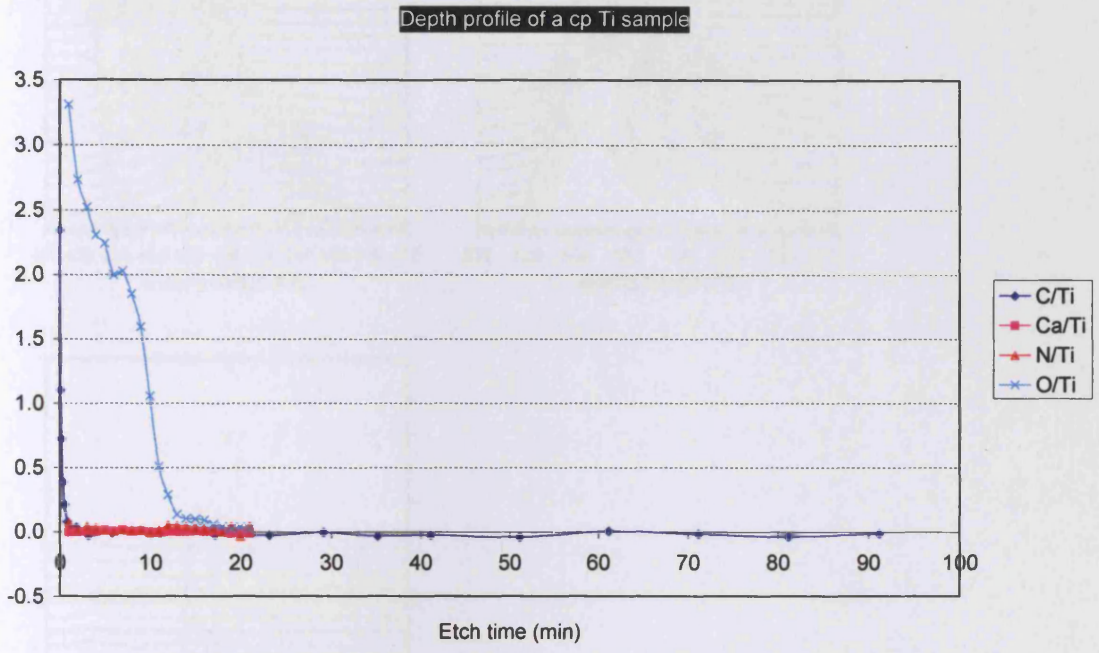

Figure 3. 41 Depth profile including the O/Ti, C/Ti, and N/Ti ratios of a cp Ti sample as a function of the etch time.

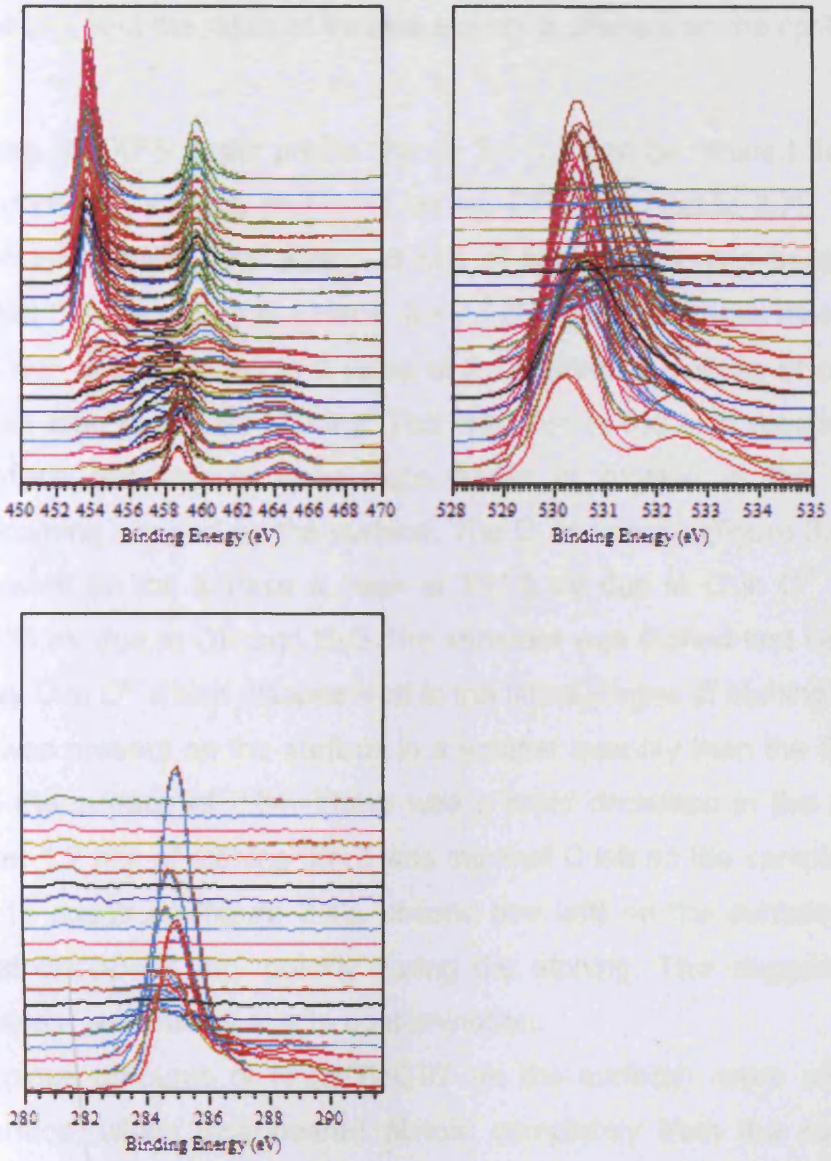

Figure 3. 42 XPS spectra of Ti 2p (first row left), O 1s (first row right) and C 1s (second row left) regions of cp Ti sample throughout the etching analysed using a monochromated X-ray source.

Etch time (min)	O/Ti	C/Ti	N/Ti	Ca/Ti
0.0	3.31	2.34	0.07	-0.01
1.2	2.03	0.01	0.02	0.00
5.8	1.06	-0.01	0.00	0.00
23.2	0.14	-0.03	0.05	0.00
91.2	0.02	-0.01	0.04	-0.01

Table 3. 7 Elemental ratios (O/Ti, C/Ti, N/Ti, Ca/Ti) for a cp Ti sample at various intervals in the etching process analysed using a monochromated X-ray source.

Figures 3.41 and 3.42 and table 3.7 show the XPS depth profiles, the CasaXPS spectra, and the ratios of various elements present on the cp Ti surface.

From the XPS depth profile (figure 3.41) it can be noticed that a cp Ti sample had on the surface mainly O, at an O/Ti=3.31 (table 3.7). The O decreased abruptly initially, and after ~ 6 min of etching the ratio became a third of the initial O/Ti ratio on the surface. It then started to decrease more slowly, and after 23 min of etching fell to a value of 0.14. Small quantities of oxygen were found even after extensive etching. This was due to the high reactivity of the titanium surface resulting in even trace levels of oxygen in the vacuum chamber becoming trapped on the surface. The O 1s spectra (figure 3.42, first row, right) showed on the surface a peak at 531.5 eV due to O in O^{2-} and a shoulder at ~533 eV due to OH and H_2O.The shoulder was etched first very quickly, leaving only O in O^{2-} which disappeared in the latest stages of etching.

C was present on the surface in a smaller quantity than the O, with a C/Ti ratio on the surface of 2.34. There was a rapid decrease in the carbon signal and after 1.2 min of etching there was minimal C left on the sample (C/Ti=0.01). The C 1s spectrum (figure 3.42, second row left) on the surface showed C peaks that disappear very quickly during the etching. This suggested that all the C present was mainly due to contamination.

Minimal amounts of N (N/Ti=0.07 on the surface), were also noticed on the surface, which disappeared almost completely from the surface immediately following initial etching (seconds), and the ratio fell to 0.01 after 0.8 min. The N/Ti ratio then reached 0 after 5 min of etching. No Ca was detected on the cp Ti surface (Ca/Ti=0.00). The rapid decrease in these levels confirmed that both C and N were found only on the surface and did not extend into the sub-surface regions.

On etching (figure 3.42, first row left) cp Ti showed initially an increase in intensity in the Ti^{3+} region, followed by Ti^{2+} and eventually Ti^{0} metal which, as expected, dominated the spectrum in the later stages of etching.

Below are presented the Ca /Ti, O/Ti, and the carbide /Ti ratios for a Ca-Ti sample as a function of the etch time. The graphs will contain also the corresponding figures for the same ratios for the cp Ti sample.

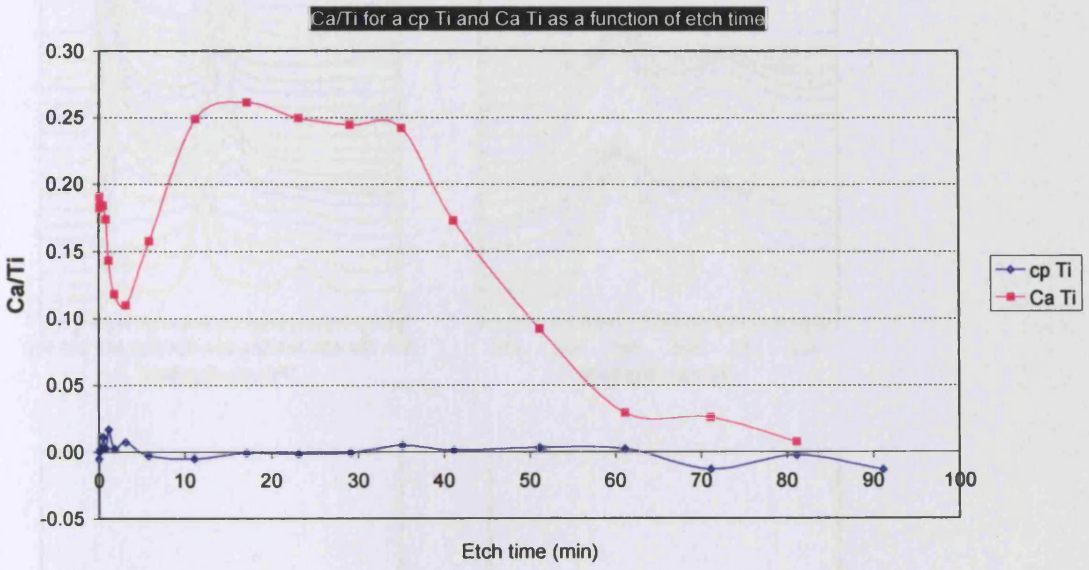

Figure 3. 43 Ca/Ti ratios for a cp Ti and Ca-Ti sample as a function of etch time.

Etch time (min)	Ca/Ti ratio
0	0.19
3	0.10
6	0.15
17	0.26
81	0.00

Table 3. 8 Ca/Ti ratios for a Ca-Ti sample throughout the etching.

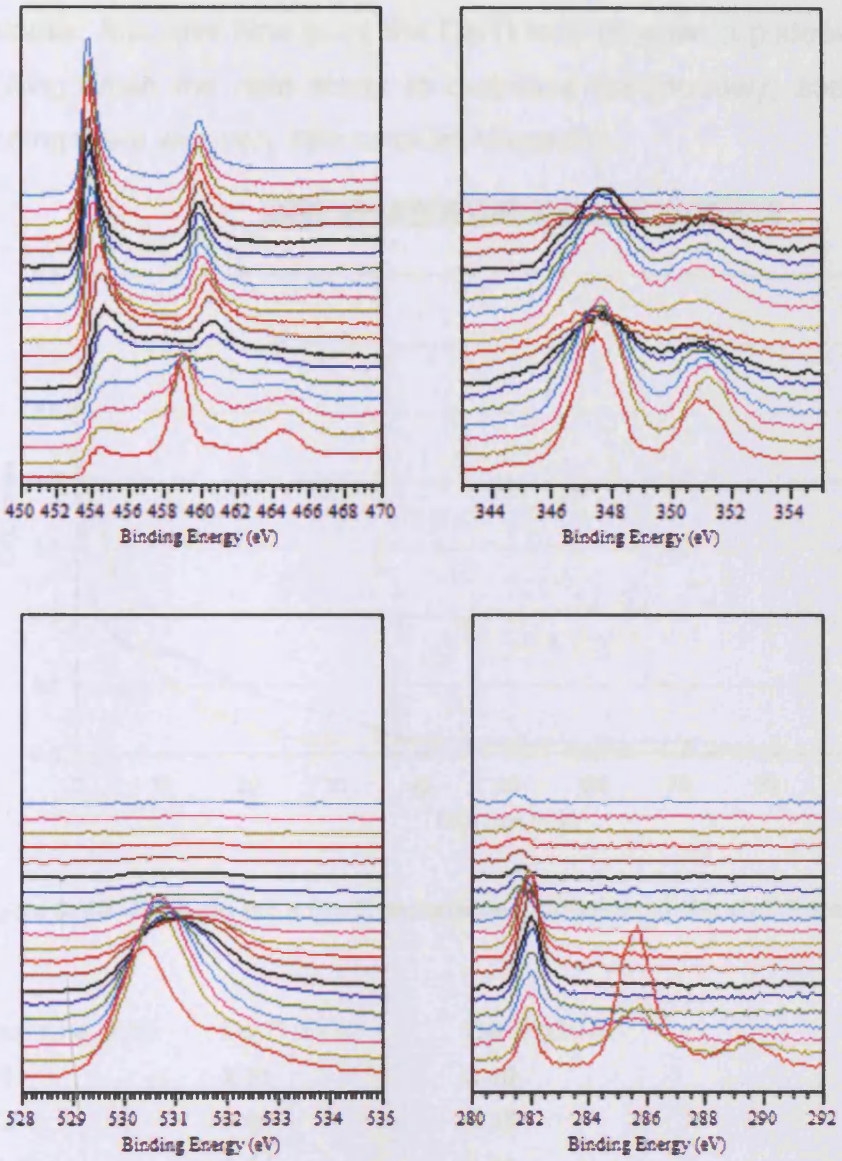

Figure 3. 44 XPS spectra of Ca 2p first row, left), Ti 2p (first row, right), O 1s (second row, left) and C 1s (second row, right) regions of Ca-Ti sample throughout the etching analysed using a monochromated X-ray source.

The as implanted Ca-Ti sample had an initial surface Ca/Ti ratio of 0.19 (table 3.8). It then dropped sharply to less than 0.1 after 3 min of etching. Following this the ratio increases very quickly, reaching 0.15 after 6 min and 0.26 after 17 minutes of etching. At this time point, the Ca/Ti ratio was found to be higher than at the immediate surface (Ca/Ti = 0.23), while the Ca 2p peaks showed further broadening (figure 3.44), with a shoulder to low binding energy possibly indicative of the presence of Ca in the metallic state, as suggested by Van

Doveren (2003), however this may be an artefact of the ion beam etching process. After this time point the Ca/Ti ratio reaches a plateau until ~30 min of etching when the ratio starts to decrease continuously, and after 81 min of etching there was very little calcium remaining.

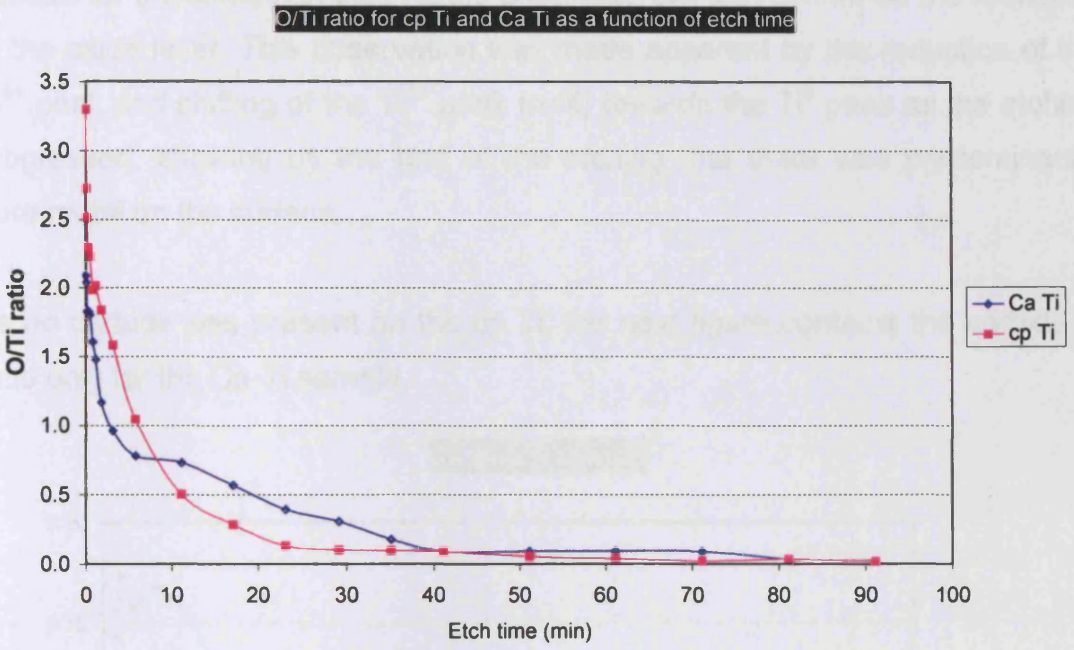

Figure 3. 45 O/Ti ratio for a Ca-Ti sample as a function of the etch time.

Etch time (min)	Cp Ti (O/Ti)	Ca-Ti (O/Ti)
0.0	3.31	2.10
3.2	1.60	0.97
81.2	0.04	0.04

Table 3. 9 O/Ti ratio for a Ca-Ti sample as a function of etch time (min).

The Ca-Ti sample had an initial surface O/Ti ratio of 2.10, smaller than the cp Ti (3.41). It then dropped sharply very quickly to less than 1 after 3 min of etching. After this it dropped gradually until there was minimal O left in the sample at the end of etching (O/Ti=0.04). This indicated that the Ca-Ti had a thicker oxide layer than the cp Ti. Minimal oxygen levels were reached in cp Ti after 23 minutes. In Ca-Ti this took 40 minutes of etching. It can be noticed that the O on the cp Ti decreased more rapidly and more sharply than Ca-Ti. The O/Ti ratios for both samples were fairly similar, although the surface O/Ti ratio for the cp Ti

was slightly elevated compared to the Ca-Ti. However, it did not show the shoulder apparent in Ca-Ti. The O 1s spectra (figure 3.44, second row, left) shows that the O decreased continuously, showing a reduction in the O peak at ~531 eV and disappearance towards the middle of the etching period. The Ti 2p spectra for the same samples (figure 3.44, first row, left) confirmed the reduction in the oxide layer. This observation was made apparent by the reduction of the Ti^{4+} peak and shifting of the Ti^{n+} peak (n<4) towards the Ti^{0} peak as the etching progressed, showing by the end of the etching that there was predominantly pure metal on the surface.

As no carbide was present on the cp Ti, the next figure contains the carbide/Ti ratio only for the Ca-Ti sample.

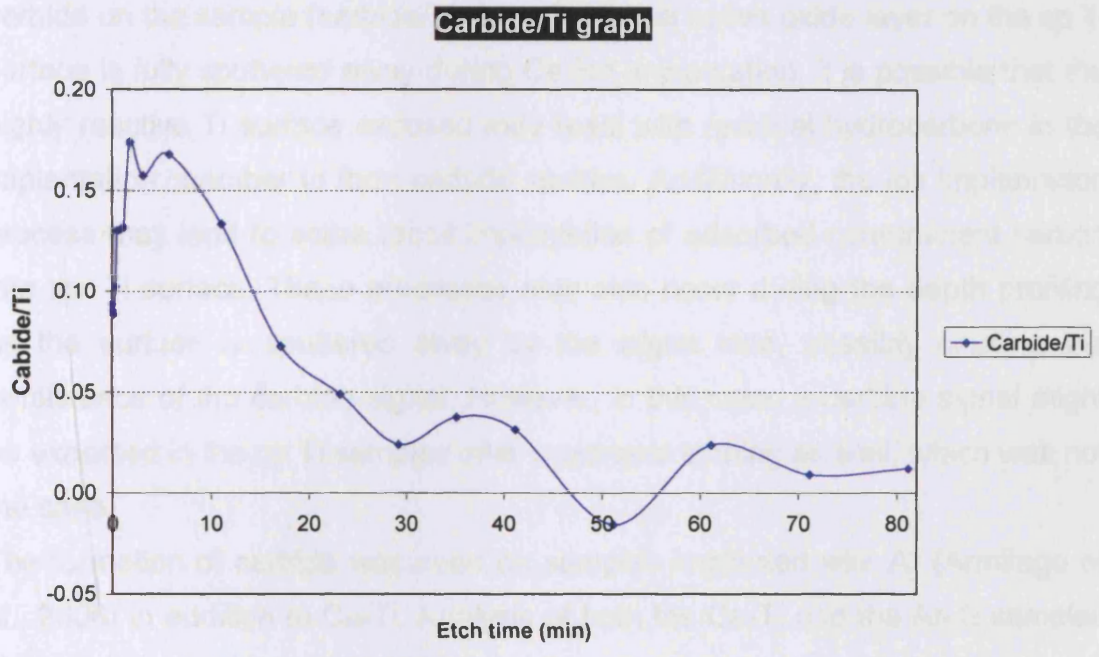

Figure 3. 46 Carbide/Ti ratios for a Ca-Ti sample as a function of the etch time.

Etch time (min)	Carbide / Ti
0	0.09
1	0.13
6	0.17
11	0.13
17	0.07
23	0.05
71	0.01
81	0.01

Table 3. 10 Carbide/Ti ratios for a Ca-Ti sample as a function of the etch time.

Carbon was found both at the surface and in the subsurface regions (figure 3.44). The surface levels were dominated by the hydrocarbon contamination typical of Ti surfaces (Lausmaa 1996) but also displayed a small peak attributable to carbide species at ~ 282 eV (figure 3.44). This is in contrast to Ca implanted Ti analysed by Hanawa et al. (1995) (18 keV, 10^{22} ions m^{-2}), where no carbide was detected. On etching, the hydrocarbon contamination peak rapidly diminished in magnitude, while the relative carbide concentration increased initially, reaching a maximum at ~1 minute (Carbide/Ti=0.13) (figure 3.46). The ratio remained at this value until minute 6 of etching and then started to decrease continuously, so that by the end of etching there was still some carbide on the sample (carbide/Ti=0.1). Since the native oxide layer on the cp Ti surface is fully sputtered away during Ca ion implantation, it is possible that the highly reactive Ti surface exposed may react with residual hydrocarbons in the implantation chamber to form carbide species. Additionally, the ion implantation process may lead to some recoil implantation of adsorbed contaminant carbon into the Ti surface. These processes may also occur during the depth profiling as the surface is sputtered away by the argon ions, possibly causing the persistence of the carbide signal. However, in this case, a carbide signal might be expected in the cp Ti samples after prolonged etching as well, which was not the case.

The formation of carbide was seen on samples implanted with Ar (Armitage et al., 2006) in addition to Ca-Ti. Analysis of both the Ca-Ti and the Ar-Ti samples showed the presence of carbide in addition to hydrocarbon contamination and depth profiling demonstrated that the relative concentration of carbide again increased on initial Ar^+ etching. The Ti 2p peak shapes of the two samples were very similar, confirming the presence of titanium carbide as well as reduced oxide species. The authors concluded that this suggested that the presence of both titanium carbide and the reduced oxides was indeed a result of the implantation process itself and not limited to the implantation of Ca. Implantation of oxygen, on the other hand, resulted in no carbide formation.

In summary, the surface chemistry of a Ca-Ti sample is characterized by a top layer which is represented by contamination. Beneath this are the surface oxide

layer, then oxide and carbide, and then more oxide represented by the sub-surface oxide layer. A more detailed representation is presented in scheme 1 below.

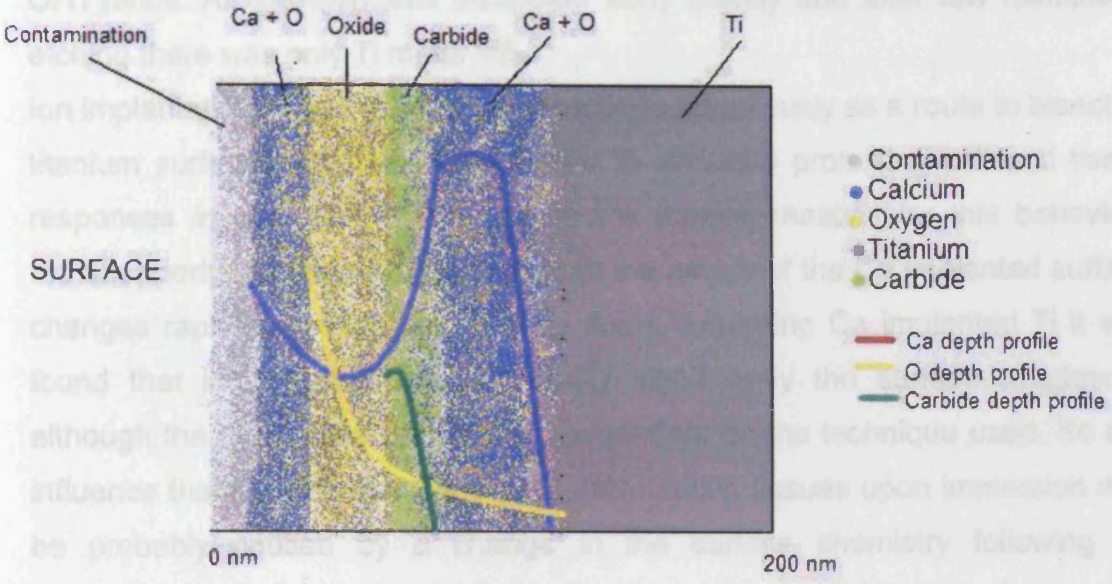

Scheme 3.1 Diagrammatic representation of as-implanted Ca-Ti surface.

The main difference in the spectrum from Ca-Ti compared to that from cp Ti was, apart from the presence of the calcium, the clear increase in the carbide component in the earlier stages of etching and also the difference in the thickness and position of the oxide layer, which was thicker than the cp Ti. Following implantation with calcium the surface of the Ca-Ti re-oxidised on removal to air. This re-oxidation occurred both above and below the maximum carbide concentration, the presence of Ca allowing greater oxygen diffusion into Ca-Ti than occurs for bare cp Ti, where the passive oxide forms very quickly, preventing further diffusion and oxide thickening.

3.3.3 Conclusions

The surface chemistry of cp Ti consists of an oxide layer present on the surface formed mainly from TiO_2. Organic contamination is common, and other impurities, like N and occasional Si, F and Al may be present. From the Ti 2p and O 1s spectra obtained for non-implanted titanium we can see that the dominant component of the surface layer is titanium oxide TiO_2. The other

components found in the layer were Ti_2O_3 and metallic titanium. The occurrence of the signal due to metallic titanium suggests that the TiO_2 layer was thin, and this is confirmed by the depth profiling which showed a rapid decrease in the O/Ti ratios. All the elements disappear fairly quickly and after few minutes of etching there was only Ti metal left.

Ion implantation of calcium has been proposed previously as a route to bioactive titanium surfaces and has been shown to stimulate promising cell and tissue responses *in vitro* and *in vivo*. While the precise reasons for this behaviour remain poorly understood, it is clear that the nature of the Ca implanted surface changes rapidly on exposure to body fluids. Analysing Ca implanted Ti it was found that implantation did not modify significantly the surface roughness, although the roughness values were dependent on the technique used. So any influence that Ca-Ti may have on the surrounding tissues upon immersion may be probably caused by a change in the surface chemistry following Ca implantation. During the calcium-ion implantation, the thickness of the oxide layer increased and the implanted ions exist as Ca^{2+} in the presence of O^{2-} and OH^- ions. Depth profiling showed a distribution of Ca within the sample and the existence of carbide.

The major difference in the spectrum from Ca-Ti compared to that from cp Ti was the clear increase in the carbide component, at a binding energy (E_B = 454.6 eV) markedly higher than that of the Ti^0 peaks, in the earlier stages of etching. The other major differences between the cp Ti and the Ca-Ti are the amount of hydroxide / water and the amount and nature of C on the surface. Implanted surfaces were shown to found to show more C than the cp Ti, and also more hydroxyl on the surface.

In conclusion, the surface characterisation of cp Ti using XPS and XPS depth profiling was in agreement with the literature (Nayab et al., 2003). Ca-Ti differed from the literature with regard to the carbide distribution and the presence of a subsurface oxide layer (Hanawa et al., 1996). The implantation parameters play an important role in determining the surface characteristics of Ca-Ti.

3.4 SUMMARY

Titanium is a relatively widely and successfully used biomaterial, especially in the dental and orthopaedic fields. The surface oxide which covers titanium is considered to be an important factor for the favourable tissue response obtained with Ti implants. This work describes the characteristics of cp Ti and Ca-Ti surface using various analytical methods. The main analytical techniques for the cp Ti and Ca-Ti were SEM, LP and WLI for surface roughness and XPS and depth profiling XPS for surface chemistry.

In the light of the findings presented in this chapter, a model can be proposed on the surface changes that follow Ca implantation into titanium. Ca ion implantation did not result in a modification of the surface roughness, but the changes that occurred affect mainly the surface chemistry.

During the implantation, the entire native oxide layer was sputtered off, leading to implantation into a Ti substrate and not TiO_2. Implantation results in the amorphisation of the surface, followed by surface re-oxidation upon removal from the implanter. The result is an oxide layer thicker than for the cp Ti, as evident from the absence of the Ti^0 peak from the Ti 2p spectrum of a Ca-Ti. Titanium suboxides and carbides may form as a result of the recoil implantation and surface re-oxidation.

3.5 LIST OF REFERENCES

Ahmad, M., Gawronski, D., Blum, J., Goldberg, J. Gronowicz, G. (1999)
Differential response of human osteoblast-like cells to commercially pure (cp) titanium grades 1 and 4.
Journal of Biomedical Materials Research 46(1): 121-131

Ameen, A. P., Short, R.D., Johns, R., Schwach, G. (1993)
The surface analysis of implant materials. 1. The surface composition of a titanium dental material.
Clinical Oral Implant Research 4(3): 144-150

Armitage, D.A., Mihoc, R., Tate, T.J., McPhail, D.S., Chater, R., Hobkirk, J.A., Shinawi, L., Jones, F.H. (2006)
The oxidation of calcium implanted titanium in water; a depth profiling study.
Applied Surface Science 253(8): 4085-4093

Brett, P. M, Harle, J., Salih, V., Mihoc, R., Olsen, I., Jones, F. H., Tonetti, M. (2004)
Roughness response genes in osteoblasts.
Bone 35(1): 124-133

Borsari V., Giavaresi G., Fini , M., Torricelli , P., Salito ,A., Chiesa, R., Chiusoli , L., Volpert , A.. Rimondini , L., Giardino, R. (2005)
Physical characterization of different-roughness titanium surfaces, with and without hydroxyapatite coating, and their effect on human osteoblast-like cells.
Journal of Biomedical Materials Research B: Applied Biomaterials 75(2): 359-368

Boyan, B.D., Bonewald, L.F., Paschalis, E.P., Lohman, C.H., Rosser, J., Cochran, D.L., Dean, D.D., Schwartz, Z., Boskey, A.L. (2002)
Osteoblast-mediated mineral deposition in culture is dependent on surface microtopography.
Calcified Tissue Interface 71(6): 519-529

Brown, D. (1997)
All you wanted to know about titanium but were afraid to ask.
British Dental Journal 182 (10): 393-394

Brunette, D. M. (1988)
The effects of implant surface topography on the behaviour of cells.
International Journal of Oral and Maxillofacial Implants 3(4): 231-246

Brunette, D. M., Tengvall, P., Textor, M., Thomsen, P. (2001)
Titanium in medicine.
Springer, Berlin.

Buser D., Schenk, R.K., Steinemann, S., Fiorellini, J.P., Fox, C.H., Stich, H. (1991)

Influence of surface characteristics on bone integration of titanium implants. A histomorphometric study in miniature pigs.
Journal of Biomedical Materials Research 25(7): 889–902.

Carlsson, L., Rostlund, I., Albrektsson, B., Albrektsson, I. (1988)
Removal torques for polished and rough titanium implants.
International Journal of Oral and Maxillofacial Implants 3(1): 21-24

Castellani, R., de Ruijter, A., Renggli, H., Jansen J. (1999)
Response of rat bone marrow cells to differently roughened titanium disc.
Clinical Oral Implants Research 10(5): 369-378

Chauvy, P. F., Madore, C., Landolt D. (1998)
Variable length scale analysis of surface topography: characterization of titanium surfaces for biomedical applications.
Surface and Coatings Technology 110(1-2): 48-56

Esposito, M., Hirsch, J.M., Lekholm, U., Thomsen, P. (1998)
Biological factors contributing to failures of osseointegrated oral implants.
European Journal of Oral Science 106: 527-551

Esposito, M., Lausmaa, J., Hirch, J. M., Thomsen, P. (1999)
Surface analysis of failed oral titanium implants.
Journal of Biomedical Material Research: Applied Biomaterials 48: 559-568

Feng, B., Chen, J. Y., Qi, S.K., He, L. Zhao, J. Z., Zhang, X. D. (2002)
Carbonate apatite coating on titanium induced rapidly by precalcification.
Biomaterials 23(1): 173-179

Guilherme, A.S., Henriques, G.E., Zavanelli, R.A., Mesquita, M.F. (2005)
Surface roughness and fatigue performance of commercially pure titanium and Ti-6Al-4V alloy after different polishing protocols.
Journal of Prosthetic Dentistry: 93(4): 378-85.

Hanawa, T., Ukai, H., Murakami K. (1993)
X-ray photoelectron spectroscopy of calcium-ion-implanted titanium.
Journal of Electron Spectroscopic and Related Phenomena 63: 347- 354

Hanawa, T., Asami, K., Asaoka, K. (1996a)
AES Studies on the dissolution of surface oxide from calcium-ion-implanted titanium in nitric acid and buffer solutions.
Corrosion Science 38(11): 2061-2067

Hanawa, T., Asami, K., Asaoka, K. (1996b)
Microdissolution of calcium ions from calcium-ion-implanted titanium.
Corrosion Science 38(9): 1579-1594

Hanawa, T. (1997)
Early bone formation around calcium-ion- implanted titanium inserted into rat tibia.

Journal of Biomedical Materials Research 36(1): 131-136

Hanawa, T., Kon, M., Doi, H., Ukai, H., Murakami K., Hamanaka, H., Asaoka, K (1998)
Amount of hydroxyl radial on calcium-ion- implanted titanium and point of zero charge of constituent oxide of the surface-modified layer.
Journal of Material Science: Materials in Medicine 9: 89-92

Hanawa, T. (2004)
Metal ion release from metal implants.
Materials Science and Engineering: C 24 (6-8): 745-752

Hiromoto, S., Hanawa, T., Asami K. (2004)
Composition of surface oxide film of titanium with culturing murine fibroblasts L929.
Biomaterials 25(6): 979-986

Jones, F.H. (2001)
Teeth and bones: Application of surface science to dental materials and related biomaterials.
Surface Science Reports 42(3-5): 75-206

Keller, J. C., Stanford, C. M., Wightman, J. P., Draughn, R. A., Zaharias, R. (1994)
Characterisations of titanium implant surfaces.
Journal of Biomedical Materials Research 28(8): 939–946

Kilpadi, D.V., Raiker, L, N., Liu, J., Lemons, J. E., Vohra, Y., Gregory, J. C., (1998a)
Effect of surface treatment on unalloyed titanium implants: spectroscopic analyses.
Journal of Biomedical Materials Research 40: 646-659

Kim, H.M. Miyaji, F., Kokubo, T., Nishigushi, S., Nakamura, T. (1999)
Graded surface structure of bioactive titanium prepared by chemical treatment.
Journal of Biomedical Materials Research 45(2): 100-107

Klokkevold, P.R., Nishimura, RD., Adachi, M., Caputo, A. (1997)
Osseointegration enhanced by chemical etching of the titanium surface. A torque removal study in the rabbit.
Clinical Oral Implant Research 8(6): 442–447

Krupa D., Baszkiewicz J., Kozubowski J. A, Barcz A., Sobczak J. W., Bilinski A.,Lewandowska-Szumie,M.,Rajchel,B.(2001)
Effect of calcium-ion implantation on the corrosion resistance and biocompatibility of titanium.
Biomaterials 22(15): 2139-2151

Krupa, D., Baszkiewicz, J., Kozubowski, J., Lewandoswska-Szumiel, M., Barcz, A., Sobczak, J., Bilinski, A., Rajchel, B. (2005)

Effect of calcium and phosphorus ion implantation on the corrosion resistance and biocompatibility of titanium.
Biomedical Materials Engineering 14(4): 525-536

Ku, C.H., Pioloetti, D.P., Browne, M., Gregson, P.J. (2002)
Effect of different Ti6Al4V surface treatment on osteoblast behaviour.
Biomaterials 23: 1447-1454

Lausmaa, J., Kasemo, B., Hansson, S. (1985)
Accelerated oxide growth on titanium implants during autoclaving caused by fluorinecontamination.
Biomaterials 6(1): 23-27

Lausmaa, J., Kasemo, B., Mattson, H. (1990)
Surface spectroscopic characterization of titanium implant materials.
Applied Surface Science 44:133-146

Lausmaa, J. (1996)
Surface spectroscopic characterization of titanium implant materials.
Journal of Electron Spectroscopy and Related Phenomena 81 (3): 343-361

Lee , T. M.. Chang , E Yang · C. Y. (2000)
A comparison of the surface characteristics and ion release of Ti6Al4V and heat-treated Ti6Al4V.
Journal of Biomedical Materials Research 50(4): 499-511

Lim, Y. J., Oshida, Y., Andres,C. J. (2001)
Surface Characterizations of Variously Treated Titanium Materials
International Journal of Oral and Maxillofacial Implants 16: 333–342

Lincks, J., Boyan, B.D., Blanchard, C.R., Lohmann, C.H., Liu, Y., Cochran, D.L., Dean, D.D., Schwartz, Z. (1998)
Response of MG63 osteoblast-like cells to titanium and titanium alloy is dependent on surface roughness and composition.
Biomaterials 19: 2219-2232

Mantel, M., Wightman, J.P. (1994).
Influence of the surface chemistry on the wettability of stainless steel.
Surface and Interface Analysis 21 (9): 595-605

Martin, J.Y., Schwartz, Z., Hummert, T.W., Schraub, D.M., Simpson, J. Lankford Jr, J., Dean, D.D., Cochran D.L., Boyan, B.D. (1995)
Effect of titanium surface roughness on proliferation, differentiation, and protein synthesis of human osteoblast-like cells (MG63).
Journal of Biomedical Materials Research 29 (3): 389–401

Michaels, C.M., Keller, J.C., Stanford, C.M., Solursh, M. (1989)
In vitro cell attachment of osteoblast-like cells to titanium.
Journal of Dental Research 68: 276-234

Misch, C.E. (1999)
Contemporary implant dentistry.
2nd Ed. Mosby, St. Louis

Morra, M., Cassinelli, C., Bruzzone, G., Carpi, A., Di Santi, G., Giardi, R., Fini, M. (2003)
Surface chemistry effects of topographic modification of titanium dental implant surfaces:1. Surface analysis.
International Journal of Oral and Maxillofacial Implants 18(1): 40–45

Natan M. (1983)
The stability of anodized titanium surfaces in hot water.
Journal of Adhesion 15:125–136

Nayab, S., Shinawi L., Hobkirk, J., Tate, T. J., Olsen, I., Jones, F. H. (2003)
Adhesion of bone cells to ion-implanted titanium.
Journal of Materials Science: Materials in Medicine 14(11): 991-997

Nayab, S., Jones, F. H., Olsen, I. (2005)
Effects of calcium ion implantation on human bone cell interaction with titanium.
Biomaterials 26: 4717-4723

Nayab, S., Jones, F. H., Olsen, I. (2007)
The human bone cell cycle is modulated by calcium ion-implantation of titanium.
Biomaterials 28(1): 38-44

Nayab, S., Jones, F. H., Olsen, I. (in press)
Effects of calcium ion-implantation of titanium on bone cell function *in vitro*.
Journal of Biomedical Materials Research A

Olefjord, I., Hansson, S. (1993)
Surface analysis of four dental implant systems
The International Journal of Oral & Maxillofacial Implants 8(1): 32-40

Ong, J. L., Lucas, L. C., Raikar, G. N., Connatser, R., Gregory, J. C. (1995)
Spectroscopic characterization of passivated titanium in a physiologic solution.
Journal of Material Science: Material in Medicine 6(2): 113-119

Shinawi, L. A. (2003)
Ion implantation as a route to enhancing osseointegration on modified titanium surfaces.
PhD thesis, UCL

Sittig, C., Textor. M., Spencer, N. D. (1999)
Surface characterizations of implant materials cp Ti, T-6Al-7Nb and Ti-6Al-4V with different pretreatments.
Journal of Material Science: Materials in Medicine 10: 35-46

Smith, D.C., Pilliar, R.M., Chernecky, R. (1991)

Dental implant materials. I. Some effects of preparative procedures on surface topography.
Journal of Biomedical Materials Research 25(9): 1045–1068

Steinemann, S. G. Eulenberger, J. Mäusli, P. ASchroeder . A. (1986)
Adhesion of bone to titanium.
Advances in Biomaterials, Vol. 6: Biological and Biomechanical Performances of Biomaterials, 409-414

Tavares, M.G., Tambasco, O. P., Nanci, A., Hwthorne, A. C., Rosa, A. L., Xavier, S. P. (2007)
Treatment of a commercial, machined surface titanium implant with H_2SO_4 / H_2O_2 enhances contact osteogenesis.
Clinical Oral Implants Research (in press)

Tengvall, P., Lundstrom, L. (1992)
Physico-chemical considerations of titanium as a biomaterial.
Clinical Materials 9: 115-134

Thomas KA, Kay JF, Cook SD, Jarcho M. (1987)
The effect of surface macrotexture and hydroxylapatite coating on the mechanical strengths and histologic profiles of titanium implant materials.
Journal of Biomedical Materials Research 21(12): 1395–1414

Ungersböck, A., Rahn, B. (1994)
Methods to characterize the surface roughness of metallic implants.
Journal of Material Science: Materials in Medicine 5: 434-440

Vanzilotta, P. S., Sader, M. S., Bastos, I. N., Soares, G. A. (2006)
Improvement of in vitro titanium bioactivity by three different surface treatments.
Dental Materials 22(3): 275-282

Wennerberg, A., Albrektsson, T. (2000)
Suggested guidelines for the topographic evaluation of implant surfaces.
International Journal of Oral and Maxillofacial Implants 15: 331–344

Yang, B. C., Weng, J., Li, X., Zhang, X. D. (1999)
The order of calcium and phosphate ion deposition on chemically treatedtitanium surfaces soaked in aqueous solution.
Journal of Biomedical Materials Research 47(2): 213-219

Yoshinari , M., Oda, Y., Kato,T., Okuda, K., Hirayama, A. (2000)
Influence of surface modifications to titanium on oral bacterial adhesion *in vitro.*
Journal of Biomedical Materials Research 52(2): 388-394

4. ION RELEASE STUDIES

4.1 INTRODUCTION

Release of ions into the tissues may follow insertion of an implant into a living host. This may affect the biological and molecular interactions around an implant, for example by inducing hydroxyapatite precipitation and subsequently enhancing bone deposition around the implant. Ions released from a material may also pass through cellular membranes and affect cell processes. Metal ion release from implants may arise due to dissolution, fretting or wear. For titanium, the rate of ion release is affected by the oxide layer, so when the surface oxide film is disrupted, the metal ion release continues and corrosion proceeds unless the surface oxide film is regenerated. Therefore, the amount of released metal ions is governed by the regeneration time of the film. Ion release into an experimental medium or bio-liquid is important because it can provide an indication of release into the surrounding tissues both *in vitro* and *in vivo*.

Released metal ions can have a beneficial or toxic effect on the cells and surrounding tissue. They do not always combine with biomolecules to produce a toxic effect. This is because they may immediately combine with a water molecule or with a nearby anion to form an oxide, hydroxide, or inorganic salt. In addition, the oxide layer present on the surface of a metallic material may play an important role as an inhibitor of ion release, which may be accelerated by even small quantities of dissolved oxygen, inorganic ions, and proteins, as well as cellular activity. In addition, there is a preferential release of specific elements during wear and fretting of metallic materials. For example, iron is preferentially released from stainless steel at passive potentials (Bruesch et al., 1985). Sasada et al., (1995) found that large amounts of molybdenum, which is a trace element in stainless steel, may be detected in the culture medium when the alloy is undergoing wear. Also relatively more nickel and manganese have been detected compared with iron and chromium after wear tests of stainless steel in a cell culture medium. In these situations cobalt is also preferentially released from Co–Cr–Mo alloy (Storp et al., 1977, Hanawa et al., 2001). These studies indicated that even trace elements in an alloy cannot be neglected from the viewpoint of metal ion release.

The complete effect of the implanted ions upon the tissues is yet to be fully understood. Because medical implants, including dental implants, are now used

widely, there are concerns with regards to their long-term localized or systemic effects on the body, especially in younger patients who will be exposed to the device for longer, or in patients who are medically compromised. Van Ginkel et al. (1993) reported abnormal deposits of aluminium in the brains of patients with Alzheimer's or Parkinson's disease, and considered this as a possible cause of the disease. Other neurological diseases have also been associated with the deposition of aluminium into the tissues (Van der Voet et al., 1991).
In the case of titanium and aluminium ion release, there is evidence that these metal ions can affect cell function *in vivo* (French et al., 1984), as well as cell proliferation and synthesis of extracellular matrix *in vitro* (Evans, 1994). Also, it has been shown that titanium, aluminium and vanadium ions can inhibit apatite formation *in vitro* (Blumenthal et al., 1989) which could have important implications for mineralisation at bone–metal implant interfaces *in vivo*. However, more recently, in a review paper, Hanawa et al. (2004) studied metal ion release from various metallic materials, including titanium and titanium alloys implanted into the human body. They found that there was only a small chance that the ion would combine with biomolecules to cause cytotoxicity, allergic reactions, and other biological influences.

Ca-ion implantation, which is studied extensively in this project, has been proposed previously as a route to bioactive titanium surfaces, and has been shown to stimulate promising cell and tissue responses *in vitro* and *in vivo* (Chapter 1). Calcium may influence cellular responses via accelerated precipitation of calcium phosphate, providing a surface with a chemical composition more similar to that of bone (details of bone composition were given in Chapter 1). This may be at least partially due to ion release from the implanted surface. Calcium could also directly influence cellular responses. Ca implanted Ti was found to have a more active hydroxyl radical than cp Ti (Hanawa et al., 1998), as the surface was charged more positively in a bioliquid than titanium. Such a surface facilitates the adsorption of hydroxyl radicals and phosphate ions in a bioliquid because of the attractive force caused by the electric charge. It is promising that more proteins or more of a specific important protein (selective adsorption) may be adsorbed by Ca-Ti than cp Ti because of the larger number of charging sites, or that they may be absorbed in a more beneficial conformation.
Hanawa et al. (1996) assumed that one of the reasons for Ca ion implanted titanium having good bone conductivity was probably the micro-dissolution of Ca

ions into the bioliquid, which could induce the precipitation of calcium phosphate onto the material by supersaturation in the adjacent bioliquid. They noted that in order to understand the behaviour of Ca implanted Ti in a biological system it was important to confirm both the dissolution of Ca and its dissolution rate. In their paper they reported the microdissolution of calcium ions from calcium-ion-implanted titanium into nitric acid solutions at several pH values (0.99, 0, 1 and 2) at 310 K for 10^3-10^6 s in scaled polyterafluoroethylene bottles. Phosphate-citric acid buffers (pH 5.2 and 7.2) were also chosen because the pH of hard tissues near to the inserted material dropped to 5.2, although their normal pH is ~ 7.2. The immersion was carried out at 310 K for 10^3 – 5 x 10^6 s. The samples were characterized using X-ray photoelectron spectroscopy. The surface oxides containing calcium were found to dissolve in the solutions. Relative levels of oxygen and titanium decreased and increased respectively as dissolution progressed. The authors stated that the changes were caused by the transformation of the surface oxide as dissolution progressed. Calcium dissolved and, consequently, the surface oxide became titanium oxide.

Brunette et al. (2001) presented a model of dissolution of the oxide layer on cp Ti following immersion. The authors have detailed the dissolution of the titanium oxide film in water 'from a thermodynamic point of view'. They stated that the oxide layer was very stable in the ambient environment but that it was not stable in the aqueous environment. The mechanism of dissolution of the oxide and release of the Ti species into water was presented by the following equation:

$\{TiO_2\}_{solid} + 2H_2O \leftrightarrow Ti(OH)_{4\,aq}$

The neutral species of $Ti(OH)_4$ formed only in small amounts, with typical concentrations in the range of 10^{-6} M. Other ionic species may be formed in much lower concentrations (10^{-10}, 10^{-11}M), as displayed in the following equations:

1. $\{TiO_2\}_{solid} + 2H_2O \leftrightarrow [Ti(OH)_3]^+_{aq} + OH^-$.
2. $\{TiO_2\}_{solid} + 2H_2O \leftrightarrow [TiO_2OH]^-_{aq} + H_3O^+$.

Small amounts of charge corrosion products were expected in addition to these species, which would elicit minimal unfavourable biochemical reactions.

The authors concluded that the dissolution rate (represented by the amount of dissolved oxides per time) depended on several factors including the oxide thickness, oxide stoichiometry, electrolyte composition, and temperature. However, they did not provide this rate or elaborate on the changes in oxide thickness following such dissolution.

Other previous studies (Shinawi, 2003) investigated cp Ti and ion implanted titanium discs (Ca-Ti, K-Ti) immersed in water for various periods of time, both at room and body temperature (37°C).The aims were to assess the mechanism and the rate of ion dissolution, and to establish if the rate of the ion dissolution was dependent on the chemistry of the surface. The samples were analysed with XPS, SEM and SIMS. For the cp Ti samples, the general appearance was not altered by the immersion. The XPS spectra showed little change following immersion except for a minor decrease in the intensity of the Ti^0 peak that was independent of the immersion temperature. However, no sound conclusions could be drawn from these studies as no statistical analyses were carried out. Regarding the Ca implanted samples analysed in Shinawi's work, their surfaces showed a blue discolouration after immersion. This was uniform for the samples immersed at body temperature but only covered some areas of the surface following immersion at room temperature. Regarding the implanted ions (Shinawi, 2003), the relative concentration of the Ca and K ions repeatedly decreased following immersion in water. For Ca up to a third of the original measured value (ion dose = 1.4×10^{17} cm^{-2}), or two thirds (ion dose = 1×10^{17} cm^{-2}) was lost. XPS measurements indicated a decrease in the Ca/Ti ratio. Three mechanisms were proposed:

a) Dissolution of the ion-containing titanium oxide layer
b) Growth of the titanium oxide film
c) Ion leaching

Both oxide layer growth and ion leaching could explain the observed decrease in the Ca/Ti ratio. While it was suggested that ion leaching was the most likely scenario, largely because the Ti 2p spectra before and after immersion were identical, suggesting no oxide layer growth, these experiments analysed only the surface of the titanium sample, and did not look at the solution to confirm whether ions were actually released. More work was also required to ascertain the mechanism of the blue coloration, which is normally indicative of oxide layer growth.

Ion release into certain solutions has been studied in detail by Hanawa et al., (1996a, 1996b), using Auger electron spectroscopy in combination with argon ion sputtering to obtain depth profiles of Ca implanted Ti. The authors stated that the dissolution of Ca from Ca implanted titanium occurred by the dissolution of the surface oxide itself on Ca implanted Ti and the dissolution of Ca by diffusion

through the surface – modified oxide layer. Hanawa (1996) also showed that the Ca ion concentration in Ca implanted titanium discs decreased on immersion in aqueous solutions. However, the ion released into the solution has not been measured to date. This chapter aims to assess whether or not Ca ions are released from Ca-Ti discs into water by analysing the solution itself, to ascertain whether the release can be followed using ion chromatography, and to correlate the results with the results of surface analysis.

4.2 CALCIUM ION RELEASE FROM CA-TI DISCS IMMERSED IN DEIONISED WATER.

4.2.1 Aims and objectives

This study aimed to observe if Ca ions were released into solution from Ca-Ti discs, and if this release could be detected using ion chromatography.

4.2.2 Materials and methods

X-ray photoelectron spectroscopy (XPS) was used to analyse the surface of the discs, and ion chromatography the solution in which they were immersed.
A preliminary study was carried out using three Ca implanted titanium discs and three cp Ti discs to determine whether ion release from a titanium disc into deionised water (DW) took place and could be detected using ion chromatography. This technique was used as a method of analysis because the amount of ions released was thought to be very small, and it may have proved difficult to detect them using other methods. Alternative techniques include ICP-AES (Inductively Coupled Plasma - Atomic Emission Spectroscopy) which uses ICP (inductively coupled plasma) to produce excited atoms that emit electromagnetic radiation at a wavelength characteristic of a particular element. The intensity of this emission is indicative of the concentration of the element within the sample. This technique is also referred to as ICP-OES (Inductively Coupled Plasma Optical Emission Spectrometry), ICP-MS (Inductively Coupled Plasma Mass Spectrometry) which

actually could not detect Ca due to mass interference from the Ar ions (also with mass 40 a.m.u.). All use different measurement techniques for assessing the ions in the plasma. Another method for detecting ions in solution is Atomic Absorption Spectroscopy (AAS).

Since the preliminary study was successful a second study was performed. In this six implanted Ca-Ti discs ($^{40}Ca^{+}$, 40 keV, 1 x $10^{17}cm^{-2}$) were analysed using XPS, employing the monochromated X-ray source, the protocol being described in Chapter 2.
Before immersion, the samples were ultrasonically cleaned in deionised water for 5 minutes, to ensure a direct comparison with previous studies carried out by Shinawi. They were then immersed in 1 ml DW at 37°C in plastic well plates. As controls, six 1 ml samples of deionised water (DW) and six cp Ti samples, which were also immersed in DW (1 ml), were placed in well plates. After 24 h at 37 °C all the solutions were removed from the well plates with pipettes, using one new pipette for each well plate in order to avoid possible contamination from one solution to the other. The solutions were then placed in new chromatography vials and analysed using ion chromatography. The Ca-Ti samples were removed from the well plates using plastic tweezers, dried using compressed air and re-analysed using XPS.
Three of the Ca-Ti discs were then re-immersed in fresh DW and placed in the incubator at 37°C for a further 47 h. On the basis of previous experiments, it was anticipated that by this time they would be completely blue in colour. The samples were removed from the solution using plastic tweezers, dried with compressed air, and their surface re-analysed using XPS. The solutions were analysed using ion chromatography (full details on the technique are given in Chapter 2).

4.2.3 Results and discussions

4.2.3.1 Appearance

The general appearance of the Ca-Ti discs before immersion was similar to that of the cp Ti discs (shiny silver) and was not altered by the implantation process. This was different from the Ca-Ti samples used in Hanawa's work in which the samples were described as `gold coloured'. Possible differences in the colour were

discussed earlier in Chapter 3.

After immersion in DW for 24 h, the surface colour of the Ca-Ti samples changed and they presented blue patches distributed non-uniformly over the surface, alternating with unchanged silver zones. After a further 47 h immersion, the samples became a uniform pale blue.

Lausmaa et al., (1985) suggested that the blue discoloration of autoclaved titanium surfaces may be due either to light absorption as a result of contamination layers following deposition during autoclaving, or light interference following oxide growth of >100 Å. These authors believed that the blue colour may result from either the reduction of Ti^{4+} in the oxide to Ti^{3+} or from growth of the oxide layer to an estimated thickness of 100-700 Å. Also the blue colour was reported by Pan et al. (1996) on cp Ti samples (grade 1) immersed in a PBS solution with added H_2O_2 after 1-4 weeks of immersion. They suggested that the blue colour was caused by optical interference effect due to an increase in the oxide layer, although hydrogen induced changes of the oxide properties cannot be excluded as an additional cause. They also stated that although Ti^{3+} may be formed as an intermediate during the oxidation process of titanium, the reduction of Ti^{4+} in the oxide to Ti^{3+} is unlikely. A blue colour was also observed on titanium implant samples with a 10-fold increase in the oxide layer due to fluorine contamination in the preparation process (Lausmaa et al., 1986).

The colour modification of the samples in this work was less pronounced than for the samples described by Shinawi (2003), who observed that the samples became fully deep blue after immersion in water at 37°C for 24 h. In her work, the blue discoloration was tentatively attributed to thickening of the oxide layer, since XPS analysis showed that the Ti^{4+} was the dominant valence in the oxide layer. However, since no increase in Ti^{4+} relative to Ti^{n+} peak ($n<4$) was observed following immersion, there was little evidence to support this. It would be interesting to explore a possible association between the colour modification of the samples in this work and any changes in the surface chemistry or ion release.

The blue colour observed in this work however was in disagreement with previous work carried out by Hanawa (1996 a and b), who stated that their samples were initially gold coloured. Following immersion in nitric acid and phosphate-citric buffer, the gold colour of the specimens gradually returned to the original titanium colour during immersion. This may be due to the thinning of the oxide layer following immersion in acid.

4.2.3.2 Surface analysis (XPS)

The surface of Ca-Ti before and after immersion in UPW was analysed using XPS. The Ti 2p and Ca 2p spectra for three samples before immersion (0 h) and after 24 h, and 24h + 47h immersion are presented in figures 4.1 and 4.2. All the XPS spectra presented below have been normalised to the Ti 2p peak maximum for each sample. A more detailed explanation about the normalisation of the data was given in section 2.7.2.

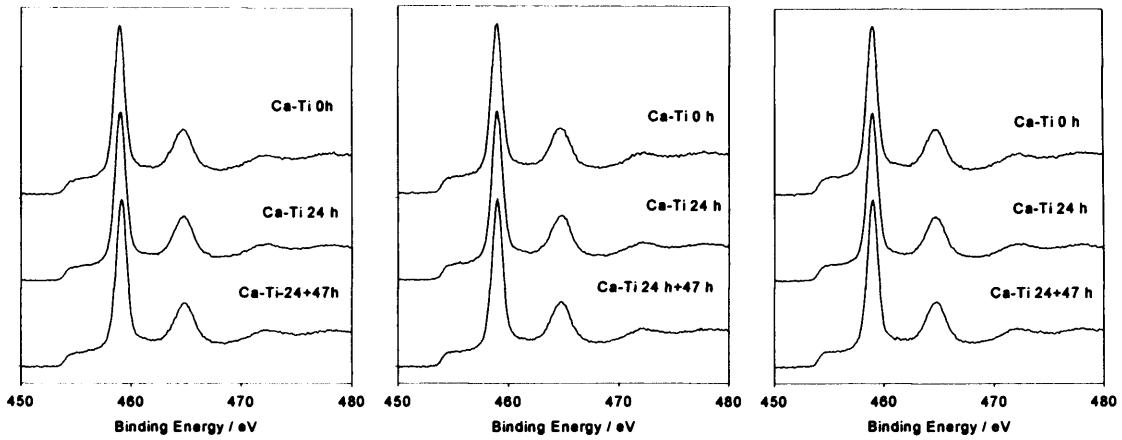

Figure 4. 1 The Ti 2p spectra from the 3 Ca-Ti samples before immersion in water (0 h), following 24 h immersion in DW (24 h) and following a further 47 h immersion in DW (24 h + 47 h).

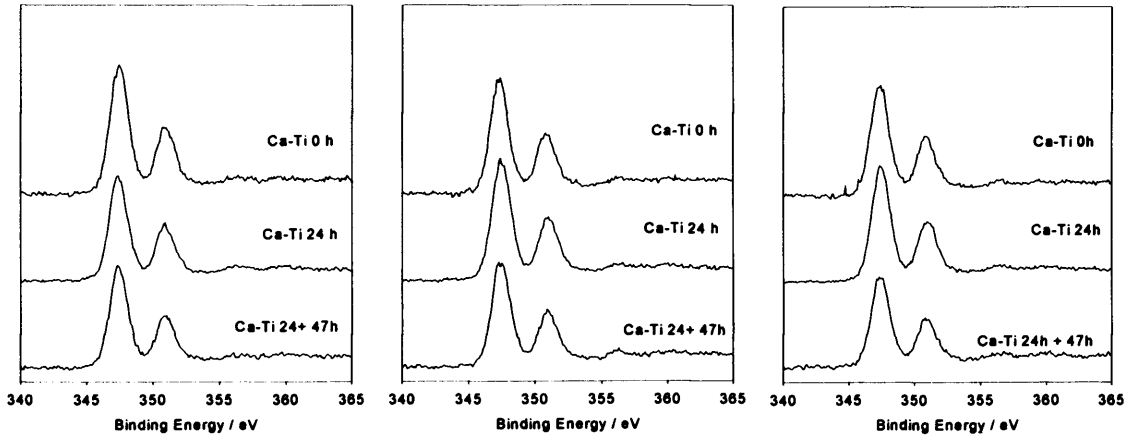

Figure 4.2 The Ca 2p spectra from the 3 Ca-Ti samples, before immersion in water (0 h), following 24 h immersion in DW (24 h) and following a further 47 h immersion in DW (24h + 47 h).

Before immersion (0 h), the Ti 2p spectra were similar for all three samples and

were typical for Ca implanted titanium. The Ca 2p spectra presented two very well defined peaks, at 347.3 eV and 350.7 eV, which were the $2p_{3/2}$ and $2p_{1/2}$ components of the spin orbit doublet.
After 24 h immersion in water, the Ti 2p and Ca 2p spectra did not change significantly in terms of shape and were very similar to the '0 h' spectra, for all the samples. The statistical analysis showed that there was no significant change in the Ca/Ti ratio following immersion in DW. The surface calcium was expected to drop by one third, as found in the pilot study carried out before this experiment, but this was not the case. Shinawi (2003) also showed in her work that the Ca/Ti ratio at the surface drops by ~ 1/3 on immersion in water at body temperature for 24 h. However, the samples analysed by Shinawi had higher Ca/Ti ratios (0.29) than those analysed in the current work. One possible explanation for this minimal drop of calcium on the surface was that the samples were ultrasonically cleaned in deionised water before immersion to remove possible surface contaminants. However, Shinawi' s samples were also ultrasonicated, and yet retained higher Ca/Ti ratios. Additionally, a different quantification technique was used, which may also give slightly different results.

After a further 47 h immersion in DW, the Ti 2p and Ca 2p spectra were unchanged in terms of peak shape, and presented only a slight decrease in the intensity of the Ca 2p peaks in comparison with the samples immersed for 24 h. The reduction in Ca/Ti ratio (Table 4.2) was not significant different following immersion.

The atomic percentages (average and SD) for 6 Ca-Ti samples are presented in table 4.1. A quantification table of various elements (Ca, O and C) is also presented for all time points (table 4.2). The averages in this table were calculated from 6 samples for the 0 h and 24 h samples and from 3 samples after a further 47 h immersion.

Ca-Ti	**Ca 2p %**	**O 1s %**	**Ti 2p %**	**C1s%**
Composition (atomic percentage [%])	*3.5 ± 0.5*	*58.6 ± 3.4*	*20.6± 1.9*	*17.3 ± 5.4*

Table 4. 1 Elemental composition of Ca-Ti samples measured in atomic percentages (averages and SD) recorded using monochromated X-ray source.

Immersion time	Ca/Ti	O/Ti	C/Ti
0 h	0.17 ± 0.02	3.27 ± 0.41	1.30 ± 0.42
24 h	0.16 ± 0.01	2.74 ± 0.31	0.73 ± 0.39
24 h + 47 h	0.15 ± 0.01	2.70 ± 0.07	0.79 ± 0.02

Table 4. 2 Elemental ratios (averages and SD) measured using XPS, before immersion (0 h), and after immersion (at 24 h and a further 47 h).

The analysis of the surface at various time points showed minimal modification, both qualitative and quantitative. Also the spectra presented in figures 4.1 and 4.2 showed consistencies in the behaviour of all the samples, at all the time points.

4.2.3.3 Ion Chromatography

In Table 4.3 calcium ion concentrations measured in ppm (averages and standard deviations) are presented for the deionised water (control 1) and the solutions in which the cp Ti (control 2) and Ca-Ti samples were immersed. They were calculated by taking the average from 6 values for DW, cp Ti, and Ca-Ti (24 h) and from 3 values for Ca-Ti samples re-immersed for a further 47 h.

Sample	Immersion Time	Ca ion release (ppm) Average ± SD
Control 1 (DW)	24 h	0.04 ± 0.004
Control 2 (Cp Ti)	24 h	0.17 ± 0.27
Ca-Ti	24 h	0.71 ± 0.31
Ca-Ti	47 h	0.35 ± 0.16

Table 4. 3 Ca ion concentration measured in ppm (average and standard deviation) for control (DW) and the solutions in which the cp Ti and Ca-Ti.

The average Ca concentration observed for the deionised water (0.042 ± 0.004 ppm) suggested that Ca ions were present in DW in very small amounts. The average Ca concentration for the cp Ti samples (0.169 ± 0.271 ppm) was not significantly higher than the DW average calcium concentration. This suggested, however, that contaminant Ca was present on the cp Ti samples. This was in

agreement with the literature, where Lausmaa et al. (1990) reported calcium present on the majority of samples they analysed, but no Ca/Ti ratio was given. However, among the samples analysed in this experiment there was a large variability between samples indicated by the high standard deviation. Considering the individual values for each of the samples, indeed, 4 out of 6 solutions analysed had minute amounts of Ca, with an average value for the 4 of 0.02 ± 0.02 ppm. There were only 2 samples (no 2 and 4) which had high values of Ca ions detected in solution, one with 0.69 ppm and the second with 0.22 ppm. These values are indeed very high and probably reflect contamination of these samples.

For Ca-Ti immersed for 24 h, the average Ca concentration was found to be 0.712 ± 0.311 ppm. This was significantly higher ($p<0.05$) than the control solutions and indicated that Ca was released from the ion implanted samples. The small standard error bars indicated that there was uniformity among the samples. Surface analysis data for these samples showed a small drop in the surface Ca. Therefore, if the Ca which was released did not come from the surface, it must have originated from the sub-surface regions of the samples.
After a further 47 h, the average Ca concentration for Ca-Ti samples was 0.351 ± 0.159 ppm, so calcium ions were still being released into solution even after a further 47 h immersion, but at a reduced rate. This value was significantly lower ($p<0.05$) than the value representing Ca ion released after 24 h, but was significantly higher ($p<0.05$) than the Ca concentration detected in the DW or the DW were the cp Ti samples were immersed.

4.2.4. Conclusions

A very small amount of Ca ions was detected in the control samples (DW and also in the DW in which the cp Ti was immersed).
The highest value of Ca ion released in solution was observed for Ca-Ti immersed at 37°C for 24 h, followed by Ca-Ti immersed for a further 47 h, a fact which confirmed the hypothesis that calcium ions are released from Ca ion implanted samples.
The ion chromatography data showed that Ca ions were detectable in solution after 24 h immersion at 37 °C. The XPS data does not show a drop in the calcium on the surface, which is not in agreement with previous studies because unlike the

previous studies (Shinawi, 2003), only a small drop in the Ca/Ti ratios at the surface of the discs was observed, in the range of 5 % compared with almost 33 % previously reported by Shinawi. As explained before this may be because the levels of calcium present in the samples used in the current studies (Ca/Ti~ 0.18, caused by the ultrasonication of the samples prior to immersion) were somewhat lower than those of the earlier work (Ca/Ti ~ 0.4 - 0.24).

As in the earlier study, ions were found to be released over the first 24 h, but were also observed in solution after a further 47 h, suggesting that the ion release continued, even though at a reduced level. Because Ca appeared to be present in the DW, ultrapure water should be used in future experiments.

4.3 VARIATION OF CA ION RELEASE FROM CA-TI SAMPLES IMMERSED IN ULTRAPURE WATER WITH TIME.

4.3.1 Aims and objectives

The XPS results (qualitative and quantitative) recorded from the analysis of the surface for the previous experiment did not clearly confirm the calcium ion release results recorded with ion chromatography, because they showed that the surface calcium dropped by only a fraction.

In order to further verify the ion release and to clarify the mechanism, a second study was carried out. This experiment used ultrapure water (Elga Labwater, Veolia Water Systems, USA) in an attempt to avoid contamination with Ca ions. In addition to standard XPS and ion chromatography, depth profiling XPS (Chapter 2) was used to analyse the sub-surface region of the samples. Newly implanted Ca-Ti discs were used, with the ion implantation carried out in the Department of Electrical and Electronic Engineering, Imperial College of Science, Technology and Medicine, London, using $^{40}Ca^{+}$ ions at a dose of 1×10^{17} ions cm^{-2}, and an implantation energy of 40 keV. Also, as it had been shown in the previous experiment that ion release was present at 24 h; a greater time range of immersion was chosen to attempt to find the peak release rate.

4.3.2 Materials and methods

Before immersion, the surfaces of thirty as-implanted Ca-Ti discs ($^{40}Ca^{+}$, 40 keV, 1 x 10^{17} cm^{-2}) and thirty polished cp Ti samples (as controls) were analysed using XPS.
XPS data for both surface and depth profiling were quantified using the CasaXPS software and Shirley background subtraction. For the depth profiling studies, Ar was excluded from the quantifications, as it is not a contaminant of Ca-Ti and it was not observed on any of the surfaces prior to etching. Any Ar observed on the surface during the etching was the result of the etching process, as Ar can be implanted into the surface from the argon ion beam used to etch the surface.
The immersion studies were carried out in 24 well cell culture plates (Corning Incorporated 3526, Corning, USA), by immersing each of the discs in 1 ml ultrapure water. The water was positioned in the well plates using a pipette and a single tip for all the samples. It was then placed in the incubator at 37°C for an hour prior to immersion, to allow the ultrapure water to reach the desired temperature. Six discs of each (Ca-Ti and cp Ti) were then immersed face upwards using plastic tweezers in the ultrapure water (1 ml per disc) for 2 min, 4 h, 24 h and 1 week in the incubator at 37° C. The well plates were sealed using parafilm (Clean Foil, Clingorap, Terinex, Prod. 235011203). A further six x 1 ml samples of ultrapure water were placed in the well plates for the same periods of time alongside the cp Ti and Ca-Ti samples, as additional controls.

After immersion the solutions were drawn off using pipettes with a new clean plastic tip for each, and placed in individual chromatography vials (Chromacol Ltd., Herts, U.K.) for analysis using ion chromatography.
The Ca-Ti and cp Ti samples were removed using plastic tweezers, dried with compressed air, (Falcon Safety Products, Inc., Branchburg, USA, Model 88010 DPSXLX) wrapped in aluminium foil (Aluchef Foil, Terinex Limited, Bedford, UK, Prod. 236401002, Supp: 11351), and placed in a desiccator until analysis.

The samples were analysed using XPS and XPS depth profiling. Details regarding the instruments were given in Chapter 2. The depth of the crater resulted after the depth profiling was measured using WLI and it was ~150 nm. As the total etching time was 191 min, the rate of etching was 0.8 nm / min. However, it has to be

mentioned that the rate of etching was quite different when etching was on the oxide layer or on the metal. Approximate etch rates calculation were attempted by Dr. D Armitage at the UCL Eastman Dental Institute, who gave very approximate etch rates of 24 nm h^{-1} and 49 nm h^{-1} for the metal and the oxide respectively, meaning that the oxide etched almost twice as fast as the metal.

4.3.3 Results and discussion

4.3.3.1 Appearance

The general appearance of the Ca-Ti discs before immersion was similar to that of the cp Ti discs (shiny silver) and was not altered by the implantation process (see section 3.3.3). After immersion, the surface colour of the Ca-Ti samples had changed and varied from fully deep blue on some of the samples, to patchy blue (samples which did not turn fully blue and had blue patches distributed over parts of the surface together with unchanged silver zones) on other samples. A few of the samples did not change colour at all and remained fully silver. This is summarised in table 4.4, which presents the data for the immersed samples, numbered 1-6 for each time point (2 min, 4 h, 24 h, and 1 week.) However, different samples were used for each time point.

Colour	2 min	4 h	24 h	1 week
Silver	all			1 sample (no 3)
Patchy blue < 50%			2 samples (no 2, 4)	2 samples (no 1,4)
Patchy blue > 85%		3 samples (no 2,4,6)		2 samples (no 2,5)
Fully blue		3 samples (no 1,3,5)	4 samples (no 1,3,5,6)	1 sample (no 6)

Table 4.4 Variations in the colour change of the Ca-Ti discs after immersion in ultrapure water for 2 min, 4 h, 24 h, and 1 week.

It can be noticed from table 4.4 that after 2 min immersion none of the samples had changed colour and all remained silver, as they were before immersion.

The situation changed after 4 h immersion, where none of the samples remained silver and all had changed colour and became blue (on the whole surface or patchy) as follows: 3 discs became fully blue while more than 85% of the surfaces of the other three were blue.
After 24 h immersion, again, none of the samples was silver, with 4 having become fully blue and 2 patchy blue, but this time the blue colour was on less than 50% of the surface.
For the samples immersed for 1 week, there was only one sample which turned fully blue. 2 of the samples became more than 85% blue and 2 less than 50% blue. One sample did not change colour at all and remained fully silver.
Comparing the results with the previous experiment where the samples turned pale blue, this time most of the samples were immersed for 4 h and more changed colour to deep blue. The colour change was similar to that recorded by Shinawi for her samples after immersion. The difference with Shinawi's samples and with those in the previous experiment is that some of the samples did not change colour over the whole surface. This may be due to the samples not being used immediately after implantation, as Shinawi did with her samples, but after ~7 months, which may have influenced their behaviour. Another factor may be that Shinawi analysed a smaller number of samples than in this experiment, hence the possibility of variation was smaller.

The blue colour of some samples may be due to an interference effect associated with oxidation of the surface. Reflected light from the air-oxide and oxide-metal interfaces interferes constructively for certain wavelengths and destructively for others, depending on the thickness and refractive index of the transparent oxide layer. Data supporting the thickening of the oxide layer is presented later in this section.

Analysing the colour modification table, it is not clear why there was such a variation in the colour of the samples. It appears that as the immersion time increased, so did the number of samples which did not turn fully blue. As mentioned before it would be interesting to investigate whether there is any association between this colour modification and the surface chemistry or the ions released from the samples.

4.3.3.2 Surface analysis

Elemental ratios (Ca/Ti, O/Ti and C/Ti) are summarised in table 4.5, and presented more clearly for Ca/Ti in figure 4.3. Quantification of the spectra was carried out in the usual manner (details in Chapter 2). The averages were calculated from 30 samples for the 0 s and 6 samples for the 4 h, 24 h and 1 week immersion. The XPS surface spectra (Ca 2p, Ti 2p, and O 1s spectra) for the Ca-Ti discs are presented in figures 4.4, 4.5 and 4.6.

Table 4.5 shows the Ca/Ti, O/Ti, and C/Ti ratios for Ca-Ti samples before immersion (0 min) and following 2 min, 4 h and 24 h immersion in ultrapure water at 37°C.

Immersion time	Ca/Ti	O/Ti	C/Ti
0 min	0.22 ± 0.01	2.59 ± 0.08	0.81 ± 0.06
2 min	0.11 ± 0.01	2.15 ± 0.04	0.74 ± 0.10
4 h	0.09 ± 0.01	2.54 ± 0.26	0.60 ± 0.18
24 h	0.09 ± 0.01	2.80 ± 0.28	0.84 ± 0.14
1 week	0.09 ± 0.01	2.92 ± 0.25	0.85 ± 0.16

Table 4.5 Ca/Ti, O/Ti and C/Ti ratios (averages + SD) for Ca-Ti discs before immersion (0 min), and after 2 min, 4 h, 24 h and 1 week immersion in ultrapure water at 37°C.

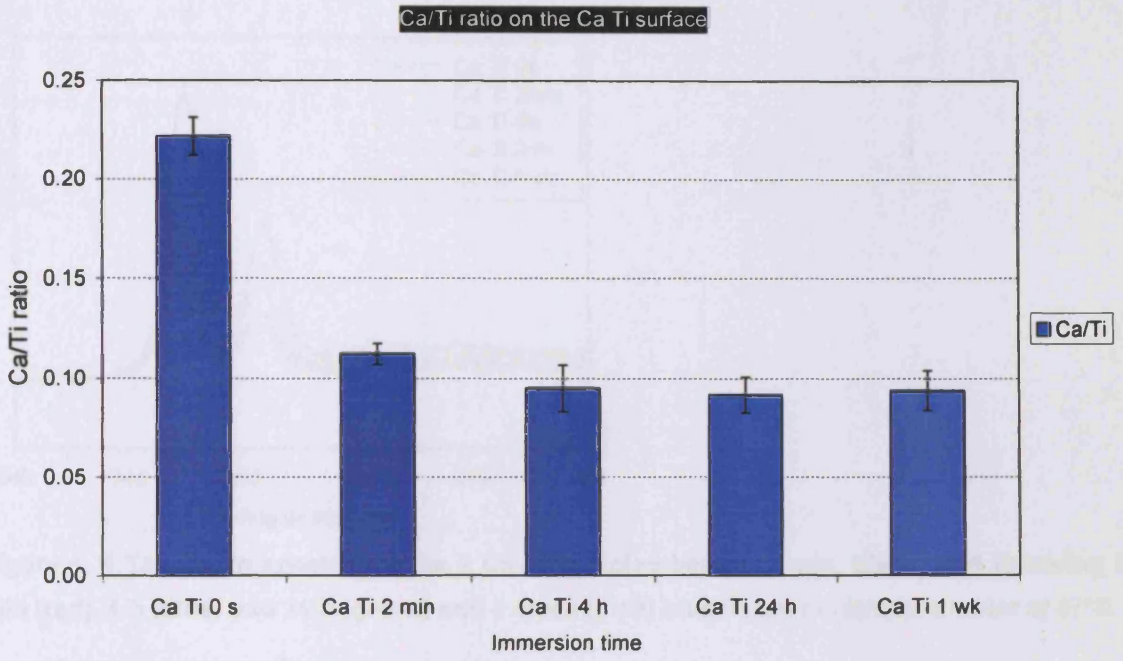

Figure 4. 3 Ca/Ti ratios for Ca-Ti discs before immersion (0 min), and after 2 min, 4 h, 24 h and 1 week immersion in UPW at 37°.

From table 4.5 and figure 4.3 can be noticed that all the elemental ratios recorded for the Ca-Ti 0 min samples and the immersed Ca-Ti samples had very low standard deviations, despite the fact that there was a huge variation in the appearance of the samples following immersion in ultrapure water. Considering that the elemental ratios presented above were calculated on samples which had variable behaviour with regards to the colour change following immersion, it appears that the colour modification does not cause variability in the surface elemental composition.

Figure 4.4 shows the Ca 2p spectra for 4 different Ca-Ti samples before immersion (0 min, black) and following 2 min (red), 4 h (blue) 24 h (green) and 1 week (pink) immersion in ultrapure water at 37°C.

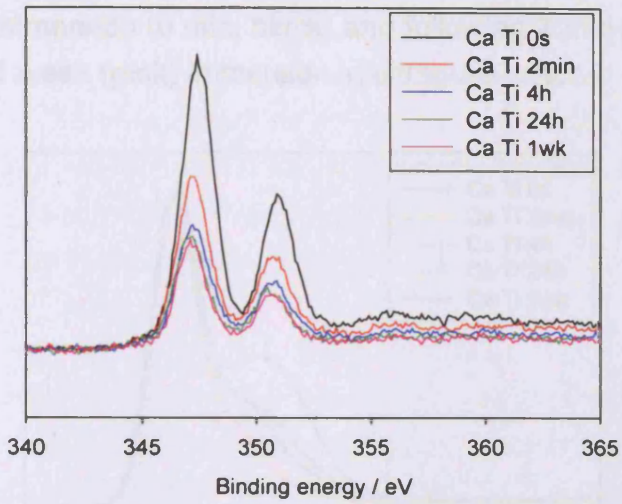

Figure 4. 4 The Ca 2p spectra for the 4 Ca-Ti samples before (0 min, black) and following 2 min (red), 4 h (blue) and 24 h (green) and 1 week (pink) immersion in ultrapure water at 37°C.

Before immersion (0 min), the Ca 2p spectrum was typical for Ca implanted titanium. The Ca 2p spectrum presented two very well defined peaks, at 347.3 eV and 350.7 eV, which are the $2p_{3/2}$ and $2p_{1/2}$ components of the spin orbit doublet. The quantification data showed that before immersion, the average Ca/Ti ratio at 0 min for the 6 samples was 0.22, with very small variation among the samples.
Following immersion in ultrapure water, the Ca 2p spectra for all the samples had not changed in terms of shape and were very similar to the '0 s' spectra. However, the intensity of the Ca 2p peaks decreased by more than 50 % after 2 min immersion, and only slightly more after that. The decrease in the Ca/Ti ratio was clearly seen in figure 4.4 and corresponds to a significant decrease ($p<0.05$) in the surface calcium after 2 min by more than half the initial value, from an average of 0.22 ± 0.01 to 0.11 ± 0.005 (table 4.5). After this time point, the Ca/Ti ratio on the surface did not change significantly ($p < 0.05$), dropping only by a fraction to 0.9, again in agreement with the appearance of the samples immersed for a longer time, where the intensity of the peaks of the Ca 2p spectra showed only a slight decrease. There was also uniformity in the behaviour of all the samples, as illustrated by the small standard deviation encountered. Immersion for a longer period did not result in a further significant decrease in the surface calcium (table 4.5).

Figure 4.5 shows the O 1s spectra from 4 different Ca-Ti samples before immersion (0 min, black) and following 2 min (red), 4 h (blue) and 24 h (green) and 1 week (pink) immersion in ultrapure water.

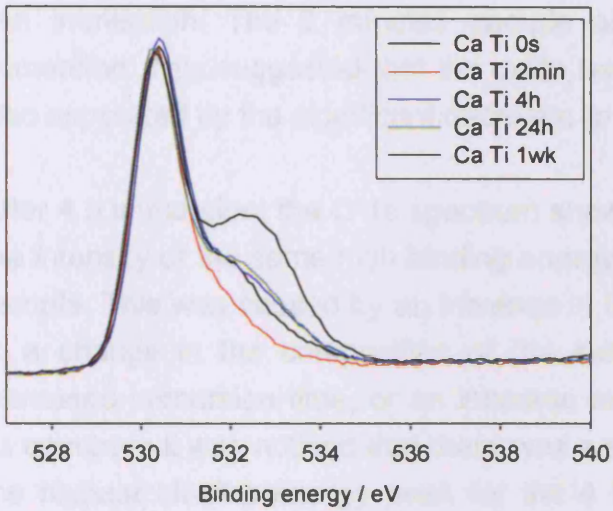

Figure 4. 5 The O 1s spectra from the 4 Ca-Ti samples before (0 min, black) and following 2 min (red), 4 h (blue) 24 h (green) and 1 week (pink) immersion in ultrapure water at 37°C.

The O 1s spectrum for the Ca-Ti 0 min sample had a single peak at ~ 531 eV due to O in O^{2-} from the oxide. The O/Ti ratio on the surface had a value of 2.59 ± 0.08. The slight shoulder, which appeared at higher binding energy, is due to OH^- on the surface, which may have been caused by a slightly different oxide layer with different composition. It may also be due to contamination, which may have come from various sources, such as the air, and the water used for the experiment etc. One possible cause of the contamination was aluminium oxide from the aluminium foil in which the samples were wrapped. However, as no Al 2p peaks were observed on the survey spectrum this could be ruled out. The shoulder at higher binding energy was therefore attributed to O in OH due to surface hydroxylation.

After 2 min immersion, the main difference in the O 1s spectrum was the decrease in intensity of the shoulder to high binding energy. Causes for this decrease may have been slight alterations in the composition of the surface oxide layer resulting in changes in the hydroxide levels, or that after 2 minutes there was a reduction in the amount of carbon contamination, resulting in a decrease in the signal due to C linked to O. After analysing the carbon spectra (spectra not presented) it was concluded that there was a slight decrease in the second C peak at ~287 eV due

to C-O and to the highest binding energy peak at ~289 eV due to COO^-. This suggested that one cause for the decrease in the O 1s shoulder may be a decrease in C contamination due to organic species. Another possibility is that the OH species (which could include C-O etc) are being washed off the surface after 2 min immersion. The 2 minutes sample also did not change colour following immersion. This suggested that the oxide layer decreased in thickness, which was also supported by the significant decrease ($p < 0.05$) in the O/Ti ratio (table 4.5).

After 4 h immersion, the O 1s spectrum showed a significant increase ($p < 0.05$) in the intensity of the same high binding energy shoulder as compared with the 2 min sample. This was caused by an increase in the OH from the surface, probably due to a change in the composition of the surface oxide layer present due to the increased immersion time, or an increase in contamination. After analysing the C 1s spectrum it was noticed that there was a slight increase in the carbide peak and the highest binding energy peak for the 4 h sample as compared to the 2 min sample, but a small decrease in the intensity of the hydrocarbon peak. An increase in contamination due to C linked to O could not be ruled out as one of the causes for the increase in the OH shoulder. Another possibility for the increase in the OH species was that the surface begins to hydrolyse following 4 h immersion, hence the increased shoulder. Throughout the work variable levels of OH^- were seen. This could be purely down to external factors such as the exact drying method and washing or immersion time, time from cleaning / immersion to analysis, room humidity etc. The O/Ti ratio for the 4 h sample increased significantly ($p < 0.05$) when compared to the 2 min sample, but the levels reached were still significantly smaller ($p < 0.05$) than the levels recorded before immersion. The 4 h immersed samples also changed in colour and became blue. This finding suggested that the oxide layer increased in thickness as explained previously. The O/Ti ratio increased significantly after 24 h immersion as compared with all the time points. Also the C 1s spectra (not presented) showed a slight increase in the carbide peak and the peaks at 286.8 eV and 288.8 eV due to C linked to O as compared to the 2 min. Again, it may be observed that one of the causes of the increase in the O/Ti ratio was an increase in C contamination. However, another possible cause of the increase in the O/Ti ratio could have been that the oxide layer was thicker on the surface.

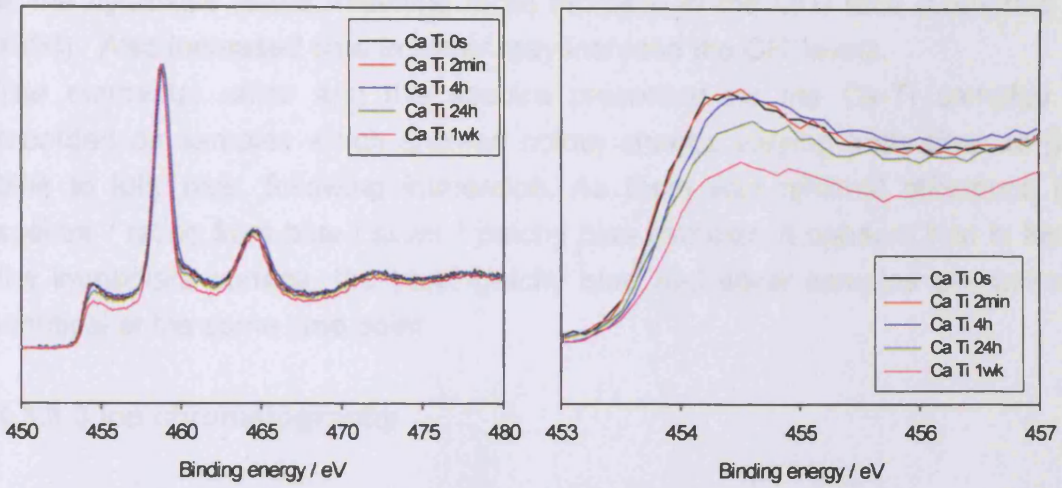

Figure 4. 6 The Ti 2p spectra (left) from the 5 Ca-Ti samples before (0 min, black) and following 2 min (red), 4 h (blue), 24 h (green) and 1 week (pink) immersion in ultrapure water. Expanded Tin+(n<4) peak (right) from the same Ti 2p spectra from the 5 Ca-Ti samples before (0 min, black) and following 2 min (red), 4 h (blue), 24 h (green) and 1 week (pink) immersion in ultrapure water (right) at 37°C.

The Ti^{4+} $2p_{3/2}$ peak at approximately 458.7 eV dominated the Ti 2p spectrum. The peak at lower binding energy was attributed to Ti^{n+} ($n < 4$) and it was noticed that this peak was much sharper than the peak from the Ti 2p spectrum presented in figure 4.1. These samples came from a different batch, and showed different amounts of carbide on the surface. Although the implantation parameters were the same, this was possibly due to the highly reactive Ti surface exposed that may react with residual hydrocarbons in the implantation chamber to form carbide species. Additionally, the ion implantation process may lead to some recoil implantation of adsorbed contaminant carbon into the Ti surface (Chapter 3).

After 2 min immersion there was no modification in the Ti^{n+} peak ($n < 4$), possibly meaning that the oxide layer stayed the same thickness. However, after both 4 h and 24 h immersion there was a reduction in the Ti^{n+} peak ($n < 4$), slightly more for the 24 h samples. This may indicate that a longer immersion resulted in an increase in the oxide layer thickness, and if this observation was correlated with the appearance, it could be assumed that a sample which turned blue reflects in an increased oxide layer. However, contamination cannot be excluded as a cause of reduction of the Ti^{n+} peak ($n < 4$) and increasing the O/Ti ratio, as time in air prior to analysis will cause an increase in the contamination, represented by an increase

in the hydroxide levels, resulting in an increase in the O/Ti ratio (Lausmaa et al. 1996). Also increased time in water may increase the OH^- levels.
The elemental ratios and the spectra presented for the Ca-Ti samples were recorded on samples which showed colour change varying from silver to patchy blue to fully blue, following immersion. As there was minimal difference in the spectra / ratios from blue / silver / patchy blue samples, it appears that in terms of the immediate surface, the blue, patchy blue and silver samples are essentially identical at the same time point.

4.3.3.3 Ion chromatography

This section presents the ion chromatography results for the immersed cp Ti and Ca-Ti described earlier. In table 4.6 calcium concentrations (averages) are presented for ultrapure water and the solutions in which the cp Ti and Ca-Ti were immersed. The values are presented as ppm. The averages were calculated from 6 values for ultrapure water, cp Ti, and Ca-Ti samples.

Sample	2 min	4 h	24 h	1 week
Ultrapure water	0.09 ± 0.06	0.24 ± 0.31	0.08 ± 0.03	0.20 ± 0.17
cp Ti	0.07 ± 0.04	0.07 ± 0.03	0.06 ± 0.05	0.10 ± 0.04
Ca-Ti	0.13 ± 0.09	1.27 ± 0.18	1.18 ± 0.35	1.06 ± 0.76

Table 4. 6 Ca ion concentrations (ppm) (averages and standard deviations) for ultrapure water and the solutions in which the cp Ti and Ca-Ti were immersed.

Figure 4.7 shows the concentration of calcium ions released into solution (average values and standard deviation) at the various time periods.

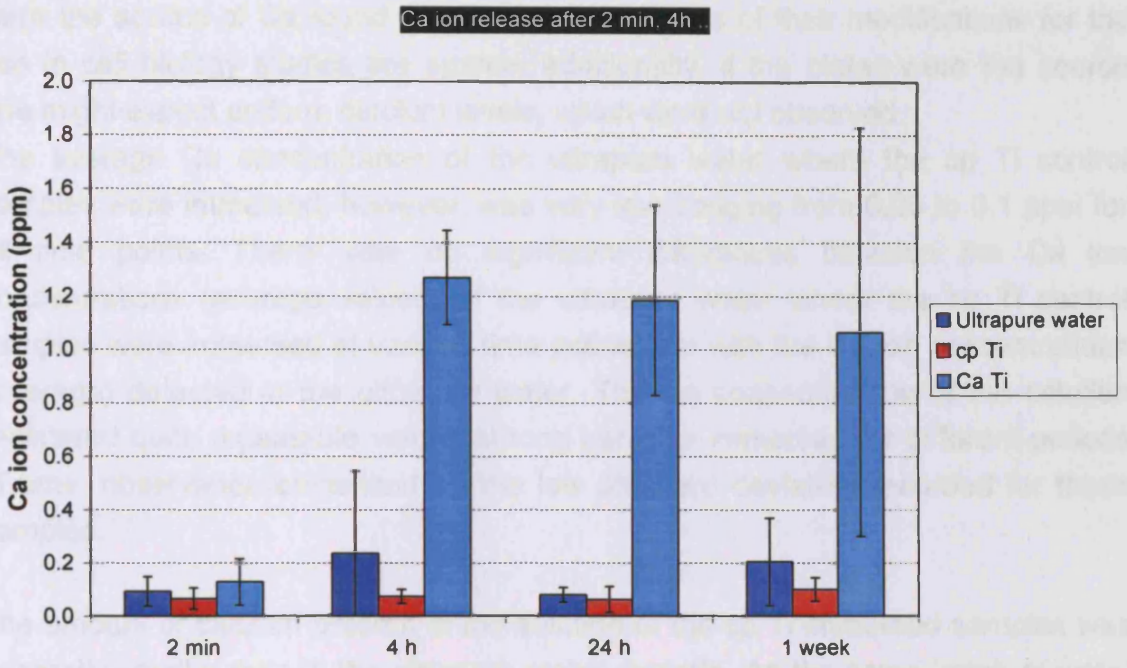

Figure 4. 7 Ca ion release (averages) control samples and from the solutions were Ca-Ti samples were immersed in UPW for 2 min, 4 h, 24 h, and 1 week

The average Ca concentration observed for the ultrapure water was generally low. However, it showed a large variability among samples, ranging from an average value of 0.09 ± 0.06 ppm for the 2 min samples, to an average value of 0.24 ± 0.31 ppm for the 4 h samples. No significant differences in calcium concentration were observed at any time point. As the same batch of ultrapure water was used in all the experiments, it was presumed that such a high variability among the samples was probably due to contamination. If the 6 individual samples were considered, the high average value and standard deviation were attributed to sample no 1 at the 4 h time point (0.86 ppm), and for the 1 week samples to sample number 4, which had a Ca concentration of 0.46 ppm. The Ca ion concentrations for the rest of the ultrapure water samples did not vary greatly from the average presented for ultrapure water (control) (0.09 ppm). As ultrapure water contains negligible amounts of Ca, it was clear that contamination caused this high increase in the calcium detected in the water. Possible sources that may contaminate the water were the well plates, the plastic tips used for removal of the solution in the well plates, or other sources (such as touching the samples). The last possibility may be excluded as gloves were used throughout the experiment in order to avoid any contamination of the samples by the hands. It is difficult to say if the well plates

were the source of Ca found in the water, as details of their modifications for the use in cell biology studies are scarce; additionally, if the plates were the source one might expect uniform calcium levels, which were not observed.
The average Ca concentration of the ultrapure water where the cp Ti control samples were immersed, however, was very low, ranging from 0.06 to 0.1 ppm for all time points. There were no significant differences between the Ca ion concentrations (average values) of the ultrapure water where the cp Ti control samples were immersed at various time points, nor with the Ca ion concentrations (average) detected in the ultrapure water. The Ca concentrations of the solution registered quite repeatable values among samples immersed for different periods of time, observation evidenced by the low standard deviation recorded for these samples.

The amount of calcium present in the solution of the cp Ti immersed samples was generally smaller than in the ultrapure water controls. As the same batch of water was used to immerse the cp Ti discs, it would have been expected that they would have at least the same amount of Ca as the ultrapure water. Since this was not the case, it could be argued that the calcium ion release might have been from the bottom of the well plates, which were covered by the cp Ti discs in the case of the cp Ti immersion, but not where only ultrapure water was placed in the wells. As the Ca ion concentrations in the ultrapure water (with the exception of two of contaminated wells) was similar to the Ca ion concentration detected in the solutions in which the cp Ti discs were immersed suggests that the wells were not source. The cause may be probably untraced contamination, a random error rather then a systematic cause.

For Ca-Ti immersed for 2 minutes the average Ca concentration of the solution was 0.13 ± 0.09 ppm; this value was not significantly higher than that for the control solutions at the same time point.

After 4 h immersion, the average Ca concentration of the solution for Ca-Ti discs had increased significantly ($p < 0.05$) to an average of 1.27 ± 0.18 ppm, much greater than either the control samples or the Ca-Ti immersed for 2 minutes. The samples were also behaving similarly, as illustrated by the small error bars. This was a clear indication that Ca ions were released from the Ca-Ti immersed for 4 h. If the ion release results were compared with the appearance of the samples after

immersion, it was observed that as the samples released Ca so they change in colour, becoming blue. Possible mechanisms for this are discussed in detail later in this chapter.

The Ca ion concentrations of the solutions had similar average values after 24 h and 1 week immersion (1.18 ± 0.35 ppm and 1.06 ± 0.76 ppm respectively) and were not statistically different to the 4 h results. This suggested that ions were fully released after 4 h immersion. The 1 week ion chromatography data shows very big standard deviation bars, indicating a very wide variability in the amount of ions released by the samples, ranging from 0.3 ppm to 1.8 ppm. One possible reason for this may be water evaporation from the well plates due to the extended time in the incubator, which increased the Ca ion concentration detected. However, the well plates were sealed whilst placed in the incubator during the experiment, so this effect should have been minimised.

The appearance of the samples and the ion release data suggested that the colour change of the samples may be related to the amount of ion release. It appears that if a sample did not change colour, ions were not released or released only in minimal amounts. It appeared that the samples that were patchy blue released more ions than the silver samples, but less ions than the samples which were fully blue. It would be necessary to analyse in detail the individual samples and compare the proportion of the area which had turned blue to the quantity of ions released (figure 4.8), in order to confirm this hypothesis.

In figure 4.8 the Ca ion concentrations released for each individual sample and percent of the sample which turned blue over 2 min, 4 h, 24 h, and 1 week are plotted separately.

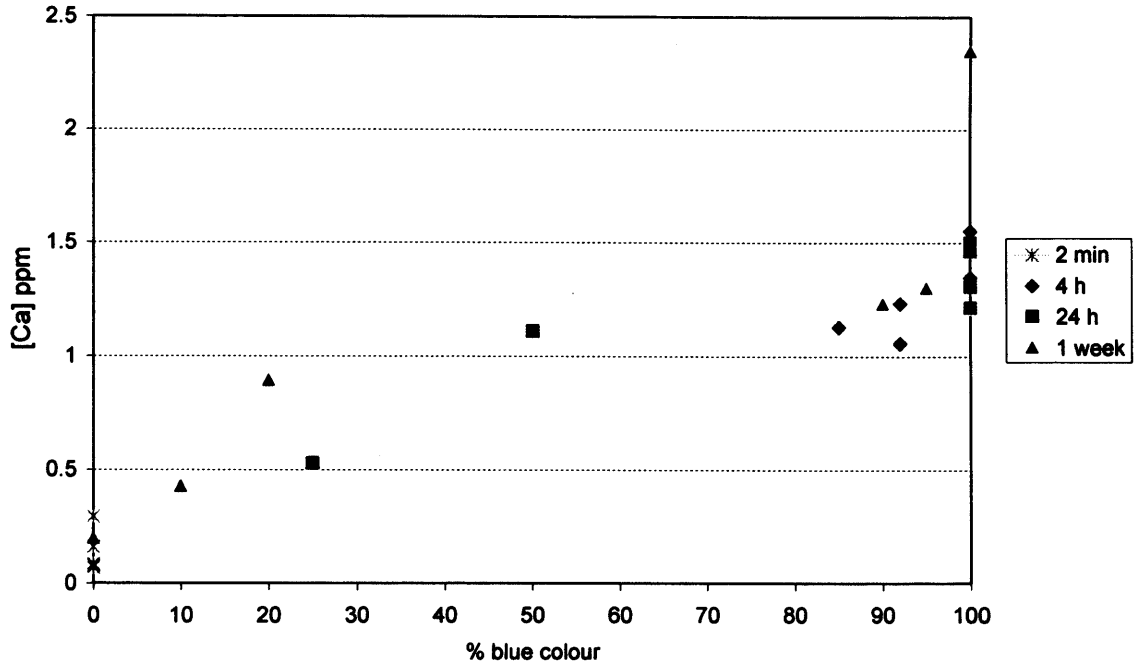

Figure 4. 8 Ca ion release from all the 6 Ca-Ti samples at 2 min, 4 h, 24 h, and 1 week and percentage of the sample area which turned blue.

The above figure (figure 4.8) shows the ion concentrations released for each individual sample plotted separately as a function of colour change. It can be seen that at 2 min all the samples behaved uniformly, releasing similar amounts of Ca ions into solution. Regarding the colour changes for this time point, again all the samples had similar behaviour, with all of the discs staying silver after 2 minutes immersion in ultrapure water.

After 4 h immersion in ultrapure water, the Ca-Ti samples were behaving similarly, as all the samples released around the same amount of ions for each time point. With regards to the colour changes for this time point, it can be observed from the graph that all the samples behaved similarly, and all the samples changed their colour from silver to blue on more than 85% of their surface after 4 h immersion. From the 6 samples, 3 of the samples turned fully blue. The amount of Ca ions released as indicated by their concentration, varied between 1.06 ppm, the smallest value which was recorded for a sample which turned 90-95% blue, to 1.55 ppm, the highest value recorded for a sample which turned fully blue. The overall amount of Ca ions released was above 1 ppm with no major differences between the samples.

The 24 h samples behaved slightly differently with regards to uniformity of ion release and colour change. Four of the six discs behaved similarly, with the amount of Ca ions released being similar and not significantly different to the Ca ions released after 4h immersion (1.2 - 1.5 ppm). These discs turned fully blue (table 4.4). Two other samples showed smaller blue areas and lower ion release, which resulted in the large standard error observed in figure 4.7.

After 1 week's immersion there was a large variability in the behaviour of the Ca-Ti samples with regards to ion release and the colour modification, with at least 2 samples of the 6 showing extreme values, with either very high or very low ion release. Three of the samples released less than 1 ppm and turned less than 50 % blue. The sample which turned 10 % blue released 0.43 ppm, more than double that of the silver sample which released 0.20 ppm, but half the amount of Ca ions released by the sample which turned 20 % blue (0.89 ppm). Also, this amount was more than double that of the sample which turned 25% blue after the 24 h immersion (0.89 ppm and 0.53 ppm respectively). This suggested that longer immersion time resulted in release of more ions.

From figure 4.8 it can be seen that there was a correlation between the quantity of Ca ions released and the colour modification. Samples which released Ca turned blue, and the ones which released less or minimal amounts had only blue patches or stayed silver.
Although it was difficult to predict how much of the sample will turn blue as a function of ion release, it appeared that for release of more than 1 ppm, the samples will turn more than 50% blue. The above results provided further evidence that modification of the appearance was linked with the amount of ion release.
From the data presented, it also appeared that an immersion time longer than 4 h resulted in an increase in the behaviour variability of the samples. It is difficult to explain this, especially as the samples were never been observed to revert back to a silver colour once they had turned blue. The effects may be purely random, or subtle outside factors such as the position of the samples in the storage desiccator or the implantation plate may have played a role.

4.3.3.4 Depth profiling

As showed earlier, the Ca ion solution concentration showed significant ion release during the first 4h, with little modification after this. However, the surface Ca dropped to half its original level after 2 min, and did not change significantly after that. In order to assess the origin of the released Ca, examination of the sub-surface chemistry was carried out using depth profiling, and the results are presented in figures 4.9 - 4.21 and tables 4.7 - 4.12. Figures 4.9, 4.10, 4.11, 4.12, 4.13, and 4.14 present the Ca/Ti, O/Ti, and carbide/Ti ratios as a function of the etching time for Ca-Ti samples immersed in ultrapure water for 2 min and 4 h. Tables 4.7 and 4.8 present Ca/Ti and O/Ti ratios for the same samples at various time points during the depth profiling. The etching time was 81 min for the as-implanted Ca-Ti sample (0 min) and 191 min for the rest of the samples.

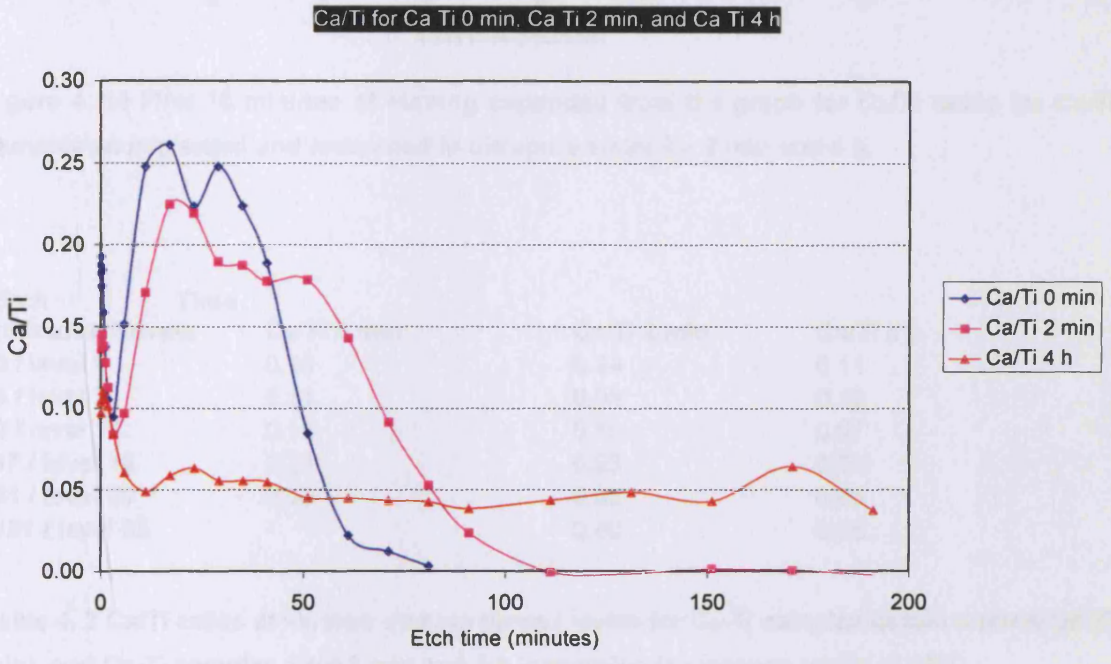

Figure 4. 9 Ca/Ti ratios for Ca-Ti samples as-implanted and immersed in ultrapure water for 2 min and 4 h as a function of the etch time.

The surface regions over the first 15 minutes of etching for as-implanted Ca-Ti and immersed Ca-Ti are shown on figure 4.10 below.

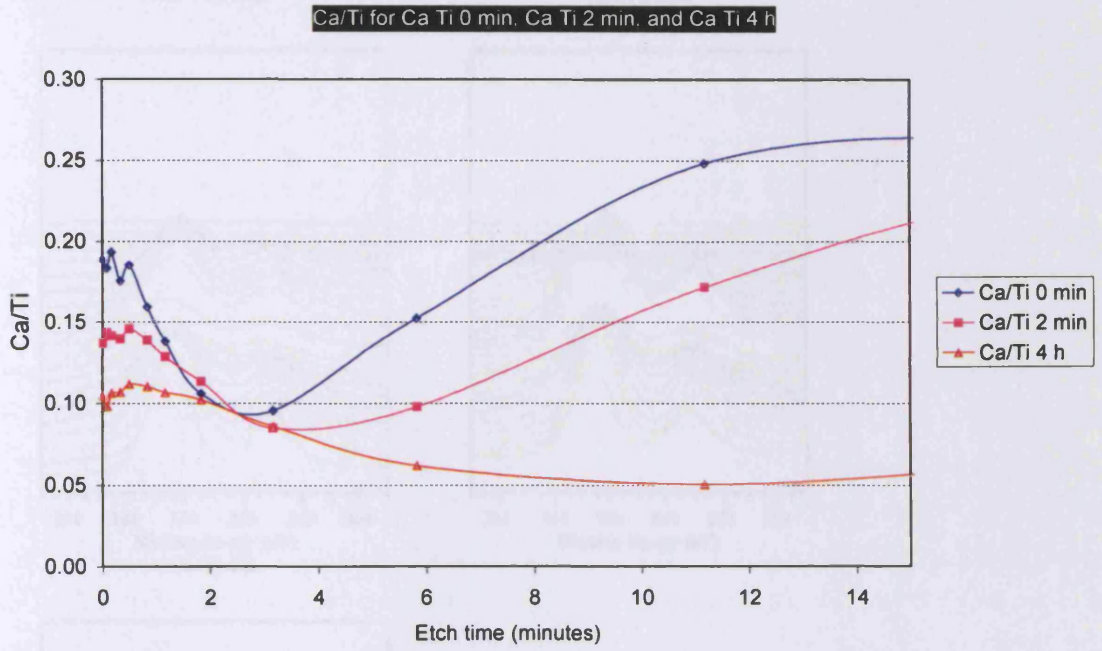

Figure 4. 10 First 15 minutes of etching expanded from the graph for Ca/Ti ratios for Ca-Ti samples as implanted and immersed in ultrapure water for 2 min and 4 h.

Etch Time (minutes)/Levels	Ca/Ti 0 min	Ca/Ti 2 min	Ca/Ti 4 h
0 / level 1	0.18	0.14	0.11
3 / level 9	0.11	0.08	0.10
6 / level 10	0.16	0.10	0.07
17 / level 12	0.26	0.23	0.07
81 / level 20	0.00	0.05	0.05
191 / level 25	-	0.00	0.05

Table 4. 7 Ca/Ti ratios at various etching times / levels for Ca-Ti samples before immersion (0 min), and Ca-Ti samples after 2 min and 4 h immersion in ultrapure water at 37°C.

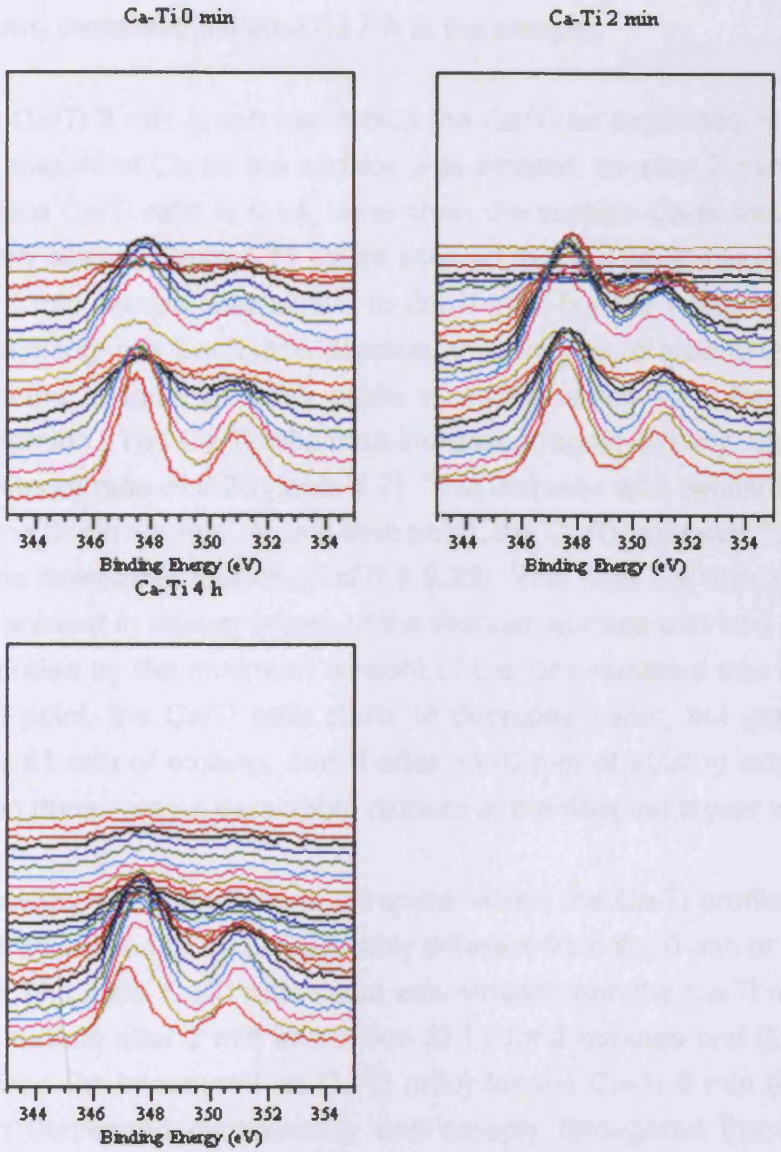

Figure 4. 11 Ca 2p XPS depth profiling spectra for Ca-Ti samples before immersion (0 min)(first row, left,) and immersed for 2 min (first row, right) and 4 h (right).

The Ca-Ti sample before immersion had an initial surface Ca/Ti ratio of 0.18. It then dropped sharply to 0.1 after 3 min of etching. This is clearly seen in figure 4.11 where the intensity of the peaks has reduced by half. The Ca level then started to increase, with the Ca/Ti ratio reaching 0.16 after 6 min and 0.26 after 17 minutes of etching. After this time point the Ca/Ti ratio decreased continuously, and after 81 min of etching there was no Ca left in the sample. Looking at the XPS spectra (figure 4.11) it can be seen that by the end of etching (last five levels

shown) there was minimal Ca left in the sample.

The Ca/Ti 2 min graph resembles the Ca/Ti as implanted, with the difference that the amount of Ca on the surface was smaller, so after 2 min immersion, the initial surface Ca/Ti ratio is 0.14, lower than the surface Ca before immersion. This was clearly seen in figure 4.11 which showed that the peak shape of the Ca 2p peak for the 2 min sample was similar to the 0 min, but the intensity was reduced by half. On etching, this Ca/Ti ratio decreased sharply up to around the 3 min etching point, reaching a value of 0.08, again a smaller value then the Ca-Ti sample before immersion. The Ca/Ti ratio then increased, again sharply, up to 17 min, reaching a maximum ratio of 0.23 (table 4.7). This increase was similar to the increase shown by the 0 min sample. At this time point, the Ca/Ti ratio was found to be higher than at the immediate surface (Ca/Ti = 0.23). This high Ca/Ti ratio confirmed that Ca is still present in deeper layers of the titanium surface and had not been released, as illustrated by the minimum amount of Ca ions released into the solution. After this time point, the Ca/Ti ratio starts to decrease again, but gradually, reaching 0.05 after 81 min of etching, and 0 after ~110 min of etching according to figure 4.10, when there was no detectable calcium in the deepest layers within the titanium.

Following 4 h immersion in ultrapure water, the Ca/Ti profile as a function of etch time was found to be considerably different from the 0 min or 2 min samples (figure 4.9). The initial Ca/Ti ratio value was smaller than the Ca/Ti ratio value detected on the surface after 2 min immersion (0.14 for 2 minutes and 0.10 for 4 hours) or the surface Ca (measured as Ca/Ti ratio) for the Ca-Ti 0 min (0.18). The Ca/Ti ratio then decreased continuously and steeply throughout the etching period which suggested that the ions have been released, as was observed by examining the Ca ions detected in solution with ion chromatography. However, it may also be that Ca ions were displaced deeper into the sample. In the end, after 191 min of etching, the Ca/Ti ratio reached 0.05, which showed that although the Ca levels within the sub-surface Ti were dramatically reduced (Ca/Ti = 0.05 at 17 minutes), there were still minute amounts of calcium left in the deeper layers within the sample, even after the depth profiling had been completed. The Ca 2p peaks for the 4 h immersed Ca-Ti sample (figure 4.11) were similar in shape and position to those of the Ca-Ti 0 min sample, although considerably reduced in intensity.

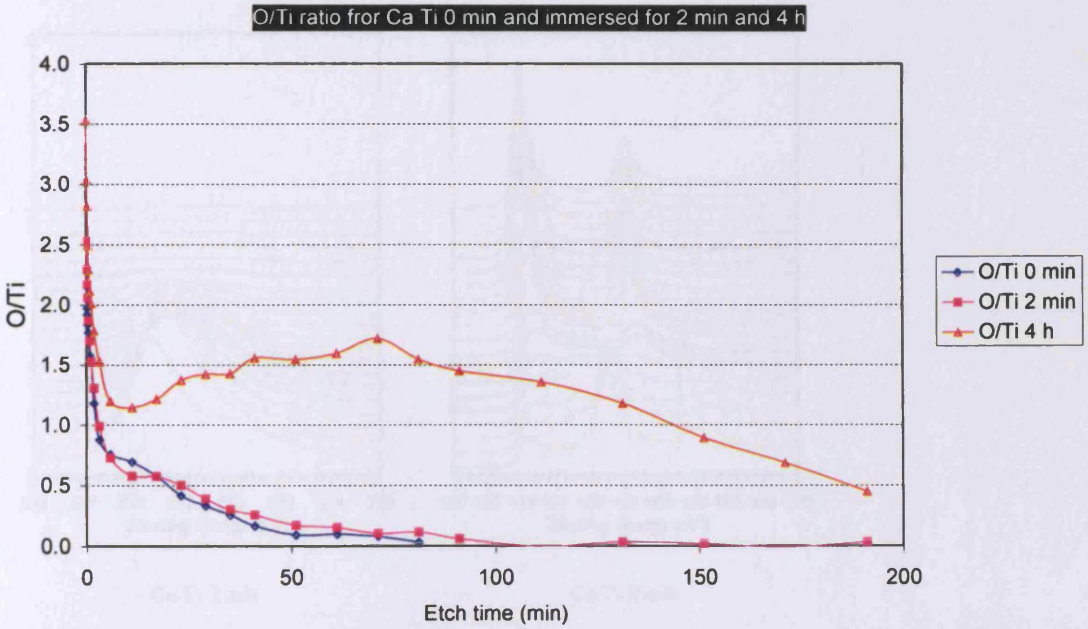

Figure 4. 12 O/Ti ratios as a function of the etching time for Ca-Ti discs before immersion (0 min), and after 2 min and 4 h immersion in ultrapure water at 37°C.

Etch time (min)/Levels	O/Ti 0 min	O/Ti 2 min	O/Ti 4 h
0 / level 1	2.16	2.53	3.58
11 / level 11	0.70	0.58	1.32
71 / level 19	0.08	0.11	1.71
81 / level 20	0.03	0.12	1.72
191 / level 25	-	0.03	0.58

Table 4. 8 O/Ti ratios at various time points throughout the etching for Ca-Ti samples before immersion (0 min), and after 2 min and 4 h immersion in ultrapure water at 37°C.

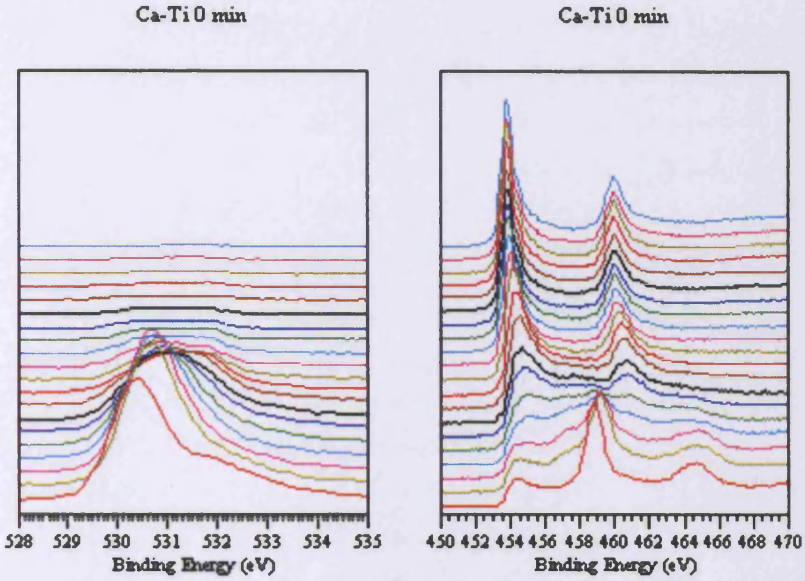
Ca-Ti 0 min
528 529 530 531 532 533 534 535
Binding Energy (eV)
Ca-Ti 0 min
450 452 454 456 458 460 462 464 466 468 470
Binding Energy (eV)

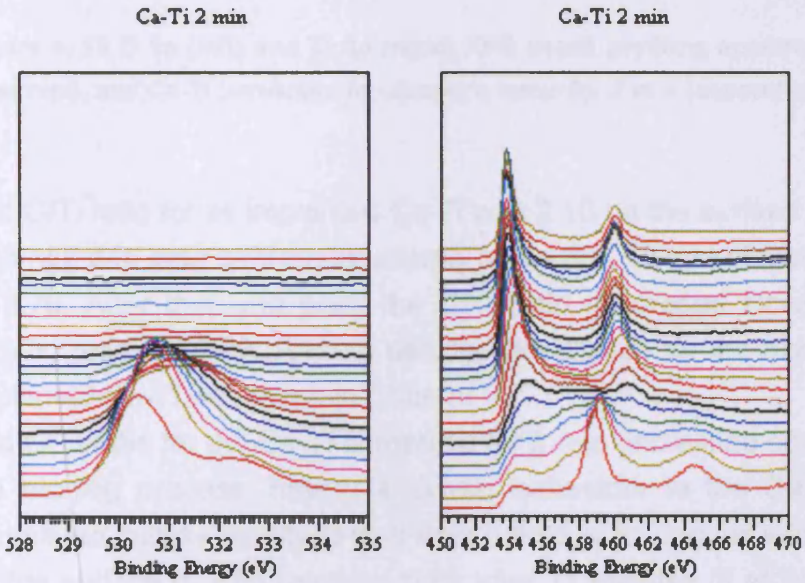
Ca-Ti 2 min
528 529 530 531 532 533 534 535
Binding Energy (eV)
Ca-Ti 2 min
450 452 454 456 458 460 462 464 466 468 470
Binding Energy (eV)

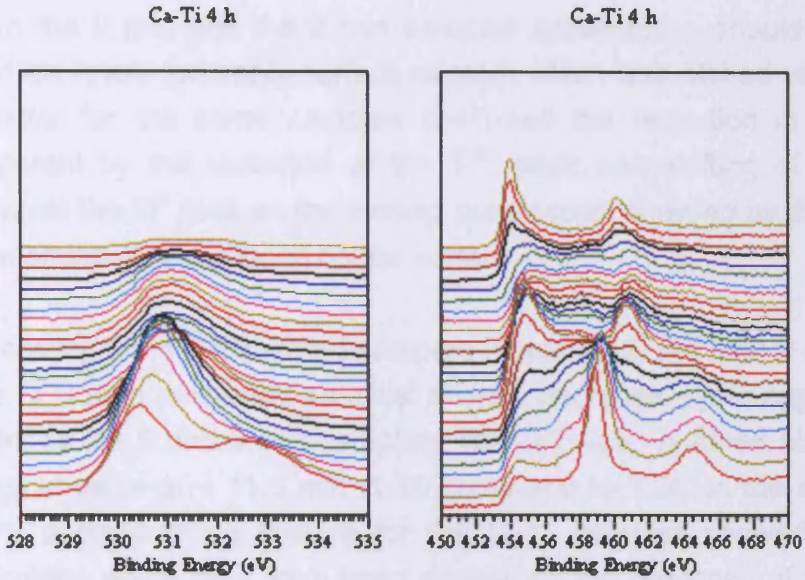

Figure 4. 13 O 1s (left) and Ti 2p (right) XPS depth profiling spectra for as-implanted Ca-Ti (first row), and Ca-Ti immersed in ultrapure water for 2 min (second row) and 4 h (third row).

The O/Ti ratio for as implanted Ca-Ti was 2.16 on the surface at 0 min (first level of etching), and then decreased sharply in the first 10 min of etching reaching a value of 0.70. After this time point the O/Ti ratio decreased slowly and at the end of etching reached 0.03. A more detailed description for the depth profile for the 'as-implanted Ca-Ti was given in Chapter 3.

The O/Ti ratio for the Ca-Ti immersed for 2 min decreased continuously throughout the etching process, having a similar behaviour to the Ca-Ti 0 min sample. It decreased initially rapidly to less than a third of its original value, from an O/Ti ratio on the surface of 2.53 reaching 0.58 after 11 minutes of etching time. At this ratio, a great deal of the oxide layer had probably been etched but the O/Ti ratio of 0.5, indicated that there was a still a significant quantity of O within the sample. After that, it continued to decrease, but very slowly and had almost disappeared after around 110 min of etching, with a value of 0.03.

The XPS depth profiling spectra throughout the etching time (figure 4.13) for both the as-implanted Ca-Ti and the 2 min immersed Ca-Ti confirmed the observation that the O decreased continuously, showing a reduction in the O peak at ~ 531 eV and disappearance towards the middle of the etching period. The O 1s spectra for

both the 0 min and the 2 min samples presented a shoulder at 532 eV for the surface levels (probably surface related) which was etched very rapidly. The Ti 2p spectra for the same samples confirmed the reduction in the oxide layer, as apparent by the reduction of the Ti^{4+} peak and shifting of the Ti^{n+} peak (n<4) towards the Ti^{0} peak as the etching progressed, showing by the end that there was predominantly pure metal on the surface.

Analysing the 4 h immersed samples (figure 4.12, red line) it can be observed that the O/Ti ratio presented an initial sharply decrease, up to approximately the same point as the 0 and 2 min samples. The O/Ti ratio reached almost one third of the original value at ~ 11.5 min (1.15 compared to 3.54 on the surface). The surface XPS depth profiling spectra for the O 1s samples showed a very pronounced shoulder, which may have been caused by the presence of very large amount of hydroxyl groups on the surface. Indeed, this may be possible, as the surface O/Ti ratio was so large, approaching 4, and may have been caused by the presence of large amounts of $Ti(OH)_4$ on the surface. This shoulder was very rapidly etched (figure 4.13), so it was probably surface related; suggesting that the hydroxylation did not extend beyond the upper atomic layers. After the initial decrease, the O/Ti ratio increased gradually up to 71 minutes of etching, when the O/Ti ratio was 1.72. This represented an increase in the thickness of the oxide layer, as shown also by the O/Ti ratio which almost reached a value of 2, indicating that it was most probably TiO_2 that was etched. The O level then started to decrease, again gradually, and at the end of etching the O/Ti ratio had a value of 0.58, which was much higher than the final ratios for the 0 min or 2 min samples which were both 0.03. The presence of a large amount of sub-surface oxygen following immersion suggested that the passive nature of the native Ti surface was compromised by the implantation of Ca. This was also shown in the XPS depth profiling spectra throughout the etching (figure 4.13). This showed the O shoulder decreasing rapidly but the O peak due to O^{2-} at ~ 531 eV was persistent throughout the etching and did not disappear completely by the end of etching. The Ti 2p spectra for the same sample showed a slower reduction in the sub-surface oxide layer, a result which was manifested by the slow reduction of the Ti^{4+} peak, and shifting of the (n<4) peak towards the Ti^{0} peak as the etching progressed. This was at a much slower rate than for the other samples, with the intensity of the Ti metal peak towards the end of etching having lower intensity than for the as-implanted Ca-Ti and Ca-Ti 2 min samples.

The blue colouration of the immersed sample could be explained by the thickening of the oxide layer. However, it was still unclear why this thickened layer could not be identified in the Ti 2p spectrum from the un-etched surface, nor why there was a large drop in the O/Ti ratio after ~ 10 min etching; the same time at which there was a shoulder in the as-implanted sample before immersion. In order to address these questions it was necessary to examine the C 1s spectrum.

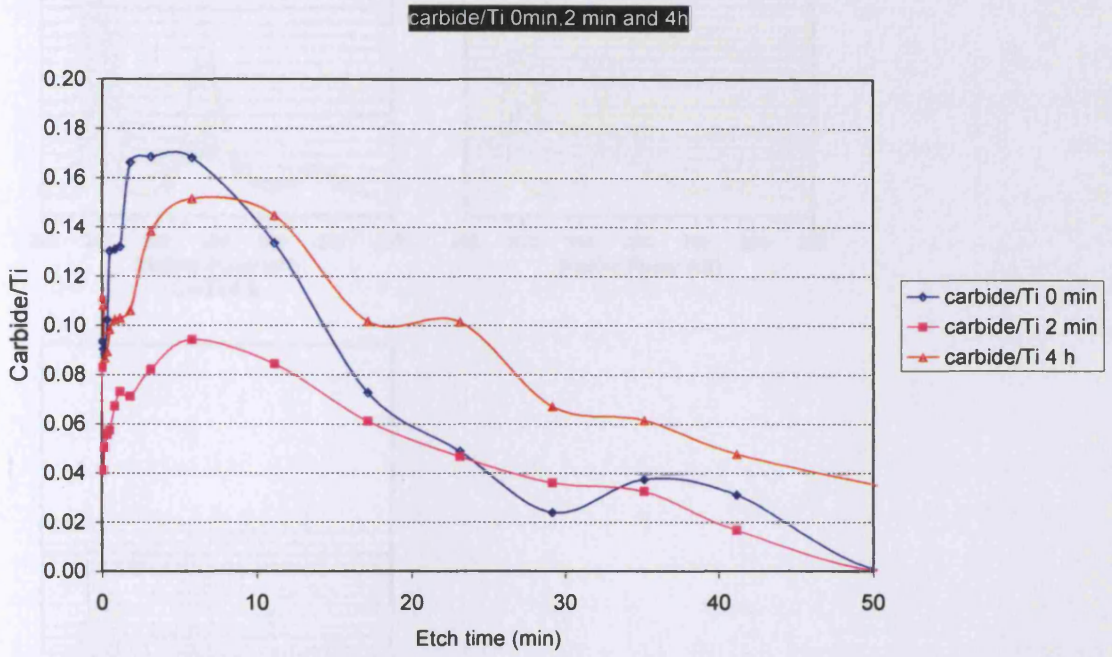

Figure 4. 14 Carbide/Ti ratios as a function of the etching time for Ca-Ti discs before immersion (0 min), and after 2 min and 4 h immersion in ultrapure water.

Etch Time (minutes)/Levels	carbide/Ti 0 min	carbide/Ti 2 min	carbide/Ti 4 h
0.00 / level 1	0.09	0.08	0.11
0.08 / level 2	0.09	0.04	0.11
0.17 / level 3	0.09	0.05	0.09
6 / level 17	0.17	0.09	0.15
51 / level 20	0.00	0.00	0.03
191 / level 25	-	0.00	0.00

Table 4.9 Carbide/Ti ratios at various time points / levels throughout the etching for Ca-Ti samples before immersion (0 min), and after 2 min and 4 h immersion in ultrapure water at 37°C.

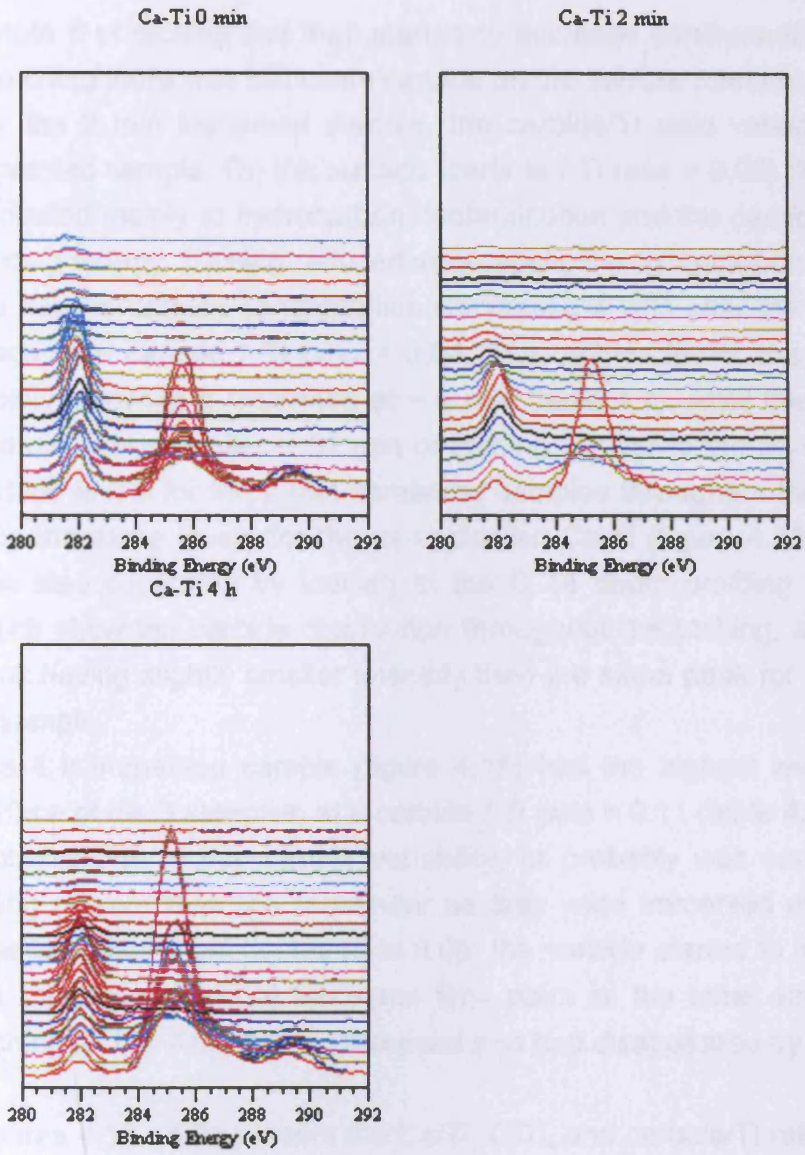

Figure 4. 15 C1s depth profiling spectra for Ca-Ti before immersion (0 min)(left), and Ca-Ti immersed for 2 min (middle) and 4 h (right).

The 0 min 'as-implanted' Ca-Ti showed carbon both at the surface and in the subsurface regions (figure 4.15). At the surface mainly hydrocarbon contamination was present and also a small peak attributable to carbide species at ~282 eV. On etching, the hydrocarbon contamination peak decreased rapidly and disappeared after 3-4 levels of etching. The relative carbide concentration increased initially, reaching at ~1 minute (carbide / Ti = 0.17). The ratio remained at this value until

minute 6 of etching and then started to decrease continuously, so that by the end of etching there was still some carbide on the sample (carbide / Ti = 0.1).
For the 2 min immersed sample, the carbide/Ti ratio varied similarly to the as-implanted sample. On the surface (carbide / Ti ratio = 0.08) there were only peaks attributed mainly to hydrocarbon contamination and the carbide peak at the lowest binding energy. Etching reduced very rapidly the hydrocarbon contamination, while the relative carbide concentration decreased a little after the first level of etching, reaching a carbide / Ti ratio = 0.04. The carbide levels then started to increase rapidly, showing a maximum at ~ 6 min (table 4.9). After this it decreased rapidly and disappeared after ~ 51 min of etching, similar to the as-implanted Ca-Ti. The carbide levels for the 2 min immersed samples throughout the etching are smaller than the same levels for the as-implanted Ca-Ti (figure 4.15 and table 4.9). This was also confirmed by looking at the C 1s depth profiling spectra (figure 4.15) which show the carbide distribution throughout the etching, and show the carbide peak having slightly smaller intensity than the same peak for the as-implanted Ca-Ti sample.
The 4 h immersed sample (figure 4.15) had the highest level of carbide on the surface of the 3 samples, at a carbide / Ti ratio = 0.11 (table 4.9). However this was probably due to the sample variability, or probably was caused by the samples being cleaner than the remainder as they were immersed more than the others. After an initial rapid decrease to 0.09, the carbide started to increase and reached the maximum value at the same time point as the other samples after 6 min of etching (0.15). After this it decreased and had disappeared by the end of etching.

Figures 4.16 - 4.21 present the Ca/Ti, O/Ti, and carbide/Ti ratios and the Ca 2p, O 1s, Ti 2p and C 1s XPS depth profiling spectra for of Ca-Ti discs on blue and silver patch respectively after 24 h immersion in ultrapure water. The XPS spectra for the silver and the blue patch were recorded on different samples. Tables 4.10, 4.11, and 4.12 illustrate the Ca/Ti, O/Ti, and carbide/Ti ratios for the same samples at various time points during the depth profiling.

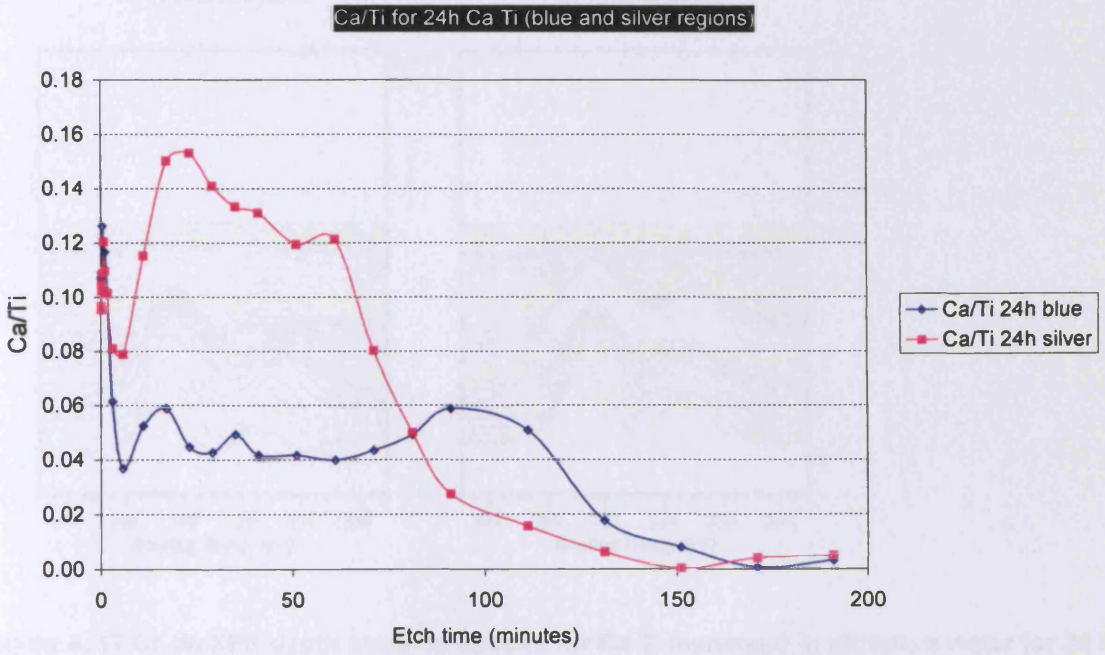

Figure 4. 16 Ca/Ti ratios on blue and silver patches of two Ca-Ti samples after 24 h immersion.

Time point (min) / Level	Ca/Ti blue	Ca/Ti silver
0 / level 1	0.10	0.12
6 / level 10	0.04	0.08
23 / level 13	0.04	0.15
191 / level 25	0.00	0.00

Table 4. 10 Ca/Ti ratios for Ca-Ti immersed for 24h in ultrapure water (blue and silver regions) at various time points.

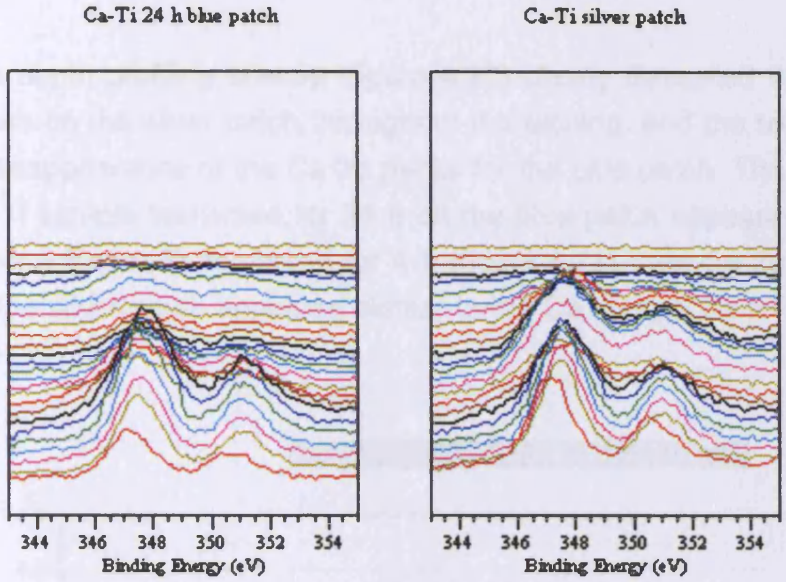

Figure 4. 17 Ca 2p XPS depth profiling spectra for Ca-Ti immersed in ultrapure water for 24 h on a blue patch (left) and silver patch (right).

The Ca/Ti ratios (table 4.10) showed significant differences between the blue and silver patches. Although the initial ratio at the surface was similar, they both decreased up to ~ 6 min etching time, reaching levels of 0.04 for the blue sample, and for the silver sample double that value at 0.08. After this time point, the Ca/Ti ratio on the silver patch increased sharply up to 23 min etching time, reaching 0.15. This finding suggested that Ca was not released and that there was still some left within the sample. The Ca/Ti ratio then decreased gradually (figure 4.16), until it disappeared at around 191 min etching time. On the blue patch, the Ca/Ti ratio decreased continuously (figure 4.16, blue line) and there was no Ca left after 191 min etching time. This suggested that the Ca ions were released in solution from the blue patch. Indeed, the ion chromatography results showed that Ca ions were released from Ca-Ti discs after 24 h immersion, but obviously could not specify if these came from a blue or silver patch. As the depth profiling data showed that there was more Ca left in the sample on a silver patch as compared with a blue patch, it was assumed that higher Ca release occurred on the blue patch for Ca-Ti samples immersed for 24 h than on the silver patch. The link between the ion released and changes in the colour was also discussed earlier (figure 4.8), so the depth profiling data appeared to be in agreement with the previous findings.

The depth profiling spectra (figure 4.17) clearly illustrated the presence of Ca 2p peaks on the silver patch throughout the etching, and the reduction in intensity up to disappearance of the Ca 2p peaks for the blue patch. The Ca 2p spectra for the Ca-Ti sample immersed for 24 h on the blue patch appeared similar to the Ca 2p spectra for Ca-Ti immersed for 4 h (figure 4.11). The Ca 2p spectra for the Ca-Ti on the silver patch appeared similar to the Ca 2p spectra for Ca-Ti immersed for 2 min.

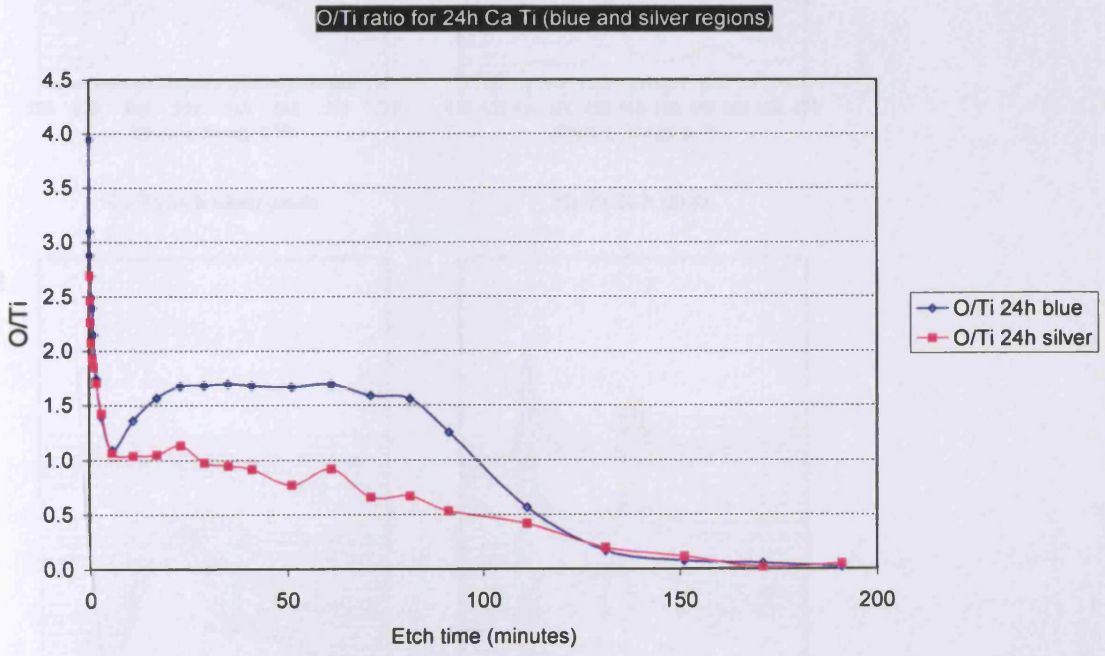

Figure 4. 18 O/Ti ratios for Ca-Ti discs after 24 h immersion in ultrapure water on the blue and silver patches on two Ca-Ti samples.

Time point (minutes) / Level	O/Ti blue patch	O/Ti silver patch
0 / level 1	3.95	2.69
6 / level 10	1.09	1.06
35 / level 16	1.69	0.94
191 / level 25	0.02	0.04

Table 4. 11 O/Ti ratios for Ca-Ti discs immersed for 24h in ultrapure water (blue and silver regions) at various time points/levels.

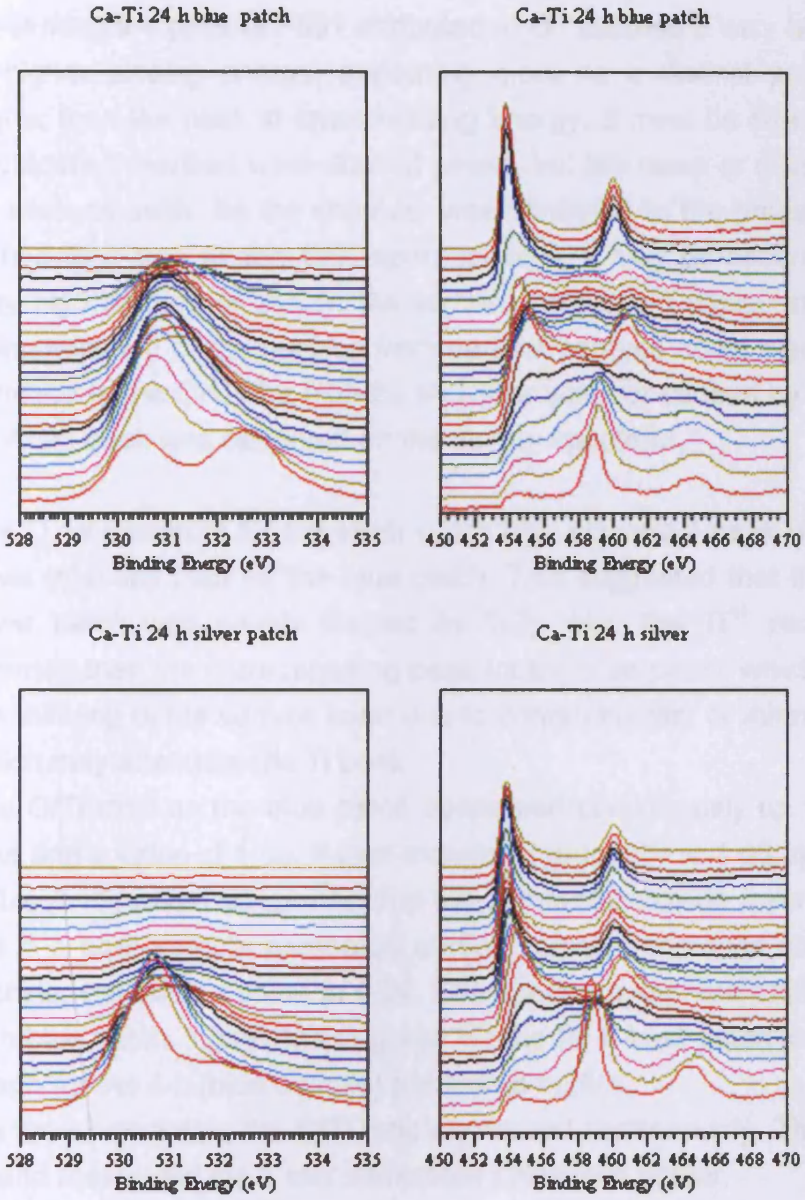

Figure 4. 19 O 1s (left) and Ti 2p (right) XPS depth profiling spectra for Ca-Ti immersed in ultrapure water for 24 h on a blue patch (first row), and silver patch (second row).

After 24 h immersion in ultrapure water, the O/Ti ratio on the blue patch on the surface was very high (3.98), much higher than the O/Ti ratio on the silver patch, which had a value of 2.57 (table 4.11). As change in colour meant thickening of the oxide layer, this indicated that the oxide layer was much thicker on the blue patch than on the silver patch, as confirmed by the depth profile (figure 4.19). The XPS surface spectra for the Ca-Ti sample on the blue patch showed the O 1s spectra

presenting the peak at ~531 attributed to O^{2-} but also a very high intensity shoulder at higher binding energy, appearing more as a distinct peak, with an intensity higher then the peak at lower binding energy. It must be stressed that most of the shoulders described were distinct peaks, but too close or of too low an intensity to be seen as such. So the shoulder was attributed to the presence of high amounts of hydroxyl, and as the O/Ti approaches 4, it may be assumed that there was a very high amount of OH on the surface, probably $Ti(OH)_4$, much more than TiO_2. Contamination of the surface from various sources could also be the cause of an increase in the OH. The high E_B shoulder was not caused by aluminium oxides as no Al 2p peak was observed on the survey spectrum.

The O 1s spectrum for the silver patch also showed a peak with a shoulder, but at lower intensity than for the blue patch. This suggested that the oxide layer on the silver patch was mainly formed by TiO_2. Also the Ti^{n+} peak ($n<4$) had higher intensity then the corresponding peak for the blue patch, which could be caused by the thinning of the surface layer due to contamination, or thinning of the oxide layer which may attenuate the Ti peak.

The O/Ti ratio on the blue patch decreased continuously up to ~ 6 min of etching time and a value of 1.09. It then increased gradually to 1.66 up to 35 min of etching (table 4.11) which suggested that the sub-surface oxide layer increased, similar to the 4 h blue sample presented earlier. It then decreased slowly until the end of etching, reaching a value of 0.04. The spectra presented thicker sub-surface O for 24h blue patch. Again, the O graph for the 24 h blue patch looked similar to the O graph for the 4 h (blue sample) presented earlier.

On the silver patch, the O/Ti ratio decreased continuously. The 24h silver had less O and resembled the 2 min immersion presented earlier.

The depth profiles clearly indicated that there was much higher oxygen concentration below the blue patch than below the silver patch, and that this sub-surface oxidation was almost certainly the cause of the blue discoloration.

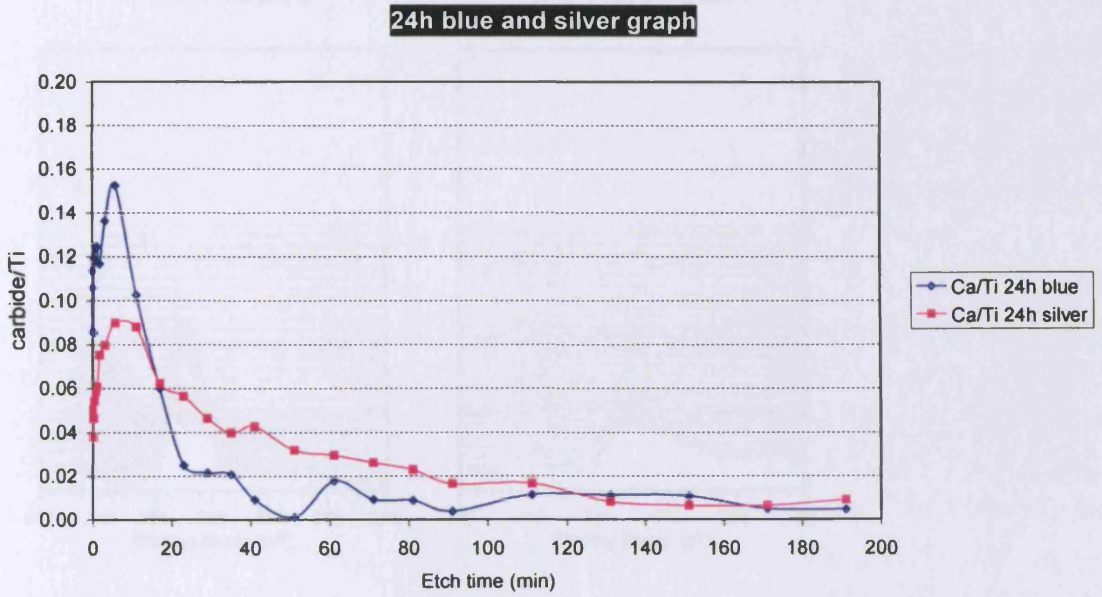

Figure 4. 20 Carbide/Ti ratios on the blue and silver patches for Ca-Ti discs after 24 h immersion in ultrapure water.

Etch Time (minutes) / Levels	Carbide/Ti 24 h blue	Carbide/Ti 24 h silver
0 / level 1	0.11	0.05
0.08 / level 2	0.09	0.04
0.17 / level 3	0.08	0.05
6 / level 10	0.15	0.09
51 / level 17	0.00	0.03
191 / level 25	0.00	0.01

Table 4. 12 Carbide/Ti ratios for Ca-Ti discs immersed for 24h in ultrapure water (blue and silver regions) at various time points/ levels.

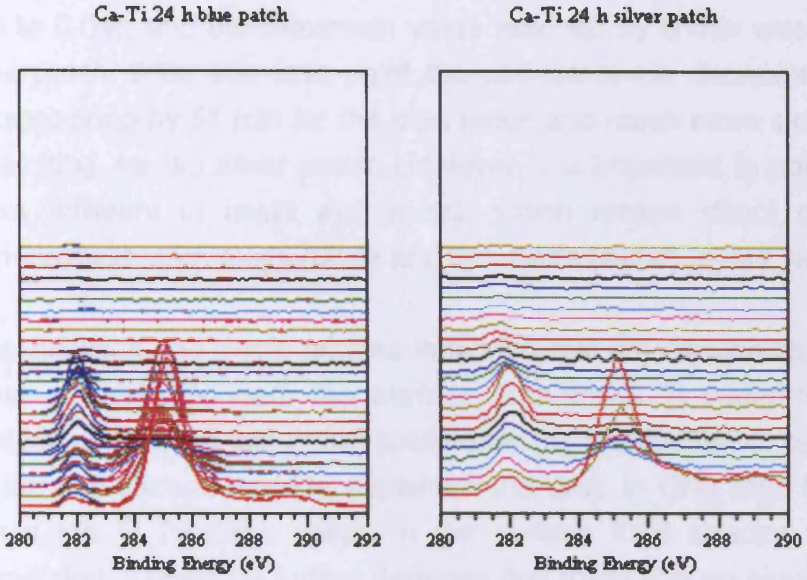

Figure 4. 21 C1s XPS depth profiling spectra for Ca-Ti immersed in ultrapure water for 24 h on a blue patch (left), and silver patches (right).

Figure 4.20 and table 4.12 show that on the blue patch at the surface there was double the amount of carbide as compared to the silver patch. This may be relevant to the difference in behaviour of the samples. For the 'as-implanted' Ca-Ti it appears that the formation of carbide and oxide following the surface sputtering that take place during implantation are two competitive processes-the highly reactive Ti may react with O or with C, perhaps depending on which is present first within the implanter. It is possible that the presence of carbide, formed by reaction with e.g. hydrocarbons in the implanter, stops the surface 'healing' properly - i.e. prevents the proper formation of the surface oxide following the implantation process. The high carbide surface is then susceptible to the slower oxidation which occurs in water. Samples (or areas of surfaces) with lower carbide may then have more fully re-oxidised after implantation and are less readily oxidised on immersion in water. However, this is only a tentative explanation for differences between the blue and silver patch and there is no other evidence supporting it. The XPS spectra (figure 4.21) showed more hydrocarbon and carbide for the blue patch than the silver patch, similar to the 4 h sample when compared with the 2 min sample. The carbide/Ti ratio for the blue patch decreased rapidly to 0.08, and then increased reaching a maximum at ~ 6 min of etching (0.15). The same behaviour was seen for the silver patch as well, with the difference that the decrease was smaller (from

0.5 to 0.04), and the maximum value reached by 6 min was smaller than for the blue patch. After this time point the carbide levels decreased for both samples, disappearing by 51 min for the blue patch and much more slowly, towards the end of etching, for the silver patch. However, it is important to note that the etch rates were different in oxide and metal, which makes direct comparison between samples with thick oxide (blue) and thin oxide (silver) layers very difficult.

In conclusion, the depth profiles indicated that the carbide was primarily located a small distance beneath the surface. Immersion in water for shorter or longer periods of time did not dramatically alter the distribution of carbide. The presence of the sub-surface carbide explained the drop in O/Ti ratio beneath the surface. Since the Ti 2p peak shape in the surface XPS spectra was little altered on immersion, it could be further deduced that there was no significant increase in the thickness of the oxide layer above the carbide layer. The Ca-modified Ti below the carbide layer was readily oxidised, but was too deep to contribute significantly to the Ti 2p peak shape in the surface spectra. The Ti 2p profile on etching (figure 4.21) showed a change in the peak shapes throughout the etching process. Initially we can see oxide and carbide on the surface, characterized by peaks at 458.7 eV for Ti^{4+} due to the surface oxide and 454 eV due to carbide (TiC). As the etching progressed the oxide was etched, as seen by a reduction in the intensity of the Ti^{4+} peak and shifting to a lower binding energy at ~ 458 eV due to sputtering of the oxygen. At the same time there was an increase in the carbide peak at ~ 454.5 eV. Then the etching penetrated the carbide and the Ti^{n+} $2p_{3/2}$ peak ($n<4$) shifted to towards lower binding energy as it started to reach the underlying metal where the Ti^0 $2p_{1/2}$ at 453.8 eV began to appear. The peak at 460.7 eV shifted to a lower binding energy and titanium oxide started to appear at 459.8 eV representing Ti^0 $2p_{1/2}$.

Immersion for 2 min did not change the distribution of Ca throughout the sample, and was similar to the as-implanted Ca-Ti. Immersion in water for more than 4 h resulted in a decrease in the Ca concomitant with a redistribution of Ca throughout the sample, and an increase in the sub-surface oxide layer. Immersion for 24 h on the silver patch did not change the Ca distribution, as opposed to the blue patch, which behaved like the 4 h immersed sample. This is not surprising in light of the ion release results which suggested that ion release was essentially complete by 4 h. The XPS data supports this result and indicate additionally that all changes in composition on immersion are complete by 4 h.

4.3.4 Conclusions

It may be concluded that the ion chromatography and the XPS results showed that Ca ions were released from Ca implanted titanium discs at 37°C. This significantly improves on other data on ion release from Ca-Ti (Shinawi, 2003) by directly measuring released ions in solution. Ion chromatography was a useful method of detecting even minute amounts of calcium ions released in solution. The data showed that the amount of calcium ions detected in solution after as little as 2 min immersion in water was not significantly different than the amount of Ca ions detected for the control samples (ultrapure water and cp Ti), and that the ion release was essentially complete by 4 h immersion, with no increase detected for longer immersion times.

The XPS results (both the surface analysis and the depth profiling) confirmed the calcium ion release from the Ca implanted samples, both from the surface and from deeper layers within the Ca-Ti. The surface calcium dropped by more than 50 % after 2 min immersion in ultrapure water, with minimal subsequent changes. The oxide layer showed an increase in thickness and also changed in composition for the samples immersed for 4 h and over. Concomitant with the increase in the oxide layer, a reduction in the Ca present in the Ca-Ti took place, which correlated with the release of the calcium ions into solution, and the redistribution of Ca throughout the thicker oxide. After 4 h immersion or more, most of the samples showed colour changes ranging from fully blue to patchy blue, which correlated with the increase in the thickness of the oxide layer. The presence of a large amount of sub-surface oxygen following immersion suggested that the passive nature of the native Ti surface was compromised by the implantation of Ca, that enables oxygen diffusion through the surface on exposure to an aqueous environment. The formation of slightly soluble $Ca(OH)_2$, and its subsequent dissolution may result in defects in the surface film, enabling further oxidation, hydroxylation and dissolution of Ca and allowing oxygen to penetrate to subsurface layers. It appears that Ca ions are both redistributed to greater depths within the oxidised Ti and released into solution.

A schematic representation of the Ca-Ti surface after 4 h immersion is given below.

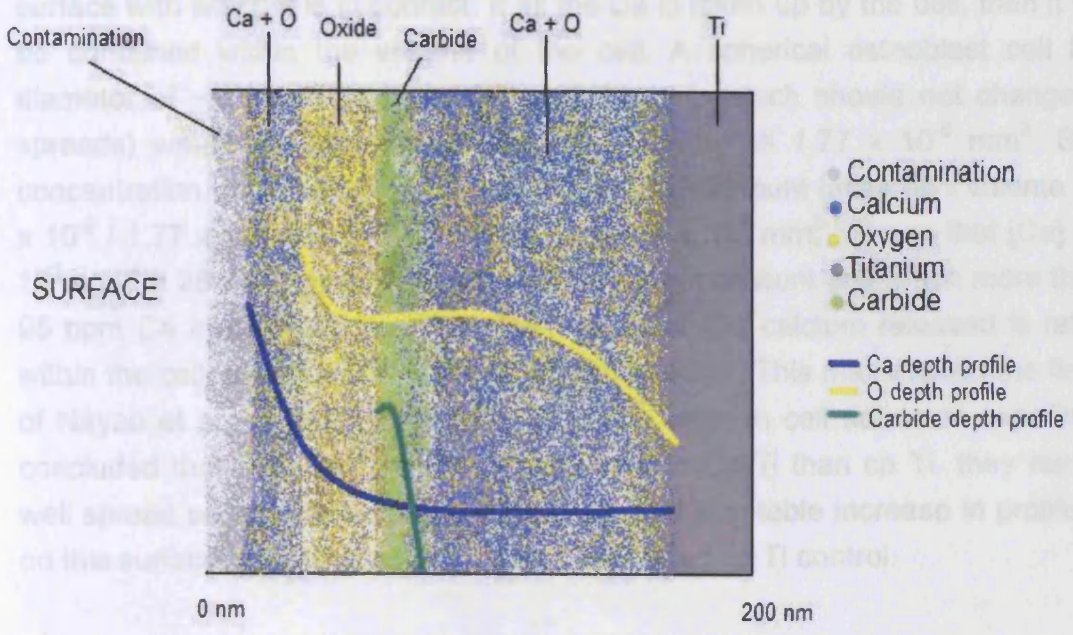

Scheme 4.1 Diagrammatic representation of the Ca-Ti surface after 4 hours immersion in water including the Ca depth profile (blue line) and O depth profile (yellow line).

The concentrations of ions released (~ 1.7 ppm maximum) were very much lower than those contained in simulated body fluids, e.g.: Hanks balanced salt solution, HBSS (66 ppm Ca) [HBSS, Invitrogen Corporation, England, Catalogue no.14025-050, [$CaCl_2 \cdot 2H_2O$] = 185 mg l^{-1}], and complete medium (95 ppm Ca), [Complete medium, Dulbeccos Modified Eagle Media, [$CaCl_2 \cdot 2H_2O$] = 264 mg l^{-1}, Gilco Invitrogen Corporation Catalogue]. This was also much less than the likely Ca concentration *in vivo* and it is therefore unlikely that the observed biological responses to Ca-implanted Ti are due to Ca-release alone. However, the amount released over the surface of the cell which was adhering to the surface was very high for that particular cell, as shown in the calculation presented below. At 4 h, a measured concentration of 1 ppm (1 mg l^{-1}) Ca in 1 ml solution indicates that 1 x 10^{-3} mg Ca has been released. An 8 mm diameter disc has a surface area of $\pi r^2 = \pi(4)^2 = 50.27$ mm^2. The average flux of Ca = $mass_{Ca}$ / (area x time) = 1 x 10^{-3} / (50.27 x 14400s) = 1.38 x 10^{-9} mg mm^{-2} s^{-1}. If we consider how much Ca each cell will see after 4 h, the amount released per unit area is: amount released / area = 1 x 10^{-3} / (50.27) = 19.9 x 10^{-6} mg mm^{-2}. The surface area of a spread osteoblast cell is 50 µm x 50 µm = 2500 µm^2 = 2.5 x 10^{-3} mm^2. So after 4 h each cell on the surface would have been exposed to 49.7 x 10^{-9} mg Ca coming out of the immediate

surface with which it is in contact. If all the Ca is taken up by the cell, then it would be contained within the volume of the cell. A spherical osteoblast cell has a diameter of ~ 15 μm, so the volume of the cell (which should not change as it spreads) would be $4/3\pi\ r^3=4/3\pi(7.5 \times 10^{-3})^3\ mm^3 = 1.77 \times 10^{-6}\ mm^3$. So the concentration of Ca within the cell would be [Ca]=amount taken up / volume =$49.7 \times 10^{-9} / 1.77 \times 10^{-6} = 0.028$ mg / mm^3. A 1l = $1 \times 10^6\ mm^3$, means that [Ca] =$28 \times 10^3 mg\ l^{-1} = 28 \times 10^3$ ppm. This is a relatively large amount and much more that the 95 ppm Ca in complete medium. Even if not all the calcium released is retained within the cell, significant adverse effects may occur. This may explain the findings of Nayab et al., (2003, 2006, 2007, in press) who, in cell adhesion experiments, concluded that although fewer cells attached to Ca-Ti than cp Ti, they remained well spread on the titanium surface and showed a notable increase in proliferation on this surface in comparison to the non-implanted cp Ti control.

4.4 VARIATION OF CALCIUM ION RELEASE FROM NITRIC ACID TREATED CA-TI DISCS IMMERSED IN ULTRAPURE WATER WITH TIME.

4.4.1 Introduction

It has been shown that various methods of implant surface preparation can significantly affect the properties of the surface, and subsequently the biologic responses and rates of cellular attachment that occur at the surface .
Passivation of cp Ti implants is performed with the aim of producing a more inert surface, minimising corrosion and removing the debris embedded on the surface (Kilpadi et al., 1998). There have been numerous reports in the literature which showed the use of passivation of titanium at various suggested dilutions, time periods and temperatures.

A passivation protocol was developed in the USA by the American Society for Testing and Materials (ASTM) to ensure that all the devices implanted into the body were cleaned following the same procedure. The ASTM-F86 was originally

developed for surgical implants made of stainless steel and cobalt chromium alloys. It consists of treatment using 20-40% nitric acid (HNO_3) for at least 1 h. Later it has been adopted for alloyed orthopaedic implants. Currently in the USA it is a requirement that all manufacturers of dental implants passivate them using this protocol. Passivation might be expected to affect both the chemical and the structural surface properties of an implant, yet no major influence on the topography or oxide composition following passivation has been reported. Sittig et al., (1999) analysed the surfaces of commercially pure titanium and of the two alloys Ti–6Al–7Nb and Ti–6Al–4V following three pre-treatments: polishing, nitric acid passivation and pickling in nitric acid-hydrogen fluoride. They found that nitric acid treatment was found to substantially reduce the concentration of surface contaminants present after polishing, but did not modify significantly the surface roughness. The oxide thickness on cp Ti and cp Ti alloys and passivated cp Ti was found to be 4.9 ± 0.1 nm. However, Kilpadi et al. (1998b) reported increased surface roughness on passivated implant-grade Ti surfaces (30% nitric acid at room temperature for 20 minutes followed by 10 minutes cleaning in deionised water) as compared to those cleaned in ethanol alone (10 minutes cleaning in 95% ethanol).

The oxide on the passivated surfaces was reported to be composed of mainly TiO_2 and some Ti_2O_3 and TiO suboxides, similar to the native oxides observed on Ti surfaces (Callen et al. 1995, Kilpaldi et al. 1998a, Brunette et al. 2001). Callen et al. (1995) studied the effect of nitric acid treatment on cp Ti and titanium alloy using graphite furnace atomic absorption spectrophotometry (GFAAS). They showed that passivation of cp Ti and Ti6Al4V reduced the oxide thickness on the alloy while having no significant effect on the pure metal. Nitric acid passivation did not influence Ti release from cp Ti. However, they also detected significantly greater levels of Ti, Al, and V in the presence of passivated compared to non-passivated Ti6Al4V. In light with these results they suggested the re-examination of ASTM-F86-based passivation protocols with respect to Ti6Al4V, as this alloy is used extensively for biomedical devices. However, Faria et al. (2003), in a study on the effect of nitric acid treatment on the *in vitro* biocompatibility of titanium, showed that passivation did not have any effect on this, as evaluated by osteoblast attachment, proliferation and differentiation. Other researchers like Ku et al. (2002) showed that passivation has only minor effects on cell behaviour.

Regarding the effects on Ca-Ti, it was shown in chapter 3 that passivation of the

Straumann samples did not alter the surface roughness. However, these samples were not treated using the ASTM-F86 passivation protocol.

There is a definite agreement that passivation of Ti alloys results in reducing the oxide layer thickness and increasing metal ion release on Ti6Al4V. Most of reports agree that passivation of the cp Ti results in thinning of the oxide film. It has been suggested that this is due to the reduction in the number of point defects on the surface of Ti, which in turn reduces the number of available ionic pathways, thus inhibiting oxide re-growth and subsequently resulting in thinning of the oxide film (Kilpaldi et al., 1998a, 1998b). However, this was not fully agreed throughout the literature (Callen et al., 1995).

4.4.2 Aims and objectives

This aim of this section of the present work was to assess whether nitric acid treatment of Ca-Ti influenced the release of Ca ions into ultrapure water at various time periods. This was assessed by analysing the solution in which the discs were immersed. The surface modifications of the discs were also analysed using XPS and XPS depth profiling.

4.4.3 Materials and method

54 as-implanted Ca-Ti discs ($^{40}Ca^{+}$, 40 keV, 1 x 10^{17} cm^{-2}) were used in this experiment. Two nitric acid treatments were used: 10% 10 min and 34% 1 h. The first treatment was chosen because it was used at the Eastman in cell biology experiments. The second treatment (34% 1 h) was selected on the basis of the recommended ASTM protocol and its use by other researchers (Lee et al., 1998).
All the discs were analysed initially with XPS. Following analysis, 36 discs were treated with nitric acid as follows:
1. 18 Ca-Ti discs were treated with 10% HNO_3 for 10 min. The nitric acid was obtained using 70 ml ultrapure water and 10 ml 70% nitric acid (AR grade). The treatment time for the discs was 10 min. After the treatment, the samples were taken out using plastic tweezers, rinsed in ultrapure water, dried with compressed air and wrapped in aluminium foil.

2. 18 Ca-Ti discs were treated with 34% HNO_3 for 1 h. The nitric acid was prepared using 21.2 ml ultrapure water and 20 ml 70% nitric acid (AR grade). The discs were treated for 1 h. Again after treatment, the samples were taken out using plastic tweezers, rinsed in ultrapure water, dried with compressed air and wrapped in aluminium foil.

Following nitric acid treatment, the 36 samples were analysed with XPS. After the analysis, all the 54 discs (as-implanted and nitric acid treated) were immersed in ultrapure water (Elga Labwater, Veolia Water Systems, USA) for various periods of time.

The immersion studies were carried out using 1 ml ultrapure water for each disc placed in (24) well cell culture plates (Corning Incorporated 3526, Corning, USA). Prior to the immersion of the discs, the water was placed in the incubator at 37°C for an hour to allow it to reach the desired temperature. Six discs of each Ca-Ti , 10 % nitric acid treated Ca-Ti (10% HNO_3 Ca-Ti) and 34% nitric acid treated Ca-Ti (34% HNO_3 Ca-Ti) were then immersed face upwards in the ultrapure water (1 ml per disc) for 2 min, 4 h and 24 h in the incubator at 37° C. The well plates were sealed using parafilm (Clean Foil, Clingorap, Terinex, Prod. 235011203). Different discs were used for different time points. A further 6 x 1 ml samples of ultrapure water were placed in the well plates for the same periods of time alongside the samples as an additional control.

After immersion, the solutions were drawn off using one clean pipette for each well plate and placed in individual chromatography vials (Chromacol Ltd., Herts, U.K.). They were then analysed using ion chromatography as detailed in Chapter 2.

The Ca-Ti and the nitric acid treated Ca-Ti samples were removed using plastic tweezers, dried with compressed air, (Falcon Safety Products, Inc., Branchburg, USA, Model 88010 DPSXLX), wrapped in aluminium foil (Aluchef Foil, Terinex Limited, Bedford, UK, Prod. 236401002, Supp: 11351) and placed in the desiccator until analysis with XPS.

A summary of the experiments carried out is presented below.

Sample	Nitric acid treatment	Immersion time	No of samples
Ca-Ti	No nitric acid treatment (Ca-Ti control)	2 min	6 samples
		4 h	6 samples
		24 h	6 samples
	10% 10 min	2 min	6 samples
		4 h	6 samples
		24 h	6 samples
	34% 1h	2 min	6 samples
		4 h	6 samples
		24 h	6 samples

The solutions in which the discs were immersed were analysed using ion chromatography. Surface analysis was carried on the discs using X-ray photoelectron spectroscopy (XPS) and depth profiling XPS.

XPS was carried out using the monochromated X-ray source. Depth profiling was carried out on 1 sample for each time point and treatment type. Blue and silver areas (where the samples did not become completely blue) on the control Ca-Ti samples which had not had nitric acid treatment were analysed. The twin anode source was used in AlK_{α} mode for the depth profiling for the nitric acid treated samples because the monochromated X-ray source was not available. Before using the twin source, a comparison between mono and twin analysis was made for 34% Ca-Ti 2 min to compare results when using different sources, and no difference was found.

4.4.4 Results and discussion

4.4.4.1 Appearance

The general appearance of the Ca-Ti discs before immersion was shiny silver.
No colour change was observed on the 10% HNO_3 Ca-Ti discs immediately after the nitric acid treatment, but after approximately 15 minutes they became dark silver in appearance. The 34% HNO_3 Ca-Ti samples became dark gold after the

treatment. As changes in colour are related to the oxide layer present on the surface, this suggested that the thickness of the oxide layer changed in response to both the 10% HNO_3 and the 34% HNO_3 treatments. The subsequent analysis of the surfaces was intended to confirm or deny this hypothesis.

After immersion in water, the surface colour of the Ca-Ti samples changed and varied from fully blue on some samples, to blue patches distributed over parts of the surface together with unchanged silver zones (patches) on others. A few of the samples did not change colour at all and remained fully silver. However, as compared with the previous experiment where most of the samples turned blue, in this experiment only a few of the samples turned fully blue, a few patchy blue and many samples remained silver or were only a little blue around the edges. The reason for this behaviour is not fully understood but it is presumed that the long interval following implantation may be the cause.
After immersion in ultrapure water the nitric acid treated samples changed colour; the 10 % HNO_3 Ca-Ti samples became dark gold and the 34% HNO_3 Ca-Ti samples pink / purple. This was probably due to the modification of the oxide layer, as there are various surface chemistry changes which might take place on acid treatment, including thickening / thinning of the oxide layer, Ca ion release, and surface etching.

4.4.4.2 Surface chemistry

The Ca 2p, Ti 2p, O 1s, C 1s and N 1s spectra for Ca-Ti, 10% HNO_3 Ca-Ti and 34% HNO_3 Ca-Ti samples are presented in figures 4.22-4.26. The elemental ratios (average) values for O/Ti, Ca/Ti and N/Ti are summarised in table 4.13. The averages were calculated from 18 samples for the 0 min and 6 samples for the 2 min, 4 h, and 24 h immersions.

Figure 4.22 shows the Ca 2p spectra for Ca-Ti samples before ('Ca Ti') and after 10% and 34% nitric acid treatment ('10% and 34%NACa Ti').

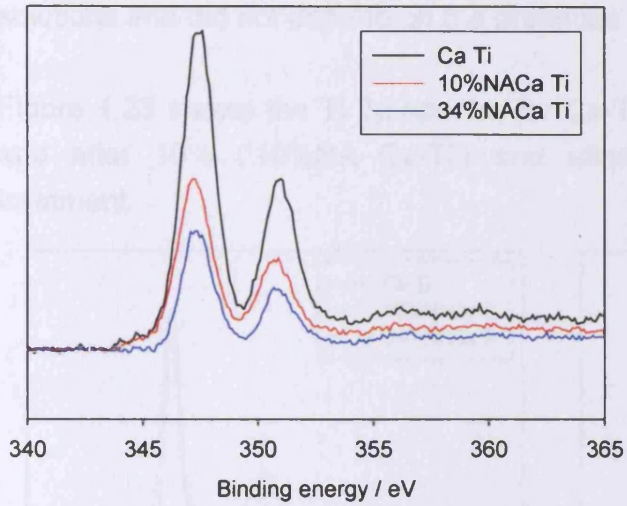

Figure 4. 22 The Ca 2p spectra for as-implanted Ca-Ti sample ('Ca Ti') and after 10% HNO_3 Ca-Ti ('10%NACa Ti') and after 34% HNO3 ('34%NACa Ti') samples.

Table 4.13 shows the elemental ratios (averages + standard deviation) for Ca-Ti, 10% HNO_3 Ca-Ti, and 34% HNO_3 Ca-Ti samples.

Sample	Ca/Ti	N/Ti	O/Ti	C/Ti
Ca-Ti	0.22 ± 0.01	0.00 ± 0.00	2.49 ± 0.09	0.85 ± 0.15
10% HNO_3 Ca-Ti	0.11 ± 0.02	0.01 ± 0.01	2.08 ± 0.11	0.50 ± 0.23
34% HNO_3 Ca-Ti	0.11 ± 0.02	0.02 ± 0.01	4.17 ± 0.15	0.51 ± 0.16

Table 4. 13 Average elemental ratios measured using XPS for Ca-Ti samples before and after nitric acid treatment.

The Ca 2p spectrum (figure 4.22) before nitric acid treatment presented two very well defined peaks, at 347.3 eV and 350.7 eV, which are the $2p_{3/2}$ and $2p_{1/2}$ components of the spin orbit doublet. These are typical for Ca implanted titanium (chapter 3). After 10% nitric acid treatment, the Ca 2p peak showed a significant decrease ($p < 0.05$) in the Ca on the surface by 50%, which is clearly seen in table 4.13, which shows a significant decrease ($p < 0.05$) in the Ca/Ti ratio from 0.22 before nitric acid treatment to 0.11 afterwards.

However, there was no significant difference in the Ca/Ti ratios between the 10% and 34% nitric acid treated samples. It is known that immersion of Ca-Ti in water for 2 min results in around a 50% reduction of the surface Ca, it is possible that this

decrease in the surface calcium was caused by the immersion in aqueous solutions and did not depend on the presence of the nitric acid.

Figure 4.23 shows the Ti 2p spectra for Ca-Ti before nitric acid treatment (Ca-Ti) and after 10% ('10%NA Ca-Ti') and after 34% ('34%NA Ca-Ti') nitric acid treatment.

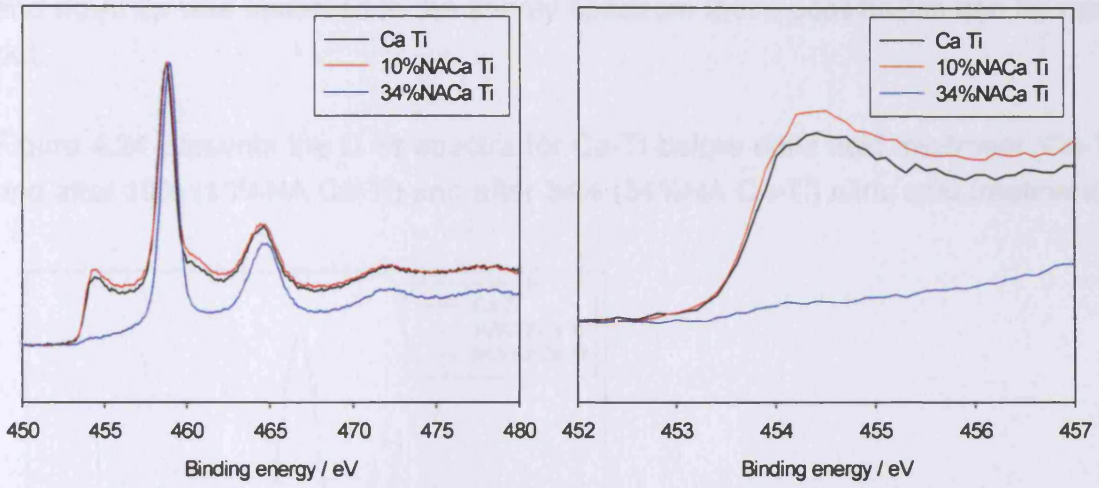

Figure 4. 23 The Ti 2p spectra for as-implanted Ca-Ti (Ca-Ti) and after 10% HNO_3 (10%NA Ca-Ti) and 34% HNO_3 (34%NA Ca-Ti). Expanded Tin+ peak (n<4) for as-implanted Ca-Ti (Ca-Ti), and after 10% HNO_3 (10%NA Ca-Ti) and 34% HNO_3 (34%NA Ca-Ti) is presented on the right of the figure.

The Ti 2p spectrum before nitric acid treatment (Ca-Ti) was typical for Ca implanted titanium. It showed the Ti^{4+} $2p_{3/2}$ peak at approximately 458.7 eV, and a peak at lower binding energy (Ti^{n+}) (n < 4) attributed to sub-oxide species including at lowest binding energy the carbide peak present on the sub-surface caused by the implantation process. After 10 % nitric acid treatment there was a slight increase in the Ti^{n+} peak (n<4) for Ti 2p which suggested that there was a slight decrease in the thickness of the oxide layer present on the surface supported also by the significant decrease ($p<0.05$) in the O/Ti ratio (table 4.13).

The Ti 2p spectrum for the 34% HNO_3 Ca-Ti changed mostly with regards to the low binding energy peak. This peak for the Ca-Ti sample treated with 34 % nitric acid was very weak at that binding energy and almost disappeared. This reduction in the peak may have been caused by a significant increase in the thickness of the oxide layer present on the surface due to the HNO_3 treatment, or by surface etching removing the top layers of the surface (including those containing the

carbide), with or without surface oxidation such that the underlying metal peaks cannot be seen (i.e oxide layer thicker than 10 nm). Analysis of the depth profiles later on will probably clarify some of these assumptions. Another cause for this peak reduction may have been an increase in the surface contamination, probably from the nitric acid treatment, or the aluminium foil in which the samples were wrapped. However, as the C 1s spectrum was not significantly altered (see below) and no Al 2p was observed in the survey spectrum these possibilities can be ruled out.

Figure 4.24 presents the C 1s spectra for Ca-Ti before nitric acid treatment (Ca-Ti) and after 10% (10%NA Ca-Ti) and after 34% (34%NA Ca-Ti) nitric acid treatment.

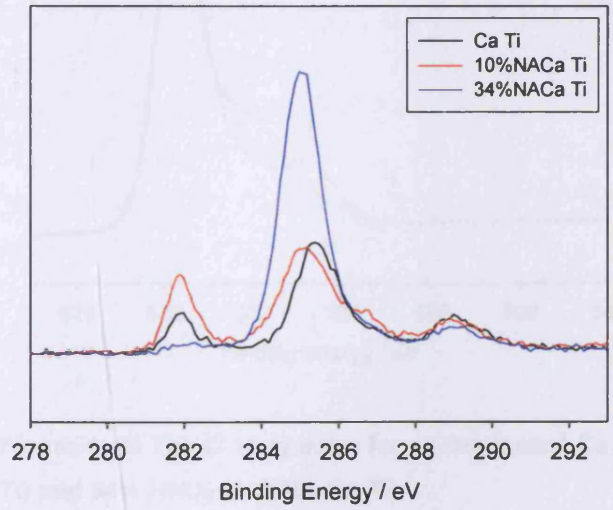

Figure 4. 24 The C 1s spectra for as-implanted Ca-Ti (Ca-Ti) and after 10% (10%NA Ca-Ti) and 34% nitric acid treatment (34%NA Ca-Ti).

The 10% HNO_3 treatment resulted in a slight increase in the carbide, and a slight decrease in the high binding energy peak. The overall C/Ti ratio decreased significantly. This suggested that slight surface etching had occurred moving carbide closer to the surface. The 34% HNO_3 treatment resulted in reduction of the carbide peak almost to disappearance, possibly indicating etching through the carbide. Alternatively, this could indicate surface oxidation with carbide buried beneath a new oxide layer. The main change in the 34% HNO_3 spectrum is a much larger hydrocarbon peak. This suggested that contamination may have increased following 34% $HN0_3$ treatment, which may have been one of the causes for the increased O/Ti ratio and reduced Ti^{n+} (n<4) peak. However, the C/Ti ratio average

actually decreased significantly ($p<0.05$) following treatment, suggesting that the contamination was not the main cause of an increase in the O/Ti ratio. It may be deduced therefore that the increase in the O/Ti ratio and the reduction in the Ti^{n+} ($n<4$) peak was due, at least in some part, to an increase in the thickness of the oxide layer, accompanied by a change in the composition of the oxide layer.

Figure 4.25 presents the O 1s spectra for Ca-Ti before nitric acid treatment (Ca-Ti) and after 10% (10%NA Ca-Ti) and after 34% (34%NA Ca-Ti) nitric acid treatment.

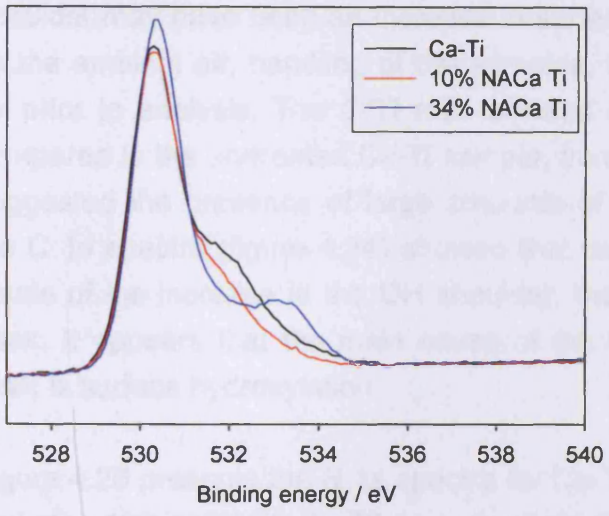

Figure 4. 25 The O 1s spectra for as-implanted Ca-Ti (Ca-Ti) and after 10% HNO_3 (10%NA Ca-Ti) and 34% HNO_3 (34%NA Ca-Ti).

The O 1s spectrum before nitric acid treatment showed a single peak at ~ 531 eV which was due to O present as O^{2-}. The slight shoulder, which appeared at higher binding energy, reflected the presence of compounds with O in OH groups at ~532 eV and H_2O at ~533 eV and other O-containing organic compounds likely to be present on the surface. It may have been due to contamination from various sources, including alumina or aluminium hydroxide from the aluminium foil in which the discs were wrapped. However this was not the case, as the survey spectra and narrow scan Al 2p spectra (graphs not presented) did not show any Al for any of the samples.

Following 10% nitric acid treatment, the O 1s peak remained unchanged in terms of peak shape. However, the shoulder decreased slightly for some of the 10% HNO_3 Ca-Ti samples remaining unchanged for others. There was also a significant

decrease ($p < 0.05$) in the O/Ti ratio following treatment, as seen in the quantification table (table 4.13). These observations, combined with the slight increase in the Ti^{n+} peak ($n<4$) for Ti 2p described earlier suggested that there was a slight decrease in the thickness of the surface oxide layer.

The O 1s spectrum for the 34% HNO_3 Ca-Ti samples showed an increase in the high binding energy shoulder; however, its intensity was very variable. The increase in the shoulder for any of the samples may have been caused by an increase in the concentration of surface hydroxyl groups, with the resultant modification of the oxide layer. Another possible cause of the increase in the shoulder may have been an increase in surface contamination, from sources such as the ambient air, handling of the samples, the nitric acid treatment, and time in air prior to analysis. The O/Ti ratio showed a significant increase ($p < 0.05$) as compared to the un-treated Ca-Ti sample, from 2.49 to 4.17 (table 4.13). This ratio suggested the presence of large amounts of $Ti(OH)_4$ on the surface. Analysis of the C 1s spectra (figure 4.24) showed that contamination could be excluded as a cause of the increase in the OH shoulder, the O/Ti ratio and reduction of the Ti^{n+} peak. It appears that the main cause of the increase of the high binding energy peak is surface hydroxylation

Figure 4.26 presents the N 1s spectra for Ca-Ti before nitric acid treatment (Ca-Ti) and after 10% (10%NA Ca-Ti) and after 34% (34%NA Ca-Ti) nitric acid treatment.

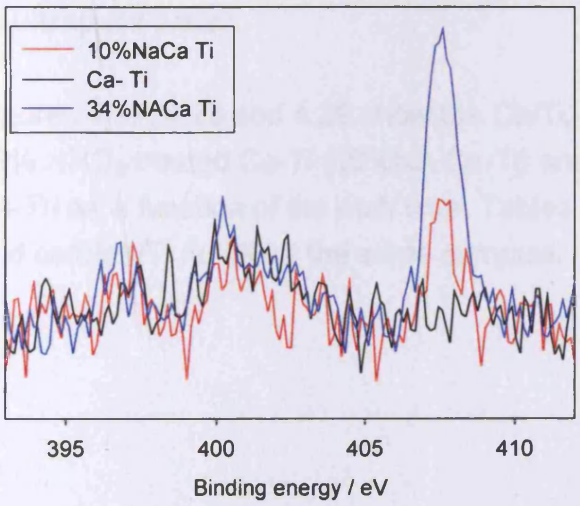

Figure 4. 26 The N1s spectra for as-implanted Ca-Ti (Ca-Ti) and after 10% (10%NA Ca-Ti) and 34% nitric acid treatment (34%NA Ca-Ti).

The N1s spectra for all the samples presented a very small single peak at ~ 400 eV due to -N-(C H) species which was probably due to contamination, possibly from handling of the samples during experiments, time in air prior to analysis etc. (figure 4.26). The N1s spectra for Ca-Ti and 34% HNO_3 Ca-Ti show another peak at ~407 eV, caused by the presence of nitrate (NO_3). There was also another small peak for all the samples, at ~ 397 eV due to titanium nitride, TiN, (Vasile et al., 1990), probably formed during the implantation process.

For the Ca-Ti sample the peaks were very low in intensity and almost non-existent, as confirmed by the quantification table where the measured N/Ti ratio had a value of 0. This again confirmed that N was not a major contaminant of the Ca-Ti.

Following 10% nitric acid treatment, neither the shape nor the intensity of the peaks was significantly altered, with only the higher binding energy peak showing a slight increase in the intensity. However, the quantification table showed no significant change in the N/Ti ratio.

The 34 % HNO_3 spectrum kept the same shape of the N1s peaks as the 10% HNO_3 spectrum but the intensity, especially for the peaks at higher E_B more than doubled when compared with the 10% HNO_3 treated titanium. The N/Ti ratio increased significantly ($p < 0.05$) to 0.02 (table 4.13) following 34% nitric acid treatment. This suggested that 34% nitric acid treatment resulted in more surface nitrogen.

4.4.4.3 XPS depth profiling for nitric acid treated samples before immersion in ultrapure water.

Figures 4.27, 4.28 and 4.29 show the Ca/Ti, O/Ti and carbide/Ti ratios for Ca-Ti, 10% HNO_3 treated Ca-Ti (10%NA Ca-Ti) and 34% treated HNO_3 Ca-Ti (34%NA Ca-Ti) as a function of the etch time. Tables 4.14, 4.15 and 4.16 show Ca/Ti, O/Ti and carbide/Ti ratios for the same samples.

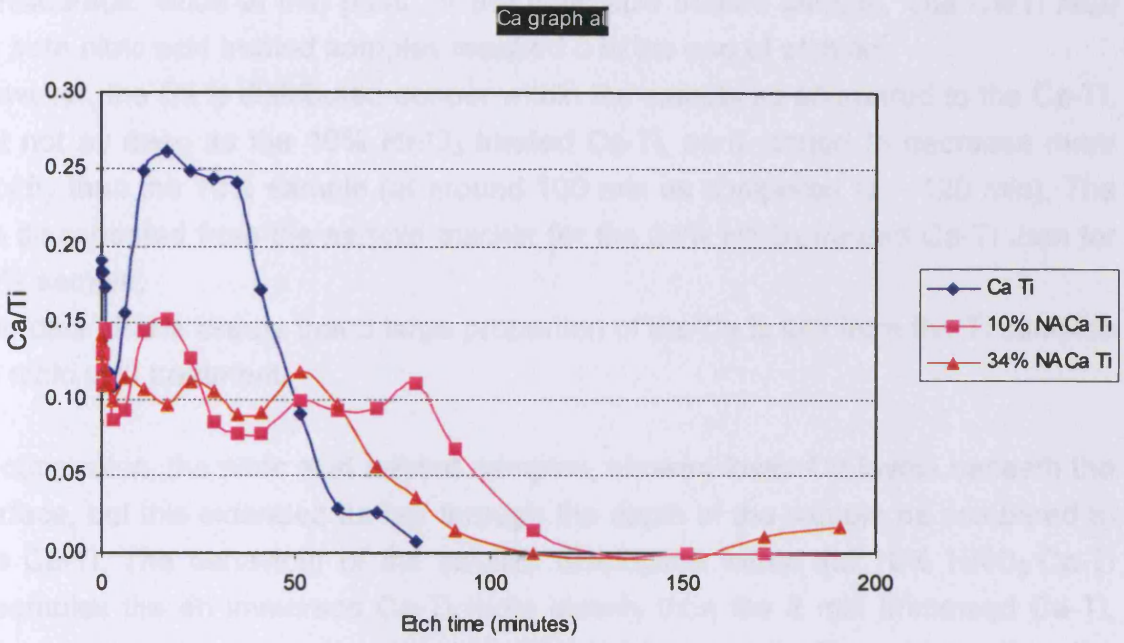

Figure 4. 27 Ca/Ti ratios for Ca-Ti as-implanted, 10% HNO3 treated Ca-Ti discs and 34% HNO_3 treated Ca-Ti as a function of etching time.

Etch time	Ca-Ti	10% HNO_3 Ca-Ti	34% HNO_3 Ca-Ti
0	0.18	0.13	0.14
3	0.11	0.09	0.10
17	0.26	0.13	0.11
81	0.01	0.11	0.04
191		0.00	0.00

Table 4. 14 Ca/Ti ratios for Ca-Ti and 10% HNO_3 treated Ca-Ti and 34% HNO_3 treated Ca-Ti.

The surface calcium level was higher for Ca-Ti as compared to both 10% HNO_3 treated Ca-Ti and to the 34% HNO_3 treated Ca-Ti. The ratios for all the samples decreased rapidly initially, reaching after 3 min, 0.11, 0.10 and 0.09 respectively. From this point they increased slightly for Ca-Ti and 10% and hardly at all for the 34%, reaching a maximum of 0.26, 0.13 and 0.11 after 17 min of etching. It is clear that at this point there was a lot more calcium beneath the surface for Ca-Ti as compared to 10% HNO_3 treated Ca-Ti. After this time point the Ca for both samples started to decrease, but at a lower pace for 10% HNO_3 treated Ca-Ti. After 81 min of etching, the Ca disappeared for Ca-Ti, but was still at a

considerable value at that point for the nitric acid treated sample. The Ca/Ti ratio for both nitric acid treated samples reached 0 in the end of etching.
However, the Ca is distributed deeper within the sample as compared to the Ca-Ti, but not as deep as the 10% HNO_3 treated Ca-Ti, as it started to decrease more rapidly than the 10% sample (at around 100 min as compared to ~ 120 min). The Ca disappeared from the sample quicker for the 34% HNO_3 treated Ca-Ti then for 10% sample.
The data shows clearly that a large proportion of the Ca is lost from the Ti samples on nitric acid treatment.

In conclusion, the nitric acid treated samples, showed lower Ca levels beneath the surface, but this extended further through the depth of the sample as compared to the Ca-Ti. The behaviour of the calcium distribution within the 10% HNO_3 Ca-Ti resembles the 4h immersed Ca-Ti more closely than the 2 min immersed Ca-Ti, although the calcium levels within the 10% HNO_3 treated Ca-Ti are higher than the 4h Ca-Ti. The 34% HNO_3 Ca-Ti showed slightly more Ca on the surface compared to the 10% HNO_3 Ca-Ti and similar distribution of Ca within deeper layer of the samples. The Ca started to decrease slightly quicker than the 10% HNO_3 Ca-Ti showing that maybe some Ca had been released, anyway more than the 10% sample.
Ca had been released from both samples. It appeared that the release was overall slightly less from 10% than 34% nitric acid treated samples, but this is highly debatable.

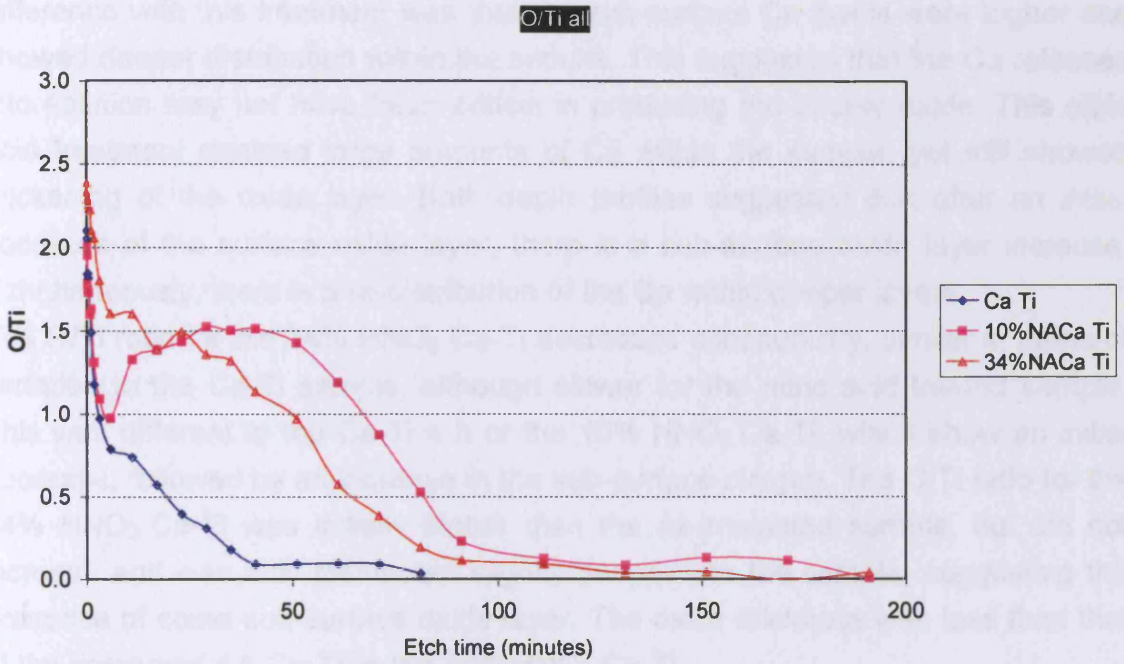

Figure 4. 28 O/Ti ratios for Ca-Ti, 10% HNO_3 treated Ca-Ti and 34% HNO_3 treated discs as a function of etching time.

Etch time (min)	Ca-Ti	10% HNO_3 treated Ca-Ti	34% HNO_3 treated Ca-Ti
0	2.10	2.00	2.33
6	0.79	0.97	1.60
41	0.09	1.51	1.13
81	0.04	0.52	0.20
191		0.01	0.04

Table 4. 15 O/Ti ratios for Ca-Ti, 10% HNO_3 treated Ca-Ti, and 34% HNO_3 treated Ca-Ti.

The O/Ti ratios for the Ca-Ti sample decreased continuously throughout the etching, with a shoulder at ~ 10 min. O had eventually gone by ~ 80 min as discussed previously (figure 4.12). The 10% HNO_3 treated Ca-Ti sample had initially less O on the surface as compared to the Ca-Ti. The O/Ti ratio decreased rapidly initially, reaching, after 6 min of etching, 0.97. It then increased rapidly, reaching 1.51 after 41 min of etching, far greater than the O/Ti ratio for Ca-Ti at this point (0.09). This suggested that the subsurface O increased and approximately followed the distribution of the calcium. The shape of the curve for the 10% HNO_3 treated Ca-Ti was similar to the O/Ti curve shape beneath the surface for 4h immersed Ca-Ti where the oxide layer was observed to thicken considerably. The

difference with this treatment was that the sub-surface Ca levels were higher and showed deeper distribution within the sample. This suggested that the Ca released into solution may not have been critical in producing the thicker oxide. This nitric acid treatment retained large amounts of Ca within the sample, yet still showed thickening of the oxide layer. Both depth profiles suggested that after an initial decrease of the surface oxide layer, there is a sub-surface oxide layer increase. Simultaneously, there is a re-distribution of the Ca within deeper layers.
The O/Ti ratio for the 34% HNO_3 Ca-Ti decreases continuously, similar in terms of variation to the Ca-Ti sample, although slower for the nitric acid treated sample. This was different to the Ca-Ti 4 h or the 10% HNO_3 Ca-Ti, which show an initial decrease, followed by an increase in the sub-surface oxygen. The O/Ti ratio for the 34% HNO_3 Ca-Ti was initially higher than the as-implanted sample, but did not increase and was only distributed slightly deeper into the sample, suggesting the presence of some sub-surface oxide layer. The oxide thickness was less than that of the immersed 4 h Ca-Ti or the 10% HNO_3 Ca-Ti.

Figure 4.29 present the carbide/Ti ratio for Ca-Ti and 10% HNO_3 treated Ca-Ti treated Ca-Ti discs as a function of the etching time. The carbide/Ti ratio for 34% HNO_3 treated Ca-Ti has not been presented in the figure as carbide decreased for this sample following treatment and was not detectable on the surface and hence not quantifiable.

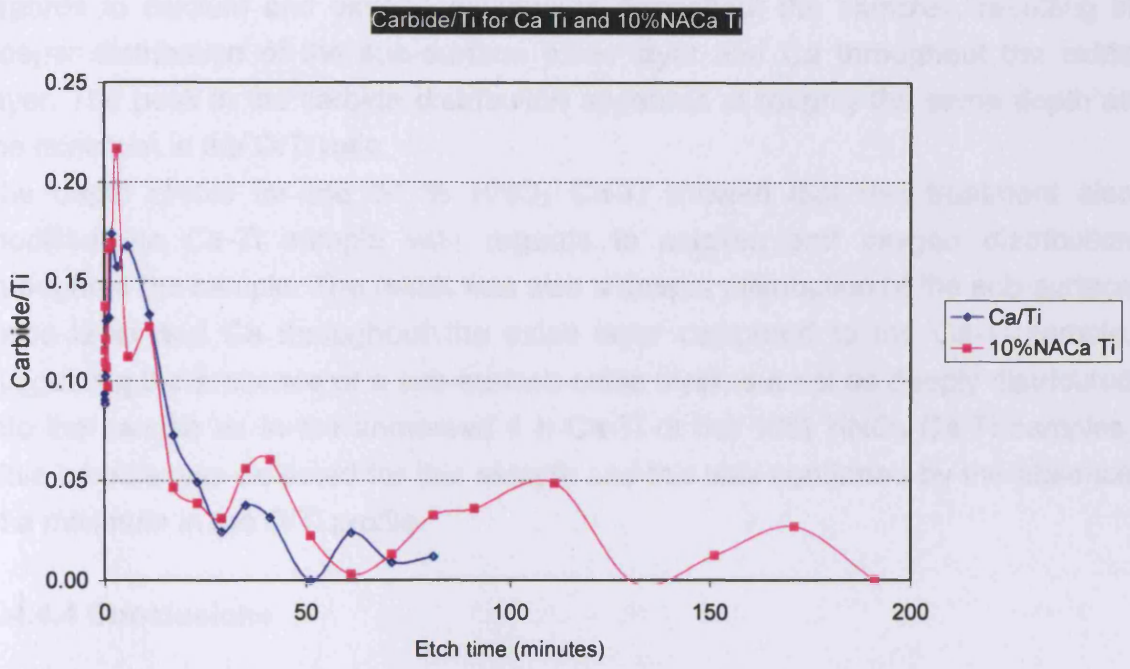

Figure 4. 29 Carbide/Ti ratios for Ca-Ti and 10% HNO_3 treated Ca-Ti discs (10%NA Ca-Ti) as a function of the etching time.

Etch time (minutes)	Ca-Ti	10% HNO_3 Ca-Ti
0	0.09	0.12
3	0.16	0.22
6	0.17	0.11
81	0.01	0.03
191	-	0.00

Table 4. 16 Carbide/Ti ratios for Ca-Ti and 10% HNO_3 Ca-Ti.

The carbide for both samples varied in similar way throughout the etching process. There was more carbide on the surface for 10% HNO_3 Ca-Ti initially, and then both samples showed a rapid increase, after 3 min of etching reaching 0.16 for Ca-Ti and more for 10% HNO_3 Ca-Ti (0.22). The carbide for Ca-Ti increased slightly more up to a carbide/Ti ratio = 0.17 after 6 min of etching. In the same time, the carbide for the nitric acid treated samples decreased rapidly, being reduced to half (0.11). The decrease continued until the disappearance of the carbide for both samples by the end of the etching of each sample. One possible explanation for this rapid decrease in the carbide for the nitric acid treated sample was that carbide could be closer to the surface as a result of the nitric acid treatments.

It is clear from the depth profile that 10 % HNO_3 modified the Ca-Ti samples with

regards to calcium and oxygen distribution throughout the samples, resulting in deeper distribution of the sub-surface oxide layer and Ca throughout the oxide layer. The peak in the carbide distribution appeared at roughly the same depth as the minimum in the O/Ti ratio.
The depth profile for the 34 % HNO_3 Ca-Ti showed that this treatment also modified the Ca-Ti sample with regards to calcium and oxygen distribution throughout the sample. The result was also a deeper distribution of the sub-surface oxide layer and Ca throughout the oxide layer compared to the Ca-Ti sample, suggesting the presence of a sub-surface oxide layer, but not as deeply distributed into the sample as in the immersed 4 h Ca-Ti or the 10% HNO_3 Ca-Ti samples. Little carbide was detected for this sample and this was confirmed by the absence of a minimum in the O/Ti profile.

4.4.4.4 Conclusions

Nitric acid treatment resulted in colour change of the treated Ca-Ti samples, with the 10%HNO_3 treated Ca-Ti becoming dark silver and the 34% becoming gold. As colour change is linked to the modification in the thickness of the oxide layer, it appears that the 10% resulted in a decrease and 34% an increase in the surface layer, probably the oxide layer, and surface etching which removed the top surface layers containing carbide.
The depth profiling data showed that for both treatments Ca is both lost from the sub-surface and re-distributed with the growth of the oxide layer.

4.4.4.5 Immersion of nitric acid treated samples in ultrapure water

After analysis, all the discs were immersed in ultrapure water following the protocol described in section 4.3.2. Following immersion, the discs were analysed with XPS and the spectra are presented in figures 4.30 - 4.36. The elemental ratios for the samples are presented in tables 4.17 - 4.18.

The XPS surface spectra for Ca-Ti immersed in water (control) were similar to those in previous experiments and are not included to avoid repetition. Any differences found in this experiment as compared with the previous ones were however addressed.
The surface calcium had similar values to the previous experiment (Ca/Ti = 0.22)

and the surface drop in Ca on immersion was not significantly different following immersion for any time period. The O/Ti ratio again did not vary significantly after 2 min and 4 h immersion, but increased significantly ($p<0.05$) for the Ca-Ti immersed for 24 h (O/Ti = 3.40 ± 0.43) for this experiment as compared the to the O/Ti ratio of 2.80 ± 0.28 presented in experiment 4.2. The reason for this could not be fully understood. One explanation may be that the oxide layer on these samples was thicker, which however was not seen in the Ti 2p spectra. Possibly more contamination was present on these samples, such as increased C contamination, which would have resulted in a higher C/Ti ratio and more pronounced C 1s peaks. However, the C 1s spectra showed less pronounced peaks in comparison with the C 1s spectra for the Ca-Ti samples analysed in experiment 4.2, and the C/Ti ratio showed no significant differences between the two experiments. Another explanation for the increase in the O/Ti ratio for the Ca-Ti samples analysed in this experiment might be the presence of more hydroxide species on the surfaces of the samples. Indeed, the O 1s spectra showed a more pronounced shoulders for these samples as compared to the previous experiment.

Below are presented the Ca 2p, Ti 2p, and O 1s spectra (figures 4.30-4.36) and the elemental ratios for 10% HNO_3 treated Ca-Ti before and after immersion for 2 min, 4 h, and 24 h (table 4.17). Representative spectra were selected from all the samples.

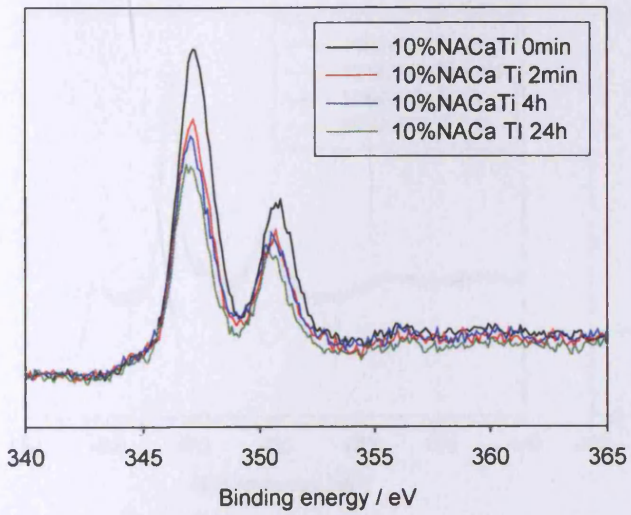

Figure 4. 30 The Ca 2p spectra for 10% HNO_3 Ca-Ti before (0 min), and after 2 min, 4 h and 24 h immersion in ultrapure water.

Samples	Ca/Ti	O/Ti	C/Ti	N/Ti
10% HNO_3 Ca-Ti 0 min	0.11 ± 0.02	2.08 ± 0.11	0.50 ± 0.23	0.01 ± 0.01
10% HNO_3 Ca-Ti 2 min	0.10 ± 0.01	2.17 ± 0.17	0.95 ± 0.37	0.02 ± 0.01
10% HNO_3 Ca-Ti 4 h	0.08± 0.00	2.15 ± 0.16	0.62 ± 0.08	0.01 ± 0.01
10% HNO_3 Ca-Ti 24 h	0.08± 0.01	2.70 ± 0.72	0.83 ± 0.11	0.02 ± 0.01

Table 4. 17 Elemental ratios (averages and standard deviations) for 10%HNO3 Ca-Ti samples measured before (0 min), and after immersion (at 2 min, 4 h, 24 h) in ultrapure water.

The Ca 2p spectra again did not change in terms of shape but showed a small decrease in the intensity of the peaks. This was seen also in the quantification table (table 4.17), where the Ca/Ti ratio on the surface dropped, but not significantly from 0.11 ± 0.02 before immersion to 0.10 ± 0.01 after 2 min. This was different from the Ca-Ti samples immersed for 2 min, which showed a 50% significant reduction in the surface calcium. However, this may have been caused by the fact that the surface calcium of the samples had already halved following nitric acid treatment.

The Ca/Ti ratio on the surface dropped significantly ($p < 0.05$) from 2 min to 4h and 24h (0.08 for both the 4 h and 24 h immersed samples). This was different to the Ca-Ti samples immersed for 4 h and 24 h, where, after 2 min the drop in the surface Ca was not significant.

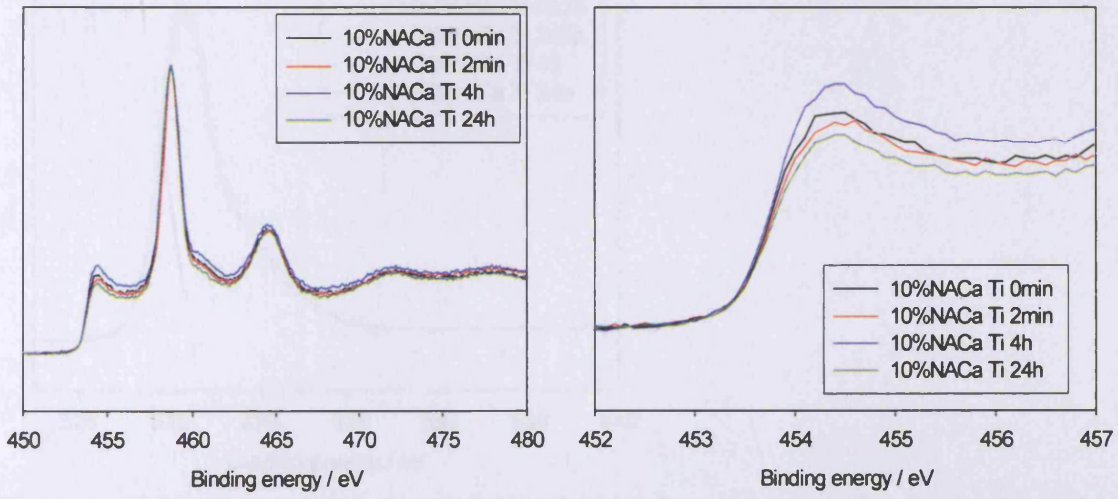

Figure 4. 31 The left panel shows Ti 2p spectra for 10% HNO_3 Ca-Ti (10%NACa Ti) before (0 min), and after 2 min, 4 h and 24 h immersion in ultrapure water(10%NACa Ti 0 min, 2 min, and 4h). The right panel shows the expanded Ti^{n+} peak (n<4) for 10% HNO_3 Ca-Ti before

(10%NACa Ti 0 min), and after 2 min, 4 h and 24 h immersion in ultrapure water.

The Ti 2p spectra for all the samples showed that the peak shape did not change at any time point. However, there was a modification in the intensity of the Ti^{n+} peak ($n < 4$) as a function of time, seen more clearly in figure 4.31, right. The Ti^{n+} peak ($n < 4$) decreased slightly after 2 min immersion, and more after 24 h immersion. There was an increase in the same peak after 4 h immersion. However, as a different sample was analysed at each time point, this variation may have been random.

Possible explanations for the decrease / increase in the intensity of the Ti^{n+} peak ($n < 4$) for the samples could be: a decrease/increase in the oxide layer thickness or a decrease/increase in the contamination. Considering the elemental ratios for the 10% HNO_3 Ca-Ti samples following immersion (table 4.17) it was observed that after 2 min immersion there was a significant increase ($p < 0.05$) in the C/Ti and N/Ti ratios as compared to the 0 min samples. This suggested that the contamination increased following immersion in ultrapure water for 2 min, and this may have produced a decrease in the Ti^{n+} peak ($n < 4$). Immersion for both 4 h and 24 h did not change significantly the C/Ti and the N/Ti ratios in comparison to 0 min. This suggested that the variation in the Ti^{n+} peak ($n < 4$) intensity might not have been caused by contamination.

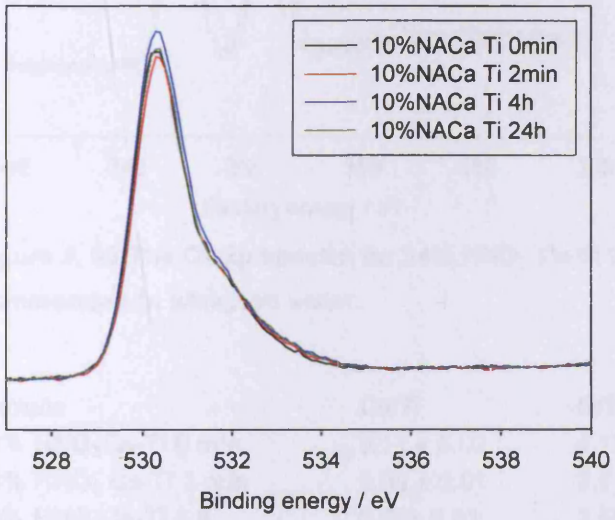

Figure 4. 32 The O 1s spectra for 10%HNO_3 Ca-Ti before (0 s), and after 2 min, 4 h and 24 h immersion in ultrapure water.

The O 1s spectra remained unchanged following immersion in ultrapure water (figure 4.32). The quantification table showed there was no significant difference in the O/Ti ratio between the samples at any time point. The fact that the O/Ti ratio did not increase significantly suggested that the thickness of the surface oxide layer may not have changed following immersion. This was supported by the fact the Ti^{n+} peak ($n < 4$) did not show any major intensity change (figure 4.31).
To summarise, immersion of 10% HNO_3 Ca-Ti samples for 2 min did not result in a change in the O/Ti ratio or modification of the surface calcium concentration. Longer immersion times (4h and 24 h) did not modify the O/Ti ratio but resulted in a significant decrease in the surface calcium.

The Ca 2p, Ti 2p, and O 1s spectra and elemental ratios for 34% HNO_3 treated Ca-Ti before and after immersion are presented in figures 4.33, 4.34, and 4.35 and table 4.18.

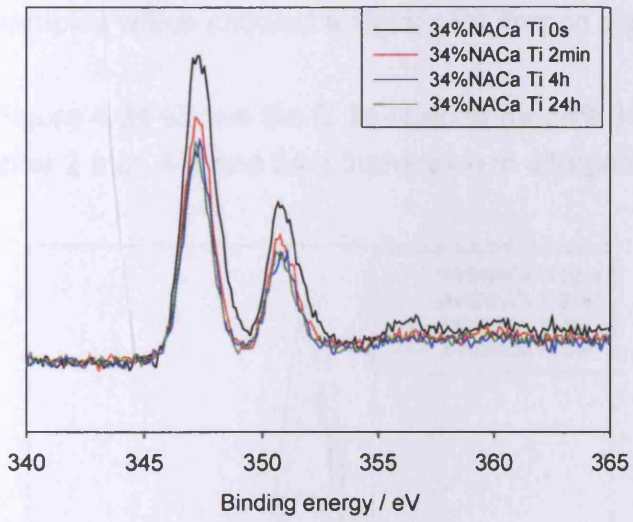

Figure 4. 33 The Ca 2p spectra for 34% HNO_3 Ca-Ti before (0 min), and after 2 min, 4 h and 24 h immersion in ultrapure water.

Sample	Ca/Ti	O/Ti	C/Ti
34% HNO_3Ca-Ti 0 min	0.11 ± 0.02	4.17 ± 0.15	0.51 ± 0.16
34% HNO_3 Ca-Ti 2 min	0.08 ± 0.01	2.51 ± 0.09	0.90 ± 0.47
34% HNO_3Ca-Ti 4 h	0.07± 0.01	3.58 ± 1.52	1.25 ± 0.47
34% HNO_3Ca-Ti 24 h	0.07± 0.01	2.58 ± 0.08	0.65 ± 0.05

Table 4. 18 Elemental ratios (averages + standard deviation) for 34% HNO3 Ca-Ti before (0 min), and after 2 min, 4 h and 24 h immersion in ultrapure water.

The Ca 2p spectra (figure 4.33) displayed consistent peak shapes but showed a pronounced decrease in the intensity of the peaks for the 2 min samples. This was also supported by the Ca-Ti ratios presented in the quantification table (table 4.18) where the Ca/Ti ratio on the surface dropped significantly ($p < 0.05$) from 0.11 ± 0.02 before immersion to 0.08 ± 0.01 after 2 min. This was similar to the un-treated Ca-Ti samples immersed for 2 min, which showed a 50% significant reduction in the surface calcium, although the drop was not so pronounced (only ~25%). However, the surface calcium drop was different to that of the 10% HNO_3 Ca-Ti samples which showed only a small drop in the surface Ca which was not significant.

Longer immersion times resulted in further significant ($p < 0.05$) decrease in the surface Ca, with a value of 0.07 ± 0.01 after 4 h, and no change after that. Again, this was different to the Ca-Ti samples, which showed no significant drop in the surface calcium after 2 min. However, this was similar to the 10% HNO_3 Ca-Ti samples which showed a significant drop in the surface calcium.

Figure 4.34 shows the C 1s spectra for 34% HNO_3 Ca-Ti discs before (0 min), and after 2 min, 4 h and 24 h immersion in ultrapure water.

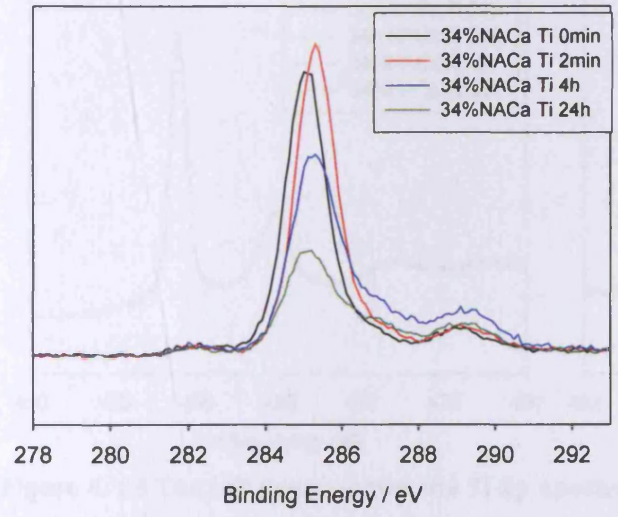

Figure 4. 34 The C 1s spectra for 34% HNO_3 Ca-Ti discs before (0 min), and after 2 min, 4 h and 24 h immersion in ultrapure water.

The 34% nitric acid treatment resulted in a significant decrease in the carbide peak. This could either have been caused by the etching of the surface, an effect

which the 10% HNO_3 samples showed only slightly. It was also possible that outward oxide growth resulted in the carbide being displaced from the surface. In comparison to the 0 min samples, immersion for 2 min resulted in non-uniformity in the samples' behaviour. There was also a significant increase ($p < 0.05$) in the C/Ti ratio.

Longer immersion times resulted in an increase in the higher binding energy peaks and significant increase in the C/Ti ratio for the 4 h samples as compared to 0 min. The 24 h samples did not show a significant difference as compared to 0 min samples, but decreased significantly ($p < 0.05$) as compared to 4 h samples. There was also non-uniformity in the samples' behaviour for 4 h and 24 h with regards to the spectra. This non-uniformity is almost certainly due to varying amounts of surface contamination arising from the immersion process and subsequent storage. Although the C/Ti ratios are a bit higher than the 10% HNO_3 treatment, they are just as variable, actually suggesting that the surfaces are quite susceptible to contamination following these nitric acid treatments

Figure 4.35 shows the Ti 2p spectra for 34% HNO_3 Ca-Ti discs before (0 min), and after 2 min, 4 h and 24 h immersion in ultrapure water.

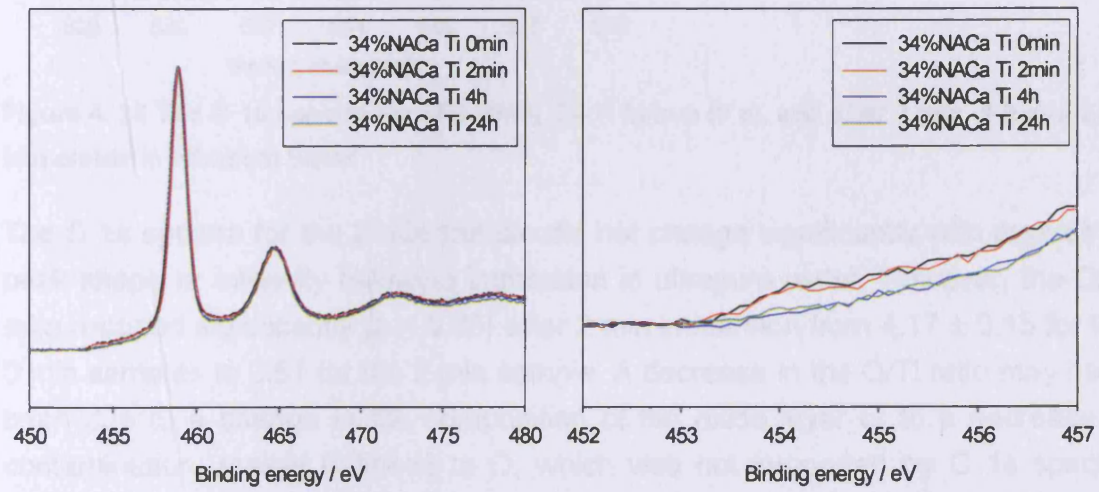

Figure 4. 35 The left panel shows the Ti 2p spectra (left) for 34% HNO_3 Ca-Ti before (0 min), and after 2 min, 4 h and 24 h immersion in ultrapure water. The right panel shows the expanded Ti^{n+} peak ($n < 4$)(right) for 34% HNO_3 Ca-Ti before (0 min), and after 2 min, 4 h and 24 h immersion in ultrapure water.

From figure 4.35 it can be seen that the Ti 2p spectra for all the samples appeared

to remain unchanged in terms of peak shape and intensity throughout the immersion. Considering the expanded Ti^{n+} ($n < 4$) peak (figure 4.35, right) it can be observed that this peak was reduced in intensity for the 4 h and 24 h samples when compared with the 0 min and 2 min samples. This suggested an increase in the surface oxide layer. In order to confirm this, the O 1s spectra and O/Ti ratios would need to be analysed.

Figure 4.36 shows the O 1s spectra for 34% HNO_3 Ca-Ti discs before (0 min), and after 2 min, 4 h and 24 h immersion in ultrapure water.

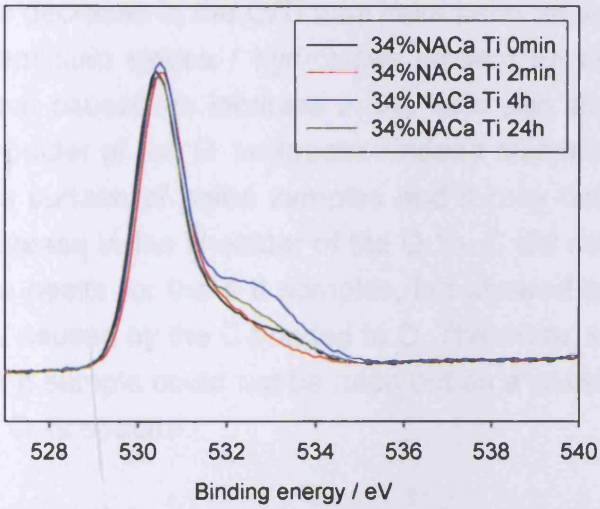

Figure 4. 36 The O 1s spectra for 34% HNO_3 Ca-Ti before (0 s), and after 2 min, 4 h and 24 h immersion in ultrapure water

The O 1s spectra for the 2 min sample did not change significantly with regards to peak shape or intensity following immersion in ultrapure water. However, the O/Ti ratio dropped significantly ($p < 0.05$) after 2 min immersion from 4.17 ± 0.15 for the 0 min samples to 2.51 for the 2 min sample. A decrease in the O/Ti ratio may have been due to a change in the composition of the oxide layer or to a decrease in contamination, mainly C linked to O, which was not supported by C 1s spectra (figure 4.36). Another explanation may be that immersion in ultrapure water for short period (2 min) of 34% HNO_3 Ca-Ti resulted in a decrease in the oxide layer and also of the surface calcium. However, it is unlikely that water would reduce the thickness of the oxide layer.

With regards to the 4 h and 24 h immersed samples, the shape of the O 1s spectra did not change shape significantly but showed a small increase in the shoulder at

~533 eV. The O/Ti ratios after 4 h and 24 h immersion in ultrapure water did not modify significantly, when compared to the O/Ti ratios for the 2 min immersed samples, and reached similar values to the average value registered for the 0 min samples before immersion (3.58). The O/Ti ratio after 24 h immersion reached a value significantly lower ($p < 0.05$) than the O/Ti ratio for the 0 min sample.
An increase in the O/Ti ratio and increase in the shoulder of the O 1s peak may have had various causes. An increase in the thickness of the oxide layer may have been one cause. Immersion for both 4 h and 24 h resulted in a decrease in the Ti^{n+} ($n<3$), which may suggest that the oxide layer thickness increased. Also at this point the surface calcium continued to decrease significantly. Another reason for the decrease in the O/Ti may have been an increase in contamination, for example aluminium oxides / hydroxides present on the surface, or C bonded to O could have caused an increase in the ratio and also an increase in the intensity of the shoulder of the O 1s spectra. Indeed alumina was detected in small quantities on the surface of some samples and it may have been a contributing factor for the increase in the shoulder of the O 1s. C did not show an increase in the intensity of the peaks for the 4 h samples, but showed a slight increase in the peak at 286.8 eV caused by the C bonded to O. Therefore, an increase in C contamination for the 24 h sample could not be ruled out as a possible cause of change in the O/Ti ratio or O 1s spectra.

From the above data it appears that nitric acid treatment certainly did modify the oxide layer, but immersion of the treated samples in water had virtually no effect at all on the surface spectra. We might therefore expect to see that the nitric acid treated samples show little ion release and little change in the depth of the sample.

4.4.4.3 Ion Chromatography

In Table 4.19 calcium ion concentrations (averages and standard deviations) are presented for the control samples (ultrapure water) and the solutions in which the Ca-Ti (control) and nitric acid treated Ca-Ti were immersed. The values are measured in ppm. The averages were calculated from 6 values for all the samples.

Sample	2 min	4h	24h
UPW (control)	0.04 ± 0.06	0.04 ± 0.05	0.02 ± 0.01
Ca-Ti (control)	0.03 ± 0.02	0.04 ± 0.03	0.61 ± 0.49
10% HNO_3 Ca-Ti	0.03 ± 0.03	0.04 ± 0.02	0.04 ± 0.03
34% HNO_3 Ca-Ti	0.10 ± 0.03	0.11 ± 0.04	0.21 ± 0.19

Table 4. 19 Averages and standard deviations of Ca concentration for the solutions in which the Ca-Ti and nitric acid treated Ca-Ti were immersed (ppm).

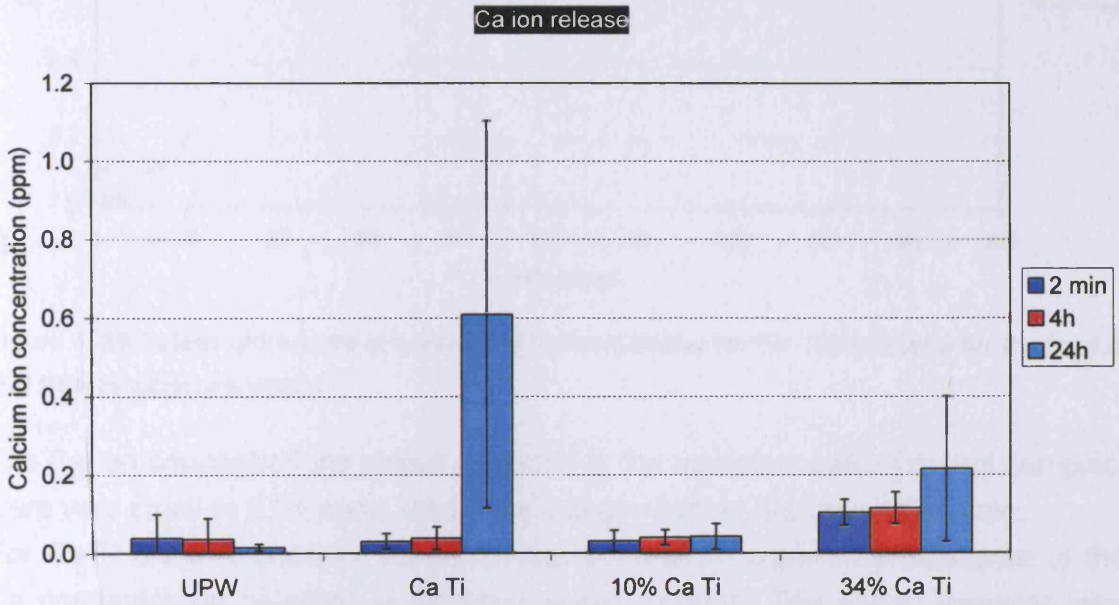

Figure 4. 37 Ca ion release from Ca-Ti, 10% Ca-Ti and 34% Ca-Ti (averages and standard deviation) after 2 min, 4 h and 24 h immersion in ultrapure water at 37°C.

Figure 4.38 below shows the concentration of calcium ions released into solution at the various time periods (average and standard deviation) for all the samples as a function of colour change.

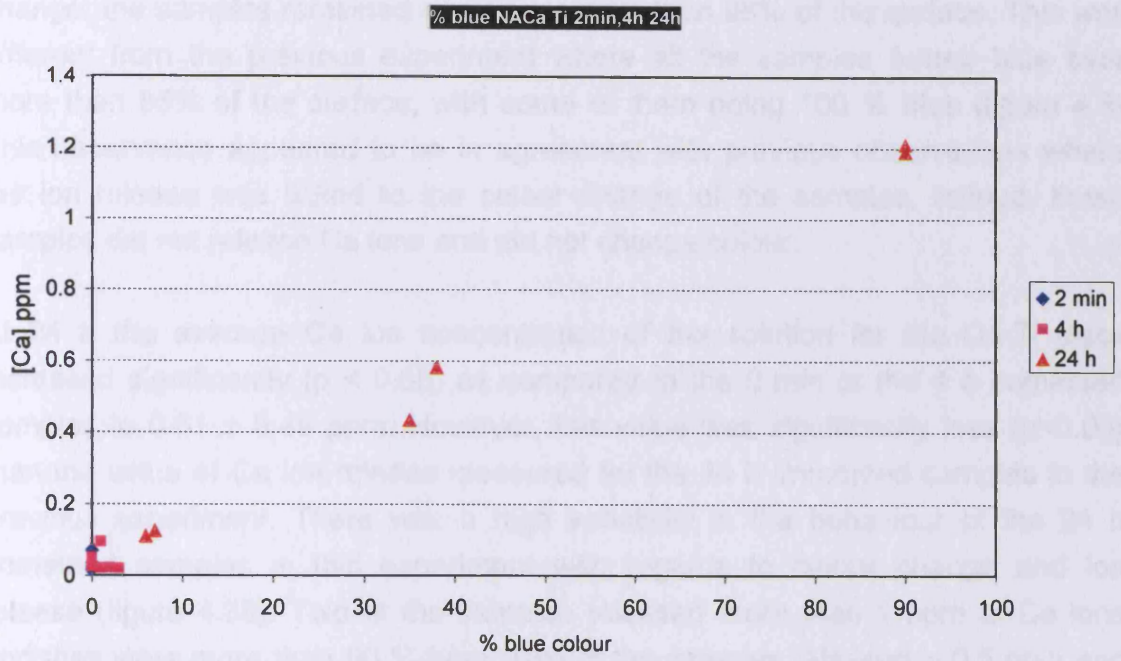

Figure 4. 38 Colour change as a function of Ca ion release for Ca-Ti immersed for 2 min, 4 h, and 24 h in ultrapure water.

The Ca ion concentrations values detected in the ultrapure water (control samples) were very small (~ 0.04 ppm), and were independent of the immersion time.
For Ca-Ti discs, immersion for 2 minutes showed no significant difference to the Ca concentration detected in ultrapure water (control). The value, however, was significantly smaller ($p < 0.05$) than the values recorded in the previous experiment (4.2), where values of 0.13 ± 0.09 ppm were recorded after 2 min immersion. It has to be noted that that both sets of samples had the same surface Ca/Ti ratio before immersion of 0.22. As the XPS studies showed that the surface calcium dropped by about half after 2 min, it may be assumed that the Ca detected in solution comes from the surface only. With regards to the colour change, none of the samples changed colour and all remained silver, similar to the behaviour of the Ca-Ti samples immersed for 2 min in the previous experiment.

After 4 h immersion, the average Ca concentrations of the solutions for the discs were very similar to the values at 2 min immersion time. This suggested that no appreciable amount of Ca was released, and was not what was expected from the Ca-Ti immersed for 4 h, with significantly higher ($p < 0.05$) values being measured in previous experiments of the order of more than 1 ppm. The colour also did not

change; the samples remained silver over more than 98% of the surface. This was different from the previous experiment where all the samples turned blue over more than 85% of the surface, with some of them being 100 % blue (figure 4.8) This observation appeared to be in agreement with previous observations where the ion release was linked to the colour change of the samples. Indeed, these samples did not release Ca ions and did not change colour.

At 24 h the average Ca ion concentration of the solution for the Ca-Ti discs increased significantly ($p < 0.05$) as compared to the 0 min or the 4 h immersed samples to 0.61 ± 0.49 ppm. However, this value was significantly less ($p<0.05$) than the value of Ca ion release measured for the 24 h immersed samples in the previous experiment. There was a high variability in the behaviour of the 24 h immersed samples in this experiment with regards to colour change and ion release (figure 4.38). Two of the samples released more than 1 ppm of Ca ions and they were more than 90 % blue. Two of the samples released ~ 0.5 ppm and were 35-40% blue. The last 2 samples released around 0.1 ppm Ca ions in solution and they were less than 6-7% blue. Again it appeared that there was a correlation between the amount of Ca ions released and the colour change. The discs were behaving in the same way as before, but it appeared that these may have been randomly selected poor samples, or that the longer storage times had affected their ability to release calcium.

The low release continued for the nitric acid treated samples as well, with values of 0.03 ppm for the 10% HNO_3 Ca-Ti after 2 min. The average Ca ion concentration of the solution after 4 h immersion showed only a minute increase to 0.04 ppm, which was not significant. After 24 h, the value did not change, suggesting that even at 24 h very little Ca was released into solution from 10% HNO_3 Ca-Ti. Regarding the colour change following immersion, the samples behaved uniformly, with all samples changing to a dark gold appearance following immersion. This suggested that the oxide layer on the surface had been modified.
The Ca ion release for the 34%HNO_3 Ca-Ti after 2 min immersion (0.1 ppm) was significantly higher than for the Ca-Ti or 10% HNO_3 Ca-Ti samples. However, the overall amount was still small. It did not change significantly after 4 h and more than doubled after 24 h reaching an average Ca concentration of 0.21 ppm, but again this was not significant. Following immersion in ultrapure water, again all the samples changed their colour, and became pink / purple following immersion. This

is an indication that the oxide layer changed, as indicated by the surface analysis as well.

In conclusion, the Ca ion release for the control samples was much lower than the values expected, especially after 4 h and 24 h immersion. The low release is correlated with the fact that the samples did not turn blue. For the sample which did, the ion release was at expected values (more than 1 ppm). The reasons for which the samples did not release Ca ions and did not modify their colour remain poorly understood. It may be due to the long storage time of the samples, although the samples were kept in a desiccator. However, the XPS data did not show any modifications of the surface chemistry.

One major reason for little ion release from the nitric acid treated samples is that quite a lot of Ca ions have been lost from the samples during the nitric acid treatments, which was illustrated by the depth profiles for the treated samples.
The fact that minimal Ca ions were released from the nitric acid treated samples may mean that the surface was modified and was made more passive, with the result that the Ca ions were not released quickly. Although it is difficult to draw this conclusion, as the Ca-Ti samples did not release Ca as expected, and it could be argued that the surface changed anyway, it can be tentatively suggested that the minimal release was caused by the nitric acid treatment, which passivated the surface. This observation may be sustained by the result which showed that the Ca-Ti surfaces did not change their colour, but all the nitric acid treated samples did. The fact that they all changed their colour suggests that they were not passivated.

4.4.4.4 XPS depth profiling for immersed nitric acid treated samples.

Figures 4.39, 4.40 and 4.41 show the Ca/Ti, O/Ti and carbide/Ti ratios for 10% HNO_3 Ca-Ti before immersion (0 min) and after 2 min, 4 h, and 24 h immersion in ultrapure water as a function of the etch time. Tables 4.20, 4.21 and 4.22 show Ca/Ti, O/Ti and carbide/Ti ratios for the same samples.

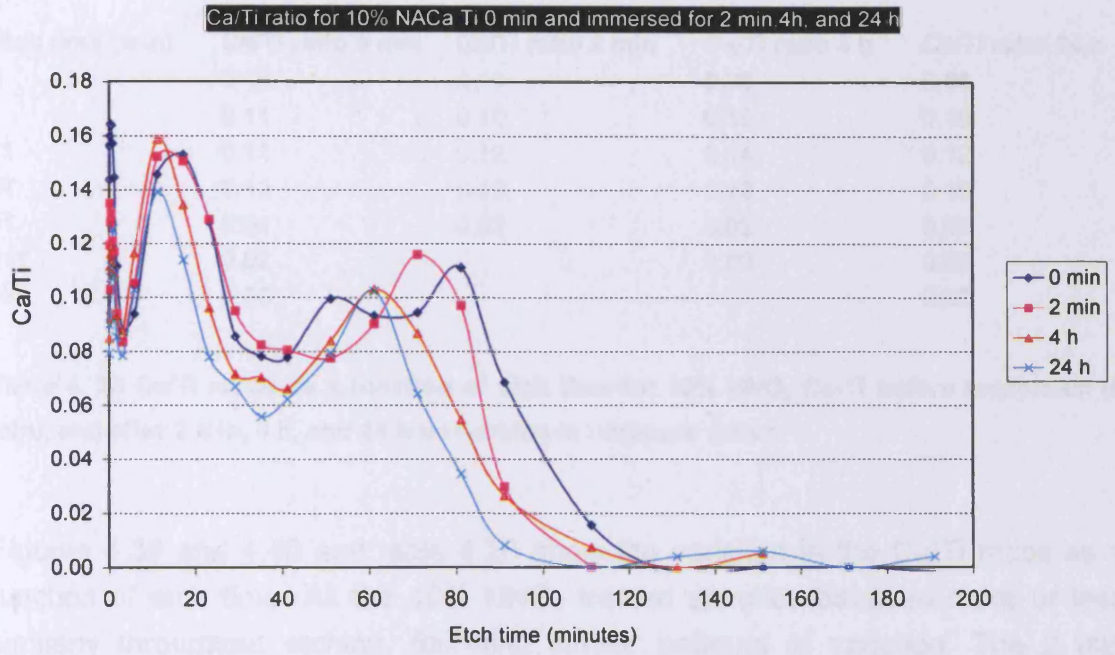

Figure 4. 39 Ca/Ti ratios as a function of etch time for 10% HNO_3 treated Ca-Ti discs before immersion (0 min) and after 2 min, 4 h, and 24 h immersion in ultrapure water.

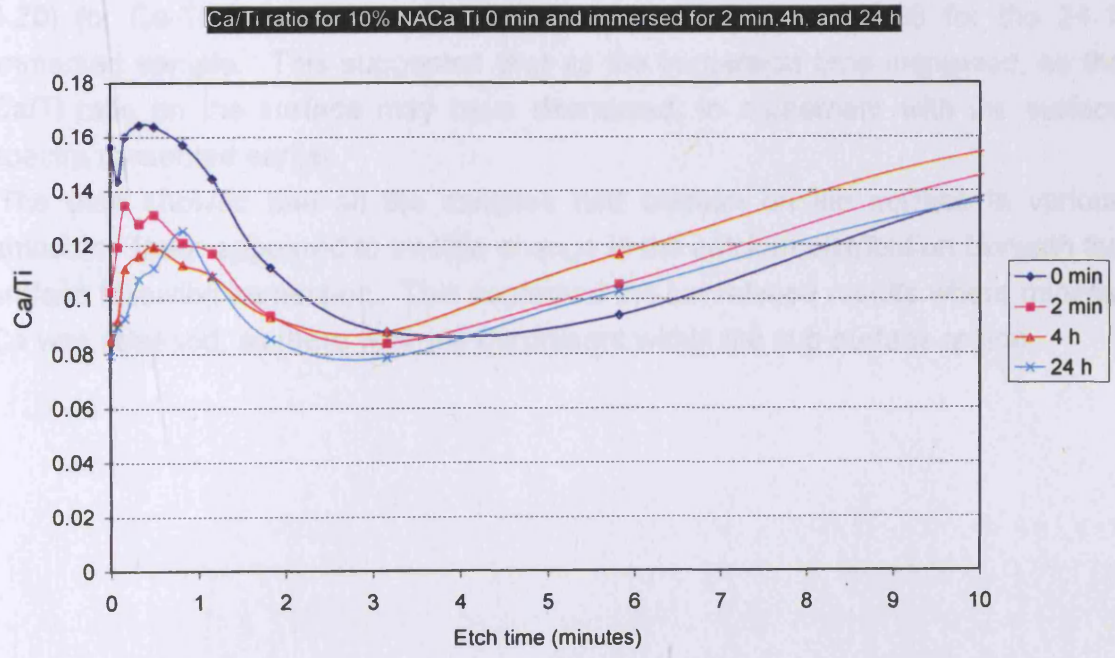

Figure 4. 40 Expanded graph of Ca/Ti ratios for 10% HNO_3 treated Ca-Ti discs before immersion (0 min), and after 2 min, 4 h, and 24 h immersion in ultrapure water.

Etch time (min)	Ca/Ti ratio 0 min	Ca/Ti ratio 2 min	Ca/Ti ratio 4 h	Ca/Ti ratio 24 h
0	0.16	0.11	0.09	0.08
1	0.11	0.10	0.10	0.10
11	0.11	0.12	0.14	0.12
17	0.13	0.13	0.12	0.10
91	0.04	0.02	0.02	0.01
111	0.02	-	0.00	0.00
191	0.00	-	-	0.00

Table 4. 20 Ca/Ti ratios as a function of etch time for 10% HNO_3 Ca-Ti before immersion (0 min), and after 2 min, 4 h, and 24 h immersion in ultrapure water.

Figures 4.39 and 4.40 and table 4.20 show the variation in the Ca/Ti ratios as a function of etch time. All the 10% HNO_3 treated samples behaved more or less similarly throughout etching, following similar patterns of variation. The 2 min behaved more like the 0 min sample, and the variation of the 4 h sample was similar in terms of shape to the 24 h sample.

The above figures showed that the amount Ca on the surface was greater for the non-immersed samples than for the immersed ones, with a ratio of 0.16 (table 4.20) for Ca-Ti 0 min compared with the smallest ratio of 0.08 for the 24 h immersed sample. This suggested that as the immersion time increased, so the Ca/Ti ratio on the surface may have decreased, in agreement with the surface spectra presented earlier.

The data showed that all the samples had calcium on the surface in various amounts. There appeared to be little change in the calcium distribution beneath the surface following immersion. This confirmed the ion release results where minimal Ca was released, as there was still Ca present within the sub-surface region.

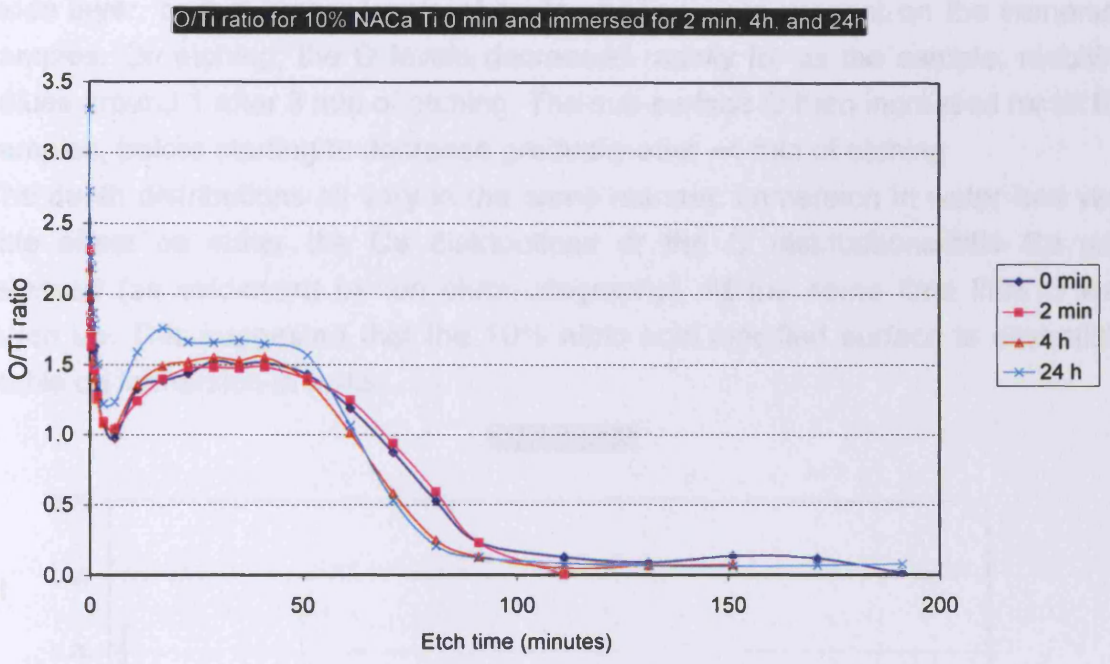

Figure 4. 41 O/Ti ratios as a function of etch time for 10% HNO_3 Ca-Ti 0min and 10% HNO_3 treated Ca-Ti discs after 2 minutes, 4 h, and 24 h immersion in ultrapure water.

Etch time (min)	0 min	2 min	4 h	24 h
0.0	2.08	2.29	2.20	3.27
3.2	0.95	0.98	0.93	1.02
41.2	1.41	1.42	1.43	1.53
51.2	1.38	1.32	1.24	1.37
91.2	0.16	0.23	0.09	0.08
111.2	0.07	-	0.03	0.05
151.2	0.06	-	0.05	0.04
191.2	0.04	-	-	0.05

Table 4. 21 O/Ti ratios for 10% HNO_3 Ca-Ti 0min and 10% HNO_3 treated Ca-Ti discs after 2 minutes, 4 h, and 24 h immersion in ultrapure water.

Figures 4.41 and table 4.21 show the O/Ti ratios recorded for all the samples throughout the etching. They show that the O level on the surface was different for each sample, with the smallest amount of 2.08 being measured for the 0 min sample. Following immersion, it could be observed that the oxide layer on the surface increased and reached the highest value of 3.27 for the 24 h sample. This suggested that longer immersion time may have resulted in an increase in the

oxide layer, or that higher levels of contamination were present on the immersed samples. On etching, the O levels decreased rapidly for all the sample, reaching values around 1 after 3 min of etching. The sub-surface O then increased for all the samples, before starting to decrease gradually after ~4 min of etching

The depth distributions all vary in the same manner: immersion in water had very little effect on either the Ca distributions or the O distributions-little Ca was released (as evidenced by ion chromatography). At the same time little O was taken up. This suggested that the 10% nitric acid modified surface is essentially stable on immersion in water.

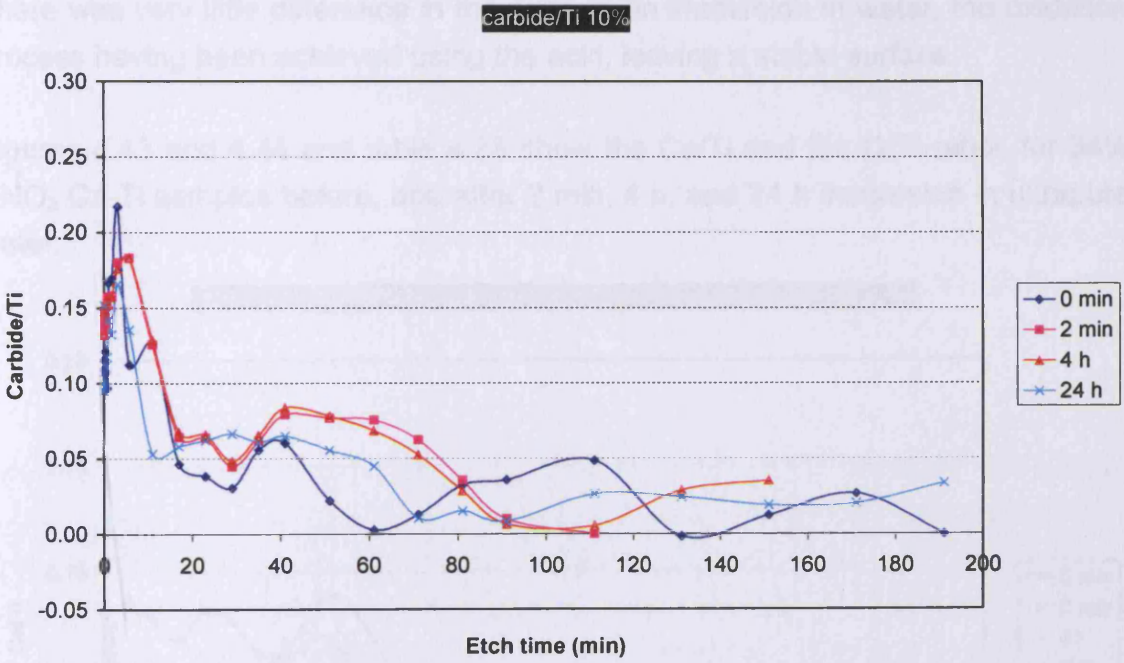

Figure 4. 42 Carbide/Ti ratios as a function of etch time for 10% HNO_3 Ca-Ti 0 min and 10% HNO_3 treated Ca-Ti discs after 2 min, 4 h, and 24 h immersion in ultrapure water.

Etch time (min)	0 min	2 min	4 h	24 h
0	0.12	0.15	0.13	0.10
3	0.22	0.18	0.18	0.17
111	0.05	0.00	0.01	0.03
151	0.01	-	0.04	0.02
191	0.00	-	-	0.03

Table 4. 22 Carbide/Ti ratios as a function of etch time for 10% HNO_3 Ca-Ti before (0 min) and after 2 min, 4 h, and 24 h immersion in ultrapure water.

The carbide/Ti ratio profiles behaved in a similar manner for all time points. The carbide levels increased rapidly for all the samples, reaching by 3 min the highest value for the 0 min sample this time (0.22). After this increase the carbide started to decrease for all the samples, reaching 0 for the 0 min sample first, and by the end of etching al the carbide levels approached 0. The carbide levels for the immersed samples disappeared more slowly than for the 0 min sample.
In conclusion, immersion of 10% HNO_3 Ca-Ti samples for various periods of time resulted in a decrease in the surface Ca, with little change in the sub-surface Ca. There was very little difference in the surface on immersion in water, the oxidation process having been achieved using the acid, leaving a stable surface.

Figures 4.43 and 4.44 and table 4.23 show the Ca/Ti and the O/Ti ratios for 34% HNO_3 Ca-Ti samples before, and after 2 min, 4 h, and 24 h immersion in ultrapure water.

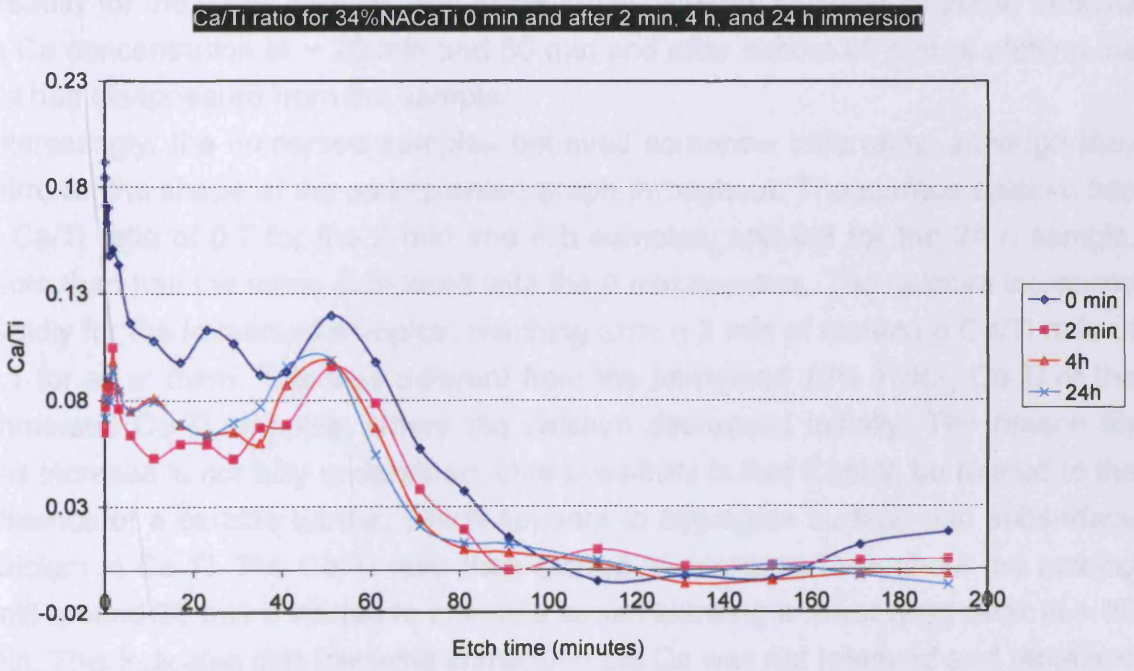

Figure 4. 43 Ca/Ti ratios as a function of etch time for Ca-Ti and 34% HNO_3 treated Ca-Ti discs after 2 min, 4 h, and 24 h immersion in ultrapure water.

Etch time (min)	0 min	2 min	4 h	24 h
0	0.19	0.06	0.07	0.07
2	0.15	0.10	0.10	0.09
29	0.11	0.05	0.06	0.07
35	0.09	0.07	0.06	0.08
51	0.12	0.10	0.10	0.10
61	0.10	0.08	0.07	0.05
131	0.00	0.00	0.01	0.00
191	0.02	0.00	0.00	0.01

Table 4. 23 Ca/Ti ratios as a function of etch time for 34% HNO_3 Ca-Ti before (0 min) and after 2 min, 4 h, and 24 h immersion in ultrapure water.

As can be seen from figure 4.43 and table 4.23, the amount of Ca present on the surface of the 34% HNO_3 0 min sample (C/Ti = 0.19) was greater than that on the 10% HNO_3 0 min sample, and more than twice the values recorded for the immersed 34% HNO_3 Ca-Ti samples. Following etching, the Ca/Ti ratio decreased steadily for the 0 min sample, with some small increase showing localised maxima in Ca concentration at ~ 20 min and 50 min and after almost 92 min of etching the Ca had disappeared from the sample.

Interestingly, the immersed samples behaved somehow differently, although they mirrored the shape of the as implanted graph throughout. The surface calcium had a Ca/Ti ratio of 0.7 for the 2 min and 4 h samples, and 0.8 for the 24 h sample, more than half the value compared with the 0 min samples. The calcium increased rapidly for the immersed samples, reaching after ~ 2 min of etching a Ca/Ti ratio of 0.1 for all of them. This was different from the immersed 10% HNO_3 Ca-Ti or the immersed Ca-Ti samples, where the calcium decreased initially. The reason for this increase is not fully understood. One possibility is that it could be related to the absence of a carbide barrier, which appears to segregate surface and subsurface calcium in Ca-Ti. The Ca/Ti ratio then started to decrease throughout the etching until around 20 min it started to increase again, showing a lower lying peak at ~ 50 min. This indicates that following immersion the Ca was not released and remained spread throughout the oxide layer, similar to in the 0 min samples. By 81 minutes for the 24 h sample and 91 min for the other samples there was no Ca left in the samples. This was similar to the time point where the calcium disappeared from the 0 min sample.

Two minutes immersion of 34% HNO_3 Ca-Ti samples showed a big decrease in Ca both at the surface and beneath it, as shown in table 4.23 Immersion for longer

periods appeared to have little effect on the quantity or distribution of calcium across the surface. This is broadly in agreement with the ion chromatography data which showed significantly more Ca release than the Ca-Ti (2 min, and 4 h) or 10% HNO_3 Ca-Ti (all time points), but no significant difference between release at 2 min, 4 h, 24 h.

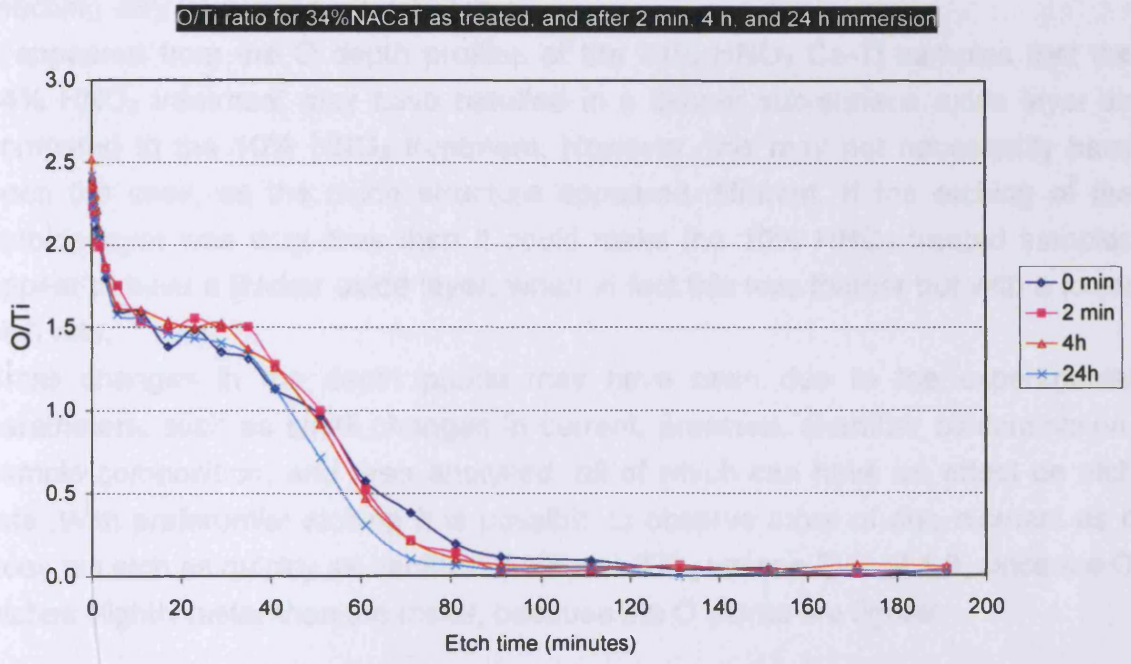

Figure 4. 44 O/Ti ratios as a function of etch time for 34% HNO_3 treated Ca-Ti discs before and after 2 min, 4 h, and 24 h immersion in ultrapure water.

Etch time (min)	0 min	2 min	4h	24h
0	2.33	2.28	2.53	2.42
6	1.60	1.75	1.63	1.58
41	1.13	1.28	1.26	1.13
171	0.00	0.01	0.07	0.03
191	0.04	0.04	0.06	0.03

Table 4.24 O/Ti ratios as a function of etch time for Ca-Ti and 34% HNO_3 treated Ca-Ti discs after 2 min, 4 h, and 24 h immersion in ultrapure water.

Figure 4.44 and table 4.24 show the variations in O /Ti ratios during the etching of the 34% HNO_3 treated Ca-Ti samples following immersion in water. The depth profile for all the samples was described earlier (figure 4.40). The 2 min sample varied similarly in terms of shape of the curve compared with the plot for the 0 min

samples throughout the etching. The ratio on the surface was smaller than for the 0 min samples being 2.28. The 4 h and the 24 h samples had the most O on the surface, with O/Ti values of 2.53 and 2.42 respectively. The shape of the depth distributions were almost indistinguishable in fact all the samples varied similarly regarding the O content, and the O/Ti ratios decreased throughout the etching, reaching very low values after 192 min.
It appeared from the O depth profiles of the 34% HNO_3 Ca-Ti samples that the 34% HNO_3 treatment may have resulted in a thinner sub-surface oxide layer as compared to the 10% HNO_3 treatment. However, this may not necessarily have been the case, as the oxide structure appeared different. If the etching of the carbide layer was very slow then it could make the 10% HNO_3 treated samples appear to have a thicker oxide layer, when in fact this was thinner but with a lower etch rate.
Small changes in the depth profile may have been due to the experimental parameters, such as small changes in current, pressure, chamber contamination, sample composition, and area analysed, all of which can have an effect on etch rate. With preferential etching it is possible to observe more of one element as it does not etch as quickly as another. If we etch TiO_2 we see Ti/O of 1.8, since the O etches slightly faster than the metal, because the O atoms are lighter.

In conclusion the 34% HNO_3 treated Ca-Ti samples contained more Ca than the 10%HNO_3 treated sample, which may subsequently be released over a longer period. The different calcium and oxygen distributions may enable implant designs which could provide ion release appropriate to a particular clinical requirement.

4.4.4 Conclusion

Both types of treatment result in a sort of passivation of the surface, although leaving a different chemistry. Presumably, the nitric acid treatment is healing the non-passive surface oxide resulting from the implantation.
The 10% HNO_3 Ca-Ti samples were observed to undergo a slow colour change, which suggested some modification of the surface. The XPS spectra showed also a reduction in the surface calcium by 50% following treatment, similar to the Ca-Ti sample immersed for 2 min. Immersion of 10% HNO_3 Ca-Ti for 2 min in water resulted in no change in the O/Ti ratio, and no modification in the surface calcium,

although the surface was observed to change colour again. If there is colour change between 0 and 2 min immersion then something may have happened to the oxide layer. However, the surface spectra and the XPS depth profiles did not indicate that the oxide layer had particularly thinned or thickened, so it is possible that there was a different effect occurring. One possibility is H uptake from the solution which could possibly change the refractive index (or some optical property of the surface layer). However, H cannot be detected using XPS but there are some nuclear techniques that could be used to follow its uptake. Another possibility is that the film colour is very sensitive to small changes in the oxide thickness which might be too small for the depth profile to pick up, or there may be changes in the carbon film thickness.
Ion chromatography showed that the 10% nitric acid treated Ca-Ti showed minimal ion release for all the time points. Looking at the XPS depth profile, O and Ca were distributed across a greater depth beneath the surface. This resulted in a thicker oxide, which retained more Ca than the 4 h water treatment.

By contrast, 34% HNO_3 resulted in a gold coloured surface, which was linked to the thickening of the surface oxide layer. The XPS spectra confirmed this by showing a significant reduction in the Ti^{n+} peak ($n<4$) following treatment. Immersion of 34% HNO_3 Ca-Ti samples in ultrapure water for a short period of time (2 min) resulted in a significant decrease in surface calcium. Immersion for 4 h resulted in a further decrease in the surface calcium concentration. 24 h immersion resulted in no further surface calcium decrease or ion release. Depth profiling XPS showed a more rapid loss of Ca (supported by the ion chromatography results) and O than the 10% HNO_3.
There was a clearly different behaviour of the 34% HNO_3 Ca-Ti samples as compared to the immersed Ca-Ti or immersed 10% HNO_3 Ca-Ti samples. The behaviour of 10% HNO_3 Ca-Ti was more uniform and not influenced by the immersion times, as opposed to the 34% HNO_3 treatment. Indeed, nitric acid treatment resulted in a passivated surface, with the least ion release observed for a shorter and less strong treatment (10% 10 min) with regards to concentration.

4.5 SUMMARY

Ca ion release occurred from Ca-Ti at 37°C and can be detected using ion chromatography. The majority of Ca ion release occurred within 4 h. The quantity is sufficient to possibly adversely influence cell behaviour.
The XPS results (both the surface analysis and the depth profiling) confirmed the calcium ion release from the Ca implanted samples, both from the surface and from deeper layers within the Ca-Ti. The surface calcium dropped by more than 50 % after 2 min immersion in ultrapure water, with minimal subsequent changes.
The oxide layer showed an increase in thickness and also changed in composition for the samples immersed for 4 h and over. Concomitant with the increase in the oxide layer, a reduction in the Ca present in the Ca-Ti took place, which correlated with the release of the calcium ions into solution, and the redistribution of Ca throughout the thicker oxide.
After 4 h immersion or more, most of the samples showed colour changes ranging from fully blue to patchy blue, which correlated with the increase in the thickness of the oxide layer. The presence of a large amount of sub-surface oxygen following immersion suggested that the passive nature of the native Ti surface was compromised by the implantation of Ca which enables oxygen diffusion through the surface on exposure to an aqueous environment.

Nitric acid treatment of Ca-Ti resulted in a modification in the surface oxide layer, as shown by the colour change of the samples following treatment. Significant amounts of Ca have been lost from the Ca-Ti samples following nitric acid treatment.
Immersion of the nitric acid treated samples in water resulted in minimal modification in the surface spectra, little ion release and little change in depth profiles. Both nitric acid treatments (10% and 34%) repassivated the Ca-Ti surface.

4.6 LIST OF REFERENCES

Bruesch, P., Muller, K., Atrens, A.,Neff, H. (1985)Corrosion of stainless steels in chloride solution: An XPS investigation of passive films.
Applied Physics A: Materials Science and Processing 38(1): 1-18

Blumenthal, N. C., Cosma, V. (1989)
Inhibition of apatite formation by titanium and vanadium ions.
Journal of Biomedical Materials Research 23: 13–22.

Braceras, I., Alava, J. I., Oñate, J. I., Brizuela, M., Garcia-Luis, A., Garagorri, N., Viviente, J. L., de Maetzu, M. A. (2002)
Improved osseointegration in ion implantation-treated dental implants.
Surface and Coatings Technology 158-159: 28-32

Brunette, D. M., Tengvall, P., Textor, M., Thomsen, P. (2001)
Titanium in medicine.
Springer, Berlin

Buchanan, R. A., Rigney, Jr. E. D., Williams, J.M. (1987)
Ion implantation of surgical Ti-6Al-4V for improved resistance to wear-accelerated corrosion.
Journal of Biomedical Materials Research 21(3): 355-366

Callen, B. W , Lowenberg, B. F., Lugowski, S., Sodhi, R. N., Davies, J. E. (1995)
Nitric acid passivation of Ti6Al4V reduces thickness of surface oxide layer and increases trace elements release.
Journal of Biomedical Materials Research 29(3): 279-90

Evans, E.J. (1994)
Cell damage in vitro following direct contact with fine particles of titanium, titanium alloy and cobalt–chrome–molybdenum alloy.
Biomaterials 15: 713–717

Faria, A. C. L., Belotti, M. M., Rosa, A. L. (2003)
Nitric Acid passivation does not affect *in vitro* biocompatibility of titanium.
International Journal of Oral and Maxillofacial Implants 18: 820-825

French, H.G., Cook, S.D., Haddad, R.J. (1984)
Correlation of tissue reaction to corrosion in osteosynthetic devices.
Journal of Biomedical Materials Research 18: 817–828

Hambleton, J. C., Schwartz, Z., Windeler, S. W. (1994)
Culture surfaces coated with various implant material affect chondrocyte growth and metabolism.

Journal of Orthopaedic Research12 :542-552

Hanawa, T., Asami, K., Asaoka, K. (1996a)
AES Studies on the dissolution of surface oxide from calcium-ion-implanted titanium in nitric acid and buffer solutions.
Corrosion Science 38(11): 2061-2067

Hanawa, T., Asami, K., Asaoka, K. (1996b)
Microdissolution of calcium ions from calcium-ion-implanted titanium.
Corrosion Science 38(9): 1579-1594

Hanawa, T., Hiromoto, S., Asami, K. (2001)
Characterization of the surface oxide film of a Co–Cr–Mo alloy after being located in quasi-biological environments using XPS.
Applied Surface Science 183(1-2): 68-75

Hanawa, T., H. Ukai, K. Murakami, and K. Asaoka, (1995)
Structure of surface-modified layers of calcium-ion-implanted Ti6Al4V and Ti56Ni.
Materials Transactions Jim, 36(3): 438-444.

Hanawa, T. (2004)
Metal ion release from metal implants
Materials Science and Engineering: C: 24 (6-8): 745-749

Kilpadi, D. V., Raiker, L, N., Liu, J., Lemons, J. E., Vohra, Y., Gregory, J. C., (1998a)
Effect of surface treatment on unalloyed titanium implants: spectroscopic analyses
Journal of Biomedical Material Research 40: 646-659

Kilpadi, D. V., Weimer, J. J, Lemons, J. E. (1998b)
Effect of passivation and dry-heat sterilisation on surface energy and topography of unalloyed titanium implants.
Colloids and Surfaces 135: 89-901

Kilpadi, D.V., Weimer, J. J, Lemons (2000)
Cleaning and heat treatment on unalloyed titanium implant surfaces.
International J Oral and Maxillofacial Implants 15: 219-230

Krupa, D., Baszkiewicz, J., Kozubowski, J., Barcz, A., Sobczak, J., Bilinski, A., Rajchel, B. (2001)
The influence of calcium and/or phosphorus ion implantation on the structure and corrosion resistance of titanium.
Vacuum 63:715-719

Ku, C. H., Pioletti, D. P., Browne, M., Gregson, P. J. (2002)
Efect of different Ti6Al4V surface treatments on osteoblast behaviour.

Biomaterials 23: 1447-1454

Lausmaa, J., Kasemo, B., Hansson, S. (1985)
Accelerated oxide growth on titanium implants during autoclaving caused by fluorine contamination.
Biomaterials 6: 23-27

Lausmaa, J., Mattsson, H., Rolander, U., Kasemo, B., (1986)
Chemical composition and morphology of titanium surface oxides.
Biomedical Materials, Materials Research Society Symposium Proceedings 85: 351-359

Lausmaa, J., Kasemo, B., Mattsson, H. (1990)
Surface spectroscopic characterizations of titanium implant materials.
Applied Surface Sciences 44:133-146

Lausmaa, J. (1996)
Surface spectroscopic characterization of titanium implant materials.
Journal of Electron Spectroscopy and Related Phenomena 81: 343-361

Lee, T. M., Chang, E. (1998)
Surface characteristics of Ti6Al4V alloy: effect of materials, passivation and autoclaving.
Journal of Materials Science: Materials in Medicine 9: 439-448

Pan, J., Thierry, D., Leygraf, C. (1995)
Hydrogen peroxide toward enhanced oxide growth on titanium in PBS solution: blue coloration and clinical relevance.
Journal of Biomedical Material Research 30 (3) :393-402

Sasada, T., Morita, M., Mabuchi, K. (1995)Evaluation of wear toxicity for implant materials through cell culture method.
Proceedings of International Tribology Conference Yokohama: 1957-1962

Sittig, C., Textor. M., Spencer, N. D. (1999)
Surface characterizations of implant materials cp Ti, T-6Al-7Nb and Ti-6Al-4V with different pretreatments.
Journal of Material Science: Materials in Medicine 10: 35-46

Storp, S., Holm, R. (1977)
ESCA investigation of the oxide layers on some Cr containing alloys.
Surface Science 68:10-19

Shinawi, L. A. (2003)
Ion implantation as a route to enhancing osseointegration on modified titanium surfaces.
PhD thesis, UCL

5. AMINO ACID ADSORPTION ONTO TITANIUM AND MODIFIED TITANIUM SURFACES

5. 1. INTRODUCTION

The biocompatibility of Ti is largely determined by its surface properties, which have a direct effect on the cellular response to the material. When a dental material is implanted in the body, its surface is almost immediately covered with blood and its component serum proteins. The interactions of proteins with the Ti surface are very important because they can regulate cell adhesion and subsequent tissue attachment to the Ti surface, which can lead to an increased rate of normal tissue regeneration. It is believed that a layer of adsorbed protein exists on the surface of all implanted materials, and that the presence of this adsorbed protein layer is important in mediating cellular responses to the implant (Horbett et al., 1982). The adhesion of proteins and other biological macromolecules such as attachment molecules and growth factors is important in the regeneration of tissue or bone (Puleo et al., 1999). Biomolecules can also determine and modify the chemical and physical properties of hard tissue, for example by stabilising the mineral content (Robinson et al., 1992). On the other hand, it may be detrimental for proteins to be adsorbed onto a surface; for example the adsorption of blood proteins onto an implant could cause the formation of a thrombus (Ratner 1993). Proteins may also play a role in bacterial adhesion and the formation of biofilms built up from harmful micro-organisms (Charaklis et al., 1990). It is therefore highly desirable to be able to formulate a surface such that favourable proteins or other organic species remain stable, whilst unwanted biomolecules rapidly desorb.

The interaction of proteins with non biological surfaces plays an important role in the acceptance or rejection of implants in the living tissues. A variety of studies, *in vivo* as well as *in vitro* has been carried out to observe the condition under which proteins adsorb from solution onto non biological surfaces. In

general terms, in aqueous solution, it is likely that on hydrophilic surfaces, such as that of titanium (Lausmaa et al., 1990), molecules will tend to bind with the hydrophilic end towards the surface (Kasemo et al., 1999). The attractions between molecules in solution and a surface may include electrostatic and van der Waals' forces. Additionally, a major driving force for macromolecules adsorption at a surface in aqueous solution is thought to be entropic, resulting from changes in conformation and water release from both protein and the surface (Norde et al., 1979).

Since proteins are highly complex macromolecules, it can be technically extremely demanding to analyse their adsorption on surfaces in terms of orientation, binding sites etc. Several investigators have therefore studied the adsorption of amino acids, the building blocks that make up proteins. This allows more fundamental interactions with the surface to be analysed.
Amino acids are used for biomaterial studies because of their relatively simple structure, in comparison with proteins, and since they are the building blocks in the latter, amino acids can be used as model systems for studying some aspects of protein-surface interaction. Amino acid adsorption at surfaces is also of relevance for a number of applications including solid-phase peptide synthesis, the development of organic mass spectrometry, and promotion of cell adhesion by immobilized peptides. The latter has practical importance, e.g. in the areas of biomaterials, medical implants and biomedical sensors.

Adsorption of various amino acids has been studied on a variety of surfaces, including Cu, Au, Pt, and Ti. As adsorption onto Ti is more relevant for this study, a more detailed representation of experiments found in the literature will be described below.
Adsorption of homocysteine from solution onto titanium surfaces was studied by Schmidt in 1991 using XPS. It was concluded, on the basis of binding energies, that ligand exchange occurred between basic OH groups on the hydroxylated Ti cations and the deprotonated, singly bound O of the homocysteine carboxyl group. However, no spectra were shown and no indication was given as to the nature of the surface prior to adsorption.

Schmidt (2001) studied adsorption of amino acids from aqueous solution onto oxidised titanium surfaces as a function of pH using X-ray photoelectron spectroscopy (XPS). The selected model substances, amino acids, were adsorbed from aqueous saline solutions with various pH (range 2 - 11) values onto evaporated titanium layers. The following amino acids were used: alanine, β-alanine, aspartic acid, cysteine, glutamic acid, glycine, homocysteine, lysine, methonine, praline, serine, and tryptophane. The evidence of adsorbates was determined by XPS. The results showed that methionine, alanine, and β-alanine did not adsorb in detectable quantities in the studied pH region. For the other amino acids, no adsorption at basic pH was detected (only adsorption of Na ions from the saline solution) under the given experimental conditions. In acidic aqueous solutions, amino acids tended to adsorb onto TiO_2 surfaces via their carboxyl groups replacing a basic hydroxyl on a Ti site. The titanium surface preferentially formed a surface complex with the carboxyl groups of the amino acids in an acidic solution. The resulting positions of the adsorbed molecules were investigated through evaluation of the line intensities. The results showed clearly that there was a chemical bonding between the titanium surface and the organic substances. The authors also said that it remained unclear why some amino acids are more strongly adsorbed, while others are not at all or so weakly bound that they desorb again during rinsing. Because of their chemical similarity, such a difference in adsorption behaviour was not expected. This makes it difficult to predict reactions on the surface of Ti in living organisms.
Assuming that a comparable situation occurs *in vivo*, such processes, or similar ones, can be viewed as preliminary stages in osseointegration (Schmidt 2001).
Lausmaa et al. (1999) considered the adsorption and co-adsorption of water and glycine (the simplest amino acid), on thermally oxidised titanium foil using thermal desorption spectroscopy (TDS). The study showed that the amount of hydroxylation of oxidised titanium surfaces could be increased by treatment in vacuum or other treatments that increased the density of surface defects. TDS is a powerful method for characterizing biomaterial surfaces with regard to their interaction with biologically relevant molecules. The titanium foil used, on the basis of AES and XPS data, was assigned as having a composition

approximating to TiO_2, although it was pointed out that the surface contained grain boundaries, multicrystallites of different orientation, mono- and multiatomic steps, oxygen vacancies, dislocations and various other structural defects. Glycine mono- and multi layers did not resorb at room temperature, and were not affected by water vapour. Water adsorption was primarily molecular at 120 K, although pre-annealing the surface in vacuum was found to result in an increase in hydroxylation. Desorbed glycine molecules were observed, both intact (multilayers and ~40% of the first monolayer) and dissociated. Decomposition as well as desorption was observed on heating. The co-adsorption of water did not affect the glycine desorption spectra. Glycine on the other hand was found to displace water, resulting in a more hydrophobic surface. The C-C bond was found to break and carboxyl fragments desorbed, leaving behind the methylamine group bonded to the surface via the original α-carbon of the glycine molecule. This was inconsistent with the finding of Schmidt (2001) that glycine bound to the surface via the COOH group.

Ojamae et al. (2006) studied the adsorption of various organic species onto TiO_2. Nanocrystalline TiO_2 powders of the rutile polymorph, synthesized by a sol–gel method, were treated with water solutions containing formic, acetic, and citric acids together with glycine in order to study the adsorption properties of these organic species. The samples were characterized by FTIR, Raman, powder XRD, and TEM. The authors found that formic, acetic, and citric acids were adsorbed onto the rutile surface but glycine was not, as evidenced by the Raman spectrum.

Various surface modifications have been carried out on titanium, in order to improve the adsorption of amino acids. Full details of these surface modifications were given in Chapter 1. However, they included, among others, alkali and acid treatments and ion implantation with various ions.

Gold et al. (1989) studied amino acid adsorption at titanium surfaces using XPS. Cysteine was adsorbed for 6 - 12 hours from a 0.37 M solution in 1M NaCl (pH 0.5 - 12.8) onto Ti plates, which were chemically etched, mechanically polished, rinsed and ultrasonically cleaned in bi-distilled water. It was concluded that adsorption and bonding of amino acid to the Ti surface

was a strong function of pH. Extreme low and high pHs prevented cysteine adsorption.

It has been shown that HA coated surfaces bind more proteins than pure titanium (Gottlander et al., 1992, Biesbrock et al., 1995). Therefore, the question has been posed as to whether it is possible to create a surface that will behave like HA in terms of protein adsorption, but without establishing a coating. If this could be achieved, then the disadvantages of coatings (fragility, risk of fracture) could be eliminated.

Studies of titanium surfaces modified by ion implantation (calcium, potassium and argon) showed enhanced cell spreading on the calcium-implanted surfaces compared with argon-implanted surfaces, and non-implanted surfaces (Nayab et al., 2003, 2006, 2007, in press). This indicated that ion implantation may be used to alter the surface chemistry of titanium in order to fabricate implant surfaces, which may integrate more rapidly *in vivo*.

The surface chemistry of titanium may be modified by processes such as ion implantation in order to fabricate an implant surface which will integrate more rapidly. It is likely that differences in cell attachment, spreading and proliferation will be influenced by the presence and configuration of proteins and other macromolecules on the modified titanium surfaces.

In order to try to improve the understanding of the biological response to titanium surfaces modified by simple techniques such as alkali treatment, or technically demanding techniques such as ion implantation, the adsorption of simple biological molecules onto modified titanium surfaces requires further study.

The adsorption of amino acids onto Ca-implanted titanium has not been studied to date. Although the literature does not mention amino acid adsorption on Ca-Ti, Lori et al., (2004) investigated the role of electrostatic interactions in the adsorption of mucin (a salivary protein) to titanium and Ti modified with Ca (not Ca-ion implanted) *in vitro*. The binding profile of mucin to titanium was analyzed according to an adsorption isotherm. Mucin was dissolved and the solution suspended with native, calcium, magnesium, or potassium treated commercially pure Ti powder, at pH 3.0 and 7.4. The

amount of unabsorbed protein in the supernatant fluid was measured. The maximum amount of adsorbed mucin was 0.11 mg / 1.0 g of Ti. The mucin-Ti association constant was estimated to be 2.91 ml / mg. The authors concluded that pretreatment of Ti with calcium, or magnesium alone, or combined, resulted in increased adsorption of mucin to Ti. No increase in adsorption was recorded following pretreatment of Ti with potassium.

A series of experiments, therefore, was required to assess how amino acids interact with titanium surfaces modified by alkali treatments and Ca ion implantation. Such interactions may be studied using X-ray photoelectron spectroscopy (XPS). This method is considered one of the most powerful tools available for analysing the extreme surface of a material.

In this part of the research the aim was to assess the effects of several chemical surface modifications on the adsorption of specific amino acids from aqueous solution. A variety of amino acids were used in experiments to date (glycine, cysteine, and lysine). However, adsorption has been found to depend strongly on experimental protocol. Systematic studies have therefore been carried out using mainly glycine (the simplest amino acid) and to a lesser extent cysteine. Glycine is the smallest amino acid. Besides being the building blocks of peptides and proteins, amino acids are interesting in biomaterial research as substances for modifying surfaces to enhance cell adhesion via immobilisation of specific amino acid sequences. Therefore, studies of amino acid surfaces have the potential for simultaneously providing a basic understanding of biomolecule-surface interactions and information useful for the preparation of biomaterial surfaces.

5. 2. ADSORPTION STUDIES

Before presenting the results for the experiments, it is necessary to show the reference spectra first in order to assess if adsorption has occurred. The glycine and cysteine powder spectra will be presented below first. The spectra were recorded by Dr. Frances Jones, were presented as part of an M.Sc.

project (Mihoc 2002) and are shown here for reference. They were recorded with the electron flood gun on to compensate for charging (details in Chapter 2).

Reference spectra - glycine powder

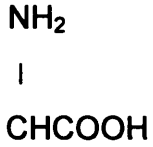

Adsorption of glycine (α-amino acetic acid, NH_2CH_2COOH), the simplest amino acid, onto various surfaces has been studied. Glycine has several functional groups. In the bulk glycine exists as the zwitterion $NH_3^+CH_2COO^-$. In solution, the molecules change from cationic through zwitterionic to anionic as the pH increases (Jones 2001).

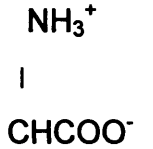

The C 1s, N 1s and O 1s spectra for the glycine powder are presented in figure 5.1. The atomic percentages and elemental ratios for the glycine powder are presented in table 5.1.

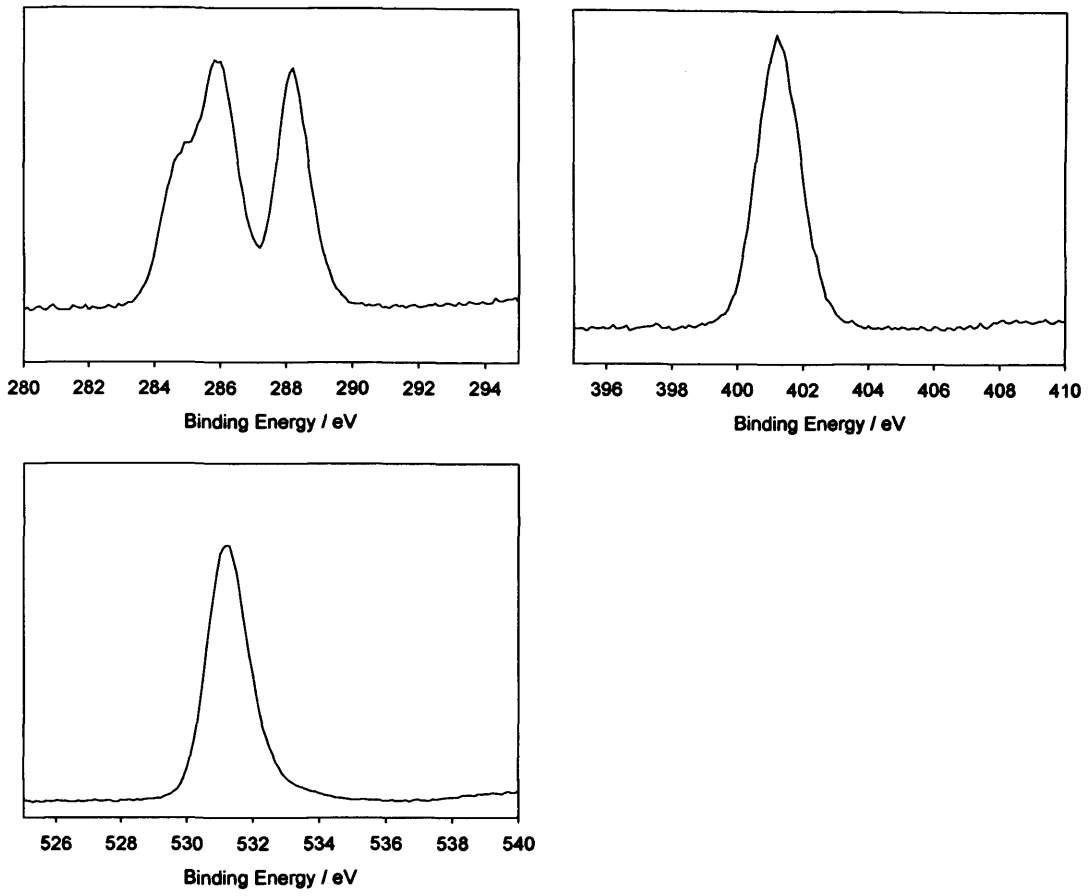

Figure 5. 1 The C 1s, N 1s, and O 1s spectra for the glycine powder.

Sample	C (atomic %)	O (atomic %)	N (atomic %)	O/C	N/C	O/N
Glycine powder	46.32	36.83	16.83	0.79	0.36	2.18

Table 5. 1 Atomic percentages and elemental ratios recorded for the glycine powder.

The spectra were characteristic of glycine (Schmidt 2001). The C 1s spectrum (first row, left panel) appears to show two photoemission peaks (285.9 eV, 288.2 eV) of similar intensity. However, the lower binding energy peak was asymmetric, suggesting that it was actually two peaks. Therefore, the C 1s spectrum can be resolved in three peaks. Glycine has no hydrocarbon-like carbon in its structure. The low binding energy peak was due to contamination. The middle binding energy carbon peak at 285.9 eV was due to carbon linked

to NH_2 / NH_3^+. The highest E_B peak was due to the C in the carboxylate group (COOH / COO^-), which is bound to two electronegative oxygen atoms.

The N 1s spectrum (first row right panel) displayed a single narrow peak at 401.2 eV, which corresponds to NH_3^+, as glycine in bulk exists as zwitterions. A peak at 400 eV may also be present on adsorbed glycine due to NH_2. Schmidt et al., (2001) stated that both peaks come from the amino group: one is neutral and one is protonated. The authors suggested that for quantitative considerations, only the total signal N = N1+N2 is meaningful. Clarks et al. (1997) also attributed the peak recorded in bulk for amino acids at 401.2 eV to NH_3^+.

The O 1s spectrum had a single peak at ~ 531 eV due to O from the COOH group (Schmidt et al., 2001).

The N/C, O/C, and O/N ratios presented in table 5.1 are 0.36, 0.79 and 2.18 respectively. It may be deduced from the glycine formula that the actual ratios should be N/C=0.5, O/C=1 and O/N =2. As the recorded ratios were smaller, this suggested that there was more C, and from the O/N ratio also more O on the surface, the most possible cause being contamination, in agreement to the large hydrocarbon peak.

Cysteine powder

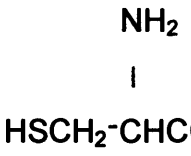

Glycine exists in bulk as a zwitterion $NH_3^+CH_2COO^-$. It is likely that cysteine exists in the bulk as zwitterions as well. Dodero et al. (2000) reported that cysteine exists in aqueous solution as zwitterions.

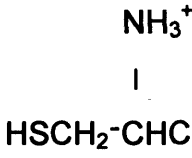

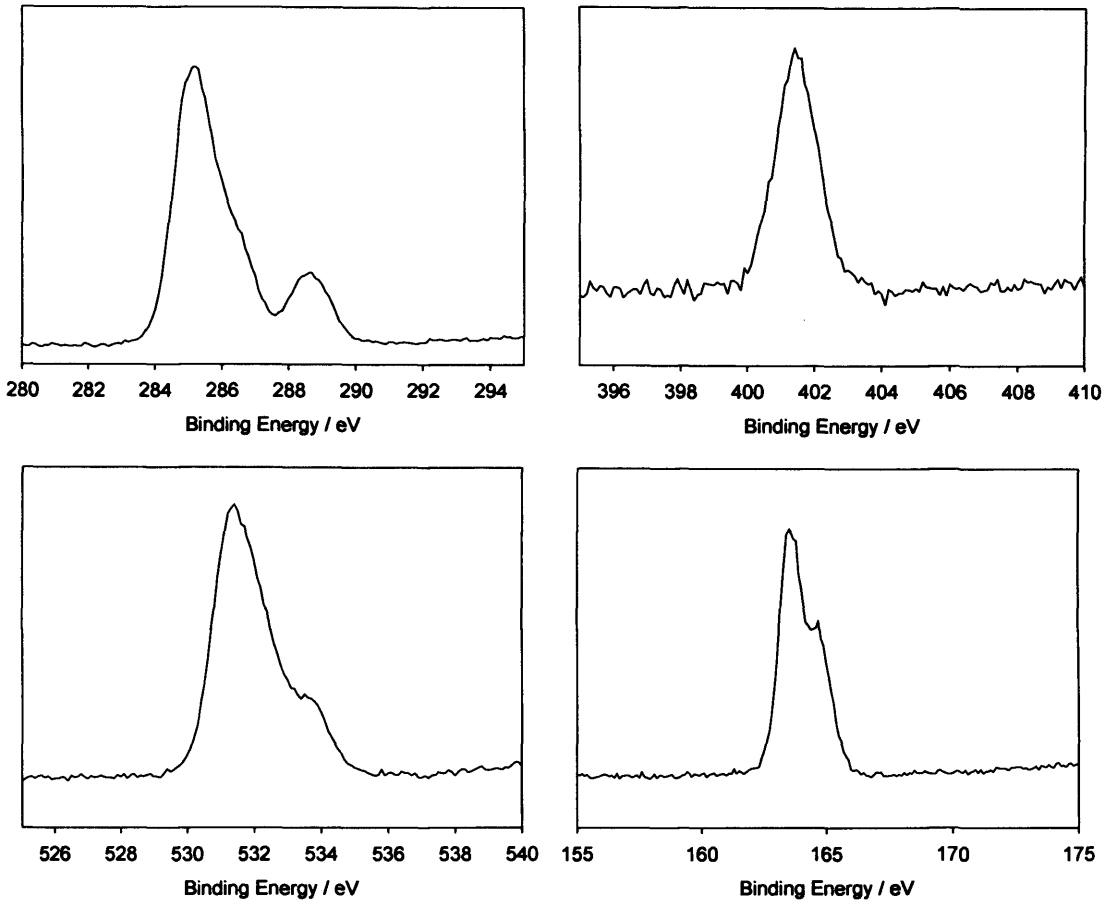

Figure 5. 2 Spectra for Cysteine powder: the C 1s spectrum (first row left), the N 1s spectrum (first row right), the O 1s spectrum (second row left), and the S 2p spectrum (second row right).

Sample	C (at %)	O (at %)	N (at %)	S (at %)	O/C	N/C	S/C
Cysteine powder	64.18	22.40	7.89	5.48	0.34	0.12	0.08

Table 5. 2 Atomic percentages and elemental ratios for the cysteine powder.

The spectra showed the characteristic peak shape for cysteine (Schmidt, 2001). The C 1s spectrum (figure 5.2) appears to shows two peaks, with decreasing intensity, with measured binding energies of 285.2 eV and 288.6 eV respectively, similar to the COOH and CNH_2 in glycine. The lower binding energy peak was asymmetric, suggesting that it is actually two peaks. The spectrum for C 1s actually presented three peaks (figure 5.2 first row, left). The lower binding energy peak at ~ 285.2 eV (C1) was due to carbon bound to

sulphur (Cavalleri et al., 2001). The highest binding energy peak at 288.6 eV is the carbon in the carboxylic acid group (Cavalleri et al., 2001). This it is at the highest binding energy value because it is linked with two electronegative oxygen atoms. These pull electron density away from the carbon atom, so the carbon atom is more positively charged. Hence, the electrons in C 1s orbital are bound more tightly and appear at higher binding energy. The middle carbon peak (C2) which is not visible as such, appeared similar to a shoulder on the first peak, was at ~ 286.5 eV and was due to carbon atoms bound to nitrogen atoms (Cavalleri et al., 2001), which are less electronegative than oxygen.

The N 1s spectrum resulted in a single broad peak (401.4 eV), which corresponds to nitrogen in the NH_3^+ group, at a binding energy similar to that observed for glycine. Again NH_2 might also be expected in adsorbed species at ~ 400 eV.

The S 2p spectrum confirmed that this amino acid contains sulphur, showing the characteristic S 2p spin-orbit splitting, due to S in the SH group (Quingwen et al., 2000). Sulphur is present in cysteine but not in glycine.

The O 1s spectrum presented a peak at ~ 531.5 eV with a shoulder at 533.5 eV. The main peak was caused by O linked with C (COOH), and the second is likely to be the result of some adsorbed water.

The elemental ratios calculated from the formula for cysteine are: O/C= 0.66, N/C=0.33, and S/C=0.33. However, the elemental ratios measured from the cysteine powder reference spectra (table 5.2) are probably much lower than expected due to hydrocarbon contamination in a similar manner to the contamination of glycine.

5. 2. 1. Glycine adsorption onto cp Ti discs (23°C).

5.2.1.1 Aims and objectives

The experiment was carried out to observe whether glycine adsorbs from solution onto the surface of commercially pure titanium discs polished in-house.

5.2.1.2 Materials and method

Six commercially pure titanium discs (cp Ti) polished in house using polishing method 1 (protocol described in section 2) were used in this experiment.
Fresh 0.37 M glycine solution was prepared using 0.69 g glycine powder (Sigma G, 7403 Sigma Ultra>99% titration -lot 51K 2506, Sigma Aldrich Chemie, Gmbh, Germany) in 25 ml deionised water (DW). As adsorption behaviour is highly pH dependant, the pH of the glycine solution was measured and was 6.15.
Each titanium disc was immersed in 5 ml of freshly prepared glycine solution, at room temperature (23°C) for 18 h. After immersion, the discs were removed from the glycine solution using plastic tweezers, rinsed with 50 ml deionised water (DW), and dried with compressed air. The discs were then stored in well plates until required for analysis with XPS.

The XPS analysis was carried out on the samples as follows:

1. XPS on the cp Ti discs (presented as 'cp Ti' spectra).

2. Due to the presence of high nitrogen and carbon contamination, the cp Ti discs were ultrasonically cleaned in acetone for 5 minutes and distilled water for 5 minutes. XPS was performed again on the same cp Ti discs (presented as 'cp Ti clean' spectra).

3. XPS on the titanium discs following immersion in glycine solution (presented as 'Ti-Gly' spectra).

5.2.1.3 Results and discussion

Table 5.3 lists the elemental ratios measured for the cp Ti samples from the XPS spectra. Figure 5.3 presents the N 1s, Ti 2p, O 1s and C 1s spectra for a cp Ti sample before and after ultrasonic cleaning, and after glycine adsorption.

Sample	C/Ti	N/Ti	O/Ti
cp Ti	2.14 ± 0.29	0.29 ± 0.06	3.15 ± 0.20
cp Ti clean	1.17 ± 023	0.18 ± 0.06	2.55 ± 0.07
Ti-Glycine (Ti-Gly)	0.98 ± 0.01	0.14 ± 0.01	2.44 ± 0.16

Table 5. 3 Elemental ratios (average and SD) for cp Ti samples before and after ultrasonic cleaning, and after immersion in glycine solution.

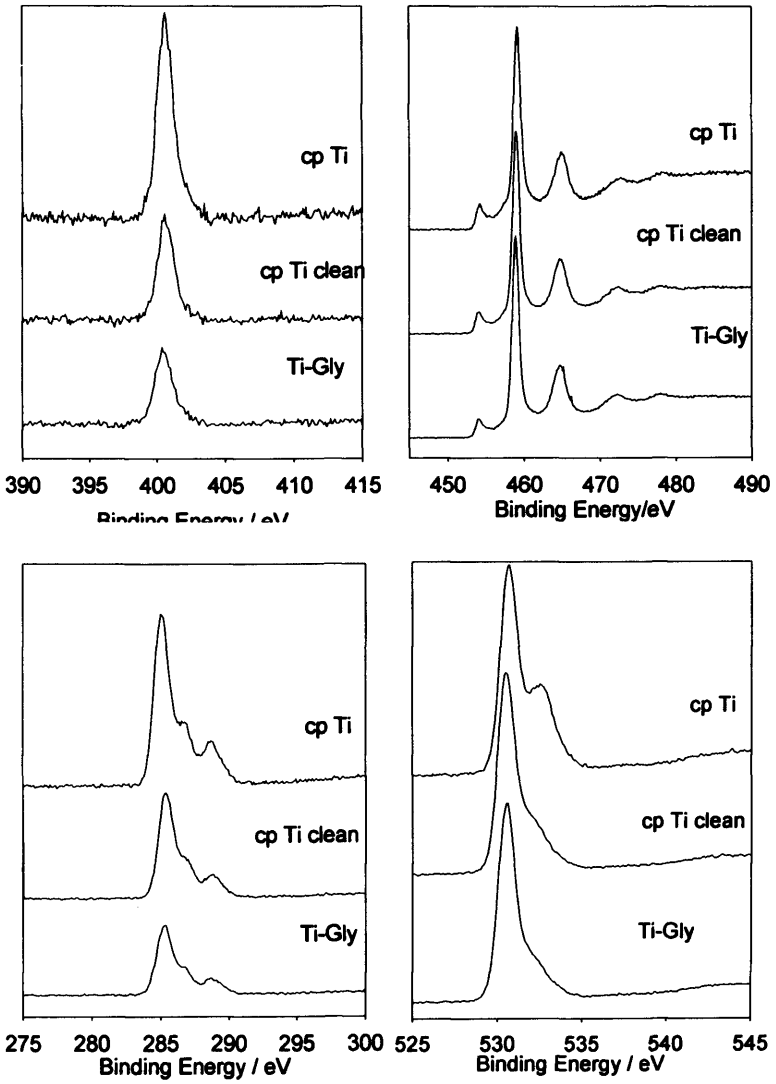

Figure 5. 3 The N 1s spectrum (first row left), the Ti 2p spectrum (first row right,) the C 1s spectrum (second row left) and the O 1s spectra (second row right) from cp Ti before, after ultrasonic cleaning, and after immersion in the glycine solution.

The quantification table (table 5.3) revealed that the as polished Ti surface shows high levels of contamination, indicated by elevated C/Ti, N/Ti and O/Ti ratios. Cleaning reduced these values, indicated by the significant decrease in the C/Ti and N/Ti ratios ($p < 0.05$). However, there was still considerable nitrogen remaining on the surface. Following glycine adsorption the C/Ti, N/Ti and O/Ti ratios showed little alteration and in some cases fall slightly. Glycine adsorption on a clean surface would be expected to be seen as an increase in C and N. O would not be expected to increase significantly since glycine contains a lower proportion of O compared to the TiO_2 surface.

Examination of the detailed spectra also did not conclusively support glycine adsorption. The expected peaks in C 1s spectrum were at 286 eV (C-N) and 288 eV (COOH), while peaks are observed at both of these energies they are not increased in relation to those on the cleaned surface. There is a very large peak at ~ 400 eV which would swamp any contribution from an amino acid adsorbate. There is no increase in the 531 eV peak corresponding to COOH.

Absence of glycine adsorption is in agreement with the literature. Schmidt et al. (2001) reported no adsorption of glycine onto titanium discs, as detailed in section 5.1. This was also in agreement with theoretical simulations of amino acids at the rutile surface in aqueous solution, where the interaction between the adsorbate and the surface was found to be severely weakened by the presence of water (Langal et.al.2003,) and with the results of experimental amino acid adsorption (Langal et al.,2003, Roddick et al., 1998).

5. 2. 2 Glycine adsorption onto NaOH treated cp Ti (23°C).

5.2.2.1 Aims and objectives

As glycine could not be detected on the cp Ti surface, it was decided to modify the titanium surface using NaOH, which has been shown to improve protein adsorption. This study aimed to show whether cp Ti modified with NaOH would influence glycine adsorption at room temperature (23°C).

5.2.2.2 Materials and methods

Six cp Ti samples were treated with 1 M NaOH solution (NaOH solution, 1 mol/l, prod.18026it-LOT 81049941, BDH Laboratory Supplies, Poole, England) for 60 minutes. The discs were dipped in water but not thoroughly rinsed after the treatment, dried with compressed air and placed in the well plates until analysed with XPS. After XPS analysis the discs were immersed in a 5 ml freshly prepared 0.37 M glycine solution at room temperature (23°C), for 18 hours. The glycine solution was prepared fresh before immersion. After immersion all the samples were removed from the well plates using plastic tweezers, rinsed with approximately 30 ml DW, dried with compressed air and stored in fresh well plates until required for analysis.

XPS was carried out on the samples before any treatment (spectra presented as 'cp Ti'), after NaOH treatment (spectra presented as 'Ti-NaOH'), and after immersion in glycine solution (spectra presented as 'Ti-NaOH-Gly').

5.2.2.3 Results and discussion

Table 5.4 presents the elemental ratios for the cp Ti samples before treatment, after NaOH treatment and after immersion in a glycine solution. Figures 5.4 and 5.5 show the N 1s, Ti 2p and Na 1s spectra for a NaOH treated cp Ti

sample immersed in glycine solution. The Na 1s spectrum is presented to show the effect of NaOH treatment on the sample. Each graph contains spectra before treatment (cp Ti), after NaOH treatment (Ti-NaOH), and after immersion in glycine solution (Ti-NaOH-Gly).

Sample	C/Ti	N/Ti	Na/Ti	O/Ti
Cp Ti	0.94 ± 0.08	0.06 ± 0.01	0.06 ± 0.03	2.52 ± 0.11
Ti-NaOH	2.92 ± 0.85	0.02 ± 0.01	4.25 ± 1.75	3.25 ± 0.20
Ti-NaOH-Gly	1.49 ± 1.53	0.07 ± 0.11	0.13 ± 0.24	2.57 ± 0.63

Table 5. 4 Elemental ratios for cp Ti, cp Ti after NaOH treatment and after glycine adsorption.

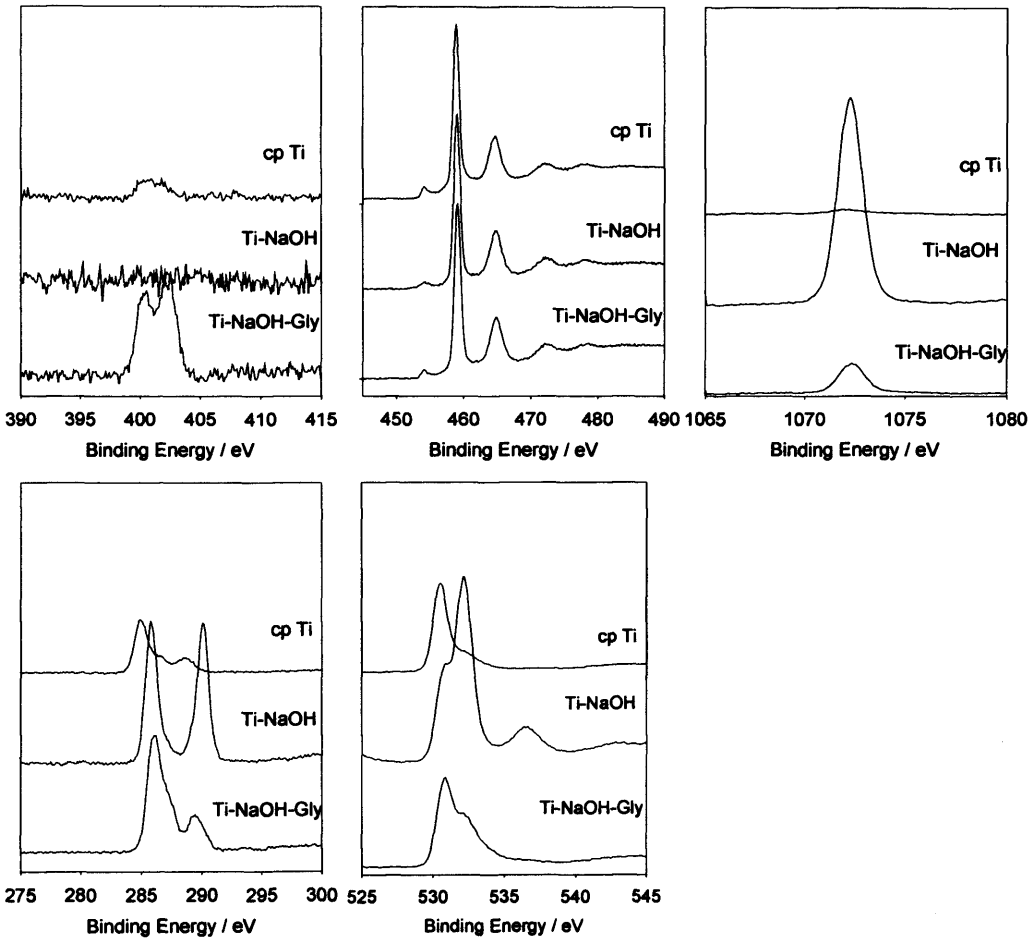

Figure 5.4 First row presents the N 1s (left), Ti 2p (middle), and Na 1s (right) spectra for a cp Ti sample treated with 1 M NaOH and then immersed in glycine (no rinsing). The C 1s (left) and O 1s spectra (right) are presented on the second row for the same samples.

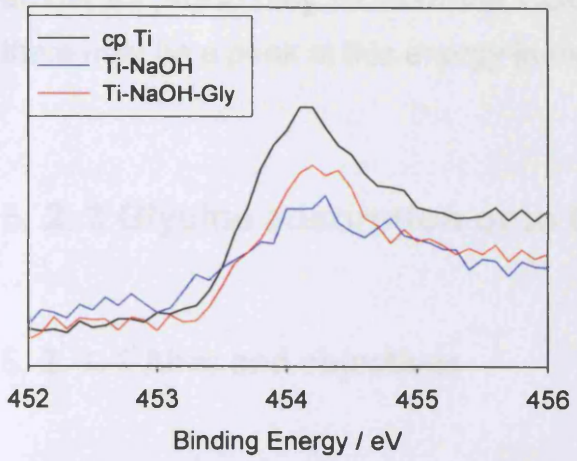

Figure 5.5 The Ti metal peak (Ti^0) for cp Ti before, after NaOH treatment, and after immersion in glycine.

The quantification showed that the NaOH treatment resulted in very low levels of nitrogen on the surface. This was at the expense of a large increase in Na, C and O, made evident by the significant increase ($p < 0.05$) in the Na/Ti, C/Ti and O/Ti ratios. Examination of the detailed C 1s spectrum (figure 5.4) for this sample revealed that there was a very strong peak at 290 eV which was consistent with carbonate. This was also supported by the increased peak at 533 eV in the O 1s spectrum. These data suggested that the surface was covered with a thin layer of Na_2CO_3. This was also supported by the attenuation of the Ti metal peak at 454 eV. This was attenuated as the substrate was further from the surface as a result of the carbonate layer.

Following immersion with glycine the Na, O and C levels were greatly reduced. This indicated that the Na_2CO_3 layer was removed from the surface. Although there appeared to be an increased level of nitrogen, this was not statistically significant. Indeed all ratios following glycine adsorption were hampered by high standard deviations. This was primarily the result of high levels of organic contamination on some samples. The N 1s spectrum for this sample (figure 5.4) showed clear nitrogen peaks at 400 eV and ~ 402 eV; this strongly suggested that NH_2 and NH_3^+ were present on this surface. This suggested that glycine had adsorbed, and may have partly altered the zwitterionic structure as the adsorption has occurred. It was also possible that the peak at 400 eV was the result of contamination. The carbon spectrum revealed a peak

at 289 eV which may be from the COOH in glycine; however it appears that there may be a peak at this energy in the Ti-NaOH spectrum.

5. 2. 3 Glycine adsorption onto Ca-Ti (23° C)

5. 2. 3. 1 Aims and objectives

The aim of this study was to assess the effect of Ca ion implantation on the adsorption of glycine from solution onto Ti surfaces at room temperature (23°C).

5. 2. 3. 2 Materials and method

Three Ca implanted titanium discs implanted (using the first method of mounting, see Chapter 2 for details) were immersed in freshly prepared 0.37 M glycine solution for 18 h at room temperature (23°C), using the method described in section 5.2.1.

After immersion, the discs were thoroughly washed with 50 ml deionised water (5 x 10 ml) using a pipette, and then dried with compressed air. The discs were then stored in cell-culture well plates and put in the desiccator until required for analysis.

The following XPS analyses were carried out:

1. XPS on the Ca-Ti discs - presented as 'Ca Ti' spectra.

2. Repeat of the XPS- after ultrasonic cleaning in ultrapure water of the samples-presented as 'Ca-Ti clean'.

3. XPS on the immersed titanium discs - presented as 'Ca Ti-Gly' spectra.

5. 2. 3. 3 Results and discussion

The Ca-Ti samples did not change with regards to the appearance following ultrasonic cleaning. Following immersion in glycine the Ca-Ti discs had a modified colour, as seen also in the experiments described in Chapter 4. However, the colour change in this experiment was not uniform over the whole surface, and the Ca-Ti samples presented blue zones alternating with silver ones. This was consistent with Shinawi's results (2003) who reported a patchy appearance, with blue zones alternating with silver zones on Ca-Ti samples immersed for 24 h in water at room temperature. A detailed explanation of the possible causes of the colour change was given in chapter 4. As a result of this variation in colour, spectra were recorded over both silver and blue zones for each sample for comparison.

Table 5.5 shows the C/Ti, Ca/Ti, N/Ti, and O/Ti ratios (average and SD) from Ca-Ti samples on blue and silver zones before and after ultrasonic cleaning, and after immersion in glycine solution. Figure 5.6 presents the Ti 2p, N 1s, C 1s, O 1s, and Ca2p spectra for Ca-Ti before (Ca-Ti) and after ultrasonic cleaning (Ca-Ti clean), and after immersion in glycine at room temperature on silver ('Ca-Ti-Gly silver'-left column) and blue ('Ca-Ti-Gly blue'-right column) zones.

Sample	C/Ti	Ca/Ti	N/Ti	O/Ti
Ca-Ti	2.57 ± 0.65	0.22 ± 0.03	0.13 ± 0.06	3.99 ± 0.83
Ca-Ti clean	2.23 ± 1.75	0.16 ± 0.02	0.05 ± 0.00	2.92 ± 0.12
Ca-Ti-Gly blue	1.32 ± 0.23	0.12 ± 0.03	0.11 ± 0.03	3.03 ± 0.42
Ca-Ti-Gly silver	0.79 ± 0.08	0.14 ± 0.00	0.04 ± 0.01	2.44 ± 0.01

Table 5. 5 Elemental ratios (average and SD) for Ca-Ti before and after ultrasonic cleaning and after immersion in glycine solution (blue and silver zones).

Silver zone **Blue zone**

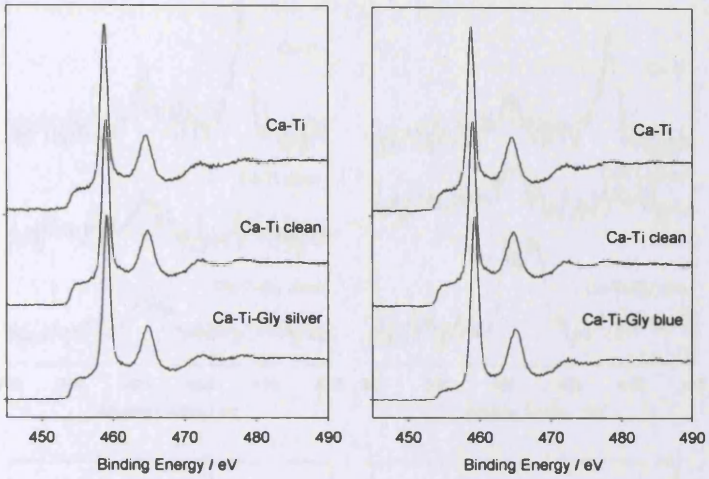

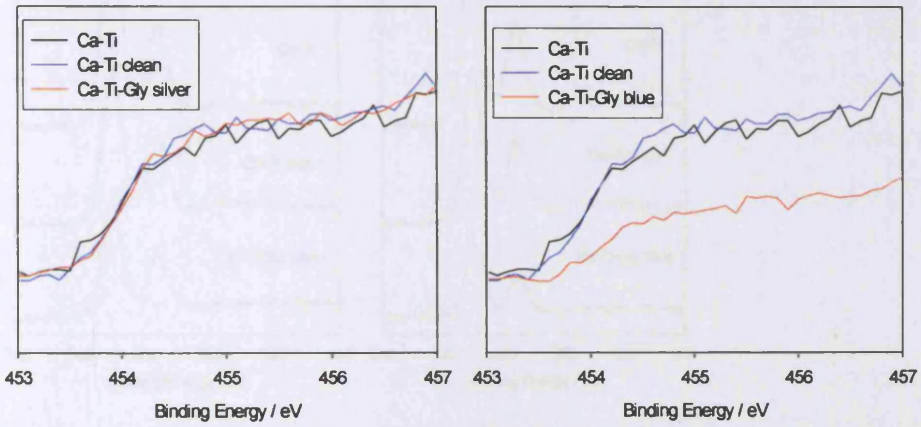

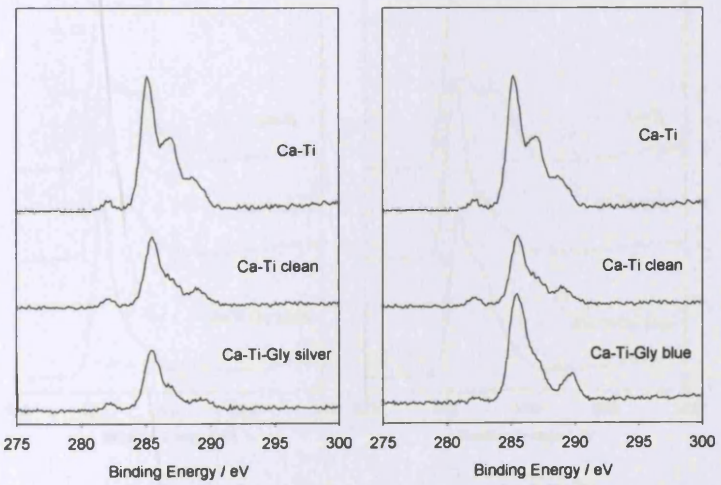

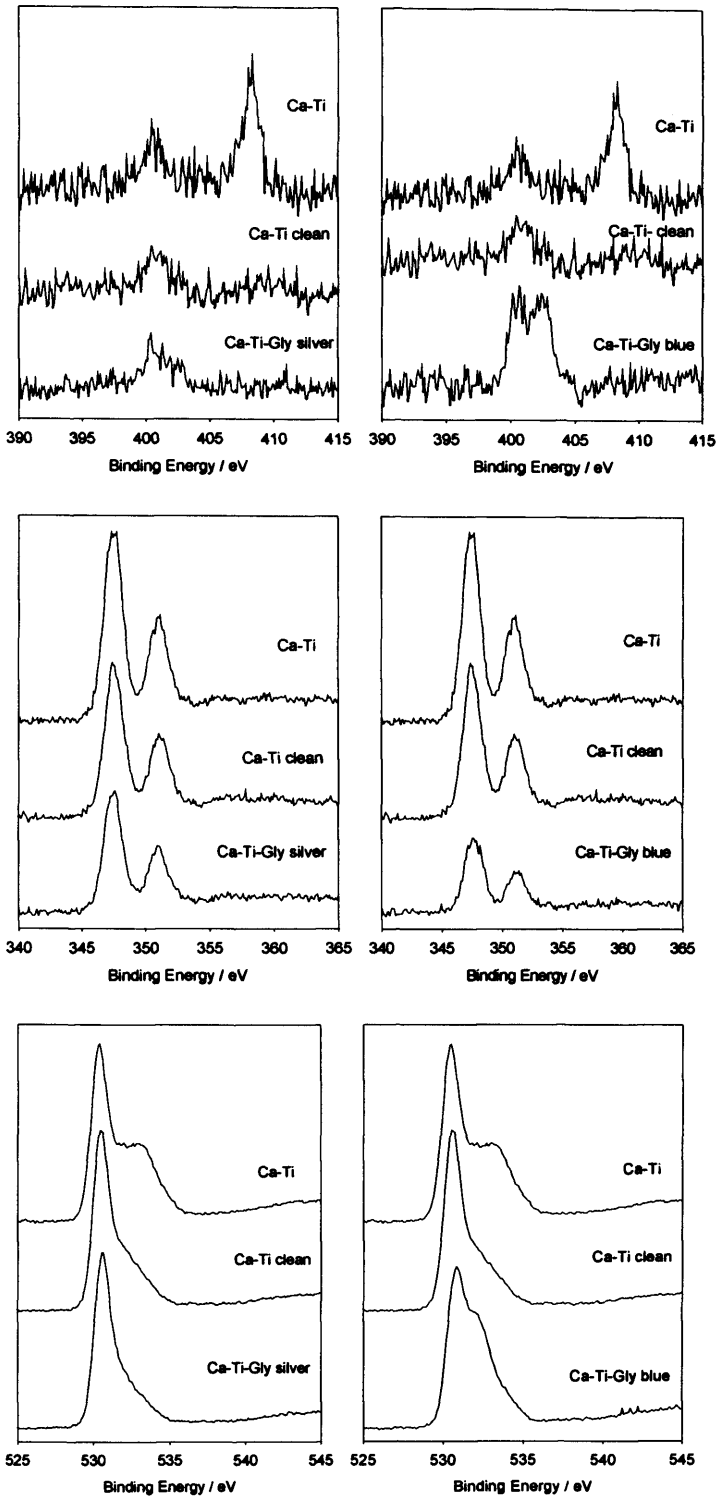

Figure 5. 6 The Ti 2p (first row), expanded Ti^{n+} peak, (n<4, second row), C 1s (third row), N 1s (fourth row), Ca2p (fifth row) and O 1s spectra (sixth row) for Ca-Ti sample before and after ultrasonic cleaning, and after immersion in glycine at room temperature: first column-silver zone, second column-blue zone.

The C/Ti, N/Ti and O/Ti ratios for the Ca-Ti samples (table 5.5) showed that the Ca-Ti samples had a small amount of surface nitrogen contamination, in addition to considerable C contamination. This was also indicated by examination of the detailed spectra, with the N 1s spectrum presenting a single peak at ~ 400 eV (due to -N-(C, H) bonds) and also a second peak at higher binding energy (408.5 eV), due to the presence of nitrate (NO_3^-). The C 1s spectrum (figure 5.6) for this sample also indicated considerable contamination and the O 1s spectrum showed a considerable shoulder at 533 eV. Cleaning reduced the contamination, indicated by the significant decrease in the N/Ti ratios ($p < 0.05$), and the reduction in C/Ti and O/Ti (table 5.5). At the same time the surface calcium was reduced due to immersion in water, caused by the Ca ion release in solution as detailed in Chapter 4. The XPS spectra also illustrated this, with the N 1s spectrum showing a reduction in the 400 eV peak and disappearance of the nitrate. The O 1s spectrum showed a decrease in the shoulder at higher binding energy, and the C 1s showed a pronounced decrease in the intensity of all the peaks. The peak at 286.5 eV was reduced further in intensity relative to the other peaks.

Following glycine adsorption there was a different behaviour with regards to glycine adsorption on blue and silver patches. The N/Ti ratio increased significantly ($p < 0.05$) for the blue patch and did not modify on the silver patch. The N 1s spectrum for the blue patch presented two peaks of similar width and intensity. The higher binding energy peak may be due to glycine adsorption. The lower binding energy peak could also be due to presence of glycine, as maybe in binding to the surface, the NH_3^+ turns to NH_2. The N1s spectrum for the silver patch presented the same 2 peaks hardly resolvable as 2 peaks, but much weaker, which suggested that if adsorption of glycine occurred, then it was minimal.

The C 1s peaks for the 'Ca-Ti Gly blue' were more pronounced than previous spectra, especially the third peak, which was consistent with COOH found in glycine, but did not modify for the silver patch. The O 1s spectrum showed an increase in the shoulder at ~533 eV for the blue patch, but again was not modified for the silver patch.

The Ti 2p spectrum for the 'Ca-Ti Gly blue' sample presented a clear reduction of the lower binding energy peak (figure 5.6, first and second row, right), suggesting an increase in the surface layer. This may be caused by the surface oxidation, as the sample also changed colour. On the basis of the results presented in Chapter 4, this seems unlikely, although the situation in glycine solution might be different to that in water, as the pH of the solution was different. Another possibility is that may also be due to an adsorbed glycine layer. The Ti 2p spectrum for 'Ca-Ti Gly silver' sample (figure 5.6, first and second row, left) did not show any modification.

The above data appeared to suggest that adsorption of glycine onto the Ca-Ti surface occurred, but was not uniform. Some areas of the sample (blue patches) showed very high adsorption when compared to areas where the colour remained unchanged and the adsorption was minimal or non existent (silver patches – figure 5.10 left column). A detailed explanation of the colour changes and patchiness was given in Chapter 4. The adsorption of glycine was illustrated by the Ti 2p, N 1s, O 1s, Ca 2p and C 1s spectra and by the significant increase in the N/Ti ratio.
If we compare these results with the glycine adsorption on cp Ti, it appears that more glycine adsorption occurred on the Ca-Ti sample -blue patch than the cp Ti sample. However, no difference in the amount of glycine adsorption (if any) for both cp Ti and 'Ca-Ti silver patch' was noticed. However, it is difficult to draw a conclusion with regards to adsorption on cp Ti and Ca-Ti due to the large amount of contamination detected on the cp Ti samples.

The results suggested that modifying the cp Ti surface by Ca-ion implantation improves the adsorption of glycine. This was in agreement with previous studies, Ca-ion implanted Ti was not used. Lori et al., (2004), carried out a pre-treatment of Ti with calcium, which resulted in increased adsorption of mucin to Ti, so it appears that the presence of Ca at the surface might affect the adsorption.

5.2.4 Adsorption of cysteine onto cp Ti and Ca-Ti

5.2.4.1 Aims and objectives

This experiment was carried out to observe whether cysteine was adsorbed onto commercially pure titanium and Ca implanted titanium discs, and if there was a quantitative difference in the adsorption on Ca-Ti as compared with cp Ti samples. Cysteine adsorption is much more easier to detect than the glycine adsorption, as this amino acid contains S, which is not normally a contaminant of cp Ti. Cysteine adsorption might also be different from the glycine because the pH of the cysteine solution is different to that of glycine solution.

5.2.4.2 Materials and method

The cysteine solution was prepared using 1.35 g L-Cysteine powder (Sigma, lot 71K 0886, Sigma Aldrich Chemie, Gmbh, Germany) in 25 ml ultrapure water. The pH of the cysteine was measured and was 5.35.

6 cp Ti and 6 Ca-Ti discs were used in this experiment. The cp Ti discs were polished using the second polishing protocol (details in chapter 2). Initially, the polished cp Ti discs were ultrasonically cleaned in acetone for 5 min and then in ultrapure water for 5 min. Following ultrasonic cleaning, the discs were dried using compressed air and placed in aluminium foil, until analysis. Ca-Ti discs were not ultrasonicated and were kept in the dessicator wrapped in aluminium foil until used in experiment.
Following analysis, the discs were immersed in 0.37 M cysteine solution (5 ml per disc) for 18 h at room temperature (23C°). After immersion, the samples were removed from solution using plastic tweezers, and then each sample was washed with 30 ml ultrapure water, to ensure that only strongly bound cysteine remained on the surface. The samples were then stored in well plates in the desiccator to minimize contamination, and were removed only when required for analysis with XPS.

5.2.4.3 Results and discussion

Table 5.6 shows the elemental ratios for cp Ti and Ca-Ti samples before and after glycine adsorption. Figures 5.7 and 5.8 present the Ti 2p, O 1s, C 1s, N 1s, and S 2p spectra for cp Ti and Ca-Ti samples, and also the Ca 2p spectra for the Ca-Ti sample before and after immersion in cysteine solution. As all the cp Ti samples had similar behaviour, only the spectra for one sample will be presented. The same applies for the Ca-Ti samples.

Sample	C/Ti	Ca/Ti	N/Ti	O/Ti	S/Ti
cp Ti 0 h	0.64 ± 0.18	0.00 ± 0.00	0.04 ± 0.02	2.19 ± 0.07	0.00 ± 0.00
cp Ti 18 h cysteine	0.77 ± 0.27	0.00 ± 0.00	0.06 ± 0.01	2.18 ± 0.05	0.01 ± 0.01
Ca-Ti 0 h	1.19 ± 0.13	0.23 ± 0.02	0.01± 0.01	2.74 ± 0.24	0.00 ± 001
Ca-Ti 18 h cysteine	0.84 ± 0.22	0.09 ± 0.01	0.03 ± 0.01	1.96 ± 0.07	0.01 ± 0.01

Table 5. 6 Elemental ratios (average and SD) for cp Ti and Ca-Ti samples before (0 h), and after 18 h immersion in cysteine solution.

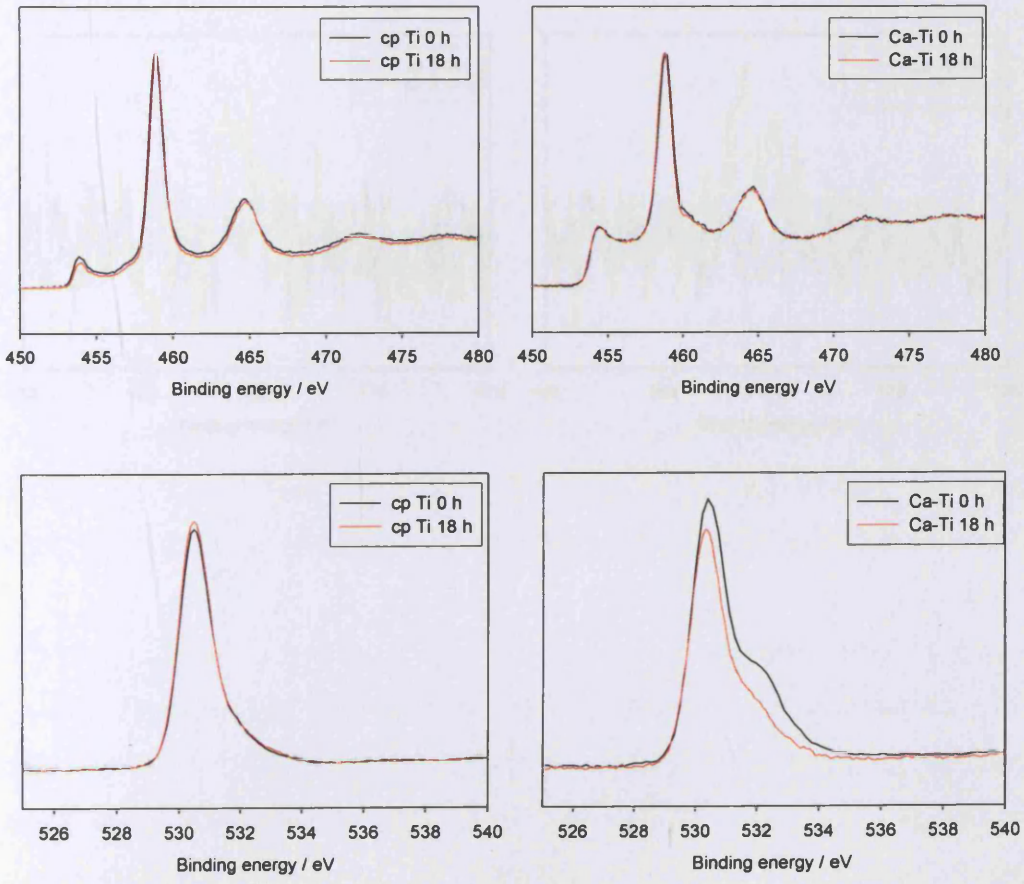

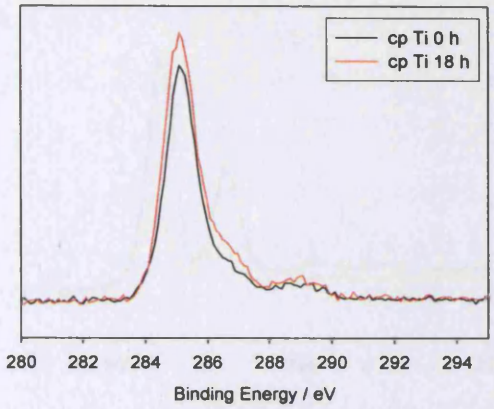
cp Ti 0 h
cp Ti 18 h
280 282 284 286 288 290 292 294
Binding Energy / eV

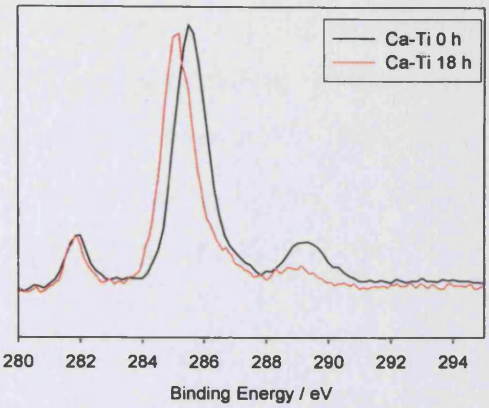
Ca-Ti 0 h
Ca-Ti 18 h
280 282 284 286 288 290 292 294
Binding Energy / eV

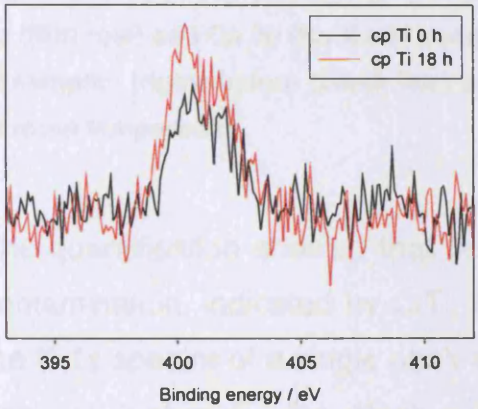
cp Ti 0 h
cp Ti 18 h
395 400 405 410
Binding energy / eV

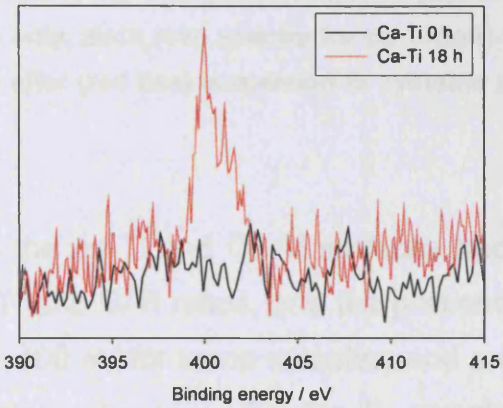
Ca-Ti 0 h
Ca-Ti 18 h
390 395 400 405 410 415
Binding energy / eV

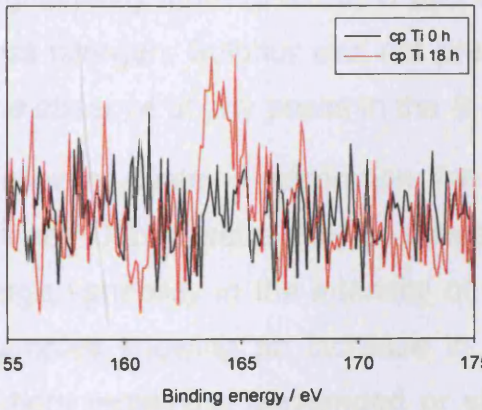
cp Ti 0 h
cp Ti 18 h
155 160 165 170 175
Binding energy / eV

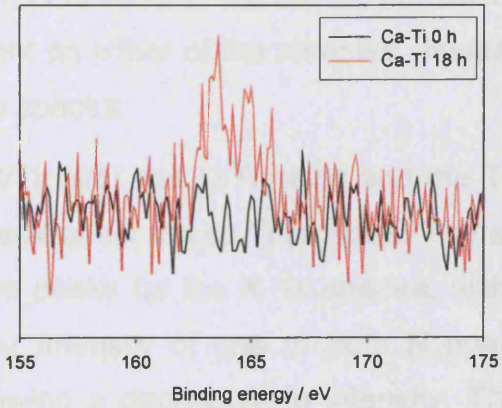
Ca-Ti 0 h
Ca-Ti 18 h
155 160 165 170 175
Binding energy / eV

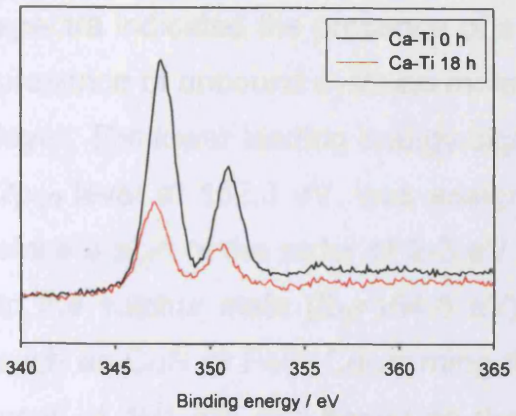

Figure 5. 7 The Ti 2p (first row), O 1s (second row), C 1s (third row), N 1s (fourth row), S 2p (fifth row) and Ca 2p (for Ca-Ti sample only, sixth row) spectra for cp Ti (left) and Ca-Ti samples (right) before (black line) and after (red line) immersion in cysteine solution at room temperature.

The quantification showed that both the cp Ti and Ca-Ti surfaces had some contamination, indicated by C/Ti, N/Ti and O/Ti ratios, and the presence of in the N 1s spectra of a single peak at ~400 eV for some samples, and a second peak at higher E_B for other samples. However, the Ca-Ti samples had significantly more ($p<0.05$) C and O on the surface than cp Ti, but significantly less nitrogen. Sulphur was not present on either of the samples, illustrated by the absence of any peaks in the S 2p spectra.

Following cysteine adsorption, the C/Ti, N/Ti and O/Ti ratios and the Ti 2p, C 1s and O 1s spectra showed little alteration for the cp Ti samples. There was a large variability in the intensity of the peaks for the N 1s spectra, with some samples showing an increase in the intensity of one or both N peaks and others remaining unchanged or showing a decreased in intensity. This was similar to the results in experiment 5.1 presented earlier, which did not demonstrate conclusively the presence of the amino acid on the surface.

However, immersion of both cp Ti and Ca-Ti in cysteine solution resulted in a change in the S 2p spectra with the appearance of a peak at ~ 164 eV. Cavalleri et al. (2001) studied L-cysteine on Au (111) from the solution phase using XPS. The authors concluded that cysteine adsorbed on gold, and by interpreting the Au 4f and S 2p spectra they noted that there was an indication

of dissociative molecular chemisorption on the metal surface. The S 2p spectra indicated the presence of a minor sulphur component attributed to the presence of unbound cysteine molecules physisorbed on the first chemisorbed layer. The lower binding energy signal of sulphur (the S1 component) with a S $2p_{3/2}$ level at 162.3 eV, was assigned to the formation of a thiolate species, since a shift of the order of 2-3 eV towards lower binding energy with respect to the sulphur state (E_B=164.0 eV) was typical of sulphur metal compounds such as CuS or FeS. Concerning the S2 component they observed a S $2p_{3/2}$ peak at 164 eV, and based on the hypothesis that this difference in binding energy could be considered significant, they assigned the 164 eV signal to physisorbed L- cysteine molecules on top of the chemisorbed layer. However in the case of this study the lower binding energy peak was not observed and the peak at ~164 eV was attributed to R-S-H due to adsorbed cysteine. The S/Ti ratio increased significantly ($p<0.05$) following immersion in cysteine, suggesting that cysteine adsorbs onto cp Ti.

Following immersion in cysteine solution the N 1s spectrum for the Ca-Ti samples showed two peaks, at ~ 400 eV and 401 eV. Clark et al. (1976) suggested that in solution there may be a shift of the adsorbed peak at 401 eV towards ~ 400 eV due to the NH_2 group. A second peak may also be present at higher E_B due to NH_3^+. The N/Ti ratio (table 5.7) increased significantly following immersion ($p<0.05$), although reaching a smaller level than in the experiment with glycine adsorption on Ca-Ti (experiment 5.3). On the basis of the presence of N peaks, and that N is not a contaminant of the Ca-Ti sample, and also because N/Ti ratios increased significantly, it may be assumed that both N peaks may be due to cysteine adsorption, although contamination causing the peak at ~ 400 eV could not be excluded. The S 2p spectrum showed a peak, at ~164 eV. The S/Ti ratio (table 5.7) increased significantly ($p<0.05$), which again suggested that adsorption occurred.

The above data suggested that cysteine adsorption occurred onto Ca-Ti samples. However, it is difficult to say if there was more adsorption onto Ca-Ti samples than cp Ti samples, as the S levels on the samples after immersion were similar for both cp Ti and Ca-Ti samples and because of the high levels of N present on the cp Ti surface.

5.2.5 Glycine adsorption onto cp Ti and alkali treated cp Ti discs.

5.2.5.1 Aims and objectives

This study was carried out to observe whether modifying the cp Ti surface by alkali treatment would influence the adsorption of glycine. Is it clear from the literature that alkali treatment is a good method to improve the bioactivity and osseointegration of titanium.
In this experiment a different alkali treatment was used compared to 5.2.2 described earlier. This method used a higher concentration of NaOH, and was similar with the method described by Kim et al. (1996), which resulted in a more bioactive Ti surface.

5.2.5.2 Materials and Methods

24 cp Ti discs were used in this experiment. The discs were polished following the second protocol for polishing (described in section 2.). The 'as-polished' cp Ti discs were then wrapped in aluminium foil and placed in the desiccator until the various treatments were carried out on them.

Preparation of Alkali solutions

A 10 M NaOH solution was prepared adding 40 g of NaOH powder (BDH Chemicals, Poole, England, prod. 26184) to UPW and making up to a total volume 100 ml.
A 0.05 M $Ca(OH)_2$ solution was then prepared using 0.35 g of $Ca(OH)_2$ powder (BDH Chemicals, Poole, England, prod. 275995C) then UPW up to 100 ml.

Discs preparation

18 cp Ti discs were treated with 10M NaOH for 24 h at 60°C (full details about the alkali treatment is given in Chapter 6). After the treatment, the discs were removed from the solution with plastic tweezers, rinsed with ultra pure water

and dried with compressed air. Then 6 cp Ti discs were heat treated at 600°C for 1 h and 12 discs with the $Ca(OH)_2$ solution for 1 h or 4 h as follows:

1. 6 NaOH treated discs were heat treated at 600 °C for 1 h.
2. 6 NaOH treated discs were immersed in the $Ca(OH)_2$ solution for 1 h at 60 °C. After treatment, the discs were dipped in water, dried with compressed air and wrapped in aluminium foil.
3. 6 NaOH treated discs were then immersed in $Ca(OH)_2$ solution for 4 h at 60 °C. After treatment, the discs were dipped in water, dried with compressed air and wrapped in aluminium foil.

Glycine solution preparation

0.37 M Glycine solution was prepared fresh using 0.69 g of glycine powder and 25 ml of ultrapure water.

A total of 24 titanium discs (18 treated titanium discs and 6 cp Ti discs-as control) were immersed in 5 ml glycine solution each in plastic jars. Immersion was carried out at in the same laboratory in which the XPS is housed to minimise contamination following immersion. After immersion, the discs were removed from the solution using plastic tweezers, washed with 30 ml ultrapure water (6 x 5 ml), dried with compressed air and then placed in well plates (to prevent anything touching the surface) with the immersed surface facing upward until analysis with XPS.

5.2.5.3 Results and discussion

Table 5.7 presents the C/Ti, Ca/Ti, N/Ti, Na/Ti and O/Ti ratios for alkali treated samples before and after immersion in glycine solution. The Ti 2p, O 1s, C 1s, N 1s, Ca 2p, Na 1s spectra for the cp Ti discs and treated cp Ti discs before and after immersion in glycine at room temperature are presented below in figure 5.9. The Ca 2p and Na 1s figures do not contain spectra for the cp Ti sample as cp Ti does not contain Ca and Na and could not be quantified.

Sample	C/Ti	Ca/Ti	N/Ti	Na/Ti	O/Ti
cp Ti	1.11 ± 0.30	-	0.06 ± 0.04	-	2.37 ± 0.05
cp Ti Gly	1.18 ± 0.35	-	0.06 ± 0.04	-	2.35 ± 0.11
Ti-NaOH	0.25 ± 0.05	0.02 ± 0.03	0.00 ± 0.01	1.67 ± 0.17	1.66 ± 0.12
Ti-NaOH-Gly	0.74 ± 0.27	0.03 ± 0.03	0.07 ± 0.01	0.29 ± 0.36	2.81 ± 0.09
Ti-NaCaOH 1 h	0.24 ± 0.10	0.94 ± 0.09	0.01 ± 0.03	0.15 ± 0.03	6.01 ± 0.46
Ti-NaCaOH 1 h-Gly	0.52 ± 0.15	0.06 ± 0.01	0.06 ± 0.02	0.17 ± 0.01	2.62 ± 0.10
Ti-NaCaOH 4 h	0.23 ± 0.10	1.38 ± 0.25	0.01 ± 0.02	0.20 ± 0.03	8.00 ± 1.17
Ti-NaCaOH 4 h-Gly	0.82 ±0.21	0.04 ± 0.00	0.09 ± 0.05	0.19 ± 0.01	2.82 ± 0.15

Table 5. 7 Elemental ratios for cp Ti and alkali treated cp Ti before and after immersion in glycine solution at room temperature.

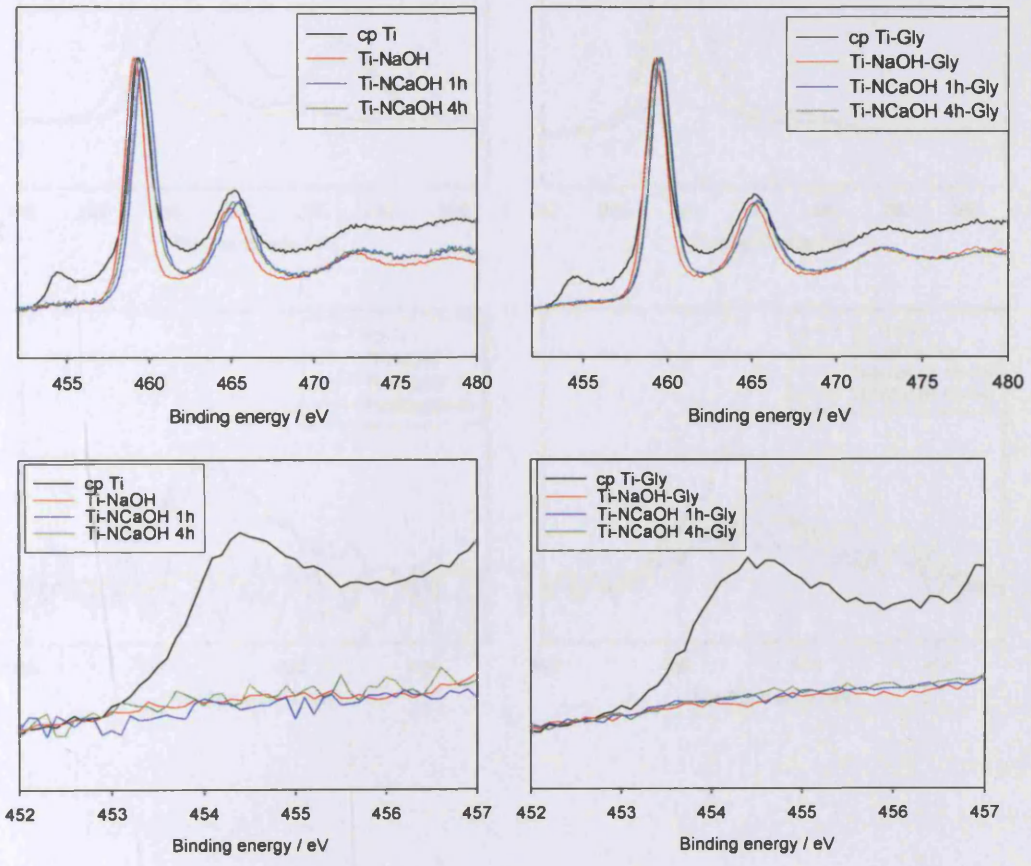

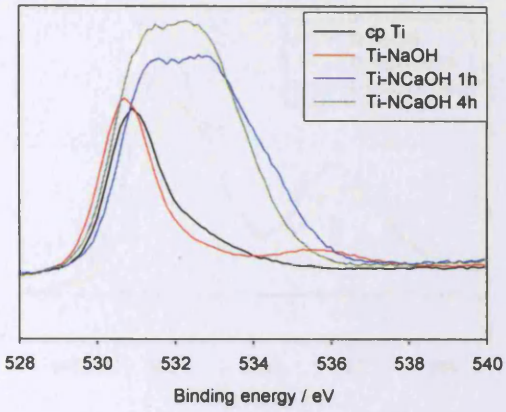
cp Ti
Ti-NaOH
Ti-NCaOH 1h
Ti-NCaOH 4h
528
530
532
534
536
538
540
Binding energy / eV

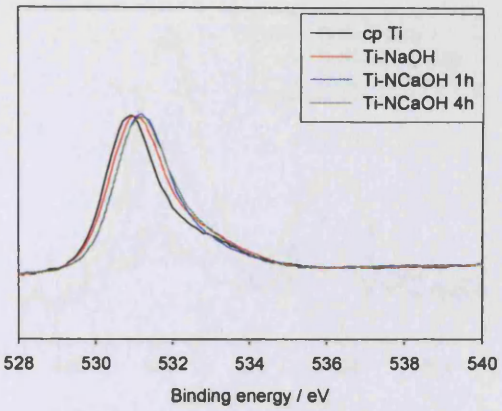
cp Ti
Ti-NaOH
Ti-NCaOH 1h
Ti-NCaOH 4h
528
530
532
534
536
538
540
Binding energy / eV

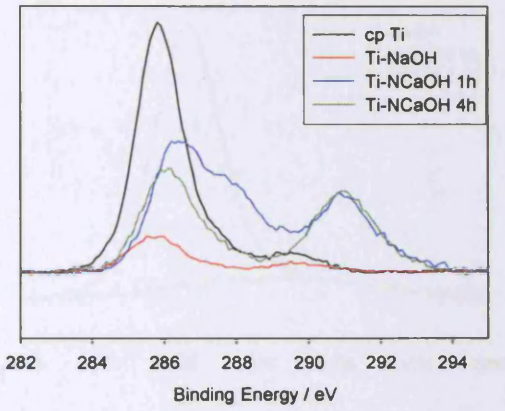
cp Ti
Ti-NaOH
Ti-NCaOH 1h
Ti-NCaOH 4h
282
284
286
288
290
292
294
Binding Energy / eV

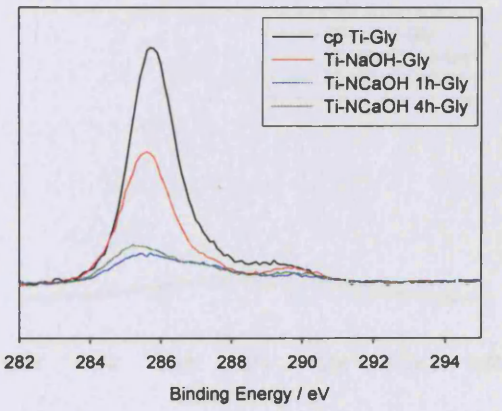
cp Ti-Gly
Ti-NaOH-Gly
Ti-NCaOH 1h-Gly
Ti-NCaOH 4h-Gly
282
284
286
288
290
292
294
Binding Energy / eV

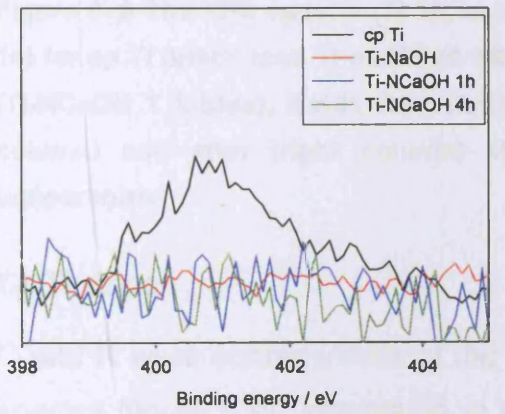
cp Ti
Ti-NaOH
Ti-NCaOH 1h
Ti-NCaOH 4h
398
400
402
404
Binding energy / eV

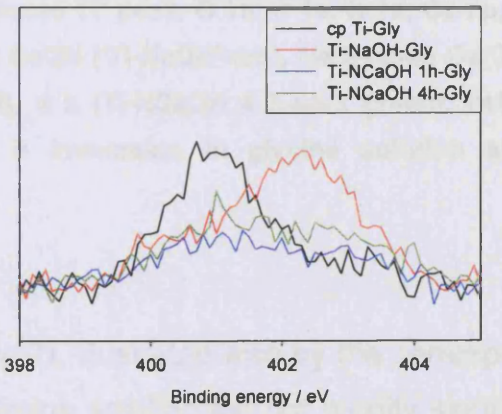
cp Ti-Gly
Ti-NaOH-Gly
Ti-NCaOH 1h-Gly
Ti-NCaOH 4h-Gly
398
400
402
404
Binding energy / eV

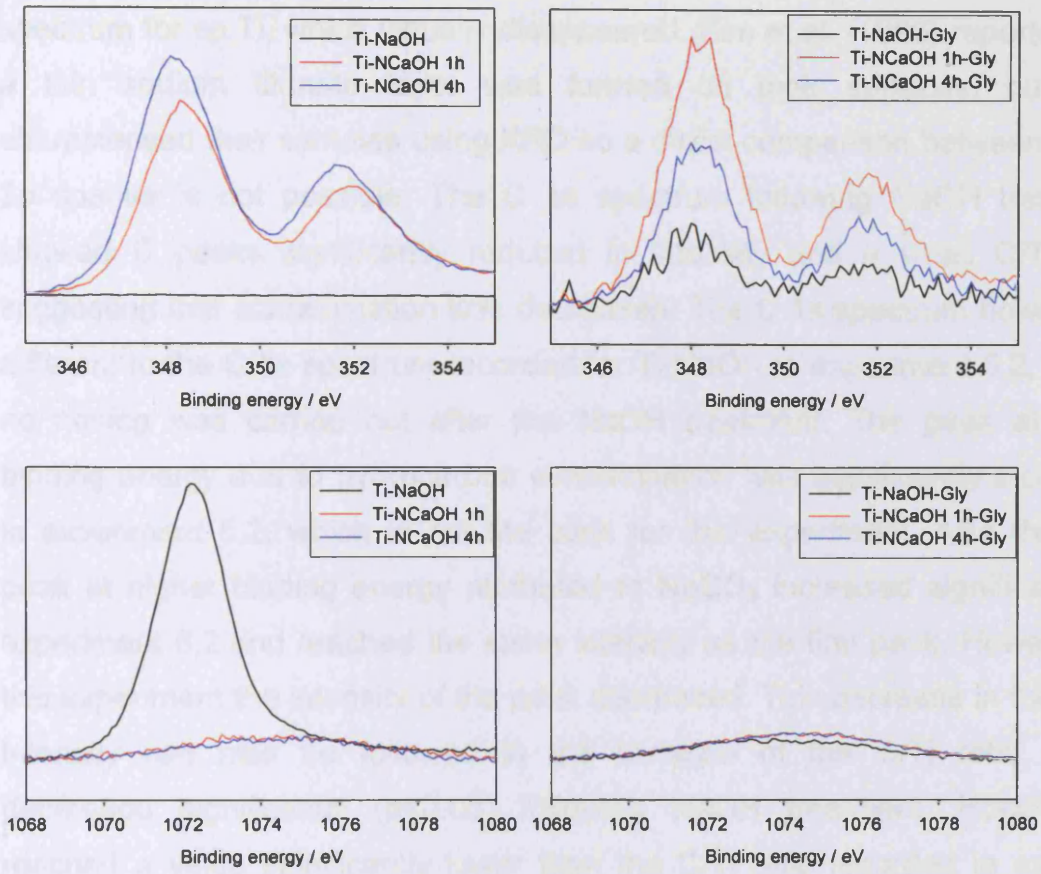

Figure 5. 8 The XPS spectra (Ti 2p, expanded Ti^0 peak, O 1s, C 1s, N 1s, Ca 2p,and Na 1s) for cp Ti (black)and Ti modified with NaOH ('Ti-NaOH'-red), NaOH then $Ca(OH)_2$ 1 h (Ti-NCaOH 1 h-blue), NaOH then $Ca(OH)_2$ 4 h (Ti-NCaOH 4 h-dark green), before(left column) and after (right column) 18 h immersion in glycine solution at room temperature.

Cp Ti discs

C and N were contaminants of the cp Ti, illustrated also by the corresponding spectra (figure 5.9). Immersion in glycine solution did not modify significantly the ratios (table 5.7), nor the spectra (figure 5.8). The results are in agreement with previous experiments with regards to the lack of glycine adsorption onto the cp Ti samples.

NaOH treated cp Ti (Ti-NaOH)

NaOH treatment of the cp Ti samples (Ti-NaOH) resulted in a significant increase in the Na presence on the sample, but decreased C and O. N and Ca were not detected on the surface. The Ti 2p spectrum showed a significant

reduction in the Ti^0 peak (figure 5.9, second row) compared to the Ti 2p spectrum for cp Ti, which virtually disappeared. Kim et al. (1996) reported that a thin sodium titanate layer was formed on their surfaces, but they characterised their samples using XRD so a direct comparison between the Ti 2p spectra is not possible. The C 1s spectrum following NaOH treatment showed C peaks significantly reduced in intensity and a small C/Ti ratio suggesting that contamination was decreased. The C 1s spectrum however is different to the C 1s spectrum recorded for Ti-NaOH in experiment 5.2, where no rinsing was carried out after the NaOH treatment. The peak at lower binding energy due to hydrocarbon contamination was significantly increased in experiment 5.2, which is not the case for this experiment. Also the third peak at higher binding energy attributed to $NaCO_3$ increased significantly in experiment 5.2 and reached the same intensity as the first peak. However, in this experiment the intensity of the peak decreased. This decrease in the peak intensity can also be followed in the variation of the C/Ti ratio, which decreased significantly ($p<0.05$) following NaOH treatment. However, it reached a value significantly lower than the C/Ti ratio recorded in exp 5.2. From this data it may be assumed that rinsing decreased contamination and Na_2CO_3 present on the surface following treatment. Concentration of NaOH was much higher too, which may have resulted in different modification of the surface.

Following glycine adsorption, the samples showed a significant increase ($p<0.05$) in the N/Ti, C/Ti and O/Ti ratios, the presence of a peak at 402 eV in the N 1s spectrum, and an increase the intensity of the lower binding energy in the C 1s spectrum, suggesting that glycine adsorption occurred. There was little sign of COOH, but this could indicate disociative binding of NH_2.
The Ti 2p spectrum did not alter; there was only a slight increase in the Ti metal peak, suggesting that the surface layer became slightly thinner.
Immersion in glycine solution reduced significantly the intensity of the Na 1s peak, illustrated also by the significant decrease ($p < 0.05$) in the Na/Ti ratio.

NaOH then $Ca(OH)_2$ treated cp Ti (Ti-NaCaOH)

As both 1 h and 4 h alkali treatment produced samples with similar characteristics, their data will be discussed together.

From the quantification table (table 5.7) it can be noticed that these treatments resulted in significant amounts of Ca and O on the surface, and minimal amounts of N. Some Na was present on the surface, but much less than for the Ti-NaOH samples. C was found to be at slightly elevated levels compared to the NaOH treated samples. The Ti 2p spectrum showed the Ti^0 peak (figure 5.8, second row, dark green) absent, similar to the NaOH treated samples. The O 1s spectrum for the NaOH then $Ca(OH)_2$ treated samples was significantly modified with regards to peak shape and intensity following the treatment. The O 1s peak at ~ 531 eV increased in intensity and became very wide, which may suggest a significant increase in the thickness of surface oxide, and also a change in the composition of the oxide layer. There was a significant increase ($p < 0.05$) in the O/Ti ratio following alkali treatment as compared to the O/Ti ratio for the cp Ti samples, or the O/Ti ratio for the NaOH treated Ti samples. Contamination could be a cause for the increased surface layer, seen by the reduction in the Ti metal peak of the Ti 2p spectrum. However, this is unlikely, given the C 1s spectrum. Probably the wide peak is a mix of O^{2-} at lower E_B and OH^- at higher E_B, the increased OH will increase O/Ti. As the NaOH was followed by heat treatment and then $Ca(OH)_2$ (just rinsed) probably this caused the difference.

Following immersion in glycine solution the N/Ti ratio increased significantly ($p < 0.05$) for both NaOH then $Ca(OH)_2$ 1 h and 4 h. The N 1s spectra (figure 5.8) presented a wide peak at ~ 402 eV. However, the values were very small. As no N was present before immersion on the samples, this may suggest that some glycine adsorption occurred, but was minimal. The O/Ti ratio decreased significantly ($p<0.05$) and the O 1s spectrum (right column, third row) decreased in intensity and reverted to the shape usually associated with the untreated cp Ti surface. Immersion in glycine decreased the intensity of the C peaks, illustrated also by the significant decrease ($p < 0.05$) in the C/Ti ratio. It also reduced significantly the intensity of the Ca 2p peaks,

illustrated by the significant decrease ($p < 0.05$) in the Ca/Ti ratio, reaching values similar to the Ca/Ti ratios for the Ca-Ti samples following immersion in water. It appeared that there was a $Ca(OH)_2$ film on the surface which came off in glycine.

As the values of the N/Ti ratios following adsorption were similar, it is difficult to say whether there is more glycine adsorbed on the alkali treated samples than cp Ti samples. Calculating the difference between the N/Ti ratio before and after immersion for each type of sample, it was found that the difference was significantly higher ($p<0.05$) for the alkali treated samples than the cp Ti samples. The N1s spectra suggested that NaOH treatment may result in adsorption with only NH_3^+ present but the $Ca(OH)_2$ treatments result in some changes to the structure, with more 401 eV N being observed.

5.3 CONCLUSIONS

Glycine adsorption onto polished cp Ti surfaces at room temperature was not detected. However, it is difficult to say whether adsorption did not occur due to the high levels of contamination, which may block the adsorption by occupying the binding sites available for the glycine. Similarly, glycine may displace the contamination, but as the contaminant contains C, N and O there is no detectable compositional change. Because of high levels of contamination on the cp Ti samples, subsequent experiments were designed to reduce contamination.

NaOH treatment with no rinsing resulted in significant amounts of Na_2CO_3 on the surface and reduced N contamination. It is difficult to say if glycine adsorption occurred, as the N/Ti ratio did not register a significant increase following immersion, due to high variability between samples. It appears that there is some evidence for glycine adsorption, provided by the detailed nitrogen spectrum of some samples. However, the rinsing procedure may have influenced the adsorption on the surface.

Adsorption of glycine onto the ion implanted Ca-Ti surface occurred. However, there was significant difference in the glycine adsorption between the blue and silver patch. It appears that Ca ion implantation of cp Ti is a good method of improving glycine adsorption.

Cysteine adsorption occurred on cp Ti and Ca-Ti samples. However, it is difficult to say whether more cysteine adsorption occurred on Ca-Ti than cp Ti due to the presence of nitrogen contamination on the cp Ti surface. There appears to be little difference in the quantity of bound cysteine.

Glycine did not adsorb onto cp Ti, a result which is in agreement with previous experiments. Modifying the cp Ti surface with 10 M NaOH appears to show that there was more glycine adsorbed on the Ti-NaOH surface than the cp Ti samples. This surface showed high levels of Na, which may influence adsorption. Changing the surface with NaOH then $Ca(OH)_2$ for 1 h also improved the adsorption as compared to the cp Ti samples. Also the NaOH then $Ca(OH)_2$ 4 h treatment of the cp Ti samples appeared to show a significant increase in the adsorption of glycine as compared to the cp Ti samples, reaching levels similar to the NaOH treated samples. The $Ca(OH)_2$ treated samples showed no Na on the surface, but high levels of Ca. The adsorbed N appeared to be in a different chemical state, suggesting that the presence of both Na^+ and Ca^{2+} may influence interaction with amino acids in solution, but probably in different ways.
However, due to the high N contamination recorded for the cp Ti samples and the fact that similar levels of N were recorded for all the samples following glycine adsorption, it is difficult to draw a definite conclusion with regards to that fact that glycine was adsorbed more on the alkali treated samples than the cp Ti samples.

5.4 SUMMARY

Ca ion implantation of the cp Ti samples resulted in both glycine and cysteine adsorption onto their surfaces. However, it cannot be said if there is more adsorption on the Ca-Ti samples than on the cp Ti samples because of high levels of contamination present, especially on the cp Ti samples.

Treatment with NaOH resulted in a modification of the surface, with the introduction of a huge amount of Na and increased C from carbonate. Also the NaOH treatment increased glycine adsorption compared to the cp Ti samples. NaOH treatment followed by $Ca(OH)_2$ treatment resulted in an increased amount of Ca on the surface, which suggested that Ca can be introduced into the cp Ti surface using a cheaper and easier method. There was rapid loss of the Ca on immersion in glycine, suggesting that the Ca was localised at the surface. However, it would be interesting to see how these modifications might influence the deeper layers of the samples. This will be examined in detail in the following chapter.
Alkali treatment resulted in more glycine adsorption on the surface compared to the cp Ti samples.

No firm conclusions could be drawn from the experiments on glycine adsorption onto cp Ti. Cysteine does adsorb onto cp Ti, illustrated by the XPS spectra and the quantification table with elemental ratios.

5.3 LIST OF REFERENCES

Biesbrock, A.R., Edgerton, M. (1995)
Evaluation of the clinical predictability of hydroxyapatite-coated endosseous dental implants: A review of the literature.
International Journal of Oral and Maxillofacial Implants 10: 712-720

Callen, B.W., Lowenberg, B.F., Lugowski, S., Sodhi, R.N., Davies, J.E. (1995)
Nitric acid passivation of Ti6Al4V reduces thickness of surface oxide layer and increases trace elements release.
Journal of Biomedical Materials Research 29(3): 279-90

Cavalleri, O., Oliveri, L., Dacca, A., Parodi, R., Rolandi, R. (2001)
XPS measurements on L-cysteine and 1-octadecanethiol self-assembled films: a comparative study.
Applied Surface Science 175-176: 357-362

Characklis, W. G., Marshall, K.C (1990)
Biofilms, Wiley, New York.

Dodero, G., De Michieli, L., Cavalleri, O., Rolandi, R., Oliveri, L., Daccà, A., Parodi, R. (2000)
Cysteine chemisorption on gold: an XPS and STM study.
Colloids and Surfaces A: Physicochemical and Engineering Aspects 175(1-2): 121-128

Gold, J.M., Schmidt, M., Steinemann, S.G. (1989)
XPS study of amino acid adsorption on titanium surfaces.
Helvetica Physica Acta (62): 247-253

Gottlander, M., Albrektsson, T., Carlsson, L.V. (1992)
A histomorphometric study of unthreaded hydroxyapatite-coated and titanium-coated implants in rabbit bone.
International Journal of Oral and Maxillofacial Implants 7: 485-490

Hanawa, T., Ukai, H., Murakami K. (1993)
X-ray photoelectron spectroscopy of calcium-ion-implanted titanium.
Journal of Electron Spectroscopy and Related Phenomena 63: 347- 354

Hanawa, T., Asami, K., Asaoka, K. (1996a)
AES Studies on the dissolution of surface oxide from calcium-ion-implanted titanium in nitric acid and buffer solutions.
Corrosion Science 38(11): 2061-2067

Hanawa, T., Asami, K., Asaoka, K. (1996b)
Microdissolution of calcium ions from calcium-ion-implanted titanium.
Corrosion Science 38(9): 1579-1594

Hanawa, T., Kamiura, Y., Yamamoto, S., Kohgo, T., Amemiya, A., Ukai, H., Murakami, K., Asaoka, K. (1997)

Early bone formation around calcium-ion-implanted titanium inserted into rat tibia.
Journal of Biomedical Materials Research 36(1): 131-136

Horbett, T. A. (1982)
Protein adsorption on biomaterials.
Biomaterials Interface phenomena and applications 233-244.
American Chemical Society.

Jones, F. H. (2001)
Teeth and bones: applications of surface science to dental materials and related biomaterials.
Surface Science Reports 42(3-5): 75-206

Kasemo, B., Gold, J. (1999)
Implant surfaces and interface processes.
Advances in Dental Research 13(Special ICOB Proceedings issue)

Kim, H.M. Miyaji, F., Kokubo, T., Nakamura, T. (1996)
Preparation of bioactive Ti and its alloy via simple chemical surface treatment.
Journal of Biomedical Materials Research 32: 409-417

Kim, H.M. Miyaji, F., Kokubo, T., Nishiguchi, T., Nakamura, T. (1999)
Graded surface structure of bioactive titanium prepared by chemical treatment.
Journal of Biomedical Materials Research 45: 100-107

Krupa D., Baszkiewicz J.,. Kozubowski J. A, Barcz A.,. Sobczak J. W., Bilinski A.,Lewandowska-Szumie,M.,Rajchel' B. (2001)
Effect of calcium-ion implantation on the corrosion resistance and biocompatibility of titanium.
Biomaterials 22(15):2 139-2151

Langel, W., Menken, L. (2003),
Simulation of the interface between titanium oxide and amino acids in solution by first principles MD.
Surface Science 538(1-2): 1–9

Lori, J. A., Nok, A.J. (2004)
Mechanism of adsorption of mucin to titanium in vitro.
Biomedical Material Engineering 14(4): 557-563

Lausmaa, J., Kasemo, B., Mattson, H. (1990)
Surface spectroscopic characterization of titanium implant materials
Applied Surface Science 44:133-146

Lausmaa, J., Lofgren, P., Kasemo, B. (1999)
Adsorption and coadsorption of water and glycine on TiO_2
Journal of Biomedical Materials Research 44 (3): 227-242

Nakagawa, M., Zhang, L., Udoh, K., Matsuya, S., Ishikawa, K. (2005)

Effects of hydrothermal treatment with CaCl(2) solution on surface property and cell response of titanium implants.
Journal of Materials Science: Materials in Medicine 16(11): 985-991

Nayab, S., Shinawi, L., Hobkirk, J., Tate, T. J., Olsen, I., Jones, F. H. (2003)
Adhesion of bone cells to ion-implanted titanium.
Journal of Materials Science: Materials in Medicine 14(11): 991-997

Nayab, S., Jones, F. H., Olsen, I. (2005)
Effects of calcium ion implantation on human bone cell interaction with titanium. Biomaterials 26: 4717.

Nayab, S., Jones, F. H., Olsen, I. (2007)
The human bone cell cycle is modulated by calcium ion-implantation of titanium. Biomaterials 38(1): 383-391

Nayab, S., Jones, F. H., Olsen, I. (in press)
Effects of calcium ion-implantation of titanium on bone cell function *in vitro.*
Journal of Biomedical Materials Research A

Norde, W., Lyklema, J. (1979)
Thermodynamics of protein adsorption. Theory with special reference to the adsorption of human plasma albumin and bovine pancreas ribonuclease at polystyrenesurfaces.
Journal of Colloid and Interface Science 71(2):350-366

Ojamae, L., Aulin, C., Pedersen, H., Kall, P.O. (2006)
IR and quantum-chemical studies of carboxylic acid and glycine adsorption on rutile TiO2 nanoparticles.
Journal of Colloid and Interface Science 296(1):71-78

Puleo, D. A., Nanci, A. (1999)
Understanding and controlling the bone-implant interface.
Biomaterials 20: 2311-2321

Qingwen, L., Hong, G., Yiming, W., Guoan, L., Jie, M. (2001)
Studies of self-assembly monolayers of cysteine on gold by XPS, QCM and electrochemical techniques.
Electroanalysis 13(16): 1342-1346

Ratner, B. D. (1993)
The blood compatibility catastrophe.
Journal of Biomedical Materials Research 27: 283-288

Robinson, C., Kirkham, J., Brookes, S. J., Shore, R. C. (1992)
The role of albumin in developing rodent dental enamel: a possible explanation for white spot hypoplasia.
Journal of Dental Research 71: 1270-1274

Roddick-Lanzilotta, A.D., Connor, P.A., McQuillan, A.J (1998)

An in situ infrared spectroscopic study of the adsorption of lysine to TiO_2 from an aqueous solution.
Langmuir 14: 6479–6484.

Schmidt, M. (1991)
Adsorption of homocysteine on titanium surfaces.
Helvetica Physica Acta 64(6): 900-901

Schmidt, M. (2001)
X-ray photoelectron spectroscopy studies on adsorption of amino acids from aqueous solutions onto oxidised titanium surfaces
Archive of Orthopaedics and Trauma Surgery 121(7): 403-410

Sultana, R., Kon, M., Hirakata, L.M., Fujihara, E., Asaoka, K., Ichikawa, T. (2006)
Surface modification of titanium with hydrothermal treatment at high pressure.
Dental Material Journal 25(3): 470-479

Takadama, H., Kim, H.M., Kokubo, T., Nakamura, T. (2001)
An X-ray photoelectron spectroscopy study of the process of apatite formation on bioactive titanium metal.
Journal of Biomedical Materials Research 55(2):185-93.

6. ALKALI TREATMENT OF COMMERCIALLY PURE TITANIUM DISCS

6.1 INTRODUCTION

The alkali and heat treatment was described initially by Kim et al. (1996) and subsequently confirmed by other authors as a route for making the Ti surface bioactive. They described the protocol for preparing Ti using an alkali treatment. The Ti samples were first immersed in 10 M NaOH or KOH solution for 24 h, followed by rinsing with distilled water and ultrasonic cleaning for 5 min. The specimens were then dried in an oven at 40° C for 24 h and finally heated to around 600–800°C for 1 h. Because of the strong tendency of titanium to oxidize, the heat treatment was performed at a pressure of 10^{-4} to 10^{-5} Torr. After the treatment, a porous surface formed on the titanium. The thin film XRD (TF-XRD) patterns acquired from the treated titanium revealed the formation of sodium titanate hydrogel on the titanium substrate. A greater amount of crystalline sodium titanate as well as rutile and anatase precipitate were formed after thermal treatment at 800°C for 1 h. After the treated titanium had been soaked in SBF for 4 weeks, bone-like apatite formed on the surface. The authors concluded that this indicated that the alkali- and heat-treated (AHT) titanium possessed good bioactivity.

Kim et al (1996) described the processes that were occurring on the Ti surface following alkali treatment. During the alkali treatment, the TiO_2 layer partially dissolved in the alkaline solution because of the attack by hydroxyl groups:

$TiO_2 + NaOH \rightarrow HTiO_3^- + Na^+$.

This reaction was assumed to proceed simultaneously with hydration of titanium

$Ti + 4OH^- \leftrightarrow Ti(OH)_4 + 4e^-$

A further hydroxyl attack on the hydrated TiO_2 produced negatively charged hydrates on the surfaces of the substrates as follows:

$TiO_2 \cdot H_2O + OH^- \leftrightarrow HTiO_3^- \cdot nH_2O$

These negatively charged species combined with the alkali ions in the aqueous solution to produce an alkalinic titanate hydrogel layer. During heat treatment,

the hydrogel layer was dehydrated and densified to form a stable amorphous or crystalline alkali titanate layer. Kim et al. (1999) stated that NaOH treatment of pure titanium (Ti) formed a sodium titanate hydrogel surface layer with a smooth graded interface structure to the Ti metal substrate. Subsequent heat treatment at 600°C of the NaOH-treated Ti formed an amorphous sodium titanate surface layer with a smooth graded interface structure similar to the Ti metal substrate. These treated Ti substrates formed an apatite surface layer with a smooth graded interface structure compared with the Ti metal substrates in simulated body fluid (SBF). Other authors also studied the effect of NaOH treatment on titanium. Himeno et al. (2001) studied the mechanism of apatite formation at various SBF soaking times It was found that the surface of the sodium titanate was highly negatively charged in SBF. The surface potential increased with increasing soaking time to a maximum positive value. Thereafter, it decreased with increasing soaking time, reached a negative value again, and finally converged to a constant negative value. On the basis of this finding, the complex process of apatite formation described above was interpreted by the authors in terms of the electrostatic interaction between the functional groups and ions in the fluid. The Ti-OH groups formed on the surface of sodium titanate after soaking in SBF were negatively charged and hence, combined selectively with the positively charged Ca^{2+} ions in the fluid to form calcium titanate. As the calcium ions accumulated on the surface, the surface gradually gained an overall positive charge. As a result, the positively charged surface combined with negatively charged phosphate ions to form amorphous calcium phosphate. The authors claimed that the calcium phosphate spontaneously transformed into apatite because apatite is the stable phase in the body environment. A similar electrostatic mechanism for apatite formation may be valid for the other functional groups described above that are effective in apatite nucleation, because all of these functional groups have isoelectric points at pH values much lower than 7, and thus should be negatively charged in the living body. Takadama et al., (2001) also stated that the bioactive titanium metal prepared by treatment with NaOH followed by an annealing stage to produce a sodium titanate layer with a graded surface structure formed a biologically active bone-like apatite surface layer in the body, and that the implant bonded to bone through this apatite layer. In their study, the authors investigated the process of

apatite formation on the bioactive titanium metal in a simulated body fluid using X-ray photoelectron spectroscopy. The bioactive titanium formed Ti-OH groups soon after soaking in simulated body fluid, via the exchange of the Na^+ ions in the sodium titanate on its surface with H_3O^+ ions in the fluid. The Ti-OH groups on the metal combined with the calcium ions in the fluid immediately to form a calcium titanate. After a long period, the calcium titanate on the metal incorporated both the phosphate and calcium ions in the fluid to form apatite nuclei. These then proceeded to grow by consuming the calcium and phosphate ions in the fluid. These results indicated that the Ti-OH groups formed on the metal induced the apatite nucleation indirectly, by forming a calcium titanate. They stated that the initial formation mechanism of the calcium titanate may be attributable to the electrostatic interaction of the negatively charged Ti-OH groups with the positively charged calcium ions.

Alkali- and heat-treated titanium is thought to bond to bones via surface apatite formation (Kim et al. 1996). Fujibayashi et al. (2001) investigated the effects of sodium removal on the bone-bonding ability of bioactive titanium prepared by alkali and heat treatment. Sodium-free bioactive titanium plates were prepared by immersion in an aqueous solution of 5 M NaOH at 60°C for 24 h, followed by immersion in distilled water at 40°C for 48 h before heating to 600°C for 1 h. The *in vivo* bioactive performance was examined mechanically and histologically after 4, 8, 16, and 24 weeks. Sodium removal was found to enhance the bone-bonding strength of bioactive titanium at 4 and 8 weeks postoperatively. However, its bone bonding strength was inferior to that of conventional alkali- and heat-treated titanium at 16 and 24 weeks. Histological examinations after the detaching test revealed breakage of the treated layer in the sodium-free alkali- and heat-treated titanium group. Sodium removal accelerated the *in vivo* bioactivity of bioactive titanium and led to faster bone bonding because of the anatase surface structure, but the loss of the surface graded structure due to the complete removal of sodium decreased the adhesive strength of the treated layer to the titanium substrate.

Nakagawa et al (2005) reported that in order to obtain early and good osseointegration after implantation of a titanium implant in the human body, the surface could be modified using NaOH or H_2O_2 treatments. In their study, titanium was hydrothermally treated with $CaCl_2$ solutions at 200°C for 24 h

($CaCl_2$-HT). Scanning electron microscope (SEM) observation clearly showed apatite deposition on the surface of $CaCl_2$-HT treated titanium faster than other chemical treated titanium during immersion in simulated body fluid. X-ray photoelectron spectroscopy (XPS) analysis demonstrated that Ti--O--Ca bonding was formed on the titanium surface by hydrothermal treatment with $CaCl_2$ solution. It was also revealed that the thickness of TiO_2, which was known to play important roles in the formation of bone-like apatite, became approximately three times greater than on as-polished titanium. The numbers of initialy attached MC3T3-E1 cells on as-polished and NaOH, H_2O_2 and this $CaCl_2$-HT treated titanium were similar. After 5 days incubation, the growth rate of MC3T3-E1 cells on $CaCl_2$-HT treated titanium was significantly higher than that on other chemically treated titanium samples. The hydrothermal treatment with 10 - 20 mmol / L $CaCl_2$-HT solution at 200°C was an effective method for the fabrication of titanium implant with good bioactivity and osteoconductivity.

Sultana et al. (2006) investigated the surface modification of titanium by means of hydrothermal treatment with a maximum pressure of 6.3 MPa (280°C) in CaO solution [$Ca(OH)_2$] or water to improve both bioactivity and biocompatibility. As a result, calcium titanate was formed on the surface of titanium. Moreover, titanium oxide and titanium hydroxide layers on the surface increased as temperature and pressure increased. The surface-modified titanium was also immersed in a simulated body fluid (SBF) to estimate its bioactivity. Needle-like apatite precipitation was observed on all hydrothermal-treated titanium surfaces after immersion in SBF for four weeks. In particular, the apatite needles of titanium treated at 6.3 MPa in CaO solution were both clearer and in greater quantity than those of all other hydrothermal-treated specimens. Furthermore, the amount of precipitate corresponded to the thickness of the surface-modified layer and the amount of calcium in the surface layer. The results suggested that surface modification of titanium with this high-pressure hydrothermal treatment seemed to improve bioactivity and biocompatibility.

Hydrothermal modification of a titanium surface in calcium solutions was also performed by Hamad et al., (2002). The apatite precipitation on the modified surface in Hanks' solution, as a simulated body fluid, was evaluated and the surface microstructure changes after the modification were characterised by thin-film X-ray diffractometry (TF-XRD) and X-ray photoelectron spectroscopy

(XPS). Hydrothermal modification in CaO solution enhanced the precipitation of apatite on the titanium surface. High pH, high pressure and high temperature of the CaO solution increased the thickness of the surface-modified layer and enhanced the synthesis of calcium titanate which possibly promoted the precipitation of apatite in Hanks' solution. Hydrothermal modification in $CaCl_2$ solution, on the other hand, showed reverse effects. The modification of titanium in CaO solution with hydrothermal treatment is expected to result in excellent osseointegration and can be easily performed by using an autoclave, a widely available clinical apparatus.

The modification of the surface properties of titanium and titanium alloy by chemical techniques has opened new possibilities to improve the bioactivity and, in general, the biological performance of such implants *in vivo*. One of the main aims is the achievement of a surface oxide layer that stimulates hydroxlapatite mineralization and, also, shows osteoconductive properties in the host.

Xue et al. (2005) characterised plasma-sprayed titanium coatings modified by alkali treatment. The changes in chemical composition and structure of coatings were examined using SEM and AES. The results obtained indicated that a net-like microscopic surface texture, which was full of the interconnected fine porosity, appeared on the alkali-modified titanium coatings. The surfaces chemical composition was also altered by alkali modification. A sodium titanate compound was formed on the surface of the titanium coating and replaced the native passivating oxide layer. Its thickness was measured as about 150 nm which was about 10 times that of the as-sprayed coating. The bone bonding ability of titanium coatings was investigated using a canine model. The histological examination and SEM observation demonstrated that more new bone was formed on the surface of alkali-modified implants and grew more rapidly into the porosity. The alkali-modified implants were found to appose directly to the surrounding bone. In contrast, a gap was observed at the interface between the as-sprayed implants and bone. The push-out test showed that alkali-modified implants had a higher shear strength than as-sprayed implants after 1 month of implantation. An interfacial layer, containing Ti, Ca and P, was found to form at the interface between bone and the alkali-modified implant by EDS analysis.

Bio-activation of titanium surfaces by Na plasma immersion ion implantation and deposition (PIII and D) was illustrated by precipitation of calcium phosphate and cell culture (Maitz et al., 2005). The bioactivity of the plasma-implanted titanium was compared to that of the untreated, Na beam-line implanted and NaOH-treated titanium samples. The data showed that the samples could be classified into two groups: non-bioactive (untreated titanium and beam-line Na implanted titanium) and bioactive (Na-PIII and D and NaOH-treated titanium). None of the four types of surfaces exhibited major cell toxicity as determined by lactate dehydrogenase (LDH) release. However, the LDH release was higher on the more bioactive PIII and NaOH-treated surfaces. From a morphological point of view, cell adherence on the NaOH-treated titanium was the best. On the other hand, the cell activity and protein production were higher on the non-bioactive surfaces. The high alkaline phosphatase activity per cell suggests that the active surfaces support an osteogenic differentiation of the bone marrow cells at the expense of lower proliferation. The authors concluded that use of Na-PIII and D provided an environmentally cleaner technology to improve the bioactivity of Ti compared to conventional wet chemical processes. The technique is also particularly useful for the uniform and conforming treatment of medical implants that typically possess an irregular shape and are difficult to treat by conventional ion beam techniques.

It is clear from the literature that alkali treatment of Ti is a good method to improve the bioactivity and osseointegration of titanium. However, the methods employed in these treatments were numerous and there are many stages involved in the preparation of Ti. This study attempts to modify the surface using a very simple and economic modification process involving only alkali treatment, rinsing and heat treatment. The ion release from these modified Ti surfaces will be measured, which has not been attempted to date. In addition, detailed characterisation of the sub-surface layers of these modified Ti samples will be carried out using XPS depth profiling, which again has not been previously reported.

6.2 ALKALI TREATMENT ON CP TI

6.2.1 Aims and objectives

The aim of the study is to introduce Ca into the titanium surface via a different route to ion implantation, which is an expensive process, not well suited to commercial applications, especially where complex implant geometries may be required. Providing this aim could be achieved, a further was to further characterise their surface and measure Ca ion release into solution (if this occurred).

6.2.2 Materials and methods

The following were investigated:
The effects of various alkali and heat treatment on cp Ti samples.
The effects of sodium hydroxide (NaOH) with and without heat treatment (HT) on the cp Ti samples (Ti-NaOH) was carried out as control.
The effect of NaOH followed by $Ca(OH)_2$ (± heat treatment), and a mixture of NaOH and CaOH on cp Ti as proposed methods for introducing Ca into the bioactive Ti surface.
The cp Ti discs used in this study were polished in-house using the second method described in Chapter 2. Before the experiment, all the discs were ultrasonically cleaned in ultrapure water for 5 minutes.
The cp Ti discs were treated with 10 M NaOH solution. This was prepared using 40 g NaOH powder (BDH Chemicals, Poole, England, prod 26184) and 100 ml ultrapure water. The discs were placed for 24 h in a covered glass beaker and then treated at 60°C using a thermostatic hot plate to regulate the temperature. A temperature sensor was kept in the beaker at all times to measure the temperature. Water was added regularly to the solution to replace that lost due to evaporation. The solution during the treatment was stirred at 400 rpm. at all times to help prevent gas bubble formation on the sample surface.
After the NaOH treatment the samples were removed from the glass beaker using plastic tweezers, dipped in ultrapure water and dried with compressed air. 18 of the treated samples were then immersed in the 0.05 M $Ca(OH)_2$ solution (BDH Chemicals, Poole, England, prod 275995C) in a glass beaker at 60°C for

1 h, 4 h, 24 h. The solution was prepared using 0.35 g $Ca(OH)_2$(BDH Chemicals, Poole, England, prod 275995C) in 100 ml ultrapure water. The experimental protocol was identical to that described in the previous paragraph with the only alterations being the treatment solution and time.
After the appropriate time, the samples were removed from the $Ca(OH)_2$ solution, dipped in ultrapure water and then dried using compressed air. Samples requiring heat treatment were treated at 600°C for 1 h. The temperature increased at a rate of 100°C / minute, was held at 600°C for 1 h, and then allowed to cool in the furnace.

A separate treatment from that described above was also attempted. Eight cp Ti discs were immersed in a mixed solution of 10 M NaOH and 0.05 M $Ca(OH)_2$. Solutions were prepared as above [40 g NaOH + 0.35 g $Ca(OH)_2$] in 100 ml ultrapure water. The cp Ti samples left for 24 h at 60° C, the process protocol was again that given previously.
Following alkali treatment, the Ti samples were immersed in ultrapure water as follows: 3 samples for each type of treatment were immersed in 1 ml ultrapure water in well plates at 37°C for 2 min. Following immersion, the solutions were removed from the well plates using a pipette and a new plastic tip for each sample (solution). These solutions were retained for analysis. Then the treated Ti samples were removed using plastic tweezers, dipped in ultrapure water and re-immersed in fresh 1 ml ultrapure water for 4 h at 37°C. The process was repeated and same samples were then re-immersed for 24 h at 37°C. The immersion procedure was different to that used in Chapter 4. As controls samples were ultrapure water and the solutions cp Ti samples were immersed for each time point.

All the Ti samples were analysed before and after alkali treatment and following immersion in ultrapure water (24 h immersion) using XPS. The retained solutions were analysed using ion chromatography (details in Chapter 2).

6.2.3 Results and discussion

6.2.3.2 Surface analysis

Elemental ratios (Ca/Ti, C/Ti, Na/Ti and O/Ti) for all the samples before and after immersion are presented in figures 6.1 and 6.2. The XPS spectra for all the samples before immersion in ultrapure water are presented in figure 6.3 for alkali non-heat treated samples (left row) and alkali heat-treated samples (right row).

Following immersion in ultrapure water, the spectra for all the samples did not alter significantly with regards to peak shape or peak positions, only the intensity of the peaks was found to change. To avoid repetition, spectra are not presented for samples following immersion in ultrapure water.

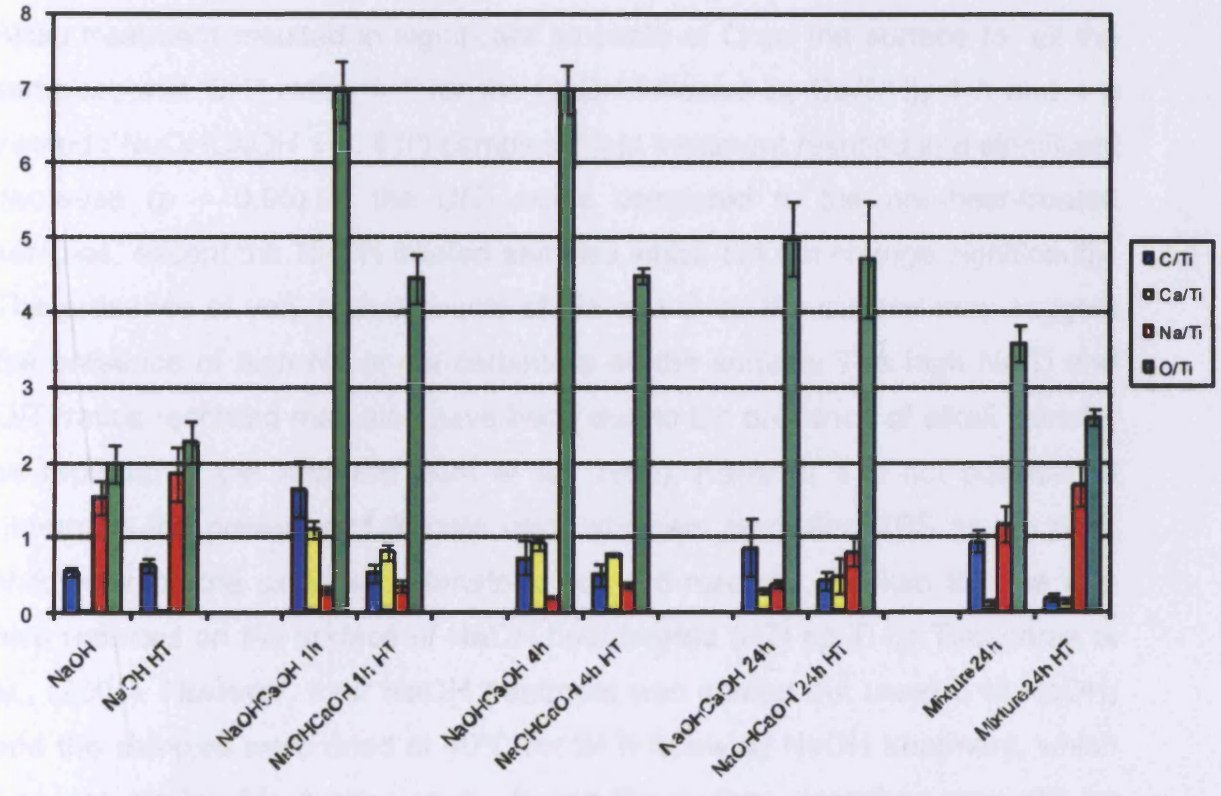

Figure 6. 1 Elemental ratios for alkali treated samples before immersion in ultrapure water at 37°C.

Figure 6.1 presents the C/Ti, Ca/Ti, Na/Ti and O/Ti ratios for alkali treated samples before immersion in ultrapure water at 37°C.

Following alkali treatment of Ti surfaces with NaOH alone, a variable amount of Na was expected to be present on the surface of the Ti samples depending on the nature of the treatment. Indeed, figure 6.1 shows that various amounts of Na were present on the surface of all the samples. The highest Na/Ti ratio was recorded for the NaOH treated samples ('NaOH' ± HT), followed by the Ti samples treated with the mixture NaOH + $Ca(OH)_2$. The Na/Ti ratio decreased significantly ($p < 0.05$) for the samples treated with $Ca(OH)_2$ following the NaOH treatment. Heat treatment (HT) increased the proportion of Na on the surface, as illustrated by the significant increase ($p < 0.05$) in the Na/Ti ratio for all the samples. However, for the samples for where $Ca(OH)_2$ was the last step in the alkali treatment, this amount was still significantly lower ($p < 0.05$) than the NaOH treated samples (± heat treatment).

Alkali treatment resulted in significant amounts of O on the surface for all the samples, with O/Ti ratios = 7 for the NaOH followed by $Ca(OH)_2$ 1 h and 4 h treated ('NaOHCaOH 1 h, 4 h') samples. Heat treatment resulted in a significant decrease ($p < 0.05$) in the O/Ti ratios compared to the non-heat-treated samples, except the NaOH treated samples which did not change significantly. The presence of very high amounts of Na and O on the surface may suggest the presence of high Na or Ca carbonate on the surface. The high Na/Ti and O/Ti ratios recorded may also have been due to the presence of alkali titanate, as reported in the literature (Kim et al., 1996). However it is not possible to determine the presence of titanate using standard resolution XPS as the peak shift between the oxide and titanate is not well resolved. Sodium titanate was also reported on the surface of NaOH heat treated (HT) cp Ti by Takadama et al., (2001). However, their NaOH treatment was carried out using 5 M NaOH, and the samples were dried at 40°C for 24 h following NaOH treatment, which was not similar this current study, hence the surface described may still be different. The most probable explanation for this high amounts of Na and O on the surface for the samples analysed here was Na and / or Ca hydroxide surface layers, which would also resulted in increased O/Ti and Na/Ti ratio, as

both hydroxides form very easily. XPS spectra presented later would confirm this.

C was also present on the surface of all the samples in various amounts, with the highest C/Ti ratio recorded for the NaOH followed by $Ca(OH)_2$ treatment for 1 h. The C/Ti ratios decreased significantly ($p < 0.05$) for all the samples following heat treatment, except the NaOH treated samples, which did not change significantly. The values of the C/Ti ratios recorded for these samples were not significantly different to the C/Ti ratio recorded for Ca-Ti and cp Ti samples. This is a good indicator that alkali treatments did not result in more C contamination and that relatively clean surfaces were achieved.

Figure 6.1 shows that following alkali treatment involving $Ca(OH)_2$ resulted in samples which had calcium on the surface. The NaOH followed by $Ca(OH)_2$ treatment for 1 h and 4 h resulted in significant amount of Ca on the surface, with Ca/Ti ratios of around ~1. Heat treatment of these samples resulted in a significant decrease ($p < 0.05$) in the Ca/Ti ratios. However, the values recorded were still significantly greater ($p < 0.05$) than the Ca/Ti ratio recorded for the other alkali treated samples. The NaOH + $Ca(OH)_2$ treated samples (the 'Ti-mixtures') had a significantly lower amount of Ca on their surface. However, the Ca/Ti ratio was still similar to the Ca/Ti ratio recorded for the as-implanted Ca-Ti.

This shows that simple chemical treatments can produce surface Ca levels greater than those found in Ca-Ti samples following Ca ion implantation.

Figure 6.2 shows the elemental ratios for alkali treated samples following immersion in ultrapure water ('I—Alkali treated Ti')

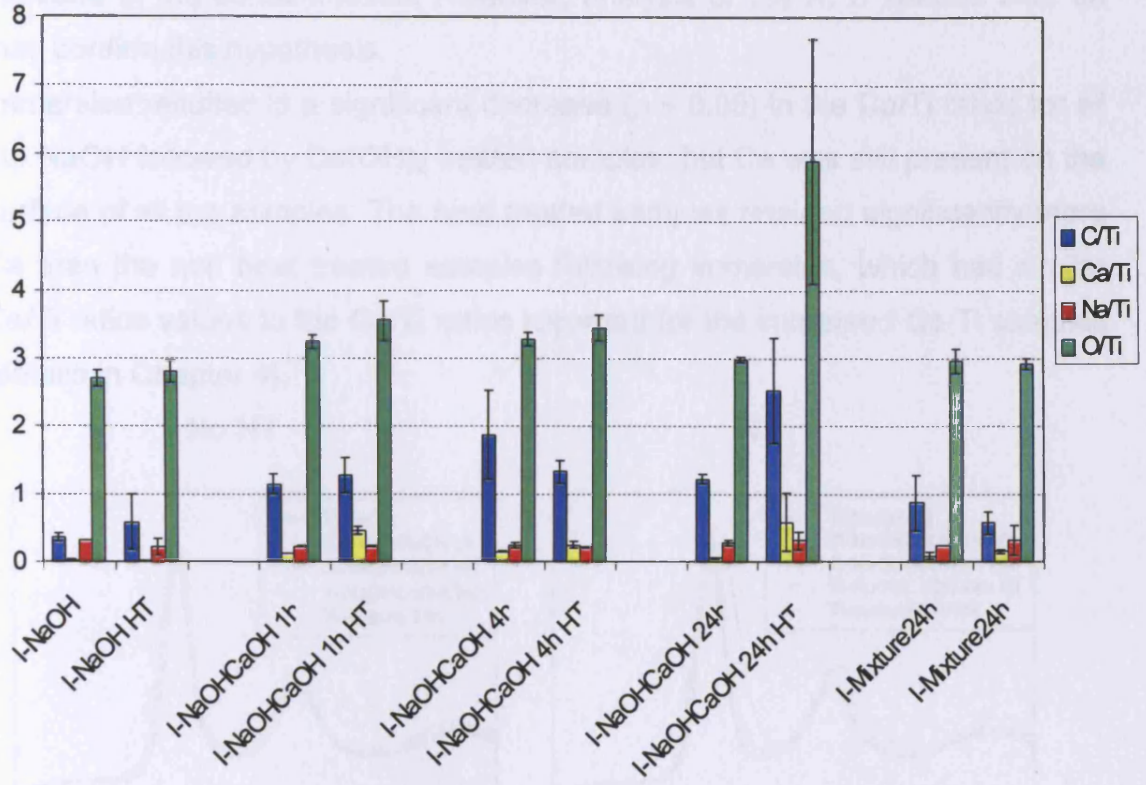

Figure 6. 2 Elemental ratios (C/Ti, Ca/Ti, Na/Ti, O/Ti) for alkali treated Ti samples after imersion (I-Alkali treated Ti) in ultrapure water at 37°C.

The NaOH treated samples presented a significant decrease ($p < 0.05$) in the Na/Ti ratio following immersion. The C/Ti ratio also decreased but not significantly. However, the O/Ti ratio increased significantly ($p < 0.05$). This may be due to and increase in the OH groups, caused probably by the presence of NaOH on the surface. The fact that Na/Ti and C/Ti ratio decreased may suggest that the Na carbonate present on the surface as a result of the NaOH treatment decreased following immersion.

The Na/Ti ratio also decreased significantly for all the other samples after immersion, with no significant difference between the non heat treated and heat treated samples. Immersion also resulted in a significant decrease ($p < 0.05$) in the O/Ti ratio for all the samples. There was a significant increase in the C/Ti ratio for all the samples following immersion. The fact that Na and O decreased may have been caused by a decrease in the Na and Ca carbonate, but a significant decrease in the C/Ti ratio was also expected. As this was not the case, it appears likely that the decrease in the carbonate was offset by an

increase in the contamination. However, analysis of the XPS spectra later on may confirm this hypothesis.

Immersion resulted in a significant decrease ($p < 0.05$) in the Ca/Ti ratios for all the NaOH followed by $Ca(OH)_2$ treated samples, but Ca was still present on the surface of all the samples. The heat treated samples retained significantly more Ca than the non heat treated samples following immersion, which had similar Ca/Ti ratios values to the Ca/Ti ratios recorded for the immersed Ca-Ti samples (details in Chapter 4).

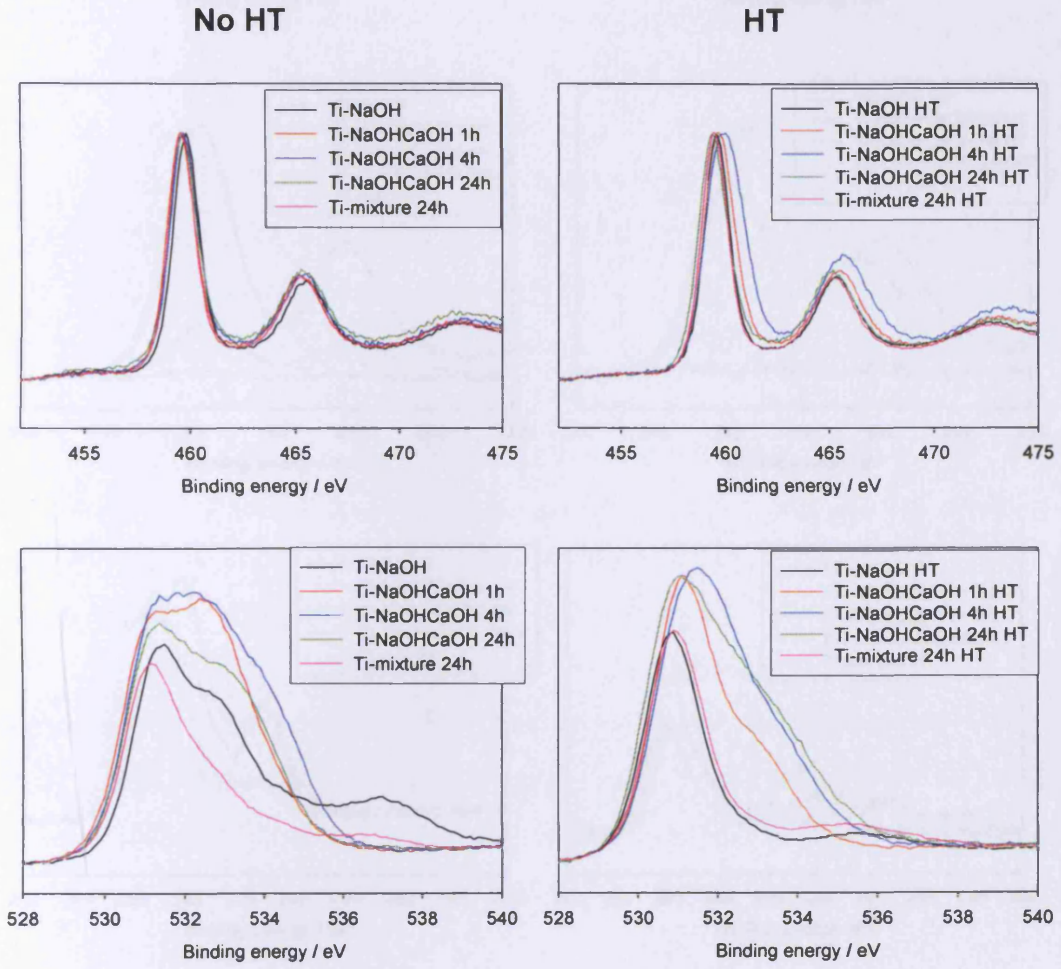

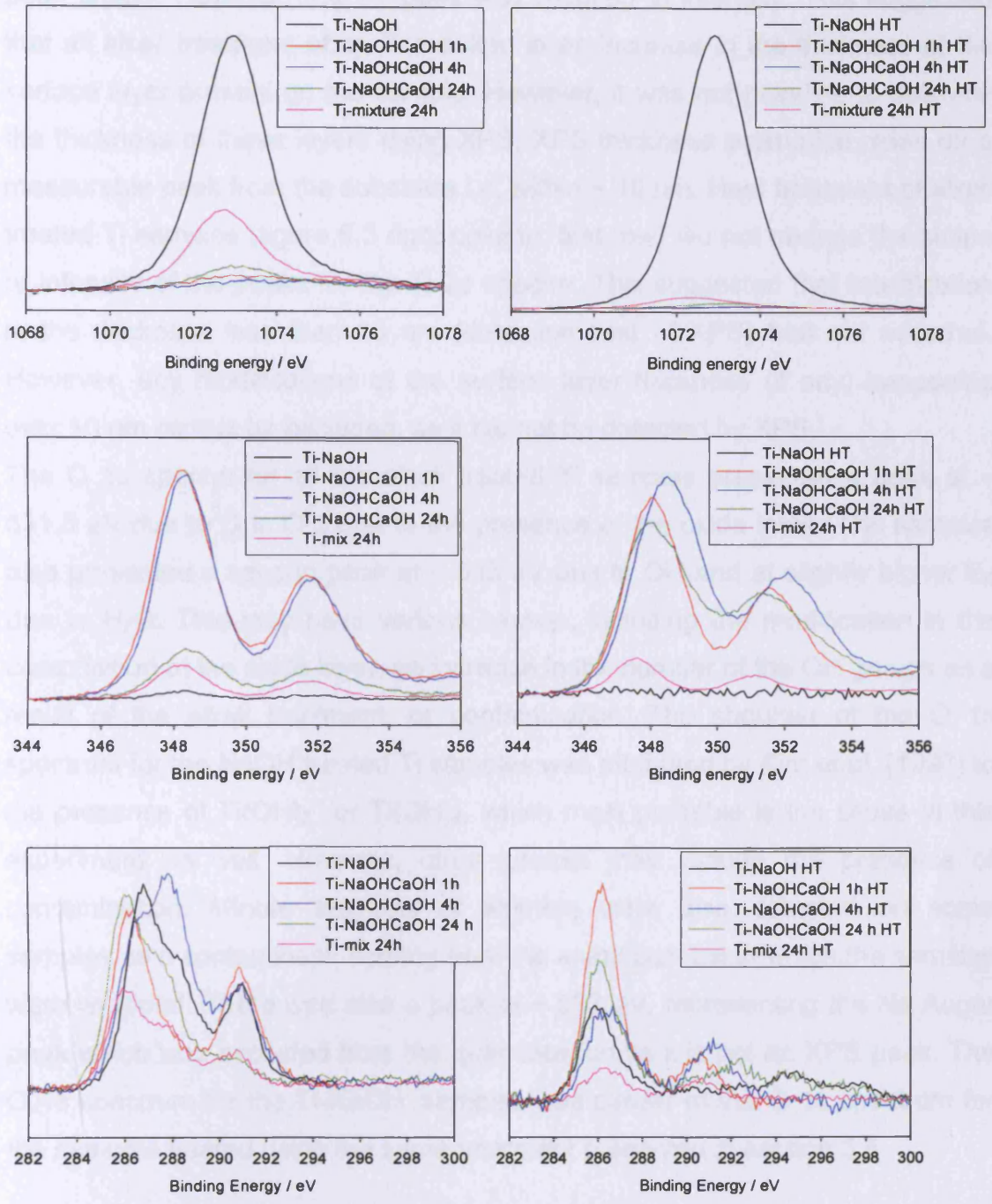

Figure 6. 3 The XPS spectra (Ti 2p, O 1s, N 1s, Ca 2p, Na 1s, and C 1s) for Ti modified with NaOH ('Ti-NaOH'-black), NaOH then $Ca(OH)_2$ 1 h (Ti-NCaOH 1 h-red)), NaOH then $Ca(OH)_2$ 4 h (Ti-NCaOH 4 h-blue), NaOH then $Ca(OH)_2$ 24 h (Ti-NCaOH 4 h-dark green), NaOH+ $Ca(OH)_2$ (Ti-mixture 24 h-pink), without (left column) and with (right column) heat treatment.

The Ti 2p spectra for all the alkali treated cp Ti samples with no heat treatment (figure 6.3 left column, first row) before immersion were similar with regards to

peak shape. However, the Ti^0 peak was reduced in intensity. This suggested that all alkali treatment of cp Ti resulted in an increase in the thickness of the surface layer present on the sample. However, it was not possible to estimate the thickness of these layers using XPS. XPS thickness estimation relies on a measurable peak from the substrate i.e. within ~ 10 nm. Heat treatment of alkali treated Ti samples (figure 6.3 right column, first row) did not change the shape or intensity of the peaks for the Ti 2p spectra. This suggested that modification in the thickness less than 10 nm (detection limit of XPS) had not occurred. However, any modifications of the surface layer thickness (if any) happening over 10 nm cannot be excluded, as it cannot be detected by XPS.

The O 1s spectra for all the alkali treated Ti samples presented a peak at ~ 531.5 eV due to O in O^{2-}, due to the presence of the oxide layer. The samples also presented a second peak at ~ 533 eV due to OH and at slightly higher E_B due to H_2O. This may have various causes, including the modification in the composition of the oxide layer, an increase in the number of the OH groups as a result of the alkali treatment, or contamination. The shoulder of the O 1s spectrum for the NaOH treated Ti samples was attributed by Kim et al. (1996) to the presence of $Ti(OH)_3^+$ or $Ti(OH)_4$, which most probable is the cause in this experiment as well. However, other causes may include the presence of contamination. Minute amounts of alumina were also detected on some samples as a contaminant, coming from the aluminium foil in which the samples were wrapped. There was also a peak at ~ 537 eV, representing the Na Auger peak which was excluded from the quantification as it is not an XPS peak. The O 1s spectrum for the Ti-NaOH' samples was similar to the O 1s spectrum for the samples treated using the same treatment presented in section 5.5.

The O 1s spectra for the NaOH followed by $Ca(OH)_2$ treated samples however, (figure 6.3, left column, second row) were significantly different with regards to peak shape and intensity compared to the 'Ti-NaOH' samples. The wide peak was a mix of O^{2-} at 530.5 eV and OH^- at 533 eV. This increased OH resulted in the increased the O/Ti ratios of the samples. The O/Ti ratio for the NaOH then $Ca(OH)_2$ 1 h and 4 h treated Ti samples was significantly greater ($p < 0.05$) than the O/Ti ratio for the NaOH then $Ca(OH)_2$ 4 h heat treated Ti or the Ti-mixture 24 h samples, which showed virtually no OH on the surface . However, there

was no significant difference between the last two treatments with regards to the O/Ti ratio value. Ca and Na formed hydroxide very easily therefore the OH peak may just reflect Na and Ca levels on the surface.

Again, these data suggested that there was an increase in the thickness of the oxide layer, accompanied by a change in the composition. The O/Ti ratio increased additionally due to the presence of Ca hydroxide on the surface as a result of the $Ca(OH)_2$ treatment.

Heat treatment reduced the second peak width for all the samples. There was also a significant decrease ($p < 0.05$) in the O/Ti ratio for the alkali samples following heat-treatment, except the 'Ti-NaOH' samples which did not change significantly. The 'Ti-mixture 24 h HT samples' showed significantly smaller O/Ti ratio ($p < 0.05$) compared to the rest of the O/Ti ratios, probably due to the lack of OH groups at ~ 533 eV. As the Ti 2p spectra for any of the samples did not show an increase in the Ti metal peak, which may have suggested that the thickness of the oxide layer was reduced, it may be assumed that this decrease in the O/Ti ratio was not due to substrate effects.

The O/Ti ratio decreased significantly ($p < 0.05$) following immersion for all the samples. This was due to reduction in the OH groups on the surface, illustrated by a further decrease in the O 1s shoulder compared to the O 1s spectra before immersion (spectra not presented). It is likely that the release of Ca was accompanied by OH^- release and hence a reduction in the O 1s shoulder. Most probably there was an NaOH or $Ca(OH)_2$ surface layer that on immersion was washing off. However, the fact that there were still strong Ti^{4+} 2p peaks seen in the Ti 2p spectra suggested that the surface layer did not contain only Na or Ca hydroxide.

The C 1s spectrum following alkali treatment for all the samples (figure 6.3, third row, left) showed 3 peaks, with different intensities. The majority of the peaks were the result of organic contamination; with peaks associated with a range of C, O and N containing species being observed. However, all the alkali treated samples presented a peak which was slightly shifted towards higher binding energy, measured at 290.8 eV, and due to (CO_3^{2-}). This suggested the presence of carbonate on the surface of all alkali treated samples. The C/Ti ratio increased significantly ($p < 0.05$) following NaOH then $Ca(OH)_2$ treatment compared to the NaOH treated samples. The C/Ti ratio for the NaOH then

$Ca(OH)_2$ 1 h treated sample was significantly greater ($p < 0.05$) than the rest of the treated samples, which did not show any significant difference in their C/Ti ratios. This suggested that there was a combination of carbon from organic contamination and also the presence of calcium carbonate and or sodium carbonate from the alkali treatments.

Following heat treatment, the intensity of the C peaks for the C 1s spectra for all the samples decreased. It is noticeable the peaks above 287eV all decreased in magnitude. This suggested that the alkali treatments tended to form a range of organic species which were burnt off the sample during the heat treatment. The C/Ti ratio for the NaOH treated samples did not modify significantly. For the rest of the samples the C/Ti ratio resulted in a significant decrease ($p < 0.05$) compared to the C/Ti ratio before heat treatment. This was in agreement with the partial removal of some of the organic contamination.

Immersion in ultrapure water did not modify significantly the peak intensities or the C/Ti ratio for the NaOH treated samples, without and with heat treatment. Immersion in ultrapure water for the rest of the samples increased the intensity of the C peaks, illustrated also by the significant increase ($p < 0.05$) in the C/Ti ratio. This may have been the result of increased organic contamination as a result of changes in the surface structure following immersion.

The Na 1s spectra showed a single peak at ~1072 eV of various intensities for all the samples. Following heat treatment, neither the Na 1s peak shape nor intensity altered for almost all the samples, illustrated by the Na/Ti ratio which did not change significantly. The Ti-mixture' sample however showed a decrease in the intensity of the Na 1s peak, illustrated also by the significant decrease ($p < 0.05$) in the Na/Ti ratio.

Immersion in ultrapure water reduced significantly the intensity of the Na 1s peak for both the NaOH treated Ti samples, illustrated also by the significant decrease ($p < 0.05$) in the Na/Ti ratios. This suggested that a great deal of the Na present on the surface had been released into solution. Immersion in ultrapure water did not modify either the Na 1s spectra or the Na/Ti ratios for the NaOH then $Ca(OH)_2$ 1 h and 4 h treated samples, but the Na/Ti ratios decreased significantly ($p < 0.05$) for the NaOH followed by $Ca(OH)_2$ 24 h treated samples and the Ti-NaOH mixture 24 h' samples. Probably on

immersion all the Na was released, and the trace levels detected were probably an artefact due to the Ti Auger peak at 1072 eV.

The Ca 2p spectrum for the 'Ti-NaOH' sample suggested that Ca was not a contaminant of NaOH treated Ti samples with and without heat treatment, in agreement with samples analysed in 5.5. This is reflected also by the Ca/Ti ratio of the samples which again approached zero.

It was shown earlier that alkali treatment involving $Ca(OH)_2$ resulted in Ca being deposited on the surface of the Ti samples. It was interesting to determine whether the Ca 2p spectra showed the same effect. Indeed all the Ca 2p spectra showed the presence of Ca on the surface of the analysed samples. The Ca 2p spectra for the NaOH then $Ca(OH)_2$ treated samples were similar with regards to peak shape to the Ca 2p spectra reported to the NaOH then $Ca(OH)_2$ 1 h and 4 h treated samples in experiment 5.5, or to previously analysed Ca-Ti samples. However, the intensity of the peaks was different between the treatments. The NaOH then $Ca(OH)_2$ 1 h and 4 h treated samples had much higher intensities than the other samples. The Ca/Ti ratios for the same samples were significantly bigger ($p < 0.05$) than the NaOH then $Ca(OH)_2$ 24 h treated samples, or the 'Ti-mixture 24 h' samples or the Ca-Ti samples analysed in previous experiments. Heat treatment resulted in a slight decrease in the intensity of the peaks, illustrated also by the decrease in the Ca/Ti ratio (figure 6.1).

The peak shapes and positions for Ca 2p were more variable than the other spectra shown. This suggested that the Ca may be found in several different binding environments, like oxide, hydroxide, titanate (Takadama et al., 2001).

Immersion in ultrapure water reduced significantly the intensity of the Ca 2p peaks, as illustrated by the significant decrease in the Ca//Ti ratio ($p < 0.05$) for all the samples.

As was seen in Chapter 4 the immersion of the Ca-Ti samples in water decreased significantly the surface calcium, with the Ca ions being released into the solution. It was clear from the above that immersion of the alkali treated samples resulted in a significantly decreased Ca/Ti ratio. It would be interesting to assess using ion chromatography whether this reduction in the surface calcium was due also to Ca ion release.

6.2.3.2 Ion chromatography

Figure 6.4 shows the Ca ion release from alkali treated samples following immersion for 2 min, 4 h, and 24 h in ultrapure water at 37°C.

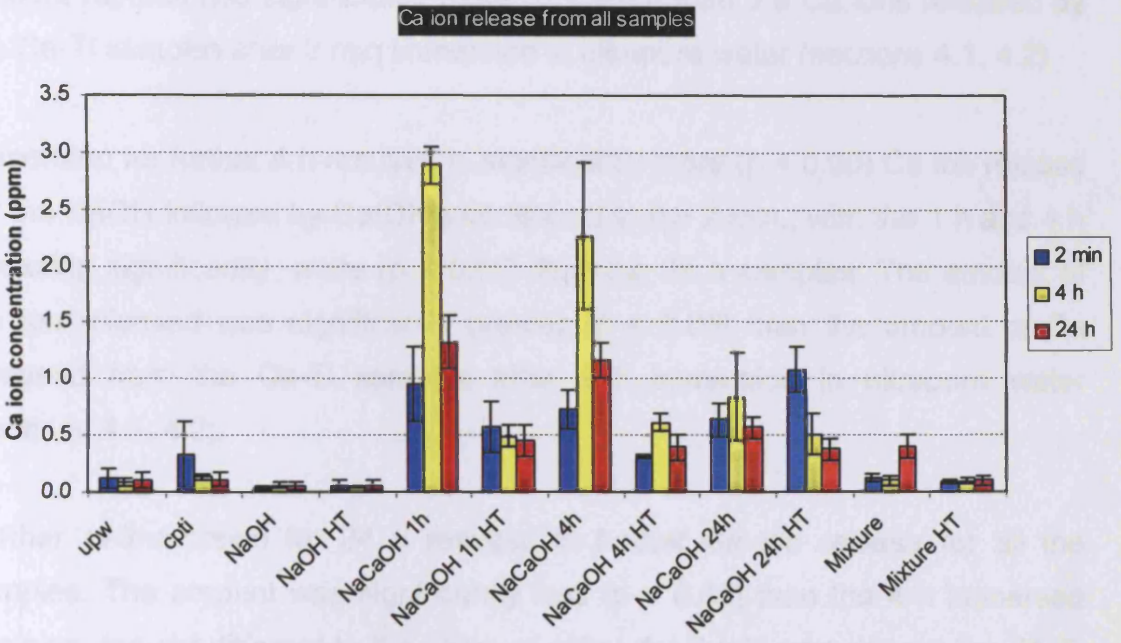

Figure 6. 4 Ca ion release from NaOH ('NaOH') and NaOH followed by $Ca(OH)_2$ treatment ('NaCaOH') and NaOH + $Ca(OH)_2$ mixture ('Mixture') for the Ti samples with (HT) and without heat treatment after 2 min, 4 h, and 24 h immersion in ultrapure water at 37°C.

As expected, all the controls showed only trace ion levels compared to the other samples at all the time points. The 2 min samples showed significantly more ($p < 0.05$) Ca ion release than the rest of the time points. This was caused by a single sample, which showed anomalous Ca ion release, most probably as a result of contamination. Possible reasons for the contamination were discussed in section 4.2. NaOH treatment of cp Ti discs showed no difference from controls so presented no discernible ion release, which agrees with no Ca detected at the surface.

Ion release from all the non heat treated NaOH followed by $Ca(OH)_2$ samples will be discussed first. Analysis of the 'Ti-mixture 24 h' samples will be carried out separately.

After 2 minutes immersion in ultrapure water, all the NaOH followed by $Ca(OH)_2$ samples resulted in a very high Ca ion release, with no significant difference in the Ca released between the treatment times (1 h, 4 h, or 24 h). However, this amount represented significantly more ($p < 0.05$) than the Ca ions released by the Ca-Ti samples after 2 min immersion in ultrapure water (sections 4.1, 4.2).

Immersion for further 4 h resulted in significantly more ($p < 0.05$) Ca ion release for the NaOH followed by $Ca(OH)_2$ compared to the 2 min., with the 1 h and 4 h releasing significantly more ($p < 0.05$) than the 24 h samples. The amount of Ca ion released was significantly greater ($p < 0.05$) than the amount of Ca released from the Ca-Ti samples after 4 h immersion in ultrapure water (sections 4.1, 4.2).

Further re-immersion for 24 h resulted in further Ca ion release for all the samples. The amount was significantly less ($p < 0.05$) than the 4 h immersed samples, but not different to the value of either the 2 min samples, or the Ca-Ti samples immersed for 24 h. This suggested that re-immersion caused further ion release, similar to the re-immersed Ca-Ti samples. However, it should be noted that the re-immersion times were very different (details in Chapter 4).

The non heat treated 'Ti-mixtures' showed the smallest Ca ion release from all the treatments involving $Ca(OH)_2$, suggesting that this was not an efficient method of laying down Ca on the surface.

Heat treatment generally slowed the Ca ion release from these samples, illustrated by the significant decrease ($p < 0.05$) in the ion release at all the time points when compared to the non heat treated samples. Unusually, heat treatment of the 24 h $Ca(OH)_2$ treated sample resulted in a significant increase ($p < 0.05$) in the ion released after 2 min, compared the all the other samples after 2 min.

In general, all the NaOH followed by $Ca(OH)_2$ heat treated looked reasonably similar in terms of their ion release, especially release after 4 h and 24 h immersion. This appeared to be in line with the XPS spectra, where both Ca 2p an O 1s spectra were reasonably similar for all heat treated samples compared to no heat treated, where the 24 h samples were quite different.

The surface analysis and ion chromatography data showed that the alkali treatment involving $Ca(OH)_2$ in the final stage resulted in a significant amount of Ca being deposited on the samples, of which some was released into solution. This behaviour is similar to the behaviour of Ca-Ti samples upon immersion into solution. Therefore, it would be interesting to see how depth distribution of Ca within the alkali treated samples compares with that of the Ca-Ti samples. It was also of interest to explore whether the sodium hydroxide pre-treatment was necessary for the incorporation of calcium in the surface. The following section presents experiments including depth profiles on a range of $Ca(OH)_2$ treated surfaces.

Depth profiling XPS

Figures 6.5, 6.6 and 6.8 and tables 6.2 and 6.3 show the Ca/Ti and O/Ti ratios and as a function of the etching time before and after 24 h immersion in ultrapure water. The Ca-Ti profile is also included in the figures for reference. Figure 6.7 shows the Ca 2p depth profiling spectra for alkali treated samples throughout the etching.

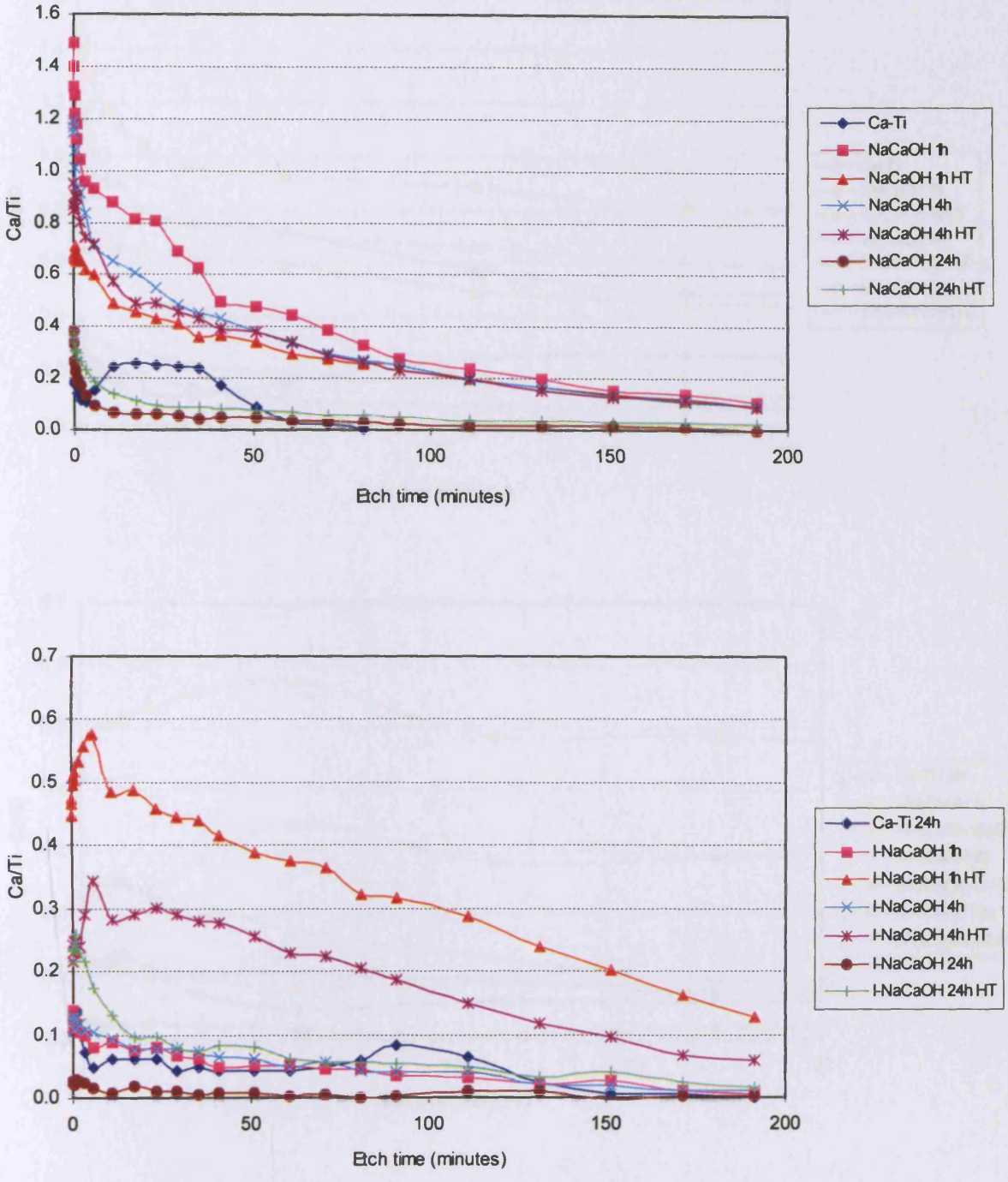

Figure 6. 5 Ca/Ti ratio for Ca-Ti and NaOH then $Ca(OH)_2$ treated Ti discs before (first row) and after (second row)24 h immersion in ultrapure water throughout etching.

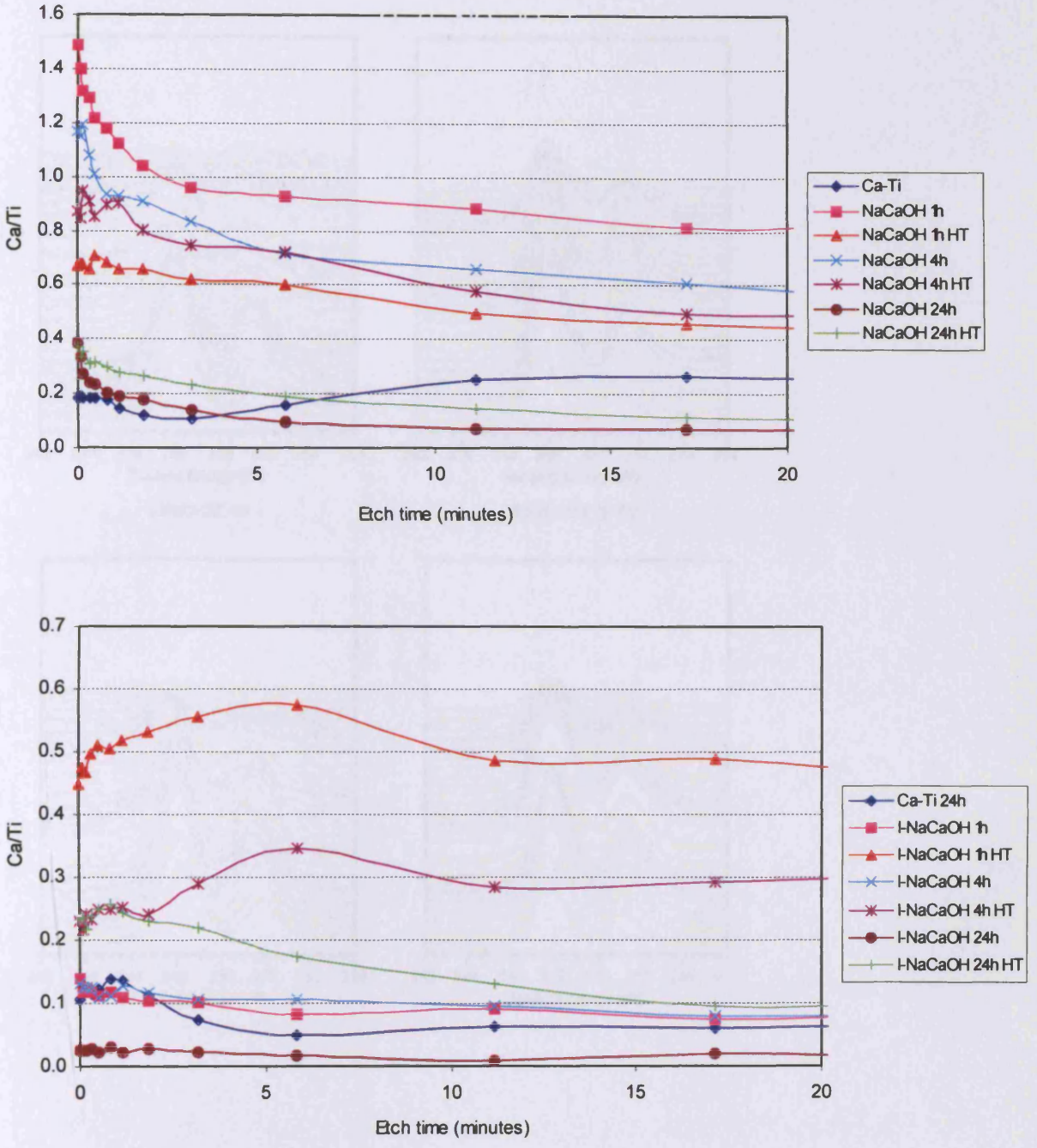

Figure 6. 6 First 20 minutes of etching for Ca/Ti ratio for Ca-Ti and NaOH then Ca(OH)2 treated Ti discs before (first row) and after (second row) 24 h immersion in ultrapure water.

I-NaCaOH 1h

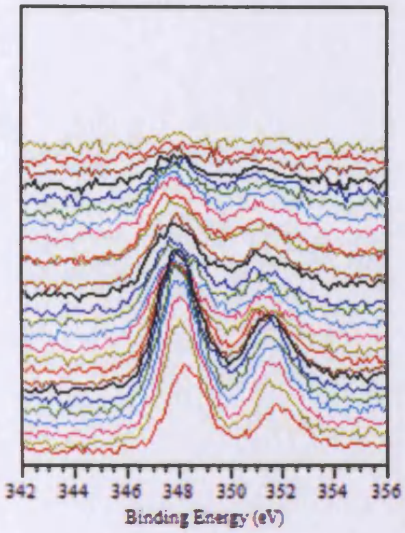

I-NaCaOH 1h HT

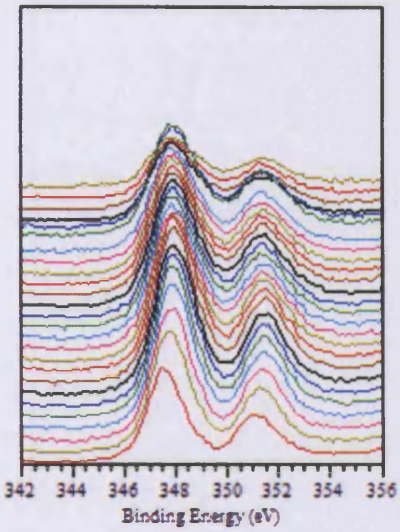

I-NaCaOH 4h

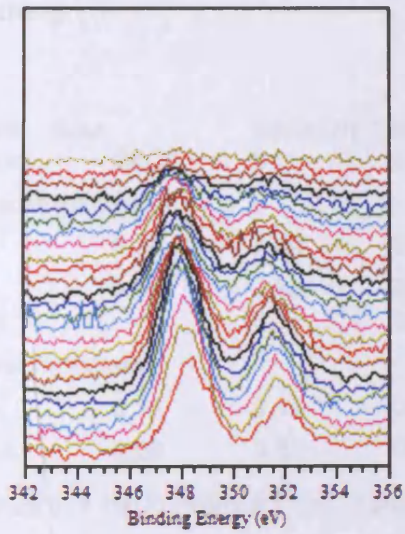

I-NaCa OH 4h HT

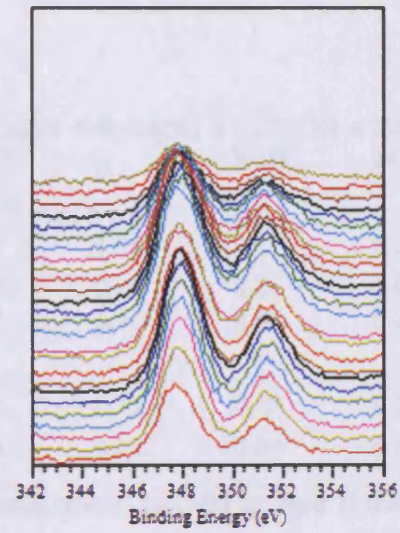

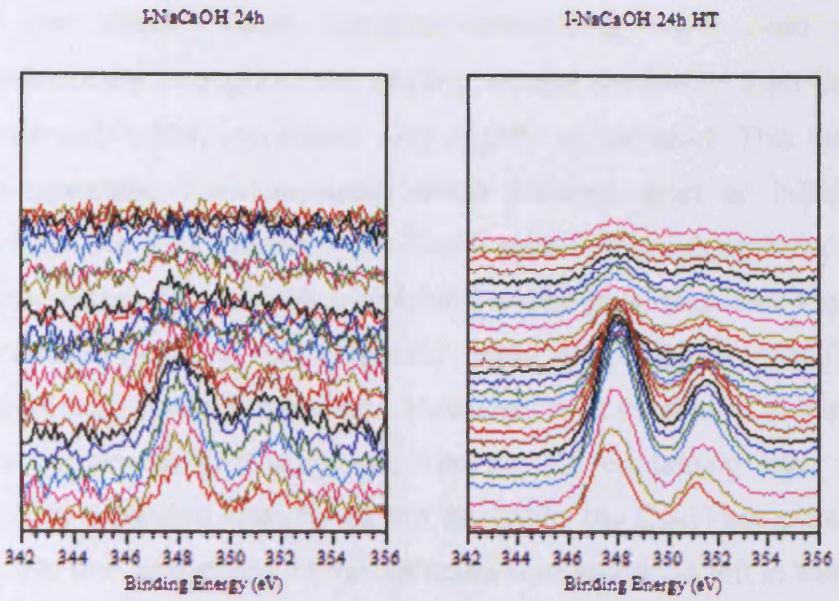

Figure 6. 7 Ca 2p depth profiling spectra for alkali treated samples throughout the etching

Etch time (min)	Ca-Ti	NaCaOH h	1 NaCaOH h HT	1 NaCaOH h	4 NaCaOH h HT	4 NaCaOH 24 h	NaCaOH 24 h HT
Before Immersion							
0	0.18	1.49	0.67	1.16	0.87	0.38	0.37
81	0.01	0.33	0.26	0.27	0.27	0.03	0.06
191		0.11	0.10	0.10	0.09	0.00	0.02
After Immersion							
0	0.10	0.14	0.45	0.13	0.23	0.03	0.23
191	0.00	0.01	0.13	0.01	0.06	0.00	0.02

Table 6. 1 Ca/Ti ratios for Ca-Ti and NaOH then Ca(OH)2 treated Ti discs before (first row) and after (second row)24 h immersion in ultrapure water at various etching times.

The graph of Ca/Ti ratio before immersion (figure 6.6 first row) shows that all the Ca depth profiles had similar shapes throughout the etching, but with different intensities, depending on the initial Ca/Ti ratio values. All the alkali treated samples had higher surface Ca than the Ca-Ti as implanted sample, with the highest Ca/Ti ratio being recorded for NaOH followed by $Ca(OH)_2$ 1 h then the 4 h treated samples. The length of the Ca treatment had a tendency to reduce the Ca present in the surface, probably because longer immersion time will reduce surface Ca.

All the alkali treated samples showed a Ca/Ti ratio which decreased continuously throughout the etching, except the NaOH then $Ca(OH)_2$ 4 h (± heat treatment) which increased very slightly at the start. This was different to the 'as-implanted' Ca-Ti samples which showed, after an initial decrease in the surface Ca, an increase in the Ca/Ti ratio in the sub-surface, followed again by a decrease. The overall trend for the samples was that the non-heat treated curves showed a considerable rapid decrease in Ca/Ti as the etched progressed below the surface. However, heat treatment of the samples reduced this considerably. It appeared that the Ca containing layer presented on the surface extended in as far as the 'as-implanted Ca-Ti samples.

By the end of etching all the samples had some Ca left in the sub-surface, with again the NaOH followed by $Ca(OH)_2$ 1 h and 4 h samples having much more than the rest (table 6.1 and figure 6.5), and 24 h the least. The amount left was greater than the as-implanted Ca-Ti which had no Ca left after 81 min of etching. At this etching time point, the NaOH followed by $Ca(OH)_2$ 1 h and 4 h treated samples had still significant amounts of Ca, with the 1 h showing much more than the rest. This appears to suggest that these alkali treatments resulted in a greater quantity and deeper distribution of the Ca in the samples sub-surface than Ca-Ti samples. Heat treatment resulted in less Ca on the surface for the NaOH followed by $Ca(OH)_2$ 1 h and 4 h treated samples, but similar amount and distribution within the sample. There was no difference in the Ca distribution between the non and HT treated NaOH followed by $Ca(OH)_2$ 24 h treated samples; both showed low Ca/Ti ratios.

Following immersion in ultrapure water, the Ca/Ti ratio on the surface decreased significantly for most of the alkali treated samples. The NaOH followed by $Ca(OH)_2$ 1 h and 4 h HT samples, however had much more Ca on the surface than the rest of the samples and even more than the Ca-Ti samples before immersion. Also these samples showed subsurface maxima in the Ca/Ti ratio after around 6 minutes of etching. This is different to the Ca-Ti samples and non-heat treated alkali treated samples. In contrast to pre-immersion, the non-heat treated shows less variation in Ca/Ti compared to the heat treated samples.

Following the surface effects all the samples showed a continual decrease in the Ca, and by the end of etching all the samples, except alkali heat treated samples, had virtually no Ca remaining (figure 6.5). The alkali heat treated samples, especially the NaOH followed by $Ca(OH)_2$ 1 h and 4 h HT samples and to a lesser extent the NaOH followed by $Ca(OH)_2$ 24 h HT samples, had significant quantities of Ca present at the end of etching (figure 6.5). In the case of the NaOH followed by $Ca(OH)_2$ 1 h HT sample the Ca/Ti ratio at the end of the etching was greater than the Ca-Ti had on its surface after immersion.

The Ca 2p depth profiling spectra (figure 6.3) clearly illustrated the presence of Ca 2p peaks on the heat treated samples throughout the etching, reaching still significant intensity at the end of etching. The Ca-Ti and the non-HT alkali treated samples however showed a reduction in intensity up to almost disappearance of the Ca 2p peaks by the end of etching.

These results showed that not all the Ca existent on the non-HT alkali treated samples has been released by 24 h, as there is still Ca closer to the surface. However, the heat treated samples show Ca left at the end of etching which was also illustrated by the lower Ca release from the heat treated samples during the 24 h immersion period. This suggested that heat treatment of alkali treated samples resulted in a deeper distribution of Ca, and the surface had become more passive in nature. Analysis of the O depth profile may suggest an explanation for this.

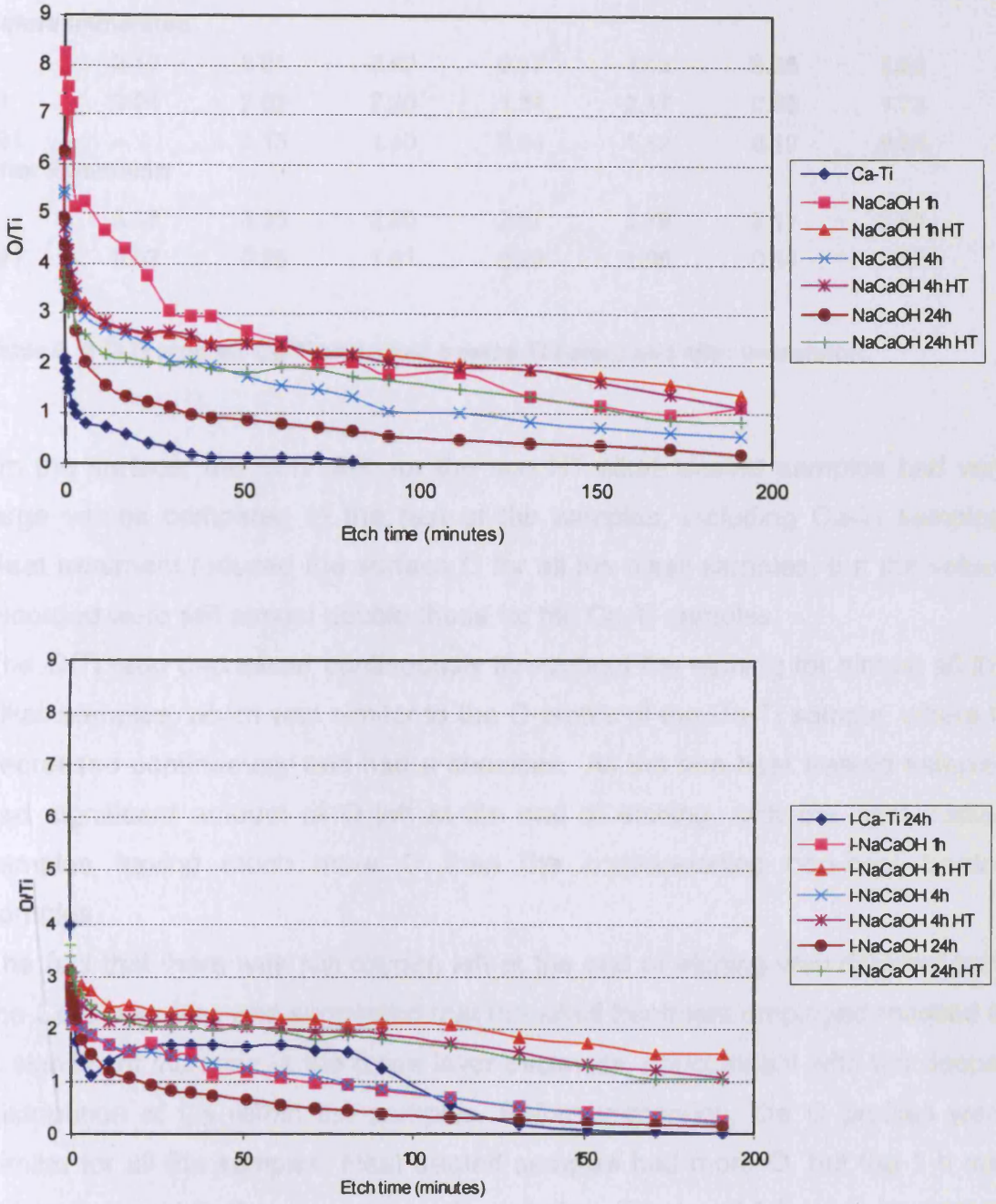

Figure 6. 8 O/Ti ratio for Ca-Ti and NaOH then $Ca(OH)_2$ treated Ti discs before (first row) and after (second row)24 h immersion in ultrapure water as a function of etching time.

Etch time (min)	Ca-Ti	NaCaOH 1 h	NaCaOH 1 h HT	NaCaOH 1 h	NaCaOH 4 h HT	NaCaOH 4 24 h	NaCaOH 24 h HT
Before Immersion							
0	2.10	8.24	3.92	6.17	4.42	6.25	3.56
81	0.04	2.02	2.20	1.34	2.17	0.66	1.73
191	-	1.13	1.40	0.54	1.12	0.19	0.83
After Immersion							
0	3.95	3.03	2.80	2.57	2.79	3.11	3.59
191	0.02	0.25	1.51	0.20	1.06	0.14	1.02

Table 6. 2 O/Ti ratio for Ca-Ti and alkali treated Ti before and after immersion.

On the surface, the O/Ti ratio for the non HT alkali treated samples had very large values compared to the rest of the samples, including Ca-Ti samples. Heat treatment reduced the surface O for all the alkali samples, but the values recorded were still almost double those for the Ca-Ti samples.

The O/Ti ratio decreased continuously throughout the etching for almost all the alkali samples, which was similar to the O profile of the Ca-Ti sample, where O decreased continuously and had a shoulder. All the non heat treated samples had significant amount of O left at the end of etching, with the heat treated samples having much more O than the corresponding non-heat treated samples.

The fact that there was still oxygen left at the end of etching was different from the Ca-Ti samples and suggested that the alkali treatment employed resulted in a significant increase in the oxide layer thickness, concomitant with the deeper distribution of Ca within the samples. Before immersion, the O profiles were similar for all the samples. Heat treated samples had more O, but the 1 h non HT had very high O in the near surface region. The trend following immersion was revealing. Profiles split into 2 groups: heat treated and non heat treated samples, with the non HT having lower ratios. The O/Ti tended to decrease for the non HT samples. This was difficult to explain but may be related to $Ca(OH)_2$ movement through the oxide lattice (i.e. the samples with high release rates are left with a highly defective titanium oxide/dioxide lattice).

6.3 CALCIUM HYDROXIDE TREATMENT OF CP TI SAMPLES.

6.3.1 Aims and objectives

The previous section showed that NaOH followed by $Ca(OH)_2$ treatments could be employed to increase the levels of Ca found on cp Ti surfaces. The work described in this section aimed to employ simpler treatments involving $Ca(OH)_2$ only. These treatments were compared to those described previously.

6.3.2 Materials and method

$Ca(OH)_2$ treatment was carried out on the surface of 12 cp Ti discs. The discs were treated with 0.05 M $Ca(OH)_2$ solution for 24 h at 60°C, using the same protocol as described earlier in 6.2.2. After the treatment, the discs were dipped in ultrapure water, dried with compressed air and placed in aluminium foil. From these 12 treated discs, 6 were heat treated at 600°C for 1 h. To enable direct comparison with the work in the previous section, 12 discs were prepared with 10 M NaOH solution followed by $Ca(OH)_2$ solution for 24 h following the protocol described in 6.2.2. After the treatment, the discs were dipped in water, dried with compressed air and placed in aluminium foil. From these discs, 6 were heat treated at 600°C for 1 h as described in 6.2.2.

The discs were immersed in well plates (lot 3526, Corning Incorporated, Corning, NY 14831) using 1 ml of UPW at 37°C.The immersion times were 2 min, 4 h and 24 h. Ultrapure water and cp Ti discs were also immersed as controls. Ca-Ti discs were also immersed to provide a complete comparison. After 2 min, first the water was removed from the well plates and placed in vials for analysis by ion chromatography. Then the discs were dried with compressed air and placed in fresh ultrapure water in new well plates each time. This was repeated at each time point. All the discs were analysed before and after immersion with XPS using an AlKα twin anode source. The solutions were analysed using ion chromatography.

6.3.3 Results and discussion

6.3.3.1 Appearance

Before immersion

$Ca(OH)_2$ treatment resulted in samples which changed their appearance. The non heat treated Ti samples were matt silver, darker than the cp Ti samples, with a slightly rough appearance. The heat treated Ti samples were matt grey-silver, with pale blue tint. The change in the colour may be attributed to a modification in the thickness of the oxide layer, as explained in section 4.2, probably accompanied by a change in refractive index.

The Ti samples treated with NaOH followed by $Ca(OH)_2$ treatment with no heat treatment were uniform with regards to the appearance and looked similar to the $Ca(OH)_2$ treated samples without heat treatment. These samples had slightly rough surface and were matt silver, darker than before the alkali treatment. The heat treated samples were again matt grey – silver, with a pale blue tint, similar with the heat treated $Ca(OH)_2$ samples. Two of the samples which were in the furnace toward the door became bluer then the other 4 which were toward the middle of the furnace. This was most likely due to either slightly different temperatures found close to the furnace door, or an effect of heating and cooling rates.

The Ca implanted discs (Ca-Ti) were shiny silver before immersion, as described in previous experiments.

After immersion in ultrapure water

None of the alkali treated samples changed colour following immersion. This suggested that the thickness of the oxide layer did not change following immersion.

The Ca implanted discs changed colour following immersion as seen in previous experiments (chapter 4), but the behaviour was not uniform. After 4 h immersion samples 1, 3 and 5 turned almost fully blue (>90%). All the other samples were ~ 10% blue at the edges. Immersion for further 24 h did not

modify the colour significantly. The blue patch on the others increased slightly (not more than 15%).

6.3.3.2 Surface analysis

Figure 6.5 and 6.6 show the elemental ratios recorded for Ca-Ti and alkali treated samples before and after immersion in ultrapure water at 37°C. Figure 6.7 show the XPS spectra for the Ca-Ti and alkali treated samples before immersion in ultrapure water. As the XPS spectra after immersion in ultrapure water did not show significant differences to the XPS spectra before immersion, they were not presented.

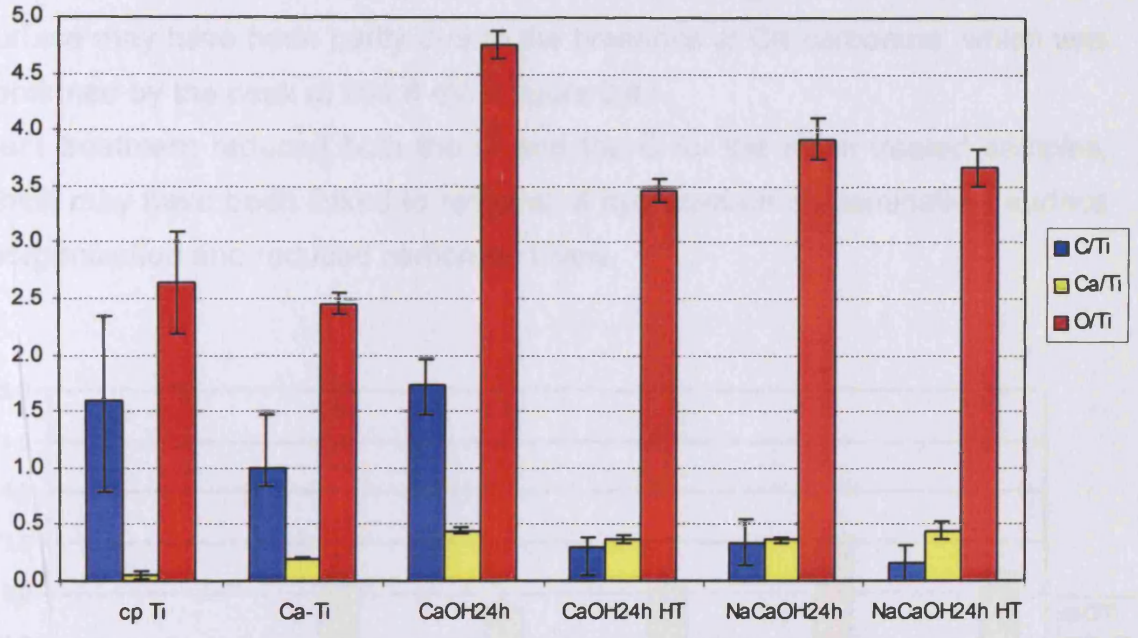

Figure 6. 9 C/Ti, Ca/Ti, and O/Ti ratios (average and SD) for Ca-Ti and alkali treated samples before immersion in ultrapure water at 37°C.

From figure 6.9 could be observed that all of the alkali treatments resulted in significantly more Ca on the surface than Ca-Ti samples. The Ca/Ti ratios did not differ between the NaOH and $Ca(OH)_2$ 24 h treatment whether heat treated or otherwise. The Ti 2p spectra showed that heat treatment reduced the

intensity of the Ti^{n+} peak, suggesting that the surface layer increased in thickness. Both alkali treatments showed some signal below the strong Ti^{4+} $2p_{3/2}$ peak; it was not possible to isolate a peak in the low binding energy region but there was a definite signal in this area. This is likely to have been due to Ti^{+}, Ti^{2+} and Ti^{3+} suboxide species. This could have been due to a highly defective structure or to the interface between the oxide and substrate being at around 10 nm from the surface.

Again large amounts of oxygen were present on the alkali treated surfaces, but there were no significant differences between the alkali treatments. The O/Ti ratios were significantly greater ($p < 0.05$) than the O/Ti ratio for the Ca-Ti samples. C was also present on the surface, significantly more for the $Ca(OH)_2$ 24 h than the rest of the samples. The presence of high O and C levels on the surface may have been partly due to the presence of Ca carbonate, which was confirmed by the peak at 291.8 eV in figure 6.4.

Heat treatment reduced both the O and the C for the alkali treated samples, which may have been linked to removal of hydrocarbon contamination, surface reorganization and reduced carbonate levels.

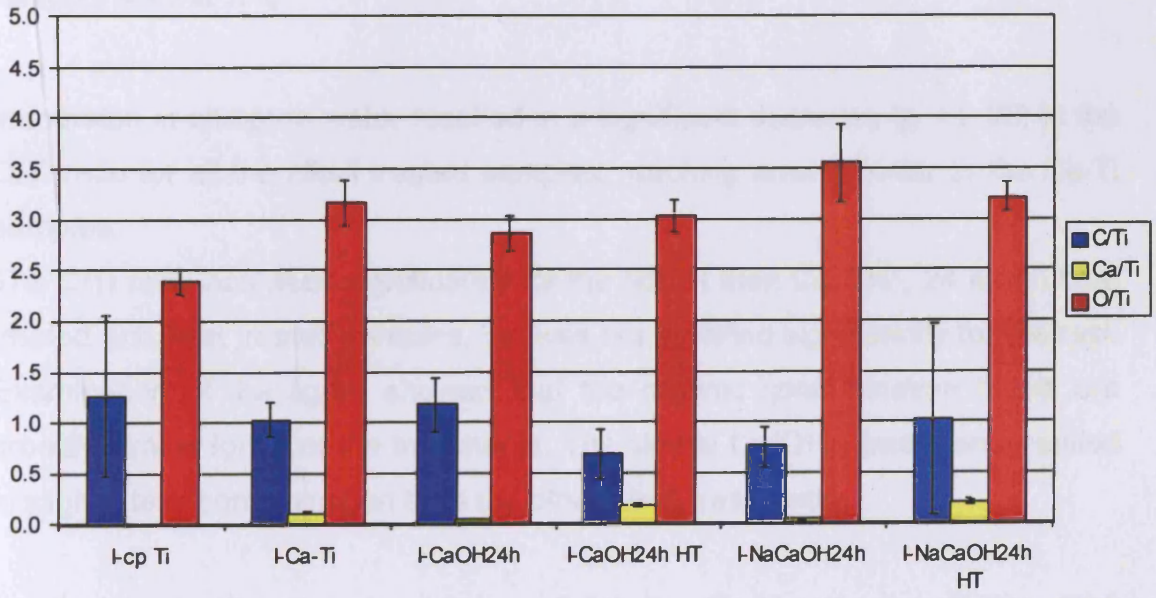

Figure 6. 10 C/Ti, Ca/Ti, and O/Ti ratios (average and SD) for cp Ti, Ca-Ti and alkali treated samples after immersion in ultrapure water at 37°C.

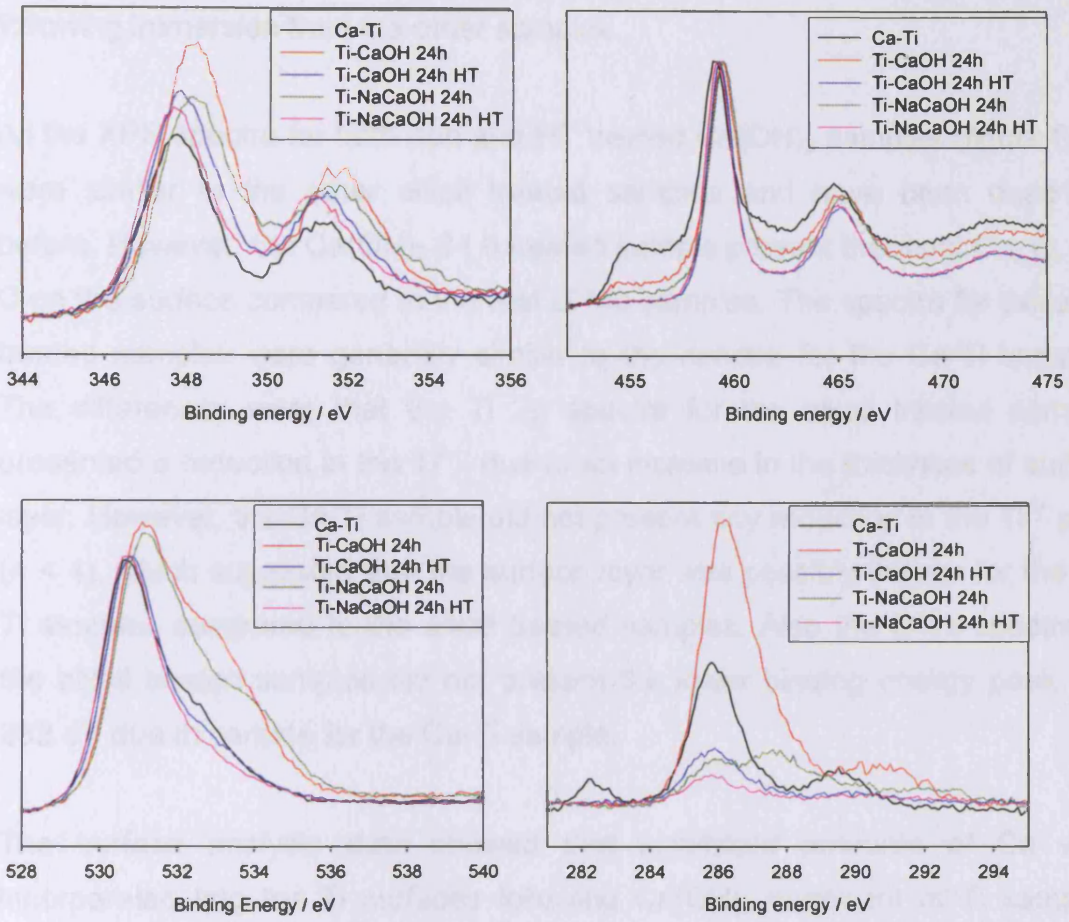

Figure 6. 11 XPS spectra for Ca-Ti and alkali treated samples before immersion in ultrapure water at 37°C.

Immersion in ultrapure water resulted in a significant decrease ($p < 0.05$) in the O/Ti ratio for all the alkali treated samples, reaching levels similar to the Ca-Ti samples.

The C/Ti ratio increased significantly for the NaOH then $Ca(OH)_2$ 24 h non heat treated and heat treated samples, but was not modified significantly for the rest. Examination of the figure showed that the organic contamination levels are broadly similar for all of the treatments. The simple $Ca(OH)_2$ treatment resulted in slightly less contamination than the other alkali treatments.

Immersion significantly reduced ($p < 0.05$) the Ca/Ti ratio for all the alkali samples analysed, similar to the Ca-Ti samples. However, both the alkali

treated HT samples retained significantly more ($p < 0.05$) Ca on the surface following immersion than the other samples.

All the XPS spectra for both non and HT treated $Ca(OH)_2$ samples (figure 6.11) were similar to the other alkali treated samples and have been described before. However, the $Ca(OH)_2$ 24 h treated sample present the most Ca, O, and C on the surface compared to the rest of the samples. The spectra for the alkali treated samples were generally similar to the spectra for the Ca-Ti samples. The differences were that the Ti 2p spectra for the alkali treated samples presented a reduction in the Ti^{n+}, due to an increase in the thickness of surface layer. However, the Ca-Ti sample did not present any reduction in the Ti^{n+} peak ($n < 4$), which suggested that the surface layer was possibly thinner for the Ca-Ti samples compared to the alkali treated samples. Also the C 1s spectra for the alkali treated samples did not present the lower binding energy peak at ~ 282 eV due to carbide for the Ca-Ti sample.

The surface analysis data showed that significant amounts of Ca were incorporated into the Ti surfaces following $Ca(OH)_2$ treatment of Ti samples. The Ca decreased significantly following immersion in water, probably as a result of release into solution. Ion chromatography measurements were carried out to confirm this.

6.3.3.3 Ion release

Figure 6.12 presents the Ca ion release for alkali treated samples Ca-Ti samples and controls (ultrapure water and cp Ti samples) following immersion in ultrapure water for 2 min, 4 h and 24 h.

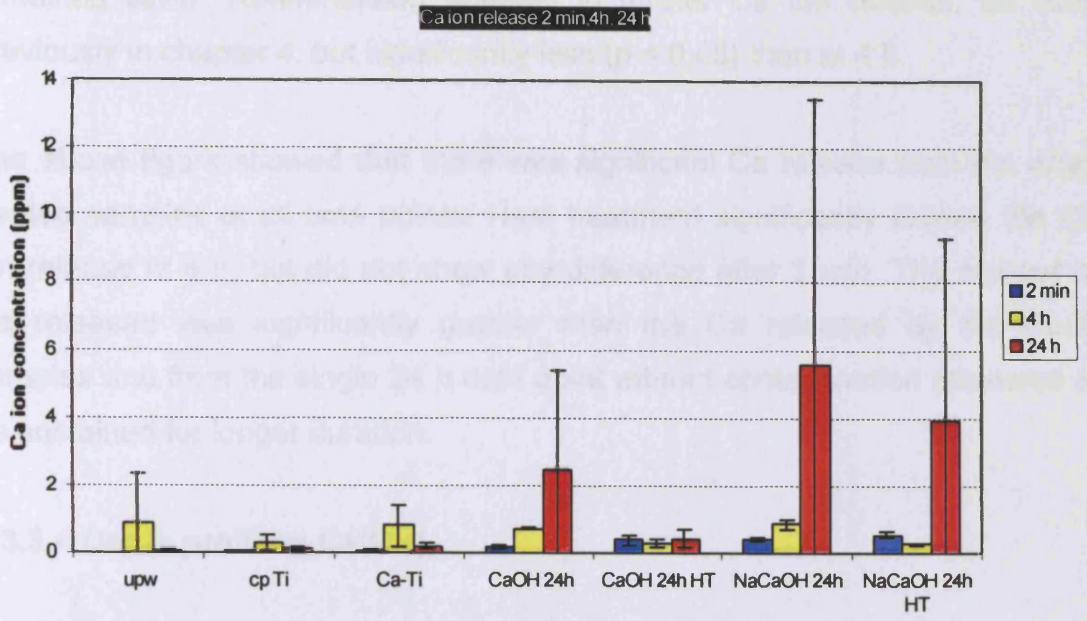

Figure 6. 12 Ca ion release from cp Ti, Ca-Ti and alkali treated Ti samples after immersion in ultrapure water.

As some contamination was experienced in these experiments, those with errors higher than the data point were likely to be from contamination and were excluded from the discussion. As three of the 4 samples at 24 h treatments were contaminated, then the results for this time point were not analysed in detail.

The control samples showed minimal Ca release in solution at any time point, except 2 min ultrapure water which showed this significantly more than other controls. This was caused by a single sample out of 6 and was most probably due to contamination

The Ca-Ti samples showed the expected release-values, similar to the levels found in the experiments in section 4.3. The release increased significantly after 4 h immersion, as seen previously.

There was again a correlation between the colour change and the amount of ions released: samples that turned blue released much more than samples that

remained silver. Re-immersion resulted in further Ca ion release, as seen previously in chapter 4, but significantly less ($p < 0.05$) than at 4 h.

The above figure showed that there was significant Ca release from the alkali treated samples at all time points. Heat treatment significantly slowed the Ca ion release at 4 h, but did not show any difference after 2 min. The amount of Ca released was significantly greater than the Ca released by the Ca-Ti samples and from the single 24 h data point without contamination appeared to be sustained for longer duration.

6.3.3.4 Depth profiling $Ca(OH)_2$

Figures 6.13 and 6.14 show the Ca/Ti ratio and O/Ti ratio for Ca-Ti and $Ca(OH)_2$ treated Ti discs before (first row) and after (second row) 24 h immersion in ultrapure water throughout etching

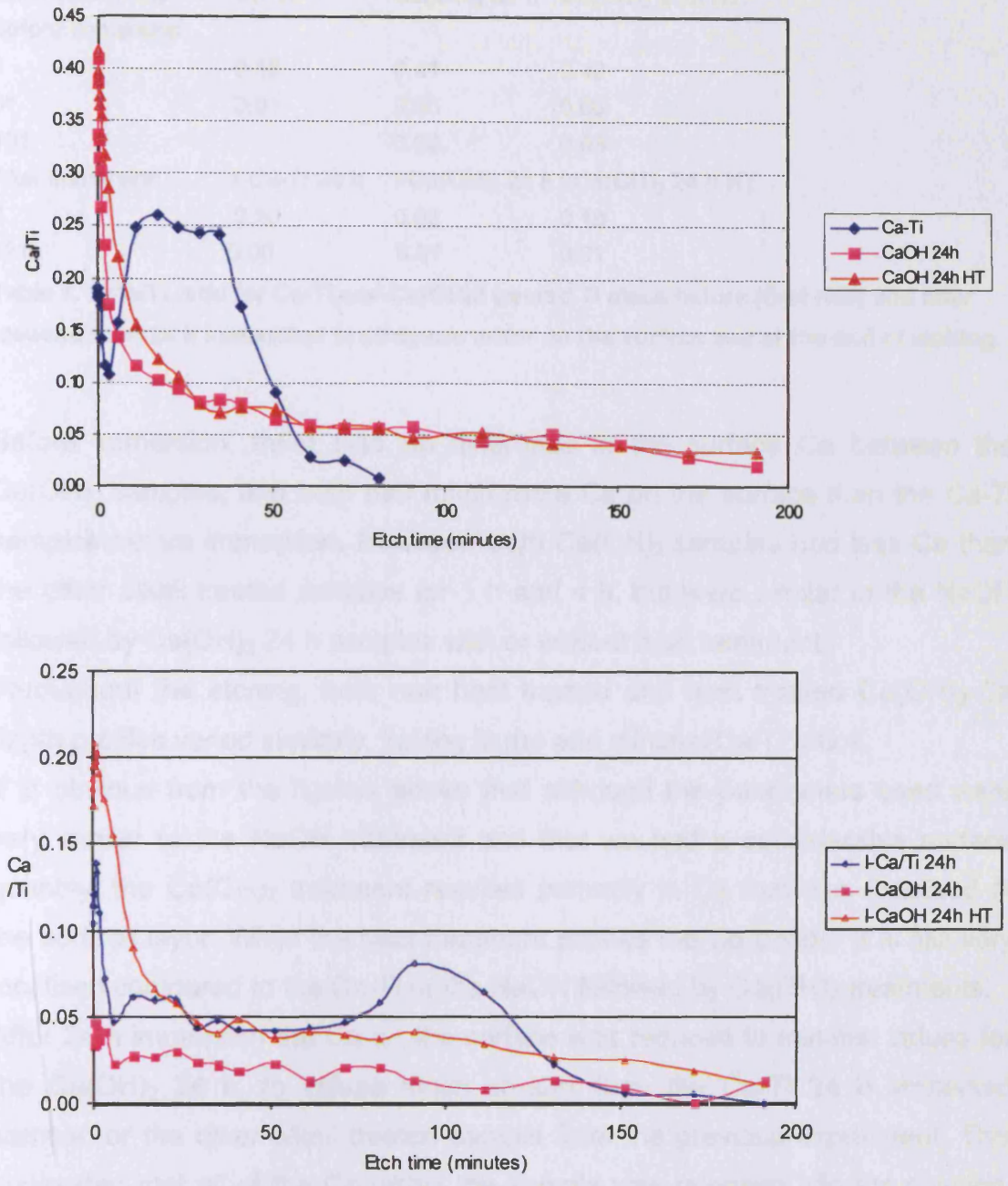

Figure 6. 13 Ca/Ti ratio for Ca-Ti and $Ca(OH)_2$ treated Ti discs before (first row) and after (second row) 24 h immersion in ultrapure water throughout etching.

Etch time (min)	Ca-Ti	$Ca(OH)_2$ 24 h	$Ca(OH)_2$ 24 h HT
Before immersion			
0	0.18	0.41	0.42
81	0.01	0.06	0.06
191		0.02	0.03
After immersion	**I-Ca-Ti 24 h**	**I-$Ca(OH)_2$ 24 h**	**I-$Ca(OH)_2$ 24 h HT**
0	0.10	0.03	0.18
191	0.00	0.01	0.01

Table 6. 3 Ca/Ti ratio for Ca-Ti and Ca(OH)2 treated Ti discs before (first row) and after (second row) 24 h immersion in ultrapure water on the surface and at the end of etching.

Before immersion, there was no difference in the surface Ca between the $Ca(OH)_2$ samples, and both had much more Ca on the surface than the Ca-Ti samples before immersion. However, both $Ca(OH)_2$ samples had less Ca than the other alkali treated samples for 1 h and 4 h, but were similar to the NaOH followed by $Ca(OH)_2$ 24 h samples with or without heat treatment.

Throughout the etching, both non heat treated and heat treated $Ca(OH)_2$ Ca depth profiles varied similarly, having in the end minimal Ca/Ti ratios.

It is obvious from the figures above that although the parameters used were very similar to the NaOH treatment and that we had a considerable surface quantity, the $Ca(OH)_2$ treatment resulted primarily in Ca that was localised at the surface layer. While the heat treatment pushes the Ca deeper it is still very localised compared to the Ca-Ti or the NaOH followed by $Ca(OH)_2$ treatments.

After 24 h immersion the Ca on the surface was reduced to minimal values for the $Ca(OH)_2$ 24 h, to values much smaller then the Ca-Ti 24 h immersed sample, or the other alkali treated sample from the previous experiment. This suggested that all of the Ca within the sample was released into the solution. The immersed HT $Ca(OH)_2$ 24 h sample did not release all of its Ca into solution. Indeed it retained a higher peak Ca/Ti ratio than the 24 h immersed Ca-Ti sample.

$Ca(OH)_2$ treatment resulted in significant amount of Ca incorporated into the surface. This Ca was released in quantities comparable to the other alkali treated samples, and significantly more than the Ca-Ti samples at the times examined. The treatment resulted in a less deep distribution of the Ca and also

O in the sample as compared to the treatments using NaOH followed by $Ca(OH)_2$. The reduced amount of Ca retained in these surfaces suggested that they should release less Ca over longer time periods than the NaOH $Ca(OH)_2$ treated samples. These $Ca(OH)_2$ only treatments may match the ion release profile of Ca-Ti better than the other treatments. Longer immersion time studies would be probably appropriate to be employed.

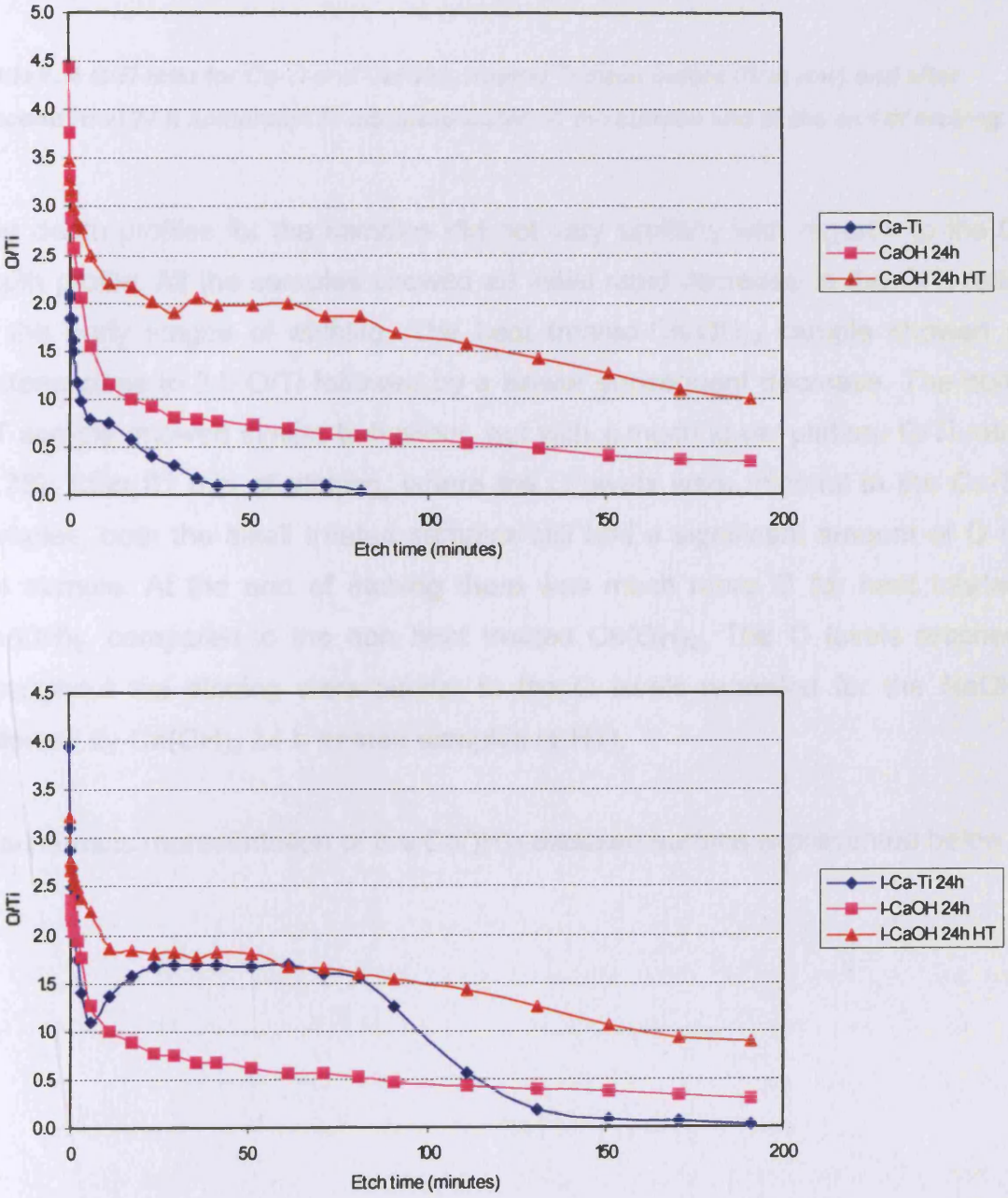

Figure 6. 14 ***O/Ti ratio for Ca-Ti and $Ca(OH)_2$ treated Ti discs before (first row) and after (second row) 24 h immersion in ultrapure water throughout etching.***

Etch time	**Ca-Ti**	**$Ca(OH)_2$ 24 h**	**$Ca(OH)_2$24 h HT**
Before immersion			
0	2.10	4.42	3.47
81	0.04	0.61	1.85
191		0.35	0.99
After immersion			
Etch time	**I-Ca-Ti 24 h**	**I-$Ca(OH)_2$ 24 h**	**I-$Ca(OH)_2$ 24 h HT**
0	3.95	2.35	3.22
191	0.02	0.29	0.88

Table 6. 4 ***O/Ti ratio for Ca-Ti and $Ca(OH)_2$ treated Ti discs before (first row) and after (second row) 24 h immersion in ultrapure water on the surface and at the end of etching.***

The depth profiles for the samples did not vary similarly with regards to the O depth profile. All the samples showed an initial rapid decrease in the O/Ti ratio in the early stages of etching. The heat treated-$Ca(OH)_2$ sample showed a plateau close to 2.0 O/Ti followed by a slower subsequent decrease. The non-HT sample showed similar behaviour, but with a much lower plateau O/Ti ratio (0.75). After 81 min of etching, where the O levels were minimal in the Ca-Ti samples, both the alkali treated samples still had a significant amount of O in the sample. At the end of etching there was much more O for heat treated $Ca(OH)_2$ compared to the non heat treated $Ca(OH)_2$. The O levels reached throughout the etching were similar to the O levels recorded for the NaOH followed by $Ca(OH)_2$ 24 h treated samples (± HT).

A schematic representation of the $Ca()H)_2$-exposed surface is presented below.

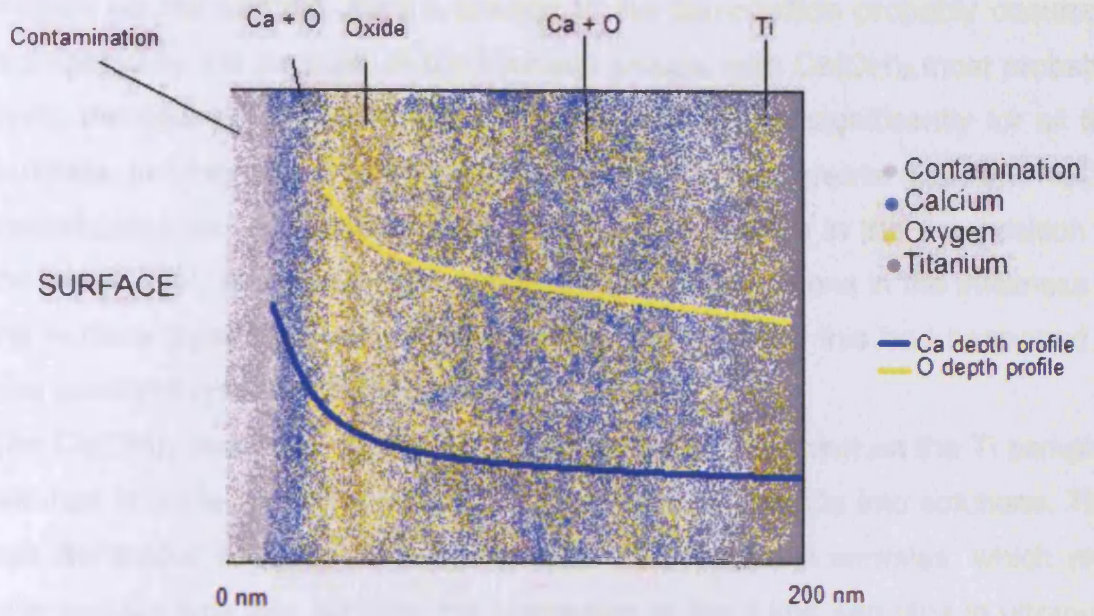

Scheme 6.1.Diagrammatic representation of the $Ca(OH)_2$–exposed surface including the Ca depth profile (blue line) and O depth profile (yellow line).

Immersion has little effect on the O/Ti for these samples, with the exception of Ca-Ti which shows the sub-surface oxidation reported extensively in Chapter 4.

6.4. CONCLUSIONS

NaOH treatment resulted in high levels of sodium on the surface with the suspected formation of Na_2CO_3, Na incorporated into the surface, the formation of titanate. Heat treatment decreased the amount of Na and carbonate groups. Ca was present only in very small amounts on the NaOH treated samples.

NaOH treatment followed by calcium hydroxide treatment resulted in high levels of calcium on the surface, independent of the time for which the $Ca(OH)_2$ treatment was performed. Heat treatment reduced the amount of Ca on the surface, except for the NaOH followed by 24 h $Ca(OH)_2$ where it increased. The highest amounts of Ca were seen for NaOH followed by $Ca(OH)_2$ 1 h o heat treatment before immersion, and the smallest for the 'Ti-NaOH mixture 24 h' no heat treatment . Following $Ca(OH)_2$ treatment, the sodium present on the surface was reduced to minimal amounts.

NaOH followed by $Ca(OH)_2$ treatment resulted in a significant increase in the O present on the surface. Also a change in the composition probably occurred, highlighted by the increase in the hydroxyl groups, with $Ca(OH)_2$ most probably being the cause. Heat treatment reduced the O/Ti ratio significantly for all the samples, but the values recorded were still significantly greater than the NaOH treated samples. This was probably caused by a change in the composition of the oxide layer, and maybe less contamination. Modifications in the thickness of the surface layer could also have been the cause, but if this had happened, it was outside the range of XPS detection.

The $Ca(OH)_2$ treatment carried out following NaOH treatment on the Ti samples resulted in surfaces that released significant amounts of Ca into solutions. This was behaviour was similar to that of 'as-implanted Ca-Ti samples, which also released Ca ions into solution. Re-immersion of the same samples in ultrapure water resulted in further ion release for all the treatments, except the mixtures. Interestingly, the amount of Ca ions released by the alkali treated samples was significantly greater than the Ca released by the Ca-Ti samples.

From the depth profiles before immersion the key results are that the samples had similar Ca and O depth profiles throughout the etching and that for some surfaces there was considerable Ca and O remaining at the end of etching. This suggested that these samples may have continued to release Ca over a longer time than the Ca-Ti which showed lower levels on Ca and O at the end of etching.

Immersion resulted in a decrease in both Ca/Ti and O/Ti ratio for all the samples. The HT alkali samples had much more Ca and O both on the surface and at the end of etching than the rest of the alkali treated samples or the Ca-Ti samples. This may suggest that HT resulted in a deeper distribution of both Ca and O throughout the samples than the rest of the samples, with the Ca being released much slower. Indeed, the ion release also illustrates a slower ion release in 24 h for the alkali HT samples.

The NaOH + $Ca(OH)_2$ treatment of Ti samples resulted in a surface which had the most Na on the surface and other contamination and the least Ca ion release from all the other treatments, so it presents the least advantages of all the alkali treatments employed.

$Ca(OH)_2$ treatment appears to be a good method of depositing Ca on the cp Ti surface. However, the amount of Ca on the surface and the ion release are smaller than the NaOH followed by $Ca(OH)_2$ treatment 1 h and 4 h (± HT).However, this method is simpler than the methods which involve NaOH treatment as a first step in the alkali treatment.

6.4 SUMMARY

Alkali treatment proved to be a very encouraging method of depositing Ca on the Ti surface, as an alterative method to Ca ion implantation. It resulted in a significant increase in the surface layer thickness compared to the cp Ti or Ca-Ti, with the formation of Na and Ca oxide / hydroxide, Na and Ca carbonate and possibly titanate, as suggested by Kim et al. (1996). However it was not possible to determine the presence of titanate using standard resolution XPS as the peak shift between the oxide and titanate was not well resolved.

The NaOH+ $Ca(OH)_2$ treated samples (the 'Ti-mixtures') had significantly lower amount of Ca on their surface compared to the other alkali treated samples. However, the Ca/Ti ratio was still similar to the Ca/Ti ratio recorded for the as-implanted Ca-Ti.

Depth profiling studies showed that the all the NaOH followed by $Ca(OH)_2$ heat treatment samples have retained large amounts of Ca within the samples. They would probably undergo longer term ion release.

There was no difference with regards to O surface characteristics and ion release between the simple $Ca(OH)_2$ treatment and the 24 h alkali treatment as the final stage the $Ca(OH)_2$ treatment. $Ca(OH)_2$ treatment resulted in similar results to the NaOH followed by $Ca(OH)_2$ 24 h ± heat treatment samples with regards to Ca and O distribution throughout the sample and the ion release, so it was probably easier to do this the first treatment, which would have eliminated the NaOH stage and potentially contaminants. However, this could have possible affected the bioactivity of the samples, as NaOH treatment results in a surface which is more bioactive and osseointegrates more quickly. However, depth profiles show that the total Ca added is far lower and the distribution far

closer to the surface. The result is that these surfaces have release characteristics similar to Ca-Ti.
Significant quantities of Ca were left at the end of etching for both non-heat treated and HT samples. This Ca however was released for the non HT samples, and was released only partially for the HT samples, suggesting that HT slows the ion release.

It appears that theses alkali methods of depositing Ca on the surface of cp Ti are successful. Their advantages compared with Ca ion implantation are lower cost, easier to perform, and widely available compared to ion implantation. However, more studies are necessary to ascertain their effect on cell behaviour.

6.5 LIST OF REFERENCES

Chosa, N., M. Taira, M., Saitoh, S., Sato, N.,Araki, Y. (2004)
Characterization of apatite formed on alkaline-heat-treated Ti.Journal of Dental Research 83(6): 465-469

Fujibayashi, S. Nakamura, T. Nishiguchi, S. Tamurhas, J. Uchida, M., Kim, H.M., Kokubo, T. (2001)
Journal of Biomedical Materials Research 56 : 235-276

Kim, H.M., Miyaji, F., Kokubo, T., Nakamura, T. (1996)
Preparation of bioactive Ti and its alloys via simple chemical surface treatment
Journal of Biomedical Materials Research 32(3): 409-417

Kim, H.M., Miyaji, F., Kokubo, T., Nakamura, T. (1997)
Bonding strength of bone-like apatite layer to Ti metal substrate.
Journal of Biomedical Materials Research 38: 121-127

Himeno, T. Kawashita, M. Kim, H.M. Kokubo, T., Nakamura T2001)
In: S. Brown, I.R. Clarke and P. Williams, Editors, Bioceramics vol. 14, Trans Tech Publishers, Switzerland 641–644.

Kokubo T, Ito S, Huang ZT, Hayashi T, Sakka S. (1990)
Ca, P-rich layer formed on high-strength bioactive glass-ceramics A-W.
Journal of Biomedical Materials Research 24: 331-343

Kokubo T, Miyaji F, Kim HM, Nakamura T. (1996)
Spontaneous apatite formation on chemically surface treated Ti.
J Amer Ceram Society ;79: 1127-1129

Nishio K., Neo, M. Akiyama, H., Nishiguchi, S., Kim, H. M., Kokubo, T. Nakamura, T. (2000)
The effect of alkali- and heat-treated titanium and apatite-formed titanium on osteoblastic differentiation of bone marrow cells.
Journal of Biomedical Materials Research 52(4): 652 – 661

Miyaji F, Zhang X, Yao T, Kokubo T, Ohtsuki C, Kitsugi T, Yamamuro T,Nakamura T. (1994)
Chemical treatment of Ti metal to its bioactivity.
In: Anderson OH , Happonen RP , Yli-Urpo A . editors. Bioceramics. Vol. 7 Oxford: Butterworth-Heinemann; 119-125

Sandrini, E., Giordano, C., Busini, V., Signorelli, E., Cigada, A (2007)
Apatite formation and cellular response of a novel bioactive titanium.
J Mater Sci Mater Med. 2007 (in press)

Spriano, S., Bronzoni, M., Rosalbino, F., Verne, E. (2005)
New chemical treatment for bioactive titanium alloy with high corrosion resistance.
Journal of Material Science Material in Medicine 16(3): 203-11

Takadama H, Kim HM, Kokubo T, Nakamura T (2001).
An x-ray photoelectron spectroscopy study of the process of apatite formation on bioactive titanium metal.
Journal of Biomedical Materials Research 55:185–193

Xue, W., Liu, X., Zheng, X. (2005)
In vivo evaluation of plasma-sprayed titanium coating after alkali modification.
Biomaterials 26(16):3029-37

7. SUMMARY

7.1 CONCLUSIONS

It is important to characterise the surface of any biomaterial, as its surface topography and chemistry will affect the biological interactions which occur at the molecular level. There is no guarantee that a material (in this case Ti) which has had changes made to its surface chemistry (i.e. via ion implantation) will function in the same manner as the unmodified material (Kasemo et al., 1986).
In the current work Ca ion implantation was found to be a very suitable method of modifying the Ti surface. The techniques used for surface analysis indicated formation of thin oxide surfaces on the Ca-Ti samples. This is consistent with a model whereby the original surface layer is sputtered away during the implantation process and the modified surface subsequently re-oxidises.
The tissue engineering group at the Eastman Dental Institute for Oral Healthcare Sciences have found that Ca-Ti discs had reduced cell growth at 4 h compared to cp Ti or Ti implanted with Ar or K (Nayab 2003). However, Ca-Ti significantly enhanced cell spreading and subsequent cell growth (Nayab et al., 2004) in contrast to K-Ti, Ar-Ti and Ti. Also implantation of cp Ti with a high ion dose of Ca (10^{17} ions cm^{-2}) was found to increase cell spreading, cell size, and cell proliferation (Nayab et al, 2004, 2005, in press) as compared to lower Ca ion doses (10^{16} or 10^{15} ions cm^{-2}) or control Ti. The effects of Ca implantation on cell function were also assessed, by measuring the production of essential bone-associated constituents (Nayab et al., in press). The results indicated that the effects of the Ca-Ti surface were mediated, at least partly, via gene activation.

Alterations in the biological response have been previously attributed to the changes in surface roughness and topography resulting from sample preparation and / or ion implantation (Lincks et al., 1998), although the exact reasons for this were not understood. However, the Ca-ion implantation process in this work was not found to affect the surface roughness, which was similar to that measured on cp Ti samples. Also, the ion implantation was not found to

alter the general appearance or the micro-topography of the Ti substrate as revealed using SEM. It appears that Ca ion implantation had no impact on the surface topography as measured with white light interferometry. So it appears that any changes in cellular responses cannot be due to topography as measured at this level. It is still possible, however, to have topographical changes at a lower level (atomic scale changes) which are not resolved by WLI, but which might still affect cellular responses. Another possibility is that the response of the cells could be purely due to chemical changes at the surface, with no influence from changes in surface topography. The surface chemistry of a Ca-Ti sample is characterized by an outer surface layer which is represented by contamination. Beneath this are the surface oxide layer, then oxide and carbide, and then more oxide represented by the sub-surface oxide layer. The main difference in the spectrum from Ca-Ti compared to that from cp Ti was, apart from the presence of the calcium, the clear increase in the carbide component in the earlier stages of etching, and also the difference in the thickness and position of the oxide layer, which was thicker than the cp Ti. Following implantation with calcium the surface of the Ca-Ti re-oxidised on removal to air. This re-oxidation occurred both above and below the maximum carbide concentration, the presence of Ca allowing greater oxygen diffusion into Ca-Ti than occurs with bare cp Ti, where the passive oxide forms very quickly, preventing further diffusion and oxide thickening.

Taking into consideration the findings presented in Chapter 3, a model can be proposed for the surface changes that follow Ca implantation into titanium. Ca ion implantation did not result in a modification of the surface roughness, at the measured level, but the changes which occurred affected mainly the surface and sub-surface chemistry.

From the cell biology studies, it appears that the presence and the nature of the implanted ion is the critical factor in determining the biological response. Indeed it was shown that implantation of either Ca or Ar produces samples with similar surface chemistry characteristics (Armitage et al., 2006). The formation of carbide was seen on samples implanted with Ar, in addition to Ca-Ti samples. The authors concluded that the presence of both titanium carbide and the reduced oxides was indeed a result of the implantation process itself and not limited to the implantation of Ca. Therefore, it appears that any influence on the

cells' behaviour was due to the Ca ions and not the implantation process itself. One possible explanation for this is the release of the implanted ions from the modified Ti surface into the biological environment. Such a release of these active ions may have a significant role in the subsequent interface interactions and could relate to the findings on cell attachments to the different surfaces.

The ion chromatography and the XPS results showed that Ca ions were released from Ca implanted titanium discs at 37°C. This significantly improves on other data on ion release from Ca-Ti (Shinawi, 2003) by directly measuring released ions in solution. Ion chromatography was a useful method of detecting even minute amounts of calcium ions released in solution. The data show that the amount of calcium ions detected in solution after as little as 2 min immersion in water was not significantly different from the amount of Ca ions detected for the control samples (ultrapure water and cp Ti), and that the ion release was essentially complete after 4 h immersion with no increase detected for longer immersion times. The XPS results (both the surface analysis and the depth profiling) confirm that the calcium ions were released from the Ca implanted samples, both from the surface and from deeper within the Ca-Ti. The oxide layer showed an increase in thickness and also changed in composition for the samples immersed for 4 h and over. Concomitant with the increase in the oxide layer, a reduction in the Ca present in the Ca-Ti took place, which correlated with the release of the calcium ions into solution, and the redistribution of Ca throughout the thicker oxide. After immersion of 4 h or more, most of the samples showed colour changes ranging from fully blue to patchy blue, which correlated with the increase in the thickness of the oxide layer. The oxidation occurred sub-surface, which was why it was difficult to detect using normal XPS.

The quantity of Ca ions detected may have beneficial effects on the cells, but may also possibly adversely influence cell behaviour. Passivation is a preclinical treatment intended to stabilise the oxide layer and decrease such ion release from the Ti surface. In this work, nitric acid treatment of Ca-Ti resulted in a modification in the surface oxide layer, as shown by the colour change of the samples following treatment. The 10% HNO_3 Ca-Ti samples were observed

to undergo a slow colour change, which suggested some modification of the surface. By contrast, the 34% HNO_3 Ca-Ti samples resulted in a gold coloured surface, which was linked to the thickening of the surface oxide layer. Significant amounts of Ca have been lost from the Ca-Ti samples following nitric acid treatment. Immersion of the nitric acid treated samples in water resulted in minimal modification in the surface spectra, little ion release and little change in depth profiles. Immersion of 10% HNO_3 Ca-Ti for 2 min in water resulted in no change in the surface oxygen or calcium, although the surface was observed to change colour again, indicating that the surface oxide layer modified. As the surface spectra and the XPS depth profiles did not indicate that the oxide layer has particularly thinned or thickened, it is possible that there is a different effect occurring. Several possibilities were suggested on Chapter 4. One possibility is that the film colour is very sensitive to small changes in the thickness of the oxide layer and there may be changes which are too small for the depth profiles to detect, or there may be changes in the carbon film thickness. Another possibility is H uptake from the solution, which could possibly change the refractive index (or some optical property of the surface layer). However H cannot be detected using XPS.

From the data it appears that both nitric acid treatments (10% and 34%) resulted in a passivated surface, with the least ion release observed for a shorter and less strong treatment (10% for 10 min). With regards to concentration, the 34% HNO_3 treated Ca-Ti samples contained more Ca than the 10%HNO_3 treated samples, which may subsequently be released over a longer period. The different calcium and oxygen distributions may enable implant designs which could provide ion release appropriate to a particular clinical requirement.

Other interactions at the surface, which may be important in cellular behaviour have also been studied. The interactions of amino acids with the Ti surface are very important because proteins are constructed from amino acids and they (proteins) can regulate cell adhesion and subsequent tissue attachment to the Ti surface, which can lead to an increased rate of normal tissue regeneration. From the data analysed in Chapter 5 it can be concluded that Ca ion implantation of the cp Ti samples resulted in both glycine and cysteine

adsorption onto their surfaces. No firm conclusions could be drawn from the experiments on glycine adsorption onto cp Ti, but cysteine did adsorb on to cp Ti discs.

Ion implantation proved a very good method for modifying the Ti surface. However, is an expensive process, not easily available and not well suited to commercial applications, especially where complex implant geometries may be required. This work aimed also to introduce Ca into the titanium surface via a different route to ion implantation, and to characterise their surface and measure subsequent Ca ion release into solution. The study showed that a range of alkali treatments can be employed but that the last stage appears to define the surface properties. Modifying the Ti surface using alkali treatment resulted in more glycine adsorption on the surface compared to the cp Ti samples. Again a wide range of different compositions, thicknesses and release rates were obtained by varying the treatment. This offers further possibilities for producing implants with controlled Ca release characteristics dependent on the clinical implant requirements.

7.2 FUTURE STUDIES

White light interferometry did not detect any change in the surface topography following Ca ion implantation of cp Ti at the micron scale. However this did not exclude changes which may occur in the surface topography at an atomic scale not detected by the technique used. This change may affect cellular behaviour. Atomic force microscopy (AFM) may prove a useful method for assessing changes that may occur in the surface topography at an atomic scale.

The release of Ca ions from Ca-Ti samples was completed by 4 h. However it should be interesting to determine the duration of this process by examining the ion release between 2 min and 4 h. Also, examining ion release from Ca-Ti samples immersed for long periods of time (months) may be assessed, as implants are placed in bone for very long period of time.

As Ca-ion implantation proved an encouraging method of changing the Ti surface, modification using different ions, e.g Na, or combination of ions may have potential merit an be worthy of investigation. *In vivo* and *in vitro* studies

have shown that modifications of Ti samples including Na (i.e. NaOH treatment) have been confirmed as a technique for making the Ti surface bioactive and have resulted in early and good osseointegration after implantation of a titanium implant in the human body (Kim et al., 1996, Nakagawa et al., 2005). In this work, simple alkali treatment of Ti was shown to be a promising method of Ti surface modification. Future studies should include assessment of the cellular response to alkali treated samples.

More work should also be undertaken to understand how the implantation process works, to detect the origin of the carbide on the samples and what happens if is altered.

7.3 LIST OF REFERENCES

Armitage, D.A., Mihoc, R., Tate, T.J., McPhail, D.S., Chater, R., Hobkirk, J.A., Shinawi, L., Jones, F.H. (2006)
The oxidation of calcium implanted titanium in water; a depth profiling study.
Applied Surface Science 253(8): 4085-4093

Kasemo, B., Lausmaa, J. (1986)
Surface science aspects on inorganic biomaterials.
CRC Critical Review of Biocompatibility 2: 335-380

Kim, H.M., Miyaji, F., Kokubo, T., Nakamura, T. (1996)
Preparation of bioactive Ti and its alloys via simple chemical surface treatment.
Journal of Biomedical Materials Research 32(3): 409-417

Lincks, J., Boyan, B.D., Blanchard, C.R., Lohmann, C.H., Liu, Y., Cochran, D.L., Dean, D.D., Schwartz, Z. (1998)
Response of MG63 osteoblast-like cells to titanium and titanium alloy is dependent on surface roughness and composition.
Biomaterials 19: 2219-2232

Nayab, S., Shinawi, L., Hobkirk, J., Tate, T. J., Olsen, I., Jones, F. H. (2003)
Adhesion of bone cells to ion-implanted titanium.
Journal of Materials Science: Materials in Medicine 14(11): 991-997

Nayab, S., Jones, F. H., Olsen, I. (2004)
Human alveolar bone cell adhesion and growth on ion-implanted titanium.
Journal of Biomedical Materials Research A 69(4): 651-657

Nayab, S., Jones, F. H., Olsen, I. (2005)
Effects of calcium ion implantation on human bone cell interaction with titanium.
Biomaterials 26: 4717-4725

Nayab, S., Jones, F. H., Olsen, I. (2007)
The human bone cell cycle is modulated by calcium ion-implantation of titanium.
Biomaterials 38 (1): 34-46

Nayab, S., Jones, F. H., Olsen, I. (in press)
Effects of calcium ion-implantation of titanium on bone cell function *in vitro*.
Journal of Biomedical Materials Research A